THE UNIVERSITY *of* EDINBURGH

The Effect of Strain Rate and Bone Quality on the Bending Behaviour of Whole Bone

Robert James Wallace

Doctor of Philosophy

University of Edinburgh

2012

Abstract

Forty ovine femurs were harvested and allocated into four testing groups; Fast-Normal, Fast-Decalcified, Slow-Normal, Slow-Decalcified. Contralateral pairings were used within these groups for closer comparison.

Dynamic testing apparatus was designed and built allowing rates of strain similar to road traffic accidents to be investigated. These strain rates were achieved by using a pneumatic actuator to apply the load. Slow rate loading was achieved by testing with a commercially available mechanical testing machine at a rate of strain similar to that created by walking. Bone quality was altered by ultrasonically assisted decalcification in EDTA. Levels of mineral dissolution equivalent to the loss of bone mineral density (BMD) of a 75 year old woman were targeted.

Whole bone was used for these experiments to facilitate comparison with real fracture radiographs obtained from NHS database. Fracture patterns and degree of comminution were similar between experimental and patient data.

Bone is often analysed as a simple beam (engineers bending theory). This method of stress analysis was compared with a method that recognised the change in cross section over the length of the bone. Accounting for this had a highly significant effect on the calculated flexural modulus ($p<0.0005$).The length to depth ratio of whole bone indicates that shear forces cannot be ignored. The effect of the contribution from shear force on the deflection was investigated. After accounting for deflections due to shear, calculated normal strains agreed with literature values. Deflection due to shear was found to make a significant contribution to the deflection

The effect of storage (freezing) on the mechanical properties at high strain rate was evaluated: no significant differences were found for force and deflection at failure.

The main body of testing gave the following results:

Normal quality bone, rate compared showed significant differences for Ultimate Stress, Ultimate Strain, Yield Strain, Flexural Modulus and Toughness. Demineralising bone resulted in no statistically significant differences between the loading rates for the Stress at failure. Yield Strain, Ultimate Strain, Flexural Modulus and Toughness did show significant differences.

The fast loading tests showed significant differences when comparing quality for Stress at failure but not at Yield. Significant differences were found when comparing toughness. Slow loading tests showed significant differences between bone qualities for Stress at failure in contralateral pairs. No significant differences were found for strain or toughness.

These results indicate that bone of normal quality can withstand higher than normal stresses for short durations. This ability is lost in demineralised bone.

The high loading rate tests revealed closely matched strains at failure for both bone qualities, lending support to the strain based failure theory for bone at traumatic strain rates.

Declaration

I hereby declare that the work presented in this thesis is all my own work unless otherwise indicated. This thesis has been composed by me alone and the material has not been submitted in whole or in any part for any other degree or professional qualification at this or any other University.

Robert Wallace

September 2011

Acknowledgements

I would like to give thanks to:

Firstly, my supervisors, Professor Hamish Simpson and Dr Pankaj for their direction, insight and support throughout this project.

Thank you to Andrew Muir for guidance and helpful comments.

Robin Henderson is thanked for his assistance with the statistical approach used to analyse the data.

John Bracken and Joan Docharty for providing the animals used in this study.

Thanks to various colleagues, Deborah MacDonald for keeping my sanity in check, David Hamilton and Paul Jenkins are thanked for their much needed humour and advice on all things medical and Antonello Spadaccino for helping me acquire the samples and supplying the office with caffeine.

Thanks to Winifred, John and Andrew Wallace for their continual love and support

And special thanks to Miriam Remally for managing to live with me during this process!

Contents

List of Figures

List of Tables

1 Introduction

1.1 Aims and research questions

Bone is known to be viscoelastic, resulting in a higher failure stress at a high strain rate. This can help protect the skeleton from traumatic incidents. It is also known that age and diseases of the bone have a negative effect on the strength, resulting in fracture from minor trauma, such as in a trip or fall.

Most fractures occur at a rate of strain greater than that which would occur in normal use (such as walking etc). Therefore, to investigate representative fractures, a representative traumatic strain rate was used.

The testing carried out in this research was carried out using whole bone. Whole bone was used for the following reasons:

- There is an existing body of research carried out using specimen machined from a larger bone.
- There is a lack of work carried out with large animal whole bone
- Assessing whole bone allows the effectiveness of all parts of bone hierarchy to be assessed
- Physiological comparisons can be drawn with health care data

This research will investigate “bone quality” as a variable, and that a variation in bone quality will be produced by decalcification alone. This study examines the effect that altering the mineral content of bone has on the bending behaviour at both low and high loading rates

1.2 Research Questions

The following research questions will be addressed in this thesis:

1. Is bone's ability to endure higher stresses before fracture maintained when there is a reduction only in the mineral content?
2. What effect does reducing the mineral content have on the stiffness of whole bone when loaded at strain rates representative of normal use?
3. What effects do traumatic rates of strain have on the toughness, yield strain and failure strain on normal quality and demineralised bones?
4. Does the contribution of shear stress have a significant effect on the stress or strain at failure?

1.3 Novel Aspects

The following elements of this study should be considered novel:

- Testing of whole bone, partially demineralised at traumatic strain rates
- Testing of whole ovine bone at traumatic strain rates
- The effect of storage (freezing) at high strain rates

2 Literature Review

Fractures cause a considerable amount of morbidity worldwide. Fractures most commonly occur as a result of experiencing a stress exceeding the level that the bone is able to cope with (Lotz 1995). Therefore people of all ages can be affected by bone fracture. However, the occurrence of fractures is not uniformly distributed among all age groups, being more prevalent, and with greater consequences, in the elderly. For example 90% of hip fractures occur in the over 70's (Hayes 1993). This is because fractures can occur at a much lower stress level in elderly bone coupled with a greater propensity for falling in the elderly (Burr 1997).

In young healthy adults, a trip or fall from a standing height will not normally result in a fracture. Fractures of the ulna/radius have a high frequency of occurrence in teenagers (Raunch, 2001). This is due to a combination of growing bones (therefore not at full strength) and a likely hood to indulge in activities that will provoke a fall.

Numerous well conducted research publications (McCalden 1993, Currey 1996, Zioupos 1998), have reported that the age of the bone affects its ability to withstand load.

Felsenberg (2005), Seeman (2006) and Compston (2006) put forward the argument that the age of the bone can be better expressed as the quality of the bone. It is argued that the aging process in bone is a consequence of a combination of a number of effects such as altered mineral content (Currey 1979), larger mineral crystals (Yerramshetty 2008), build-up of microdamage (Burr 1997), changes in the collagen network (Wang 2002) and a reduced cross sectional area (McCreadie 2006). In addition to the aging process, diseases of the bone such as osteoporosis and osteomalacia can have a significant effect on the mechanical properties (See section 2.9.1).

Another important concept that is also well established in the existing research is the viscoelastic properties of bone (Crowninshield 1974, Currey 1988, Ferreira 2006).

In the majority of current literature involving mechanical testing of bone (Burstein 1972, Reilly 1975, Carter 1977, Keaveny 1994, Garnier 1999, Turner 2001), the bone was cut and machined to give many small samples from the same bone. In many ways this is a very good method for testing as it allows many samples to be yielded from the same bone (reducing

intra-subject variability) and allows idealised shapes to be used for testing. However, due to the modular construction of bone as discussed in section 2.2, Hierarchical structure of bone, there will be an inherent scaling effect as the size of the sample increases. And, in addition to this, it is whole bone that fractures and therefore it would be more clinically relevant to study the effects of these properties at a large scale.

2.1 Properties of Bone

Bone is a complex, hierarchical material. It is essentially a two-phase porous composite arranged as a matrix of organic and inorganic components (Currey 2002, Olszta 2007). This composite arrangement imparts an anisotropic nature to the material properties.

Due to the varying amounts, and compositions, of this constituent materials used to create the bones of the skeleton it is said to be inhomogeneous. Bone also displays viscoelastic properties in its response to loading. Furthermore the amount and composition of the composite change throughout its life cycle, as a consequence of usage and age. Therefore it can be concluded that mechanical properties vary throughout life, and are different both inter and intra species. Finally, in addition to all of the above, bone is alive and is also responsible for containing life supporting systems for the whole body. Consequently, bone can be said to have the following material properties:

Hierarchical - Each structural element is also made up of structural elements.
Anisotropic - Material properties are directionally dependant: important when considering loading direction.
Inhomogeneous - Properties are different throughout the structure (Morgan 2001).
Viscoelastic - Duration and rate of loading affects the resulting stiffness and strain.

2.2 Hierarchical structure of bone

Bone, being a biological organ, is by nature a hierarchical substance. All living things are made from cells, which are in turn made from proteins. However, it is from a structural point of view that this hierarchy becomes significant (Rho 1998). The formation of bone from these smaller structures is shown in Figure 2.1 below, taken from Lakes (1993).

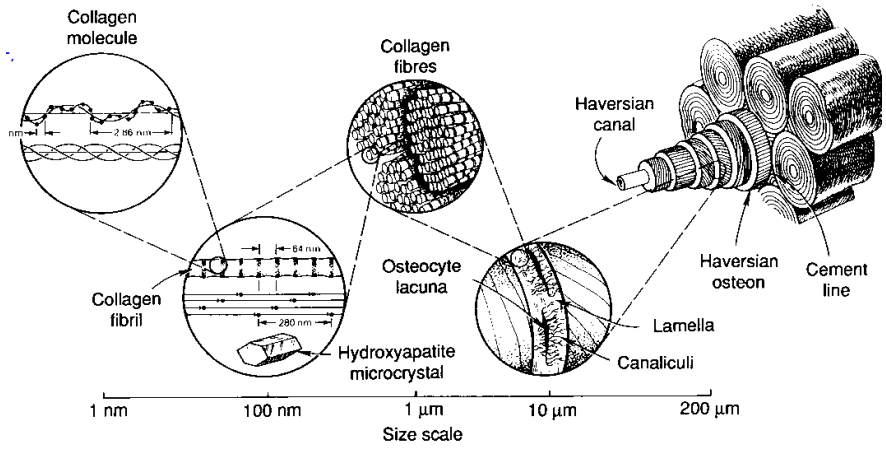

Figure 2.1: Hierarchical Structure of Bone from Lakes (1993)

At the molecular level three polypeptide chains form the triple helix structure of Collagen Type 1. These triple helix molecules strengthened by the addition of crystallised mineral to form mineralised collagen fibrils (Wiener 1992). These fibrils are aligned along their lengths to form fibril arrays, or fibres (Fratzl 2007). These arrays can take a variety of patterns (Wiener 1998), such as:

- parallel fibred – found in mineralised tendons and bovine bone (plexiform)
- woven fibred – formed in early stages of fracture repair
- radial fibred – as seen in dentin

The fibril form chosen is dependent on its function. For example, tensile applications such as tendon use parallel fibrils, while lamellar bone makes use of "plywood like" fibrillar arrays to enable it to withstand forces in many directions (Wiener 1998).

This hierarchical nature, where the structural units of the bone are themselves a composite material makes bone in effect a composite of a composite, that makes yet another composite material.

2.2.1 Cancellous and Cortical Bone

In the literature bone has been categorised as cancellous (also known as trabeculae or spongy bone) and cortical bone. The same basic building blocks outlined in section 2.2 above are used for both bone types (Currey 2002)

Cortical bone acts as the main load carrying part, and as such can be found in long bones, primarily in the diaphysis, and in other areas where strength is of primary concern, such as the skull or mandible.

Trabecular bone acts primarily as a shock absorber and as such is found in the top and bottom of long bones and in other areas where an ability to absorb load is of importance such as the vertebrae.

Osteons are the main functional units in adult cortical bone. Osteons run along the main axis of the bone and are composed of concentric layers of lamella surrounding a central canal containing the blood vessels and nerves. Marking the external boundary of the osteon is a thin layer, known as a cement line

Martin et al (1989) has shown that there can be a negative effect on the static strength properties. Kennedy (2008) believes that these features can also act as crack stoppers, preventing cracks from propagating significantly and posing a serious risk to fracture. Furthermore, they are essential to the growth and sustainability of bone.

Within the layers of lamella there are small interconnecting canals (canaliculi) allowing the transfer of blood and nutrients throughout the bone as well as providing shelter for osteocytes (Wiener 1998). This is shown in Figure 2.2 below.

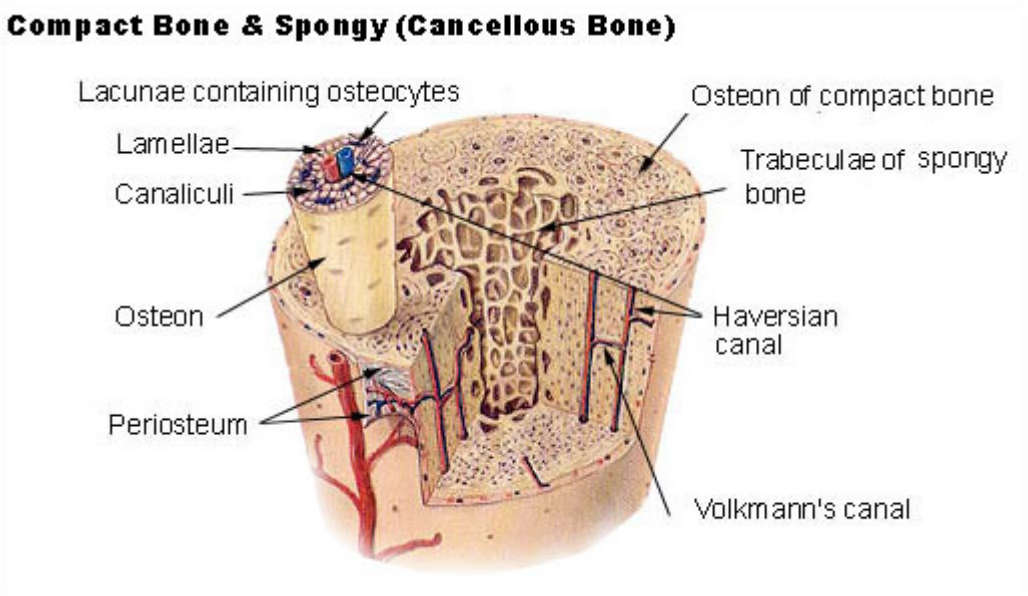

Figure 2.2: Detail of bone constituents from Wiener (1998)

Each layer of lamella has collagen fibres orientated along a different principal axis, and are of differing thicknesses (Weiner 1992). It has been reported that the orientations and thicknesses of the collagen fibres is in part governed by the requirements of Wolff's Law, which is discussed in section 2.4.

All of the different forms that bone takes, from the armour of the skull to the latticework of trabeculae are assembled from the same basic building blocks of mineralised collagen fibrils. Therefore it is the orientation of these fibres and the degree of mineralization that denotes the ultimate strength, Young's modulus and fracture properties.

The strength and resistance to fracture of the whole bone is dependent on the interaction between all these smaller building blocks. Features and voids such as Osteons and Canals may act as fracture initiation points in small tests, but in larger more voluminous structures they may act as features that arrest crack propagation (Kennedy 2008). With smaller samples taken from a larger bone, these features will have a proportionally greater effect on the mechanical properties as they form a larger proportion of the structure.

2.3 Bone Function

Bone can be classified into three main categories based on similar shape, composition and function, these are:

- Long bone, such as the femur
- Short bone, such as the vertebra
- Plate-like, such as the skull

Long bones tend to be found in the extremities where, in the lower limb, their primary function is for locomotion, and as such they act as the levers for the skeleton (Jarvinen 2005).

Taylor & Tanner (1996) have shown by both finite element modelling and a radiographic based strain analysis that the lower limbs are loaded primarily in compression during stance and walking. However, there is also a requirement for the long bones to withstand bending, be it from a fall or impact, or in the case of the upper limbs, lifting an object.

Long bones consist of a thick cortical shaft with cancellous end pieces covered by a thin cortical shell. This can be seen in Figure 2.1 below. In long bones, stiffness is more desirable than flexibility and as such these bones tend to be more highly mineralised and make efficient use of the distribution of bone material for maximum stiffness (Currey 2002)

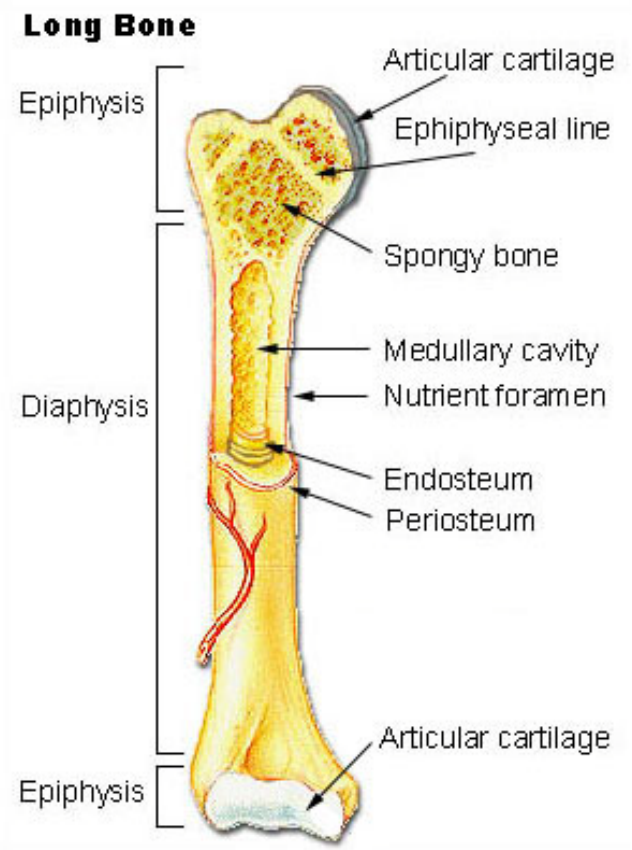

Figure 2.3: Diagram of long bone taken from www.training.seer.cancer.gov

Short bones primarily resist compressive loads and as such are densely packed with trabeculae with a thin cortical shell surrounding the outside. This type of arrangement is favoured for energy absorption and as such can undergo more deformation than long bones without suffering failure (Seeman 2008). It is interesting to note that a similar arrangement of densely packed trabeculae with a thin shell of cortical bone can also be found in the long bone. In the long bone this arrangement of material is located in the epiphysis, where the compressive loading from the body would be greatest and the bending moment due to a trauma would be minimal.

Plate-like bones have a protective function. This type of bone can be found around vital organs such as in the skull or the sternum. This type of bone, especially in the skull vault does not seem to undergo the same load based remodelling process as is described in section 2.7, and as such seem to be designed solely to resist fracture (Currey 2003).

2.4 Wolff's Law

Wolff's law states that the bones of the body will adapt to the loads placed upon it (Wolff 1892). Trabeculae are aligned in the most efficient manner for dealing with the loads they encounter. Cortical bone is thickest where the extra thickness is of most use during typical loading. However this can result in loss of bone in immobile patients as the bones adapt to the loads placed upon them. In this instance the load is less than the bone would previously have experienced and therefore less bone is needed. Further examples of load related remodelling can also be seen in athletes where different bone densities can be found on opposite limbs. For example, Sievanen (2008) has shown that the favoured arm of a tennis player will usually be thicker than the other.

What Wolff observed by this adaptation to loading was in effect the targeted remodelling of bone (Burr 2002). However, this process can also lead to bones that are still comfortably able to bear loads in the directions that they are normally loaded in, but that will be substantially more prone to fracture when a load is applied in a different direction.

A familiar example of this is the thinning that takes place in osteoporotic bone. The action of the disease results in a reduction of the bone's ability to lay down new bone (Kanis 1994) However, bone is able to remodel selectively in a way that results in bone being removed from the endosteal surface and remodelled at the periosteal surface. This results in a net reduction in cross sectional area as less bone is laid down than removed. Even with the reduction in total area, this process can conserve the second moment of area for the bone allowing it to adequately deal with the moderate bending forces caused by daily activity. However, when an out of plane load is applied, such as in a fall to the side, a fracture can result even though the total force applied is not great (Lotz 1995. Pinilla 1996). To compound this problem, the strength giving elements of bone are aligned in the direction of normal loading. This further enhances the anisotropy of bone, creating a state where even without the reduction in bone mass, the bone would be weaker in the direction of loading that would result from a fall.

2.5 The role of Mineral in Bone Strength

In 1975, Burstein stated that what is traditionally referred to as the strength of bone is provided by the mineral component of the matrix. As such bone has been historically

examined and evaluated by its static strength properties. Studies have been carried out to quantify the values for (amongst other properties) Yield strength, Ultimate strength and Young's modulus in tension, compression, bending, shear and torsion (Burstein 1972, Reilly 1975, Carter 1977, Garnier 1999). A range of values found for human bone are shown in Table 2.1 below.

BONE TYPE	Load Type	ELASTIC MODULUS, E 10^9 Pa	ULTIMATE STRESS, 10^6 Pa
Cortical	Compression	15.1 - 19.7	156 – 212
	Tension	11.1 - 19.1	107 – 172
Cancellous	Compression	0.1 – 3	1.5 – 50
	Tension	0.2 – 5	3.2 – 20

Table 2.1: Static Strength Properties of Bone

Conversely, too much mineral can make bone susceptible to brittle fracture. This is evident as an extreme example in the small auditory ossicles, which are highly mineralised to maximize their stiffness and therefore efficiency when transmitting vibrations, but are easily fractured. A counter example of this would be deer antlers, which have a comparatively low mineral content but are able to withstand repeated high energy impacts (Currey 2004). Curry had also shown in 1969 that while an increase in the static strength could be achieved with higher levels of mineralisation, this would lead to a drop in impact strength, implying that there was a compromise to be reached between the ratios of the main components of the composite material that is bone. This was expanded upon by Katz (1971), who demonstrated that there was a non-linear relationship between the matrix and the mineral. This can be thought of as a property of the hierarchical composite nature of bone (section 2.2)

The effect of mineralization on bone strength can be controversial when looking at treatment of bone diseases. It has been shown that the effects of Osteoporosis can be reduced by the use of bisphosphonates which are prescribed to those at most risk of suffering secondary fragility fractures (SIGN 2003, NICE 2010). Bisphosphonates are type of drug that acts by inhibiting the action of osteoclasts (Fleisch 1998, Rogers 2000) to increase BMD.

Allen (2008) has shown that the beneficial effects can be demonstrated for 2-5 years. After which it is thought that they may make bone more susceptible to brittle fracture due to the

increase in the mineral content and accumulation of microcracks that result from the lack of remodelling that the bone has undergone (Shahnazari 2010).

The majority of research into the mechanical properties of bone has dealt with small samples machined from a whole bone (Jarvinen 2005). This method of testing has many advantages, chiefly that many samples can be made available for testing from the same bone. This removes the intra-species variability from the test samples. However, as bone is both anisotropic and inhomogeneous, there will still be inherent variability in the samples. A further benefit is that testing small samples allows appropriate dimensions to be used to facilitate the derivation of material properties, such as stiffness or yield stress, in line with approved testing standards. Suitable standards would be ASTM D790-10 for 3-point bending and ASTM D6272 for 4-point bending. However, caution should be applied when attempting to infer mechanical responses of the whole bone from values derived in this manner (Jarvinen 2005, van der Meulen 2001).

It should be noted that testing using whole bone is not without its own drawbacks. Inferring properties like stiffness is often erroneous due to the change in stiffness of the bone along the length. This problem can be somewhat alleviated by considering the geometric changes along the bone, but the changes in Young's modulus cannot be accurately derived (Turner 1993).

2.6 Fracture Mechanics

The classic approach to structural analysis deals with the calculation of the stress in the structure. Areas of maximum stress are calculated based on long standing relationships between load and the distribution of material in the loaded body. When the maximum stress resulting from these loads is higher than the maximum allowable stress of that material, failure will occur. The influence of defects, such as cracks, in the material was not given serious consideration until after the Second World War. The sudden failure of the Liberty ships and ammunition casing at loads significantly below yield, along with the Comet air disasters of the 1950s gave a new impetus to understanding this phenomenon and the study of Fracture Mechanics was established.

A crack is a volume-less defect. As cracks do not occupy volume they are not reliant on diffusion in the material to move and therefore have the potential to move very fast. This can

lead to rapid and unexpected failures occurring at stresses considerably lower than the yield stress of the material (Demade 2006).

The presence of a sharp notch in a material leads to a stress concentration at the tip, as can be seen in Figure 2.4 below.

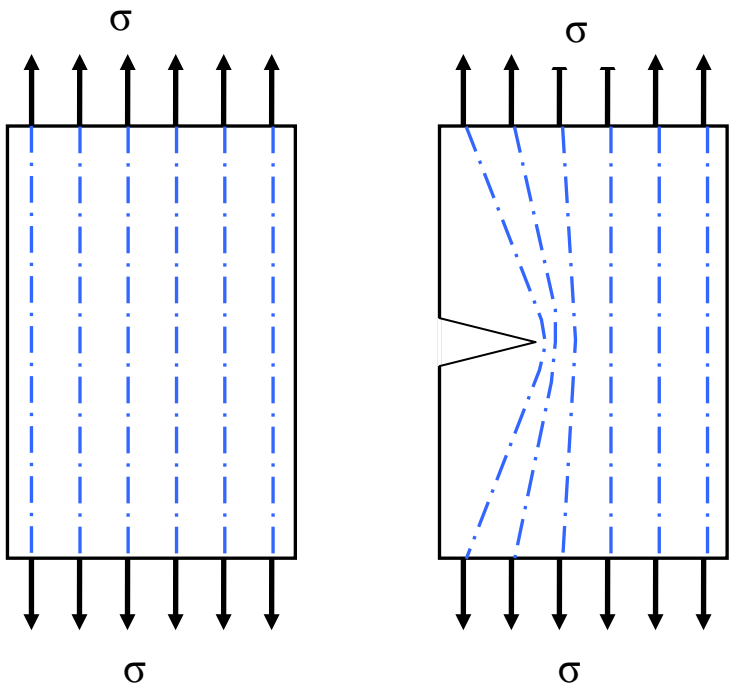

Figure 2.4: Effect of notch on stress concentration

The smaller the radius, the larger the concentration of stress will occur. As a crack has no volume, the tip can be said to have no radius, thus leading to an infinite stress field at the tip. Clearly, the presence of an infinite stress would cause failure in any material. This paradox is examined in the discipline of fracture mechanics (Kanninen 1985).

2.6.1 Fracture Mechanics – Damage Tolerance

Fracture mechanics is the study of the maximum permissible applied loads acting upon a structural component containing a crack. Alternatively, the role of Fracture Mechanics can be to establish the maximum permitted crack size that could be present in the structure without failure occurring at the maximum predicted loads that will occur in that structure (Kanninen 1985). The approach known as Damage Tolerance in Engineering uses the

principals of fracture mechanics to predict the rate at which a crack will grow before reaching this critical size (Hertzberg 1996).

2.6.2 Damage Tolerance Method in Bone Lifecycle

Skeletons provide the structural support for the body. The muscles and the skeleton are required for locomotion, allowing us to travel long distances, hunt and gather food, avoid predators and even fight with rivals. In order to achieve all these goals the skeleton must be stiff and strong and also as light as possible.

Maximum strength at minimum weight is achieved by appropriate geometry, efficient use of material and also what is known in Engineering as "Damage Tolerance". This essentially means that a structure is allowed to have small flaws, or damage, and still be operational. This is acceptable as long as those flaws are small enough not to pose a risk of causing failure.

This damage tolerance approach is essential in the aircraft industry as structures must be as light as possible in order to achieve efficient flight. Furthermore, aircraft, just like bones, are subjected to cyclic loading which causes fatigue. It is this fatigue loading which can cause both existing flaws to develop and can create new dislocations or cracks around areas of local stress concentration or material weakness.

In the aerospace industry the damage tolerance approach requires regular inspections of the components of the aircraft. The loading, access, properties of the material, consequences of failure and ease of repair or replacement are all considered when designing the aircraft and its inspection periods. As it is impossible to eliminate flaws from materials completely, the presence of small voids, dislocations or cracks must be accounted for when calculating the fatigue life or inspection interval. For safety, in the aerospace industry, the largest flaw that would be undetectable is assumed to be present in the component at the time of inspection

For the same reasons of maximum strength at minimum weight, and therefore minimum energy consumption (Currey 2003), bones are also damage tolerant (Taylor 2007). Instead of some form of inspection interval with replacements being offered, bone is continually examined for defects and these are repaired as they occur by a similar mechanism to that responsible for bone growth.

If this remodelling did not take place it has been shown theoretically that bone would have a fatigue life of approximately 3 years (Martin 2003). This reduction in bone life can be demonstrated in patients who have had to undergo a large allograft, such as when a section of whole bone is transplanted. The transplanted section is often found to fail around this period of time (Simpson 2009).

Fatigue is described graphically by plotting the stress against number of cycles at that stress that would cause failure. The number of cycles is plotted on a logarithmic scale and this chart is known as an S/N curve. To facilitate comparison, a typical S/N curve for bone, taken from (Choi 1992), is shown in Figure 2.5 with an S/N curve for steel (MILHDBK-5 1998) in Figure 2.6.

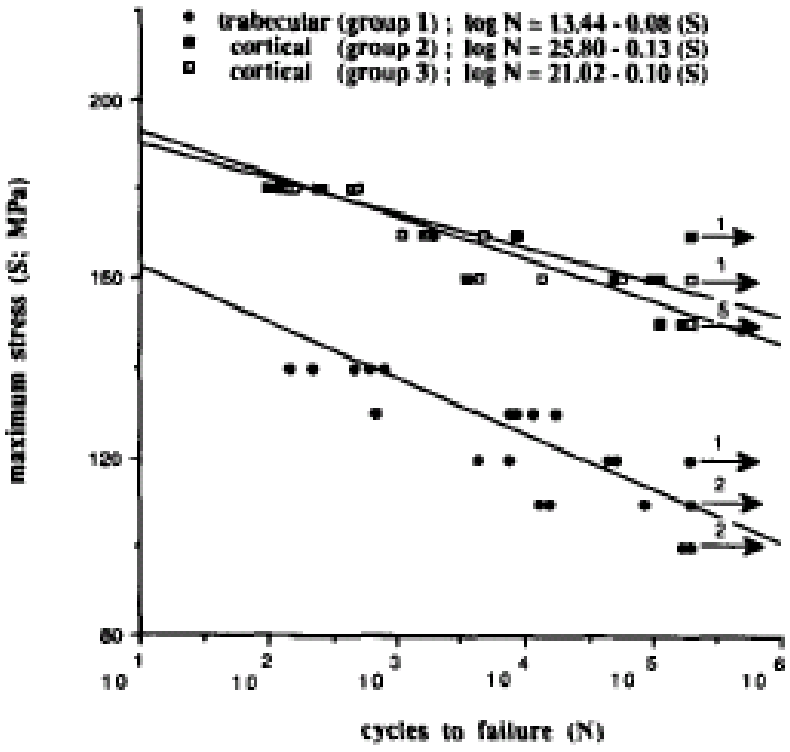

Figure 2.5: S/N curve for Bone from Choi (1992)

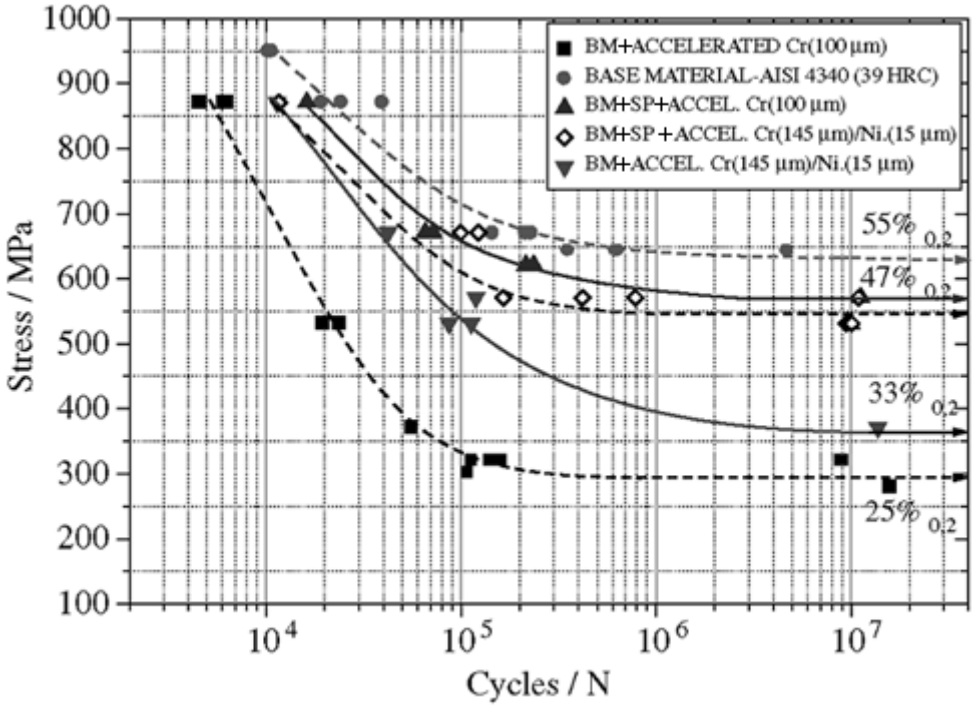

Figure 2.6: S/N curve for un-notched steel taken from MILHDBK-5 (1998)

It follows that there are two ways that the fatigue life (without remodelling) could be increased.

1. To perform less cycles on the bone. This would severely limit the function of the skeleton to 3 years worth of activity at current levels spread throughout the entire life.
2. To reduce the stress on the bones. This can be achieved by either decreasing the load on the bone or increasing the cross-section of the bone in order to reduce the stress.

Decreasing the load would again place un-achievable limits on the activities that would be possible. Bone would be required to be up to 82% thicker in cross section in order to cope with the loads placed on it without suffering fatigue failure (Martin 2003). This analysis only considers the increase in bone mass. It would be required for the muscle also to increase to cope with the increased mass of the bone. This would add further load to the area from it being a) a bigger stronger muscle and also b) it being heavier. This increased loading would result in even greater stresses: therefore the bone would have to have a greater cross section still, and so on. Remodelling of the skeleton therefore confers considerable advantages.

2.7 Remodelling

Remodelling is needed to enable all types of bone to perform two basic structural functions; they must be stiff enough to be able to transmit loads and they must also be able to absorb energy by deformation (Seeman 2008). This requirement to be both stiff and flexible, while also being as light as possible, gives rise to the phenomenon of microcracking. If the load applied to a bone is large enough that it cannot be dealt with by elastic deformation, plastic deformation must take place. In bone, this plastic deformation takes the form of the formation of a number of small microcracks. These cracks allow the release of energy, allowing the structure to dissipate the energy applied to it (Taylor 2007). The presence of these microcracks is thought to act as stimulation for remodelling of bone (Burr 2002)

The complete picture of the whole remodelling process for bone is not fully known (Olszta 2007). It is recognised that the process is dominated by the action of two cell types, the Osteoclast and the Osteoblast. The Osteoclast is responsible for the removal of bone material and the Osteoblast, which is responsible for new bone growth.

This process is shown below in Figure 2.7 and Figure 2.8, figures taken from [ICB Dent, Mechanical Properties of Bone]

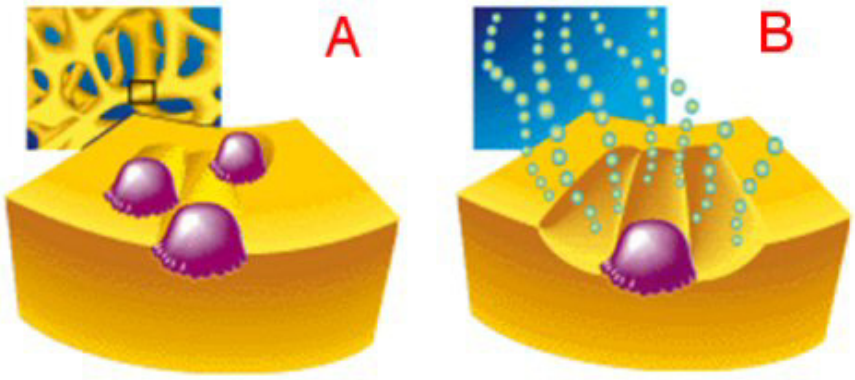

Figure 2.7: Osteoclast bone removal taken from ICB Dent, Mechanical Properties of Bone

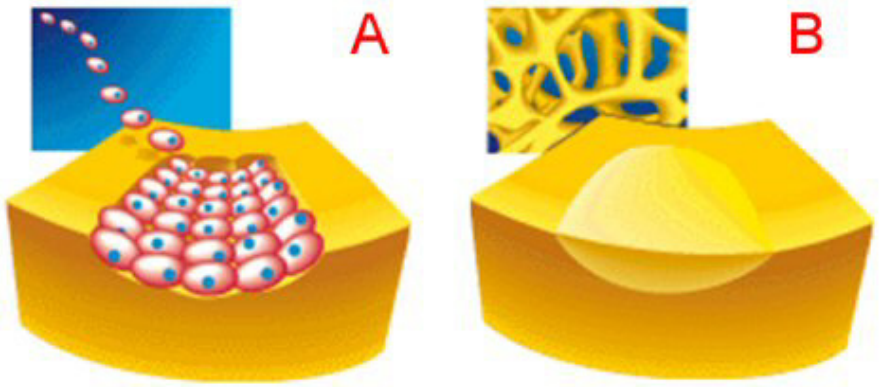

Figure 2.8: Osteoblast bone deposition taken from ICB Dent, Mechanical Properties of Bone

Fatigue fractures, which are commonly referred as stress fractures in orthopaedic literature, have been shown to occur when bone cannot remodel as fast as cracks are created. This can be a problem for athletes (O'Brien 2003) and amongst new recruits to the armed forces (Beck 2000), both groups having to perform repetitive, high intensity activities.

The healthy body attempts to achieve all the goals above in the most efficient manner. Extra bone material will add to the strength of the structure, but also the mass. If the bone is not being loaded sufficiently, the body will reduce the mass of the bone (Frost 1997).

This process is particularly evident in people confined to prolonged periods of bed rest and in the elderly, this is called "disuse osteoporosis". As many elderly people are not as active as they were in their youth, a net reduction in bone mass has been observed (Zioupos 1998). This is exacerbated by diseases such as post menopausal Osteoporosis (see section 2.9.1). This continual change in bone quality throughout the life cycle could be described as another facet of bone's inhomogeneous properties.

2.7.1 Fracture mechanics testing

Fracture mechanics testing, in bone as well as throughout the wider engineering community, relies on testing small samples of a material and applying the results to the larger material as a whole (Hertzberg 1996, Kanninen 1985). This is the most efficient way to perform a large number of tests without using a large amount of the materials under test. In the nuclear or aerospace industries, where safety is critical, tests are performed on small samples taken from the same manufactured batch of material. This takes into account defects in the

manufacturing process (Demade 2006). However, the fracture process is scale dependant (Sinclair 1987), even in homogeneous, isotropic materials such as metal alloys. Constraints on testing procedures such as the requirement for plane strain conditions can make inferring values from testing with smaller sized test pieces erroneous (Rogers 1988). It therefore follows that when a material as structurally complex as bone is tested these scale effects will not be reduced, but will in fact have a greater influence on the testing results. The size of defects compared to the overall structure will be far greater when considering the effect of osteons or micro-cracks when looking at a 2mm section than when considering the effect on a section of bone several times larger than this.

2.8 Fracture Mechanics testing on bone

From early work conducted by researches such as Bonfield (1966) and Piekarski (1970) it was clear that investigating the mechanical properties of bone such as stiffness and yield did not describe how the bone failed. To do so would require investigating the fracture properties of the material.

As with the majority of testing conducted on bone, fracture mechanics testing was performed on idealised samples machined from whole bone. Indeed the nature of fracture mechanics testing requires that regularly shaped sections are used (ASTM, 1985)

Researchers such as Bonfield (1976, 1978) and Wright and Hayes (1976a, 1977) conducted detailed studies on idealised sections of bone using Linear Fracture Mechanics to assess the fracture properties of bone. This method of analysis was found to under predict the fracture toughness of bone. It was evident from this research that bone has a toughening mechanism to provide resistance to fracture. The attributes of the composite that instil these toughening mechanisms are expanded on in section 2.9.

2.9 Toughness

Toughness is essentially a parameter relating to the absorption of energy in the material. The potential energy, the energy required to start the crack and the energy released by propagating the crack are all intimately involved in the process. The exact interactions will vary from material to material, the parameter 'toughness' allows comparison between many types of material.

Vashishth and Tanner (2000, 2003) have demonstrated by controlled crack propagation testing and detailed stereo imaging scanning electron microscopy (SEM) that toughness, or post yield load carrying ability, occurs in bone as microcracking.

It has been shown that bone displays an increased resistance to fracture with increasing crack length. This shows that an elastic – plastic fracture is occurring. Therefore exclusively using the methods of analysis of Linear Elastic Fracture Mechanics (LEFM) will provide a pessimistic analysis of the fracture properties. A more involved method incorporating these elastic – plastic effects should be used (Atkins 1985).

Methods such as the J-integral (Zioupos, 1998) or the resistance (R) curve (Vashishth 1997, 2003, Malik 2002, and Nalla 2005) have been successfully implemented on bone. In order to apply these methods, rigorous testing protocols must be employed, as can be found in ASTM E1820-11 "Standard Test Method for Measurement of Fracture Toughness"

The correct application of these testing methods to derive accurate fracture properties requires careful machining of the bone to give idealised geometric shapes. Small notches can then be made to act as crack initiation points, allowing the energy required to drive an existing crack to be derived.

Due to scaling effects that occur with fracture, and due to the physical size of many mechanisms involved in crack propagation full scale testing of bone is required to assess the contribution of these features to the overall toughness of the bone. Scaling effects of fracture include those that would be relevant in homogeneous isotropic materials such as the edge effect (zero strain at surface), and the size and frequency of internal voids relative to specimen size (Hertzberg 1996).

As stated above, true fracture mechanics tests utilize regular shapes, strict testing methodology and often notches to act as crack initiation sites. These testing restrictions would not be suitable for whole bone testing therefore fracture mechanics properties cannot be accurately derived from the testing carried out in this project. However, a knowledge the work done by many researchers in this field is required to draw any conclusions of how the energy involved in deforming and fracturing whole bone is absorbed.

2.9.1 The role of Collagen in bone toughness

The principal toughening mechanisms in bone are microcracking (Vashishth and Turner 2003, Wang 2006) and at a smaller length scale, un-cracked ligament bridging (Nalla 2003) that affects the collagen in bone. The effects of collagen are thought to operate at the smallest level of the hierarchy displayed in bone. The orientation of collagen is also thought to be of great importance in determining the Modulus of Toughness of the bone (Boskey 1999). This directional dependency is another example of the anisotropy displayed by bone, and is what would be expected when considering its composite structure and hierarchical nature.

Collagen, acting as the matrix in the composite material that is bone, can therefore be thought to be the component that provides bone with its toughness.

2.10 Aging

It has been demonstrated in several well conducted studies, by McCalden (1993, Courtney (1996) and Zioupos (1998) that there is a reduction in the fracture properties of bone, representing an increased fracture risk, that occurs with aging.

There are two proposed mechanisms that have been reported to explain this from a fracture mechanics perspective; a decrease in the quality of the collagen matrix and an increase in porosity and structural defects such as microcracks. In reality it is likely to be due to the combination of these, along with a total reduction in the amount of bone plus the increased likelihood of falls that result in the higher risk of fracture associated with otherwise healthy aging bone.

As bone ages the rate of bone turnover reduces. This increases the likelihood that there are more microcracks present as they will not be removed as efficiently by bone remodelling. Additionally, a longer life will also increase the opportunity for the accumulation of microcracks due to an increase in the number of loading cycles that the bone will have experienced. The build up of voids and microcracks can provide crack initiation points or easier pathways for propagation (Courtney 1996, Burr 1997, Vashishth 1997, Zioupos 2008). In addition to this, the presence of sufficient numbers of microcracks will have a negative effect on the stiffness (Burr 1997). This can be considered as a reduction in the mechanical quality of the bone.

2.10.1 Diseases of the Bones

Metabolic bone diseases affect the material and structural properties of bone, resulting in reduced bone quality and therefore an increased risk of fracture (Chavassieux 2007). Two such diseases are osteoporosis and osteomalacia.

2.10.2 Osteoporosis

Osteoporosis is defined by means of a measurement of bone mineral density (BMD). This is carried out using a duel energy X-ray absorptiometry (DXA) scanner. BMD measurements are compared to the young adult mean value, those with a BMD equal to or more that 2.5 SD of the young adult mean are defined to have osteoporosis. This form of assessment using standard deviations is referred to as a "t-score", which is sex and race matched but not age matched, and therefore those with a t-score of -2.5 are defined to have osteoporosis. If a t-score of between -1 and -2.5 is found this is termed osteopenia, and could indicate a risk of developing osteoporosis. (Kanis 1994, WHO 1994, Miller 2006)

Osteoporosis is a disease that is often associated with the elderly. Both the quality and the amount of bone are reduced, leading to higher stresses for any given load and less ability to cope with these stresses (Felsenberg 2005). Due to an increasing aging population it is expected that osteoporotic fractures are likely to increase in the coming years. Areas of research involving this disease remain highly relevant, it has been estimated (surgeon general, accessed 2010) that 1 in 2 Americans over the age of 50 are likely to be affected by this disease by 2020

It is recognised that both the degree of mineralization, as well as the bone mineral density, affects the strength of the bone (Boivin and Meunier 2002). This adds another complication to the way that osteoporosis increases fracture risk, as not only is there less bone overall, the bone that is present is likely to be less mineralized than normal healthy bone. The explanation for this lack of mineralization is often explained by the fact that the mineral present in the collagen matrix builds up over time. Therefore bone that has been recently deposited will not have had sufficient time to accrue sufficient mineral resulting in reduced stiffness and strength (Ciarelli 2003, Boivin and Meunier 2002)

Furthermore, the mineral that is present is likely to be older due to the reduction in the remodelling process (see section 2.7). This has implications on the size of the mineral deposits. The mineral that is present is in the form of larger crystals than would be found in young healthy bone. Larger crystals of mineral will be stiffer and therefore more likely to be a cause of stress concentration and act as an initiation point for microcracking (Yerramshetty 2008, Akkus 2004). As a greater percentage of the mineral that is present will be in the form of these large crystals, the reduction in strength that could be expected when looking at bone mineral density alone will be underestimated as the distribution and micro effects of this distribution will have an effect that has not been accounted for.

In addition to this, the reduction in remodelling will lead to a rise in the number of microcracks that are created as a consequence of normal activity (Burr 1997, Chavassieux 2007). As described in section 2.6.2, microcracks can act as locations of crack initiation. It should therefore be expected that more microcracks would lead to a greater susceptibility for a whole bone fracture.

This lack of the mineral component is one of the aspects of osteoporosis that can be replicated in the laboratory using decalcification techniques. Selective targeting of the decalcification fluid can produce patterns of demineralisation similar to those found in patients suffering from osteoporosis.

However, it is recognised that decalcification alone is not able to replicate the effects of osteoporosis. It does however mimic the lack of mineralization that would be found in osteomalacia. Therefore, the effect of the mineral reduction studied in the main body of

experiments should be considered to be a representation of the effects of the reduced mineral content encountered in osteomalacia.

2.10.3 Osteomalacia

Osteomalacia is a lack of mineral in the bone resulting in soft bones. It can be caused by a lack of vitamin D or calcium in the diet. When the under mineralisation occurs in the growth plates the disease is be termed Rickets (Chesney 2003) and often results in bowed legs (Russell 2003). In adults, as there is no growth of the bone, there will not be the characteristic bowed leg appearance. Symptoms include muscle weakness, bone pain and in severe cases fracture of the weight bearing bones (Rockville 2004)

Rickets is still regarded as an issue in developing countries as a result of malnutrition and where social or religious reasons prevent sunlight exposure (Pettifor 2002). In developed countries a resurgence in the incidences of rickets was observed towards the end of the 20th century. The epidemiology of these cases included infants who were dark skinned, exclusively breast fed and living in Northern locations with reduced hours of sunlight during the winter (Clements 1989, Pettifor 2002, Chesney 2003).

These diseases and others like them are a source of concern for health care professionals, as they can change the mechanical properties of bone making them far more susceptible to fracture or failure, as well as causing a great deal of pain and discomfort for the patients. It is therefore important to understand the failure mechanisms of these compromised bones from a structural point of view at a whole bone scale as well as the underlying biological causes of the diseases themselves.

2.11 Decalcification

Bowman et al (1996) conducted a study to examine the tensile properties of fully demineralised bovine bone. Radiographs and atomic absorption spectrophotometry were utilized to ensure complete demineralisation had occurred. Tensile tests were performed and mechanical properties similar to tendon were found. Shah et al (1995) conducted bending tests on feline bone segments that had been demineralised to different degrees. These were tested with a machine crosshead speed of 10mm/min, which is considerably slower than would be encountered in physiological activity. The viscoelastic response of demineralised

bone was acknowledged in a study by Sasaki and Yoshikawa (1993) who investigated the stress relaxation of demineralised bone. Samples of bone were machined from bovine femur and were mechanically tested by cantilever bending. No studies were found that investigated the effect of demineralised bone at traumatic loading rates.

The decalcification agent used in this study was Ethylene diamine tetra-acetic acid (EDTA). This has been used in previous studies (Shah et al 1995) and is commonly used as a means of preparation of bone samples for histology (Alers 1999). In order to speed up the decalcification process ultrasonic agitation was used. This is a validated method that has been shown not to cause morphological deteritation of the tissue (Thorpe 1963, Milan 1981)

Figure 2.9, taken from (Washington University, 2009), illustrates that a 75 year old white woman has a BMD of approximately 750 mg/cm^2. This compares with a peak BMD of 950 mg/cm^2, representing a mineral density loss of just over 20%. This is also shown in Figure 2.10, taken from Kanis 1994, which uses bone mineral content (BMC) and compares this to age and t-score. A higher percentage loss is found when expressed in terms of BMC.

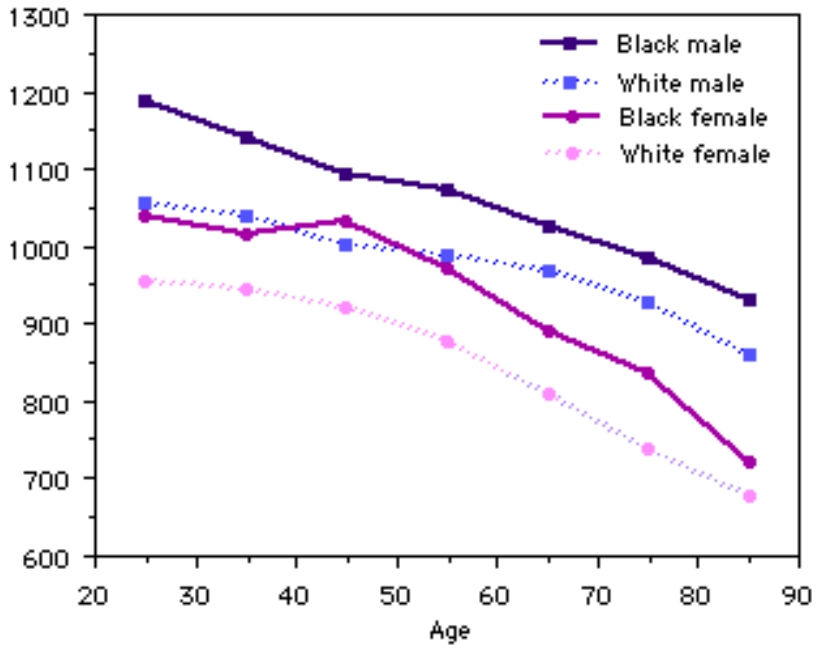

Figure 2.9: Average BMD (mg/cm^2) v Age (Washington University, 2009)

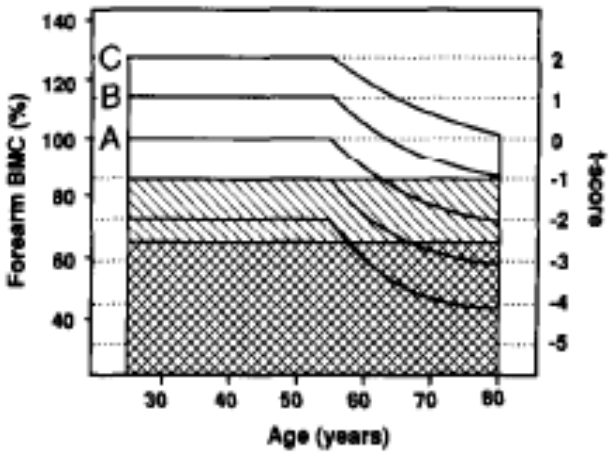

Figure 2.10: BMC, t-score and age (female distal forearm) from Kanis (1994)

2.12 Viscoelasticity

Bone is a viscoelastic material. The definition of a viscoelastic material is that which is affected not just by the amount of strain that is applied but also by the duration and rate of application (Flugge 1967). In bone this viscoelastic effect results in a stiffening response to faster loading, i.e. an increase in the Young's Modulus that is proportional to the strain rate (Wright 1976b, Raftopoulus 1993, Hansen 2008). This is shown in Figure 2.11 below, reproduced from (Hansen 2008)

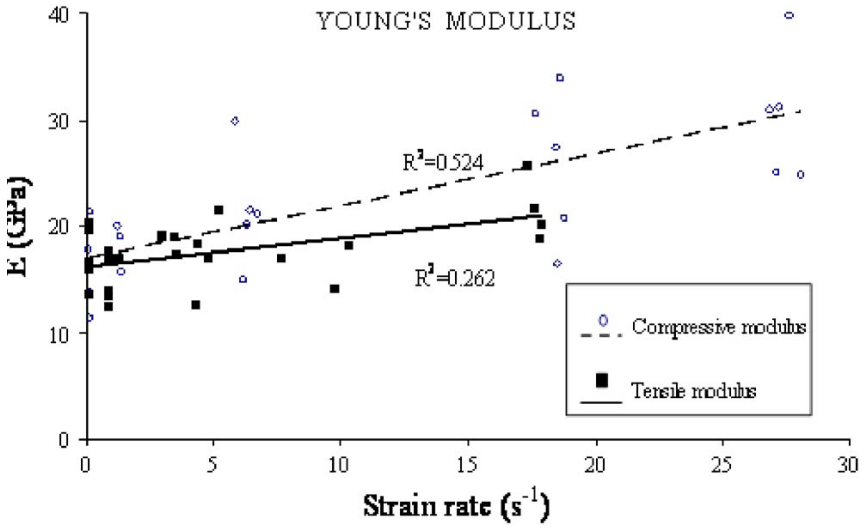

Figure 2.11: Stiffness (Young's Modulus) Vs Strain Rate taken from Hansen (2008)

It has also been recorded that a higher stress can be endured before failure due to an increase in strain rate, i.e. Max Strength is proportional to strain rate (Crowninshield 1974, Wright 1976b). Zioupos (2008) showed that the amount of post yield strain reduces with increasing strain rate. This implies that bone is not able to sustain as much damage before fracture. As its work to fracture is less, the bone has absorbed less energy, therefore more energy will be transferred to the surrounding soft tissue.

Much of the literature examines mechanical testing performed at either a very slow rate that is below that which would be would experienced in daily activity such as walking (Burstein 1972, Carter 1977) or at a rate that could only be experienced as a result of a gunshot or explosion (Ferreira 2006). There are however some examples of testing at physiological rates of loading (Wright 1976b, Hansen 2008). In all these cases however, specimens for testing have been machined from a whole bone. As previously discussed, the effects of features such as osteons or microcracks could have a disproportionate affect on small test pieces.

3 Testing Apparatus and Methods

As described in the introduction to this thesis, the effects of strain rate and bone quality on the mechanical properties of bone were experimentally investigated. To achieve these aims a source of ovine bone was identified and bones were harvested following the process outlined in section 3.1. Mechanical testing was carried out by means of 3-point bending. The methods for slow strain rate loading can be found in section 3.2.2 and the methods for high strain rate loading can be found in 3.2.3. The process for altering the bone quality is given in 3.5.

3.1 Harvest and storage of bones

Ovine bones were harvested from freshly euthanized sheep at the Bush Research Facility, University of Edinburgh. After death, the hind limbs were removed. Care was taken to ensure that no contact was made between the knife and the bone to prevent the risk that a scratch was made that could act as a fracture initiation site during testing. The larger chunks of muscle were also removed at this point to reduce the bulk of materials transported back to the University's testing facility. Each pair of limbs was placed into a thick waste grade plastic bag for hygienic transport and to ensure that each pair of limbs was kept together. This was essential in ensuring that the subjects used could be grouped into contra lateral pairs for testing.

After transportation to the orthopaedic research laboratory in the University medical school a more thorough de-fleshing process was able to take place. All soft tissues, tendons and ligaments were carefully removed from the bone with a scalpel before the bone was wrapped in gauze and soaked in a 1M PBS solution, to ensure they were kept moist. The wrapped bone was then placed in an individually labelled airtight bag before freezing at -20ºC, where they remained stored until testing. This method of storage has been shown to preserve the mechanical properties of bone (Van Haaren 2008).

3.1.1 Testing Groups

A total of 20 pairs of femurs were harvested and processed using this methodology and assigned for testing into 4 main groups of 10 femurs as follows:

- Slow rate loading, normal bone quality (SN)
- Fast rate loading, normal bone quality (FN)
- Slow rate loading, altered bone quality (SD)
- Fast rate loading, altered bone quality (FD)

Within these groups contra lateral limbs were paired, giving rise to 8 groups with 5 bones in each. Pairing of these specimens within each testing group was as follows:

- Slow Loading, Normal Quality (SNr) V Fast Loading, Normal Quality (FNr)
- Slow Loading, Normal Quality (SNq) V Slow Loading, Altered Quality (SDq)
- Slow Loading, Altered Quality (SDr) V Fast Loading, Altered Quality (FDq)
- Fast Loading, Normal Quality (FNq) V Fast Loading, Altered Quality (FDq)

This further subdivision of the groups allows for contralateral pairs to be compared within the four main tests performed.

In addition to these 40 femurs, further bones were harvested for additional experiments. One interesting additional experiment conducted examined the effect of storage on the stress to failure of bone loaded with a fast strain rate. Previous studies have examined the effect of storage media and storage duration, but all tests were conducted at slow loading rates (Turner and Burr, 1993). Strain rate is an important variable in this study therefore it stands that it was also important to investigate the effect that storage at the strain rates to be tested had upon the test subject. These sets of experiments were carried out using ovine tibias, following the methodology for dynamic testing outlined in section 3.2.3

3.2 Specification and Design of equipment

3.2.1 Mechanical Testing procedure

All of the bones were tested to failure in 3-point bending with the load applied at the midpoint of the span in all cases. This is a commonly used testing method and facilitated ease of comparison between the two loading rates.

It was recognised that 3-point bending resulted in a combination of stresses in the test specimen, as in addition to the tensile/compressive stresses caused by bending, there would also have been shear force present. While it was acknowledged that 4-point bending would have created a state of pure bending in the test specimen, the practical difficulties of applying equal forces at each of the loading points in a test piece with a variation in cross section, such as bone, are not trivial. These difficulties are further magnified when considering dynamic loading, as the short loading duration would not provide enough time for equal forces to be established at both loading points. This could result in an uneven load distribution between the 4 loading points or even result in all the load being applied at one point, giving rise to an off centre 3-point bending load. Therefore, in order to ensure a consistent loading mechanism in all tests, 3-point bending was used for all tests.

The two loading rates were applied to the bones by separate loading equipment. The devices and testing protocols are described in section 3.2.2 for the slow rate loading and section 3.2.3 for the dynamic loading.

3.2.2 Experimental Equipment for Slow Loading Rate

The slow loading rate experiments were carried out on a commercially available mechanical testing machine, Zwick/Roell z005 (Zwick GmbH & Co, Ulm, Germany). Data capture was provided by TestXpert V9.01 (Zwick GmbH & Co, Ulm, Germany). This is the proprietary software for the Zwick and as such acted as the control system for the experiments.

The test bone was loaded in 3-point bending at a constant rate of 1mm/s. This created an average strain rate in the bone 8.56 $x10^{-3}$ s-1 (± 1.42 $x10^{-3}$ SD), based on the total deflection of the bone. This strain rate is consistent with that found for walking by Burr (1996). In this

study, strain gauges were implanted onto the tibias two of the researchers. This enabled accurate measurement of the strains involved during activities such as walking and running. Strain rates between 6.44 $x10^{-3}$ s-1 and 11.43 $x10^{-3}$ s-1 were recorded for walking. This confirmed the physiological relevance of the strain rate used in the slow loading rate tests.

During testing the bone was located on rounded supports of 10mm diameter at either end. The load was applied via an aluminium cylinder with a diameter of 35mm, as used in the dynamic loading cases.

As there was no resistance to rotation at the supports, the testing can be said to have been carried out with "simple support" conditions.

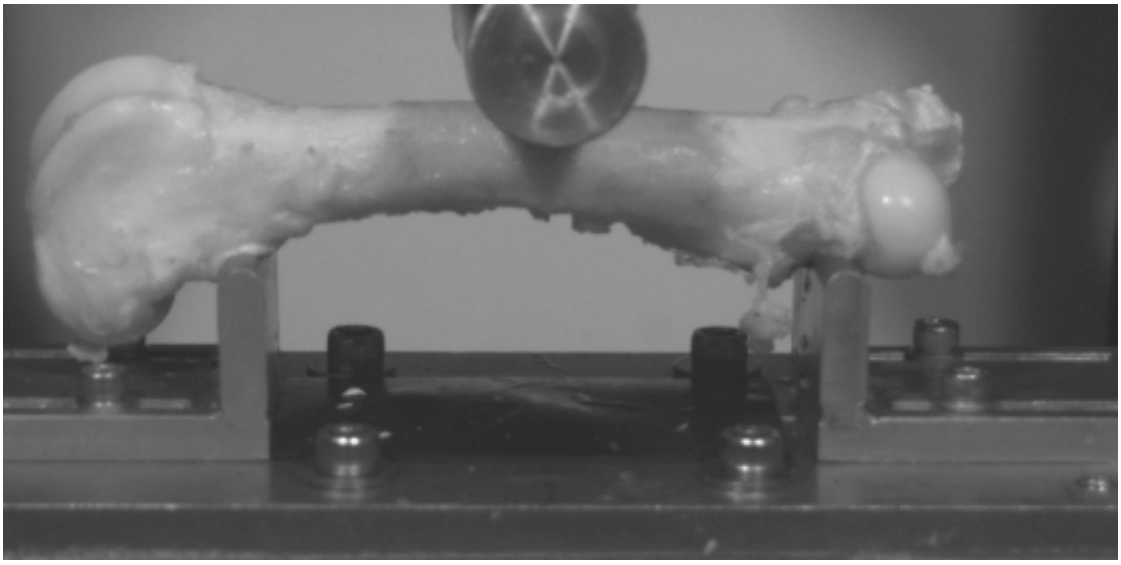

Figure 3.1: Testing at slow strain rate

3.2.3 Experimental Equipment for Fast Loading Rate

The fast rate loading was applied in 3-point bending by a custom designed experimental set up. The final set up consisted of: a bone holder, an instrumented impactor powered by a pneumatic actuator, sensors and a data capture system to monitor the loading and a camera to record the impact. This can be seen in Figure 3.2 below. The development process taken to obtain this final set up is outlined in the following sections.

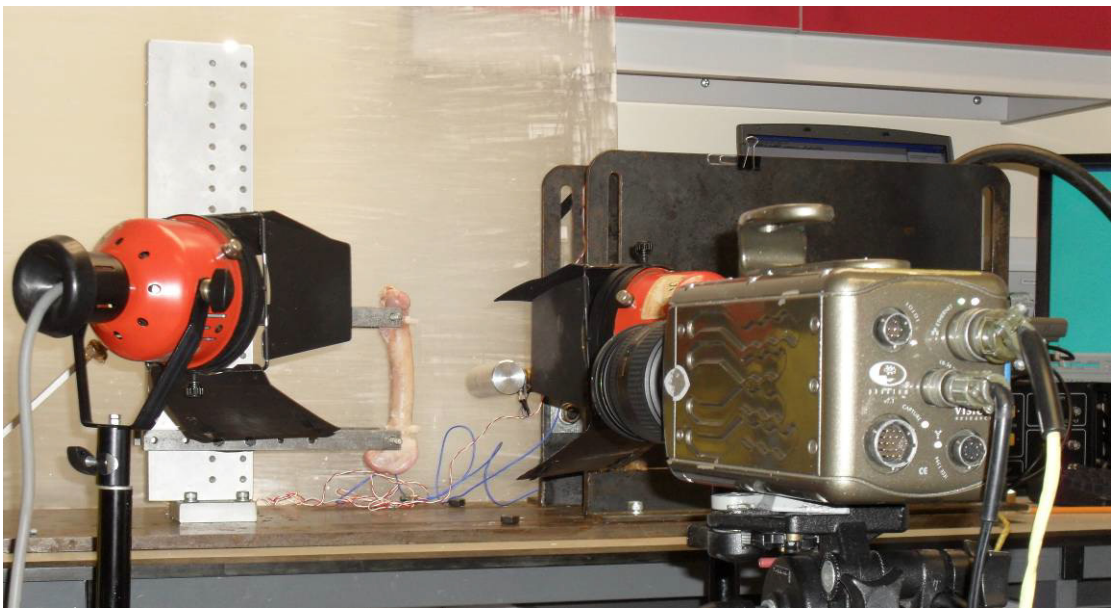

Figure 3.2: Experimental set up for fast loading rate

Calculating the rate of strain from the total deflection of the bone results in an average strain rate of 17.14 s-1 (± 8.20 SD).

Hansen et al (2008), states that a strain rate on the bone of 25s-1 provides an upper bound strain rate that is relevant to bone failures in traumatic events such as a motor vehicle accident. Therefore the rate of strain applied to the bone during the high loading rate laboratory tests can be said to be similar to those that would be encountered in traumatic conditions.

During the development phase the support structure and testing methodology went through a process of optimisation. The steps taken to improve the design of the equipment and the finished experimental protocol are outlined below.

3.2.4 Bone holder for fast strain rate loading

In order to reduce the complexity of forces interacting on the test specimen, it was desirable to have the bone held with “simple supports”. That is, supports that resist movement in the main direction of load but offer no resistance to moments. As the bone is held by a single pin at each end, there will be no resistance to moments. Therefore the bone can be said to be in 3 point loading with simple supports.

3.2.5 Design and development of bone holder

The original design of the testing apparatus secured the bone by means of an 8mm diameter bar inserted through the bone as shown in Figure 3.3.

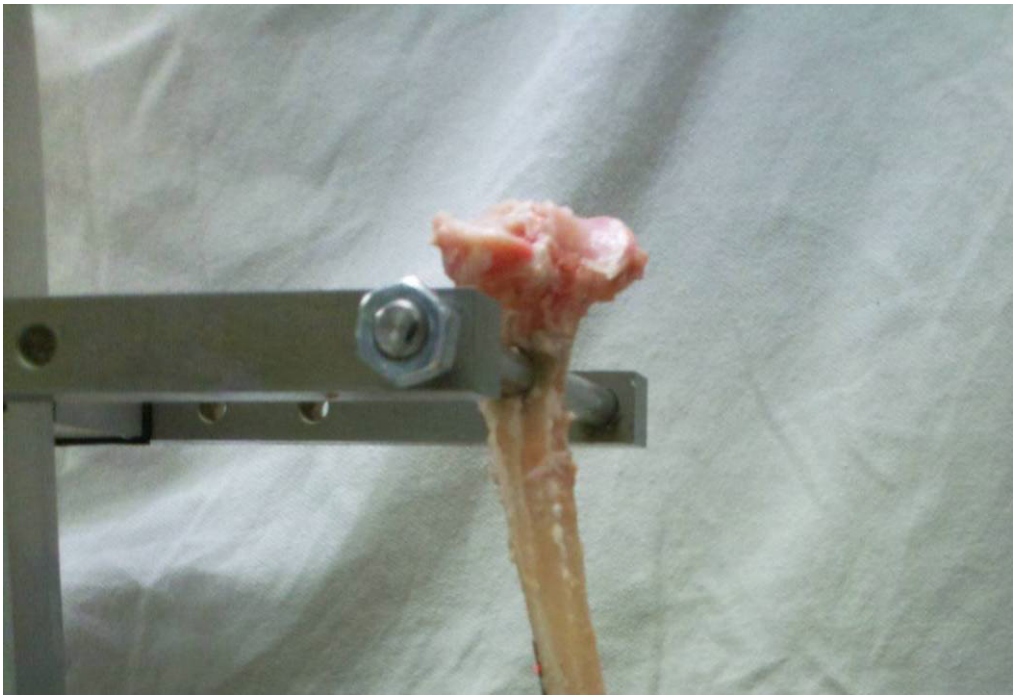

Figure 3.3: Picture of bone held in place by bar through bone

The bars then attach into the support tower via an arm on either side of the bar. The use of these bars locates the bone in a fixed position, and provides no resistance rotation, allowing simple support conditions to be used in the mechanical analysis. It became evident during initial tests that using a bar through the bone was not suitable for mechanical testing to failure, as invariably failure would occur at one of these support locations. This was due to a combination of: stress concentration factors around the hole and there simply being a reduced area at the location of the support loads, leading to greater stresses. These two factors, when combined, greatly reduced the load carrying ability of the bone around the mounting holes as shown in Figure 3.4.

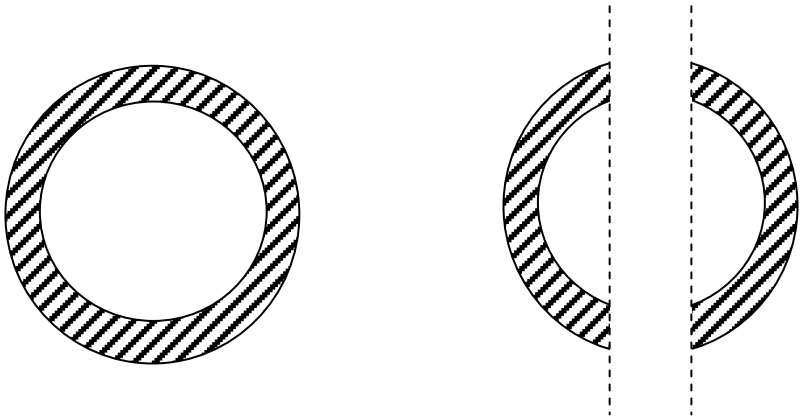

Figure 3.4: Reduction in area due to drill hole

It was therefore apparent that a method of attachment must be found that provided the same freedom for rotation at the support locations but did not involve physical modification to the bone.

A solution to this problem was found by applying cable ties to locate the bones to the pins. Two cable ties were used at each of the attachment points top and bottom. These were crossed over the bone at the front, (impact side) and also around the pin at the rear. It was recognised that this arrangement would provide resistance to any movement of the bone away from the pin, but as there was no offset perpendicular to the direction of the load, i.e. the cable ties were in line with the reaction force from the pin, there would be no resistance to rotations at this location. Therefore, the requirements of simple supports can be said to have been met.

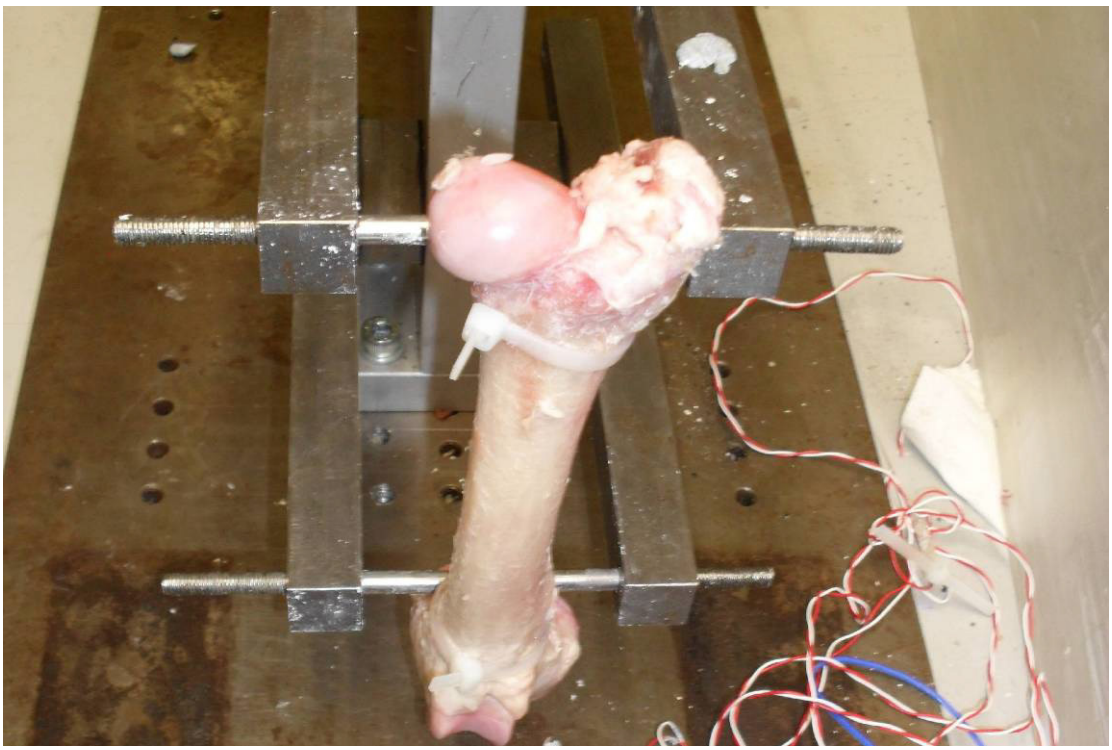

Figure 3.5: Bone secured by cable ties

Now that the bone was securely fastened to the bar without the need to create drill holes, the diameter of the bar could be increased. This was done to increase the stiffness of the bar. The improvement in stiffness of the bar and the increase in the force required to deflect the centre point of the bar can be seen in the table below for 6mm, 8mm and 10mm bars. Calculations were carried out using the formula for "both ends fixed, point load" from Roark's Formulas of Stresses and Strain 4th Edition (Young WC, 1965. p112 Table 3, ex 31) with the force applied at the centre of the beam.

Bar Diameter	Stiffness (E x I_{NA})	Max Deflection with 1 kN unit load
6 mm	12.72 N/mm^2	0.1124 mm
8 mm	40.21 N/mm^2	0.0356 mm
10 mm	98.17 N/mm^2	0.0146 mm

Table 3.1: Calculation of support bar stiffness

Modelling the applied load as a point load at the centre of the bar is a worst case condition. If, as would be expected, the load was applied to the bar via the cortical part of the bone, a 4-point bend condition would result. The deflection due to 4-point bending can be derived using the same equation as was used above, but with the loading points moved to reflect the

position of the cortex. Assuming symmetrical loading, the deflection calculation need only be done for one position and then multiplied by two in accordance with the Principal of Superposition. Only half the load should therefore be applied in this calculation.

A theoretical bone width of 20mm was used giving an offset from the centre to the location of the cortex of 10mm. This results in an estimated deflection of 0.01128 mm per Kilonewton at the centre of the bar.

3.2.6 Support Arm

As previously stated, the support arms link the bars used to support the bone during testing with the support tower. This component is made from steel to maximize stiffness. A relatively thick section of 19mm (3/4 inch) was chosen for this purpose.

The distance between these support arms was kept to a minimum as excessive distance would lead to a large bending moment being created in the bar used to support the bone during testing. However, there must be enough room to allow ease of fixation of the bone to the test structure and to prevent the arms from contacting the bone during testing. A distance of 65mm between the internal surfaces of the arms was used. This distance was achieved by the use of spacers between the arms and the support tower.

Rubber gaskets were placed at either side of the spacers in order to introduce damping in the high frequency range between the support arms and the support tower. This was done to prevent resonance occurring in the stiff support structure that could be a consequence of metal on metal contact.

3.2.7 Support Tower

The support tower was a vertically mounted aluminium plate (440mm x 100mm, with a thickness of 25mm) with threaded holes 30mm apart and with a pitch of 25mm. These holes ran the length of the plate. This configuration allowed the support arms to be located at a range of distances apart, allowing the effective bending length of the tested specimen to be altered. Additionally this configuration gave the test structure the capability to test a variety of alternative bone types and sizes. Other types of loading than 3-point bending could be supported by this arrangement. However, it was felt that this study would prove more conclusive by concentrating on only one mode of loading. Scope for further research in this area is expanded upon in section 13.3.

The support tower was securely bolted to a large steel plate that also served as a point of anchorage for the actuator. Several potential mounting locations were drilled and tapped into the anchor plate giving options upon the positioning of the tower. It should be noted that for the experiments carried out in this research, the tower location was limited to one position. The mounting plate was securely fastened to the workbench to ensure that the apparatus did not move during experimentation.

Additional stiffness is added to the support tower structure by the use of a prop support. This linkage attaches the support tower to the mounting plate at an angle of 45°. This prop support was fixed to the support tower at a similar height to the top support arm for maximum stiffness. The bone support tower assembly is shown in Figure 3.6.

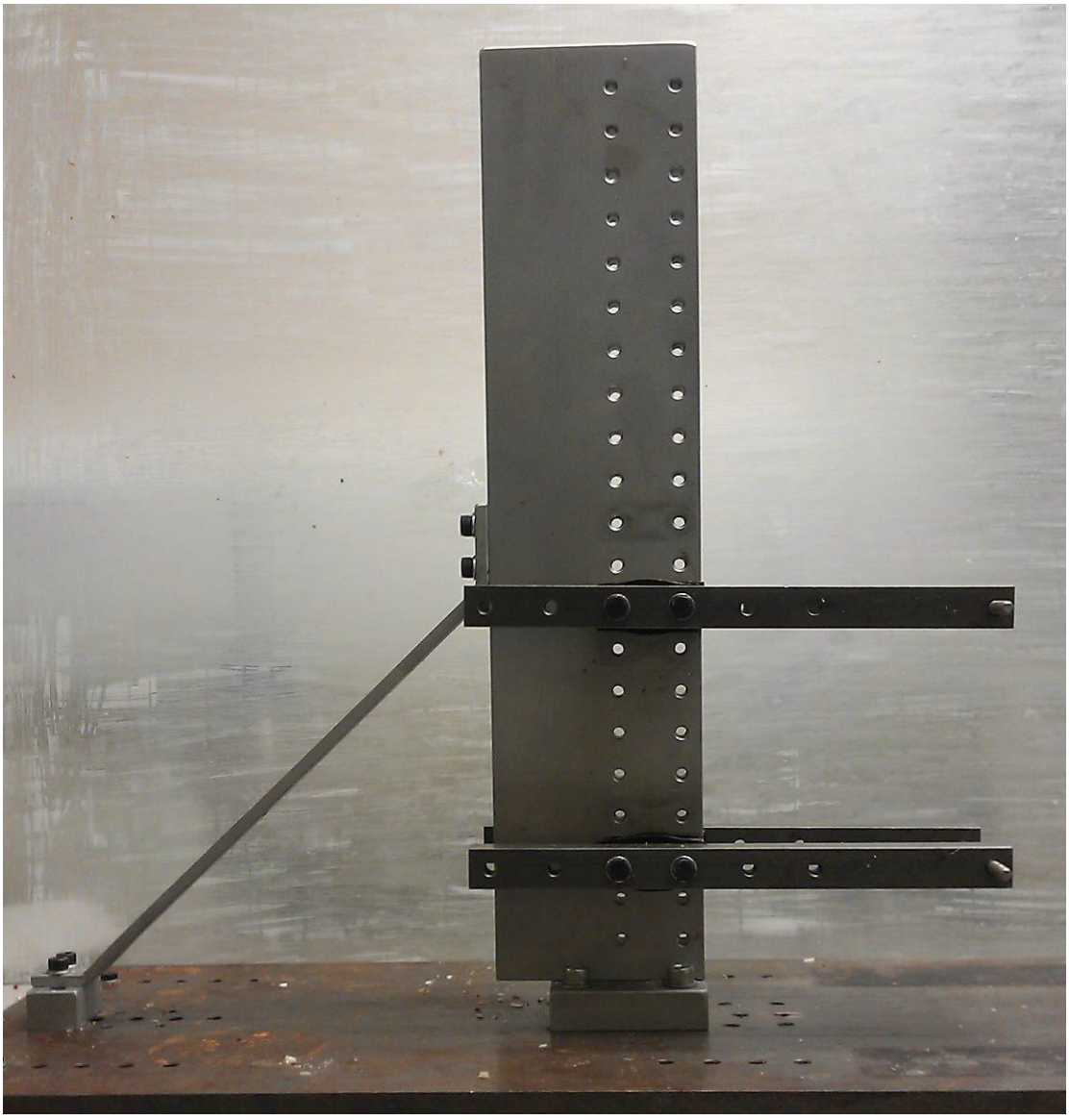

Figure 3.6: Assembled tower with support arms and prop support

3.2.8 Impact Hammer and Actuator

The impact hammer (impactor) consists of a round aluminium striker with a diameter of 35mm. This impactor is connected to a Norgren PRA/18200/200 pneumatic actuator. Nitrogen gas is supplied to the pneumatic actuator from a gas cylinder. The pressure is controlled by a regulator and released by depressing an inline switch. For the high strain rate experiments a pressure of 10bar was used. This creates a theoretical maximum force from the actuator of 7650N (Appendix A).

The actuator was securely bolted to 10mm thick steel plates at either side. These bolts allowed for the actuator to be positioned vertically ensuring that the load was applied at the midpoint of the bone span. The plates were welded to 10mm thick L-section steel along the length of the plates which were in turn bolted to the mounting plate. This prevented any horizontal movement of the actuator system from the reaction force as it was activated.

3.3 Impact Force

It is a bone's ability to cope with the mechanical stress and strain caused by the transference of force, whether slowly or rapidly applied, that will determine if it survives the experience or fractures. It was therefore imperative that the force applied to the bone during dynamic testing was known accurately. In order to achieve accuracy this part of the experimental set up was continually evaluated and improved until this goal was achieved.

Two accelerometers, coupled to a high speed data acquisition card, were initially proposed to evaluate the impact and gather measurements at important locations on the bone and test equipment. The first accelerometer would be attached to the head of the actuator, in order to measure the deceleration and allow the impact load to be derived. The second accelerometer would be attached to the bone in a location that would not be damaged by the impacting actuator to evaluate the frequency of vibrations caused by this impact.

A selection of accelerometers was available in the laboratory from previous research carried out by the Orthopaedic Engineering department at the University of Edinburgh. The highest rated of these was the PCB 353B18 (PCB Piezotronics Inc. New York, USA). It had a measurable range (that is the maximum acceleration before the signal was clipped) of 500g, where g represents the acceleration due to gravity. This was not considered a large enough range to ensure that accurate measurements were carried out.

Therefore a high specification shock accelerometer was purchased. The PCB 350B23 (PCB Piezotronics Inc. New York, USA) was selected, as this has a measurable acceleration range of 10,000g. This range is suitable for measuring short duration, large acceleration forces associated with impact. This precision sensor was located on the impacting head, where the accelerometer data could be used to derive the impact forces. Initial verification experiments were carried out with this apparatus using Sawbones (Pacific Research Laboratories inc.

Washington, USA) in lieu of real bone as it provided consistency in the mechanical properties of the tested subjects.

3.3.1 Preliminary Impact Experiments

Artificial sawbones were used during the development stage as they have consistent material properties. This gives confidence that measured changes are due to the parameters altered by the operator. These experiments facilitated the development of the signal chain and software routine for the data capture system, (section 3.4)

3.3.2 Sensor location

As can be seen in Figure 3.7, the accelerometer was mounted at a distance to the central load path between the actuator and the impactor head. This off centre location was unavoidable. Due to the complex nature of the stress waves and the resulting residual vibrations created in impact, it was felt that this eccentricity may be a source of uncertainty in the analysis of the force during impact loading.

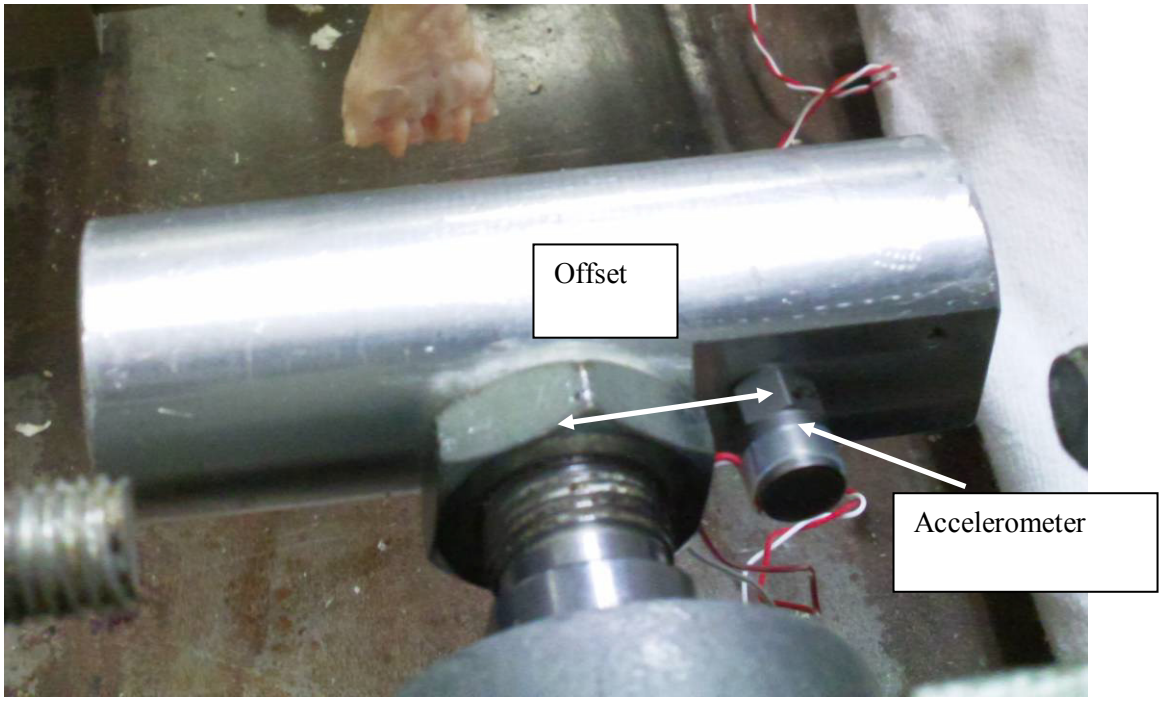

Figure 3.7: Location of accelerometer on the impactor head

It was considered that the experimental procedure would be more robust if a direct method of measuring the impact force was employed. As the requirement for this sensor was specific, i.e. all that would be required was a measure of the force, the accelerations and therefore velocities involved having already been measured in previous experiments, it was considered that a dedicated dynamic force sensor should be used.

A suitable dynamic force sensor, PCB 208C05 (PCB Piezotronics Inc. New York, USA), was identified and the impactor-actuator interface was modified to incorporate this device into the experimental set up. Due to the fast response time required in this analysis a piezoelectric type of force sensor was used. The data sheet for this sensor can be found in Appendix A. The force sensor was incorporated directly into the load path between the actuator and impactor.

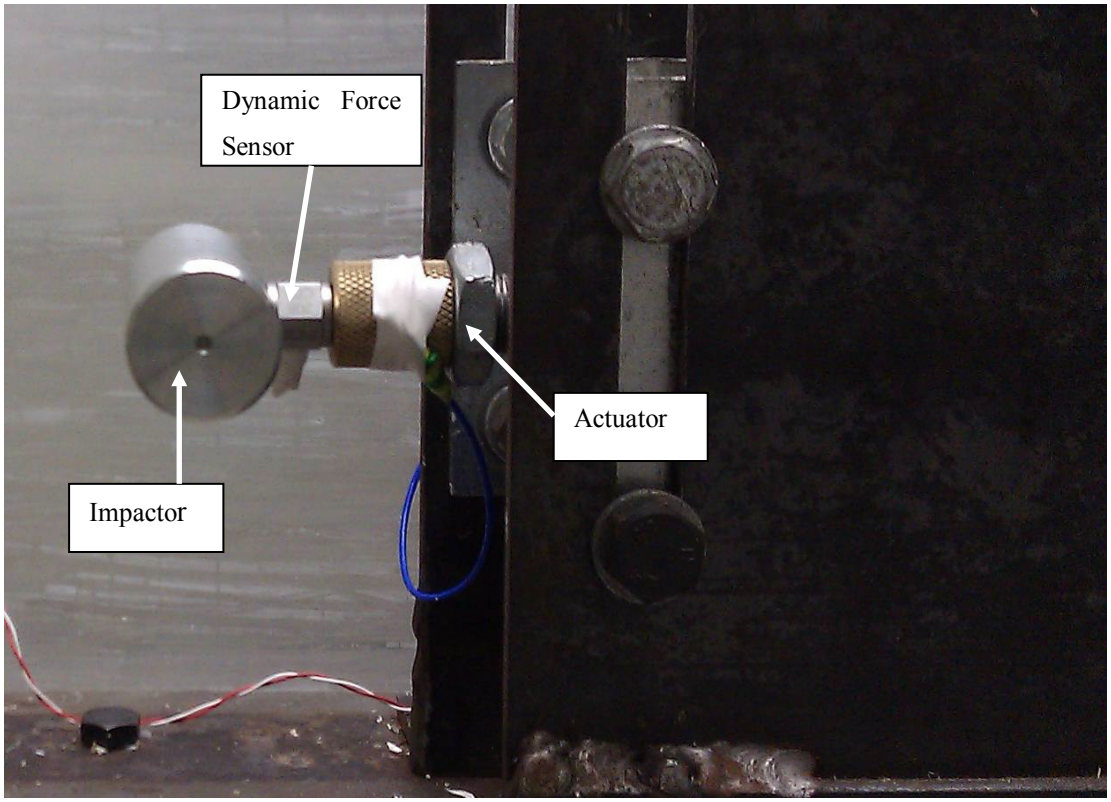

Figure 3.8: Dynamic Force Sensor

3.3.3 Bone mounted accelerometer

Mounting the dynamic force sensor to the impact head allowed the high performance accelerometer to measure vibrations in the bone resulting from fast fracture. This is in line

with the original experimental concept. Before testing a hole was drilled into the femoral head of the bone, a thread was tapped allowing a secure contact with between the accelerometer and the bone surface to be made. This is shown in Figure 3.9 below.

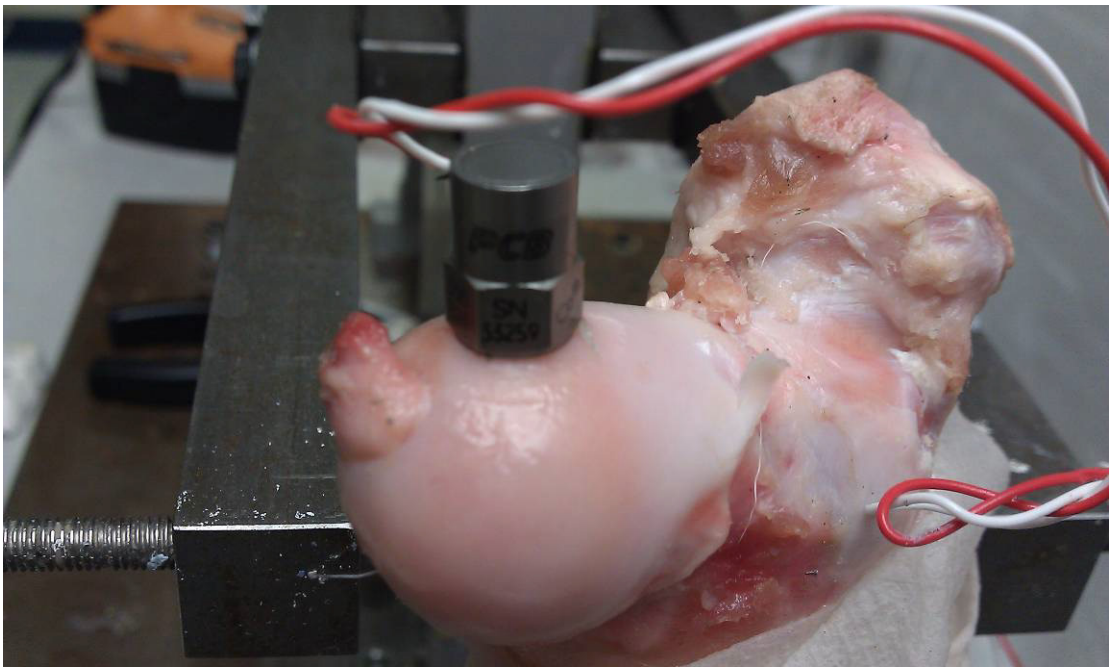

Figure 3.9: Accelerometer mounted on the bone

The frequency of the vibrations in the bone was derived from the accelerometer data by means of a Fast Fourier transform. This was carried out using MatLAB R2008a (MathWorks Inc. Massachusetts, USA). The results from this analysis can be found in Chapter 7, Accelerometer data.

It was recognised that mounting the accelerometer on the femoral head would result in the sensor being located in an eccentric position. This eccentricity could introduce error when interpreting the absolute frequency and amplitude output from this sensor. However, as the sensor location was the same for all test specimens and as it was the relative changes in the measured values that were analysed, it was considered that the secure mounting point offered by this location made it a suitable choice to attach the accelerometer.

3.3.4 Displacement

A Laser Doppler Vibrometer (LDV) (Polytec Ltd. Hertfordshire, UK) was employed as a means of non-contact displacement measurement. The device was made up of the laser unit (OFV 303) and a processing unit (OFV 3001). When the term LDV is used herein it should be assumed to apply to both units. This equipment was capable of measuring both displacement and velocity. In these experiments it was used to measure displacement only, as the velocity can be calculated subsequently from this.

This device works by focussing a laser beam onto a target measuring the amount of time it takes for the laser signal to return to the point of origin. Displacement is measured by calculating the difference in time that it takes to receive the return signal. Therefore a sufficiently reflective target is required for this method to be successful.

Bone does not reflect enough of the laser light to enable the LDV to read this return signal therefore a small section of reflective tape was affixed to the surface of the bone to provide a point of focus for the laser to provide sufficient reflection. The tape was fixed just above the midpoint of the bone, as shown in Figure 3.10. The distance between the point of laser focus and the point of loading was measured before testing.

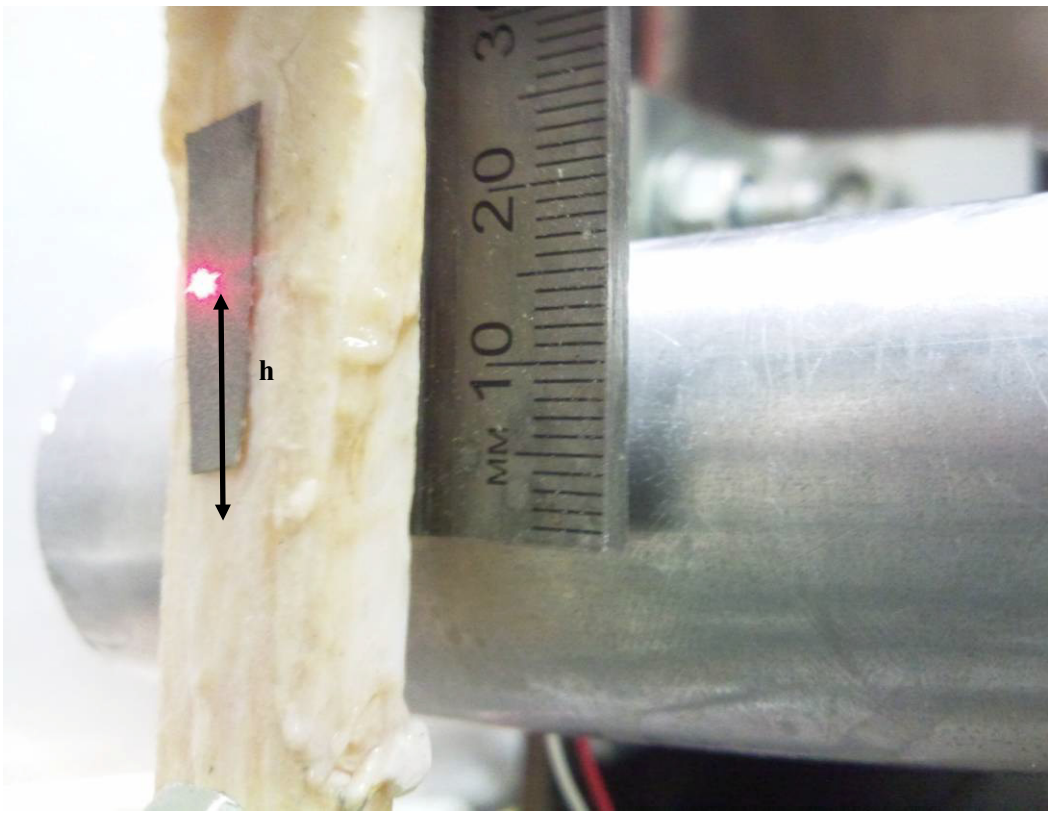

Figure 3.10: picture of reflective tape on back of bone in exp rig

It should be noted that small horizontal translation or in plane rotations in the bone during loading would have a disproportionate effect on the values measured by the LDV. This is shown below in Figure 3.11 for a typical case of a rotation and in Figure 3.12 for a horizontal translation.

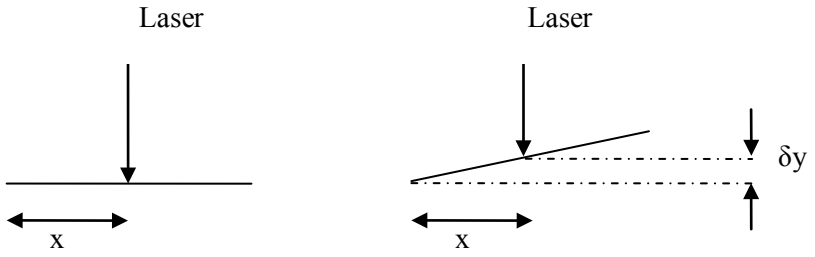

Figure 3.11: Small rotations can result in large measured displacements

.

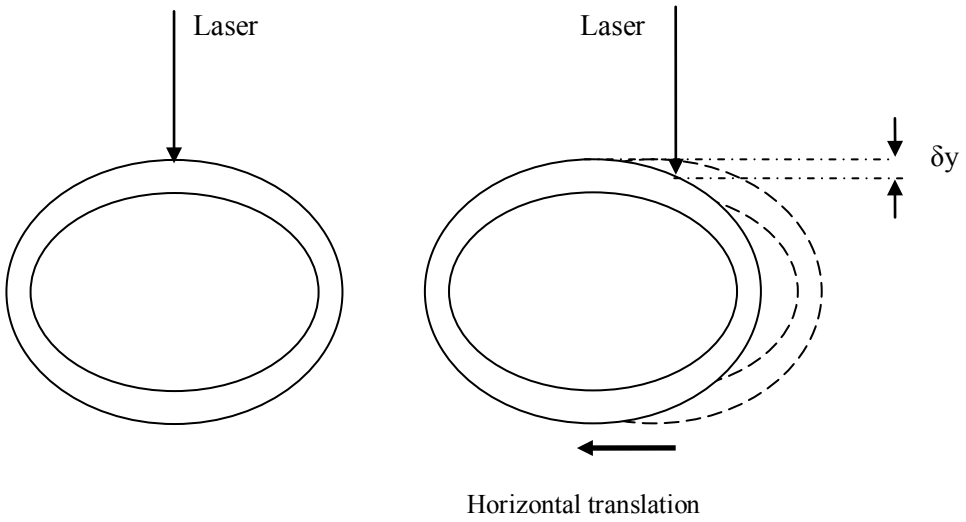

Figure 3.12: Horizontal deflection causing error in LDV measurement

There was no way of determining if any horizontal translations or rotations took place during the short period of loading. As such there would be no way of determining if the measured results were valid. Even if movement not in the plane of loading could be confirmed the effect upon displacement at any given point in time would not be known. Therefore, a different method of measuring the displacement was investigated; this is detailed in section 3.4.1.

3.4 Data Acquisition System

The term "data acquisition system" outlined below refers to the software, computer and other devices that assess and record the raw electrical output from the above sensors.

The accelerometer and piezoelectric force sensor both require a powered signal in order to operate. A PCB 442B104 (PCB Piezotronics Inc. New York, USA) signal conditioning unit was used for this purpose.

All of the measured inputs were captured by a high speed data acquisition device, a National Instruments DAQPad 6070e (National Instruments Corporation. Texas, USA). The Force and Displacement signals to the DAQ were split allowing a digital oscilloscope, Tektronix TDS 2014 (Tektronix, Oregon, USA), to capture and display these signals in real time. The

output from the DAQPad 6070e was passed via firewire high speed cable into a laptop, (Dell Inspiron 5100, P4 2.8 GHz, 768 MB RAM).

The laptop was running a self developed analysis routine in LabVIEW v7.0 (National Instruments Corporation. Texas, USA). A separate channel was assigned to each of the inputs and recorded in parallel at a sample rate of 100 kHz. A sampling duration of 3 seconds was chosen to offer sufficient margin to ensure that the acceleration, impact and fracture stages of the test were recorded. This programme was continually improved during the initial experiments carried out using artificial sawbone, as described in section 3.3.1. As there was a spare capacity of ovine bone, confirmation of the suitability of the entire data capture system was confirmed with real bone before the experiments that form the main body of this thesis were conducted.

After recording, the data was saved by the programme as a text file. This facilitated post test analysis using MatLAB and Microsoft Excel.

The inline oscilloscope was a useful addition to the data acquisition system as it was found that there was an indeterminate delay of between 1 and 2 seconds from pressing the start button in the LabVIEW programme and the start of data capture. It was considered that this delay was likely to be caused by insufficient RAM on the laptop.

The initiation of data capture by the software was signified by a small amount of noise on the oscilloscope. This confirmed to the operator that the signal was being recorded and the switch controlling the pneumatic actuator could be depressed. It should be noted that the noise displayed on the oscilloscope was thought to be due to cross talk in the signals input to this device. This noise was not present in the signal outputted from the DAQ and was therefore not present on the analysed data.

3.4.1 High Speed Camera

In order to allow the dynamic loading experiments to be witnessed in detail, a high speed camera was acquired from the Engineering and Physical Sciences Research Council (EPSRC) Equipment Loan Pool. The model used was a Vision Research Phantom v7.1 monochromatic high speed camera (Vision Research Inc. New Jersey, USA). A Nikon 24-85mm F2.8 lens was fitted to this camera.

To show the onset of failure and the crack propagation fracture process, a frame rate of 25,000 frames per second (fps) was selected from the on screen menu. This gave an actual recorded frame rate of 26,143 fps. At this recording rate a maximum resolution of 256x256 pixels was available. The on-board memory was sufficient for a total of 1.5 seconds recording time at these settings before becoming full. This amount of recordable time does not leave much room for operator error. In order to ensure that the entire loading process was captured the programme was set to record continuously, until a trigger was pressed. Pressing the trigger stopped the recording, allowing the last 1.5 seconds of footage to be transferred to a desktop PC (Pentium 4, 3.0GHz, 512 Mb RAM) for processing with the CineView 630 software (Vision Research Inc).

The exposure time at this high frame rate is very short, 38.25µs per frame. Therefore a large amount of light is required to be shone onto the subject in order to illuminate it sufficiently. This was achieved for these experiments by the use of two halogen spotlights.

The camera was positioned and focussed so that the entire loaded section of the bone could be seen vertically in the frame. At the selected resolution of 256x256 the approach of the impact hammer and the post fracture fragmentation could be seen in the horizontal direction.

The CineView software allows the footage to be converted into a variety of movie and still image files. The user can set the playback speed of the movie files, allowing the impact and fracture to be viewed away from the laboratory setting.In order to measure the deflection of the bone during dynamic loading, the series of still images between the point of striker contact and the point of fracture were identified. These images were then opened in ImageJ (National Institute of Health. Maryland, USA). This programme provides a tool for digital measurement allowing the deflection of the bone at different locations on the bone to be measured. The theoretical bending strain and flexural stiffness can then be calculated from these deflections. The formula and results for these calculations can be found in sections 10.10 and 10.4 respectively. The data capture software and high speed camera set up can be seen in Figure 3.13.

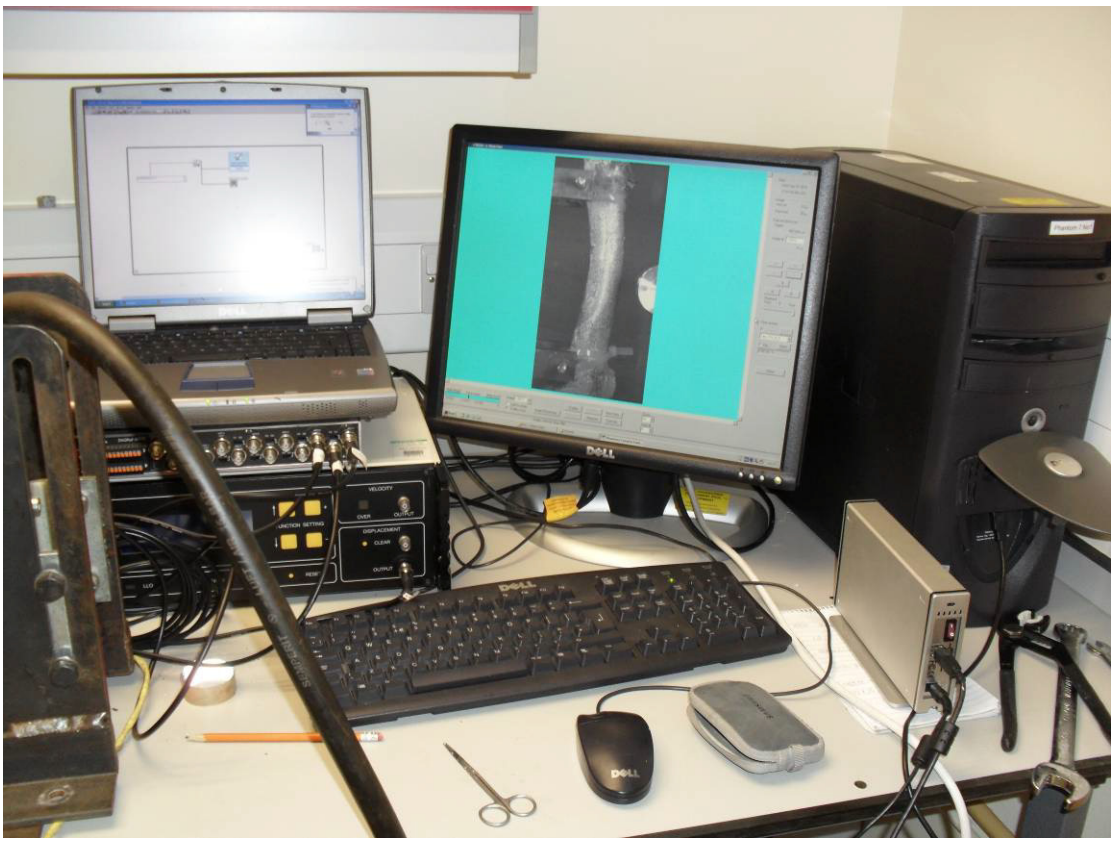

Figure 3.13: Data capture and integrated high speed camera set up

3.4.2 Applied Strain

It was considered advantageous to measure the strain directly. Strain gauges were initially considered as a means of achieving this. Although the use of strain gauges is a popular technique, it was felt that there were drawbacks with this method. Principally, strain gauges are difficult to apply proficiently, especially by the inexperienced. This could create indeterminate errors in the experiments. The likelihood of some error would be increased due to the many specimen tested.

Furthermore, it was felt that bonding these gauges to the bone, along with any form of strain relief for the wiring could interfere with the fracture patterns. The risk of interference to the fracture pattern would be increased as the specimen would have to be dried in order to fix the strain gauges. The presence of the gauge and the necessary wiring could prevent uniform re-hydration of the specimen and introduce unknown variables to the results.

It was therefore required that another method should be investigated, preferably a non-contact means. This would ensure that no external interference in the development of fracture paths was added to the structure.

As a high speed camera was being used to monitor the bone during impact, a series of images would be captured, each a set amount of time apart. Therefore, these images could be compared and relative positional differences compared to calculate the deflections and therefore the surface strains. This method is analogous with Particle Image Velocimetry (PIV), a technique more commonly associated with dynamic fluid measurements.

3.4.3 PIV

As PIV is an already established technique, various computer programmes are available to calculate the changes in relative position. For this work a free to use MatLAB code, OpenPIV (Gurka, R. 1999) was used. When being used to monitor fluid flow, a dye or equivalent is added to the fluid. This allows the camera to effectively "follow" the fluid as it flows. This technique is also applied in the study of aerodynamics; where a coloured gas or smoke is added to the flow of air so its progress can be monitored as the air flows downstream. In order for the program to identify regions of the bone, the bone was painted with a speckle pattern before testing. A layer of white primer was applied to the surface of the bone and a speckle of black flecks of paint was applied to this base layer. The bone could then be mounted for testing.

The speckle pattern was applied immediately after the base coat and then the bone was taken directly for testing. The reasoning for such quick application of both coats was that waiting for the paint to dry out would also allow the bone to dry out. As the fracture properties of bone are known to be affected by moisture content (Turner 1993), allowing the bone to dry would create non-physiologically representative conditions. The quick turnaround from paint application to testing could create difficulties in handling the bone, as any contact would result in the paint surface being marked. However, any marking of the painted surface was kept to a minimum after a small amount of practice.

A number of bones not required for the main body of testing were identified for use to develop this technique. It was found that the extra time required for application of both the

base coat and speckle pattern was between 3 to 5 minutes. It was considered that this was not sufficient time to have a significant effect on the moisture content of bone (and therefore the mechanical properties), although it should be stated that the effect of this process on the moisture content of the bone was not investigated.

Images of the bone during loading were captured at a rate of 26,163 frames per second (fps) in accordance with the dynamic testing protocol outlined in section 3.4.1. While this frame rate provided sufficient detail to show the deflection and failure process, the resolution of 256x256 pixels was not high enough for the computer PIV technique. Attempts to improve the quality of the images were made by increasing the resolution to 256x512 pixels. This allowed the camera to be located closer to the specimen and still keep all loaded parts of the bone in the frame. By moving the camera closer, the bone would be caught by a greater number of pixels. As a consequence of this the frame rate dropped to 14,035 fps. This still gave an average of 16 frames for the loading process. Even this improved resolution did not give high enough quality images for the technique to work satisfactorily.

3.5 Decalcification

Decalcification in Ethylene diamine tetra-acetic acid (EDTA) was used at a concentration of 10M in order to alter the bone quality. The process was speeded up by using ultrasonic agitation in a Kerry KC3 Ultrasonic bath (Guyson plc. Skipton, UK).

EDTA is a chelating agent. Its action is to remove the mineral element, in the case of bone this is Calcium. It achieves this function by means of a strong attraction to the metal ion, where it is bonded to the EDTA molecule by means of coordinate bonds around the centrally located metal atom. Outwith the medical uses for EDTA (which include treatment for heavy metal poisoning and as an anticoagulant for blood testing) it is used as a water softener and as a preservative in food and drink products.

By submerging the bones in the chelating agent, the process of demineralization can begin to occur where there is contact between the fluid and the bone (Verdenius 1958). Therefore, this process will begin on the outer surface.

3.5.1 Decalcification of Ovine Bone

Before the decalcification process was carried out on any of the bones allocated to the testing groups, a pilot study was carried out to ensure that the correct decalcification time and method would be used. In addition to this a small animal study using rat bones was completed (Chapter 5). As well as validating the use of the ultrasonic assistance this study showed the effect of a range of decalcification levels on the mechanical properties.

When examining bone loss due to aging, it has been observed that the bone is preferentially removed from the endosteal surface rather than the periosteal surface. This has the effect of minimising the loss in rotational or bending stiffness that occurs with reduced bone volume, as the contribution of material to the second moment of area (the geometric contribution to stiffness) is greater the further it is from the neutral axis (or the further the material is from the rotational centre in the case of torsion).

In order to have some of the decalcification occurring at the inner surface it was required to supply a flow of the chelating agent to this part of the bone. This was achieved by drilling a 6mm hole into each end of the bone through the cancellous bone structure until the medullary cavity was reached. As these holes were made outwith the loaded section of the bone they would not have an effect on the mechanical properties of the structure during loading. A section of plastic tubing was then inserted into the proximal drill hole and connected to the outlet of a peristaltic pump, (Gilson. Wisconsin, USA). This was used to continuously supply EDTA to the inner surface of the bone, via these machined holes. The inlet to the pump was placed into the fluid in the ultrasonic tank. The supply of fluid from the pump was altered between the proximal and distal drill holes every 2 hours to co-inside with the temperature readings. The fluid supply holes were made outwith the loaded section of the bone so they would not have an influence on the mechanical properties.

The peristaltic pump was set to 30 RPM, this was representative of a flow rate of 45 ml/min through the 3 mm internal diameter tubing.

The bones were decalcified in batches of two. They were placed in the ultrasonic bath which was then filled with the EDTA solution up to a level indicator mark. This required a volume of approximately 1.5 litres of the solution. The exact volume of EDTA required varied with

the volume of the bones in the tank. Both the peristaltic pump and the ultrasonic bath were switched on and the bones were left to decalcify continuously for 56 hours. The temperature of the fluid was recorded at 2 hour intervals.

To prevent excessive build up of temperature the baths were left uncovered. This did lead to evaporation of the fluid, but never to below the minimum allowable fluid level as indicated on the ultrasonic bath, and the bone remained covered by the fluid at all times. The level of the fluid was topped up as required throughout this process. After overnight operation, the reduction in level in the tank was recorded and a mean value for this reduction in fluid level of 11.71mm ± 2.88mm SD was found.

The temperature was recorded before the fluid was topped up, as the temperature reading could be adversely affected by the addition of a volume of room temperature fluid. For the same reason, the temperature measurement taken at the start of the process was not included in the range of temperature measurements, as this was when the fluid was at room temperature. The temperature range of the fluid during the decalcification process is shown in Table 3.2, all values in degrees Celsius.

Variable	Mean	SE Mean	StDev	Minimum	Q1	Median	Q3	Maximum
Temperature	39.9	0.413	4.353	32.0	37.0	39.0	43.0	51.0

Table 3.2: Temperature range (ºC) during decalcification

3.5.2 Assessment of Demineralisation

The level of mineral removed by the ultrasonic decalcification process was assessed by the aluminium equivalent thickness radiographic method (Dawson 2009). This technique assesses the amount of mineral present in a bone using a traditional x-ray image with an aluminium step wedge present in the exposure. After developing the digital radiographs, the DICOM image output was then transferred to a computer where the programme was located. The programme runs a MatLAB script that works in tandem with imageJ.

It is operated by the following procedure:

1. Load the desired image using MatLAB "load" command
2. The image will appear on the screen
3. Identify the step wedge using a rectangular box around the item
4. The program performs an automated edge detection routine to determine the location and grey level of the wedge increments
5. Background and heel effect are corrected for and an exponential calibration curve is created
6. Areas of the bone can now be selected for analysis
7. Output is in the form of equivalent aluminium thickness
8. This was then divided by bone thickness to give density (g/cm^3)

Evaluation of this technique was done by correlating the predicted amount of mineral present with that found by ash weighting, over a range of decalcification levels. An R^2 correlation coefficient of 0.98 was found using the calibrated, heel corrected curve. This was improved to an R^2 value of 0.99 when the thickness of the bone was also taken into consideration (Dawson 2009). To act as a reference for the above tests the measured grey level for the radiographs was also compared with the ash weight. An R^2 correlation coefficient of 0.07 was found. This indicates that the grey level from an image cannot be used alone to make any predictions regarding the mineral content of the bone.

To assess the level of demineralisation in the ovine bones used for this study two regions of interest were selected on each specimen, one proximal and one distal to the fracture. The methods outlined above were followed to obtain the bone mineral density for that section. The measurement of bone thickness for that section was taken from the μCT data. The values for these two regions were averaged to give a single value for the bone mineral density for the bone. Table 3.3 shows the results of this analysis

Groups Compared	Mean Density (g/cm^3)	±SD
Normal Quality	1.88	0.28
Demineralised	2.45	0.43

Table 3.3 : Measured density of bone specimens

The mean value of the mineral level in the demineralised group was 77% of the mean level of mineral found in the normal group. A two-sample t-test was performed indicating a statistically significant difference with a p-value <0.0005.

4 Analysis Methods

4.1 Manual Measurements

Measurements of the external width, external depth and thicknesses of the bones were taken after testing using a digital calliper. The external dimensions were orientated with respect to the direction of loading: the depth taken collinear to the direction of loading, the width was orthogonal to this. Measurements were taken from the proximal and distal sections allowing the dimensions at the fracture to be approximated. Thickness measurements were taken from eight locations, analogous to the points of a compass. These measurements were also taken on both proximal and distal sections, allowing an approximation of the distribution of bone thickness around the fracture site to be calculated. These measurements were taken to provide a source of reference for the computer derived properties (section 4.4.2) ensuring that the output from the programme was representative of the actual dimensions.

4.2 X-ray and µCT of tested samples

After mechanical testing, the bones were x-rayed in anterior–posterior and medio–lateral orientations. This provides a representation of the information available in a clinical situation when a patient is admitted with a fracture. After x-raying the samples the exposed x-ray plates were taken and developed on the hospital's digital x-ray system. The radiographs for all the tested specimen can be found in appendix F.

Consistent x-ray settings of 63mV and 1.8 mAs were used for all the exposures. An aluminium step wedge was placed in the centre of all the x-rays to facilitate measurement of the bone mineral density of the specimen.

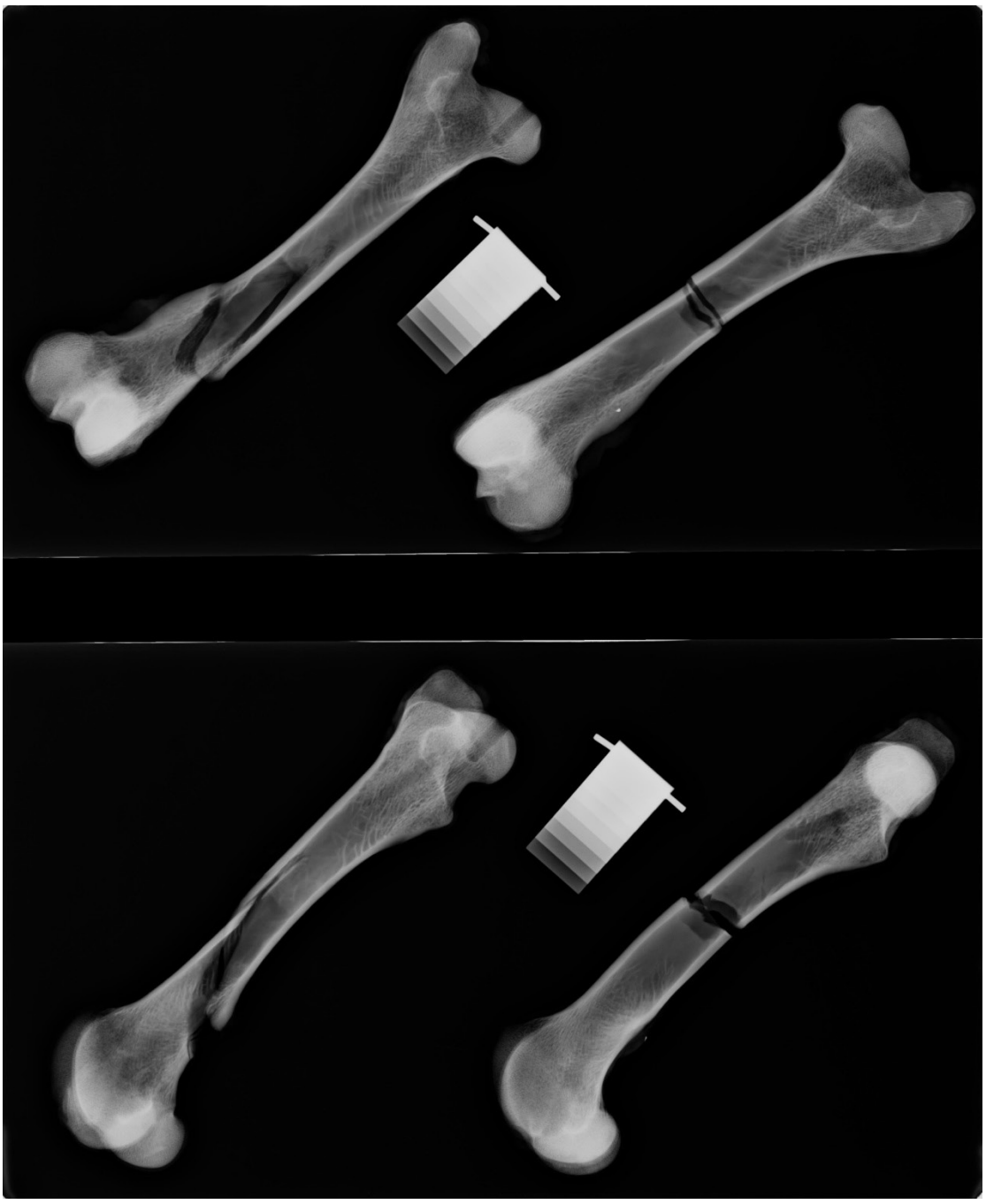

Figure 4.1: Example radiograph of fractured ovine femur

The Bone Mineral Density (BMD) could then be derived in accordance with the protocol set out by S. Dawson (2009) as described in section 3.5.3.

4.3 I_{NA} of bones

In order to accurately calculate the second moment of area, the bones were cut into small sections which were in turn scanned using a μCT scanner. The output from which was subjected to further analysis where the relevant properties were extracted, as detailed in the following section.

4.3.1 μCT of fracture site

The μCT scanner used for this analysis was a SkyScan 1172 x-ray micro tomography system (Skyscan. Kontich, Belgium). The maximum size of object that is capable of fitting into this device was 40mm. Therefore, to facilitate investigation with this equipment the bone was cut using a fine tooth manual saw into smaller sections to allow the bone to fit into the μCT scanner.

A section of bone both proximal and distal to the fracture surface and of approximately 30mm in length was removed by a fine tooth saw. Following this, a section of bone up to the location of the supports could be removed. An example of a cut section of bone containing the fracture surface can be found in Figure 4.2.

Figure 4.2: Picture of Section of bone removed for μCT scanning

Care was taken not to damage the fracture surface during the sectioning process. Fractures of an oblique nature would result in the sections containing the fracture surface having greater length than those with transverse fractures. As a result of this the number of sections for each bone varied from two to four pieces to be placed into the scanner.

The length of each section and the width of the saw were measured to account for the varying lengths of sections and allow their position on the bone to be established when analysing the output from the μCT scanner. While having consistently sized sections taken at identical locations on the bone would have been preferable, the nature of some of the fractures did not allow this. It was considered that maintaining the fracture surface for future analysis and accounting for the variation in section sizes manually was an acceptable compromise. A table showing these measurements can be found in Appendix C.

The bone sections were labelled according to the following protocol: sections cut immediate to the fracture were denoted “top” or “bottom” for the proximal and distal sections respectively. The section between the top (proximal) section and the support point was

denoted “top mid” and the section between the bottom (distal) section and the support location was termed “bottom mid”. This is shown in Figure 4.3 below

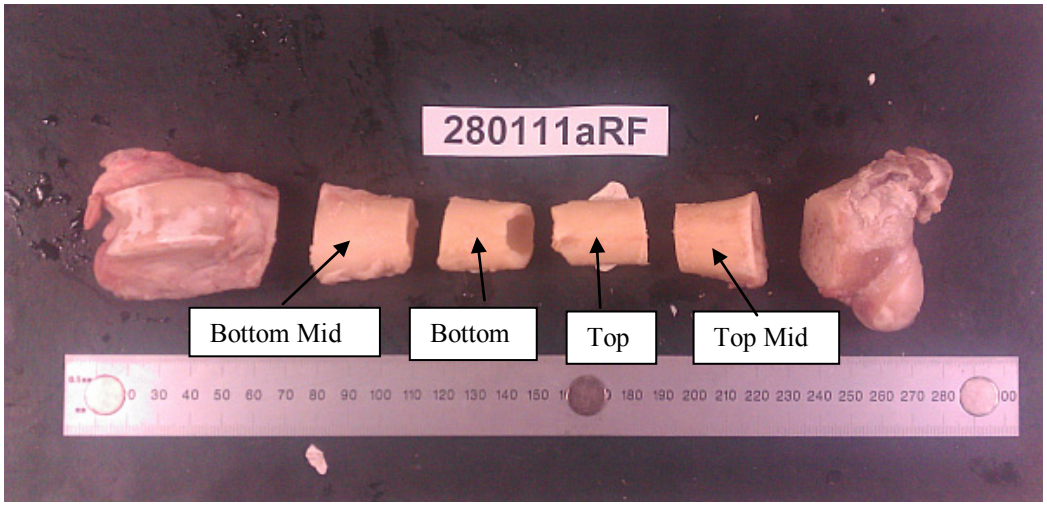

Figure 4.3: Bone after cut into sections

These sections were then scanned at a resolution of 19 µm per pixel. To obtain detailed images and 3D models from these scans the following procedure was followed.

1. The subject to be scanned was placed on a disk of polystyrene and fully encased by foam segments. Both these materials are transparent to x-ray.

2. This was attached to the stage using masking tape, which in turn was securely fastened to the holder in the µCT x-ray chamber. This must be done correctly as any movement of the sample could render the scan unusable.

3. The data from the scan could then be split by region of interest, or the whole data set could be processed if required. CTAn v1.10.10.2 (Skyscan. Kontich, Belgium) was used for this task.

4. 3D processing first involves thresholding and despeckeling the image slices to clean up the data before it can be reconstructed to give volume and solid 3D models. Skyscan’s proprietary CTVol v2.2.0.0 (Skyscan. Kontich, Belgium) was used for this. Understandably, this is a resource intensive computer task and as such a dedicated computer was used for this process (2x 3GHz Quad core 64bit CPUs, 8G Ram, NVIDEA Quadro FX 570)

4.3.2 Properties from scan data

The 19 μm resolution full section scans were also used to obtain geometric measurements of the area around the fracture. An ImageJ module, BoneJ (Doube, 2010) was used to obtain the second moment of area (I_{NA}).

In addition to locating the position of the section with regards to the whole bone it was important to ensure that they were correctly orientated. It was not practical to do this when they were placed into the μCT scanner as the surrounding layer of foam obscured the segments of bone from view and it could not be guaranteed that rotations occurred during location of the stage into the μCT scanner. Therefore, orientation of the samples was done on the output data.

Before the analysis was conducted using the imageJ plug in, BoneJ, all slices of the section to be analysed were input into the "data viewer" programme (Skyscan. Kontich, Belgium) enabling identification of suitable slices. This programme also assisted with the orientation procedure as described in section 4.4.3 by allowing the sections to be viewed by any slice and at any angle.

The following protocol was applied to the slices of scan data in order to accurately obtain the second moment of area:

- Selected slice opened with ImageJ
- Suitable threshold limit identified
- BoneJ module run to identify
    - Centre of image
    - Principal axis of cross section
- Image cropped and translated to ensure centre of bone segment in centre of image
- "Orientation" plug in to define axis of interest
- BoneJ module run again, ensuring calculations performed with respect to the defined axis
- Output in pixels therefore scaling of results required (exact 19.34 μm resolution used for this)

In addition to the second moment of area, properties such as the cross sectional area and mean cortical thickness were also extracted.

4.3.3 Orientation of scan data

As discussed in the above protocol, an axis of interest was defined to calculate the second moment of area about the correct axis. Photographs of the segments of bone along with the SkyScan data viewer programme to ensure that the correct axis was applied. Figure 4.4 to Figure 4.7 show the desired axis marked on photographs of each section.

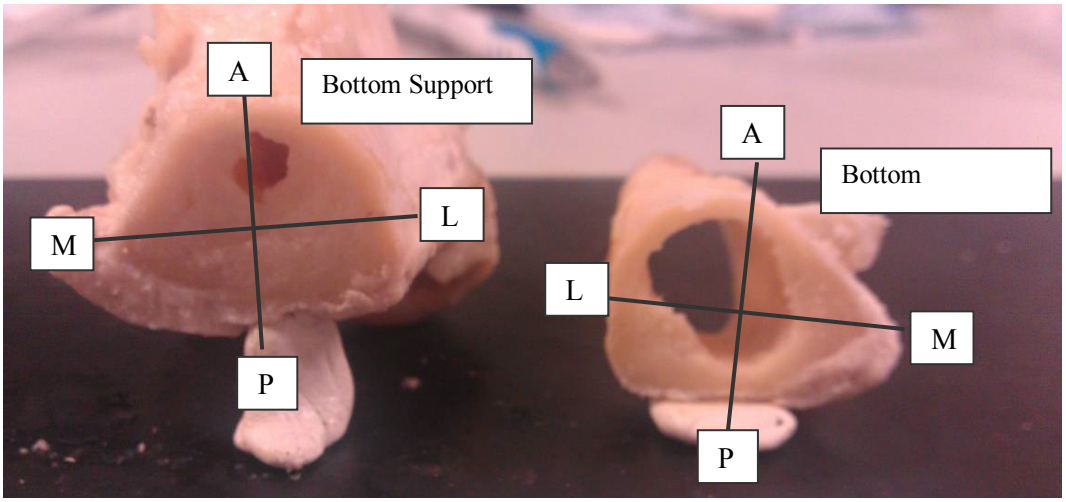

Figure 4.4: Bottom Support and Bottom Mid section

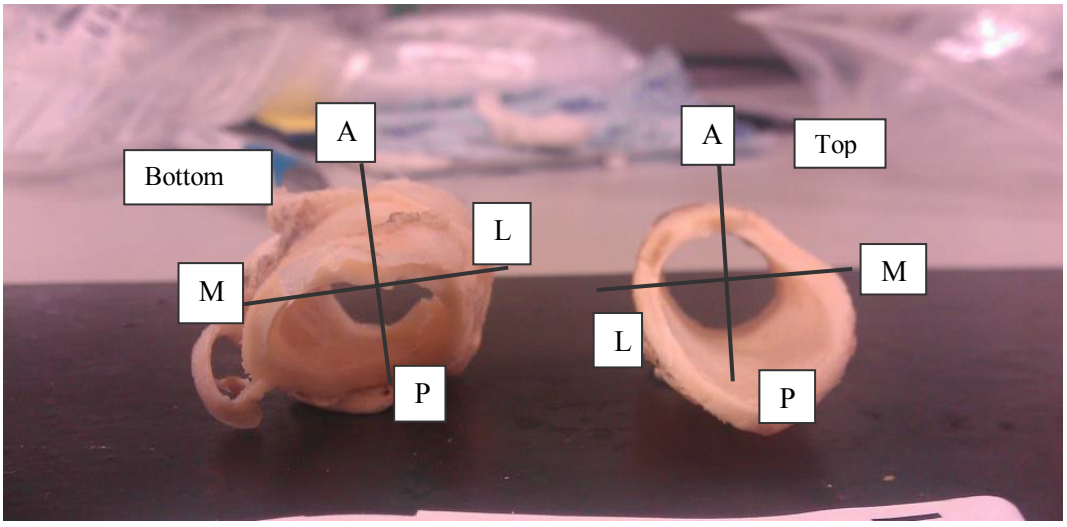

Figure 4.5: Bottom and Top section

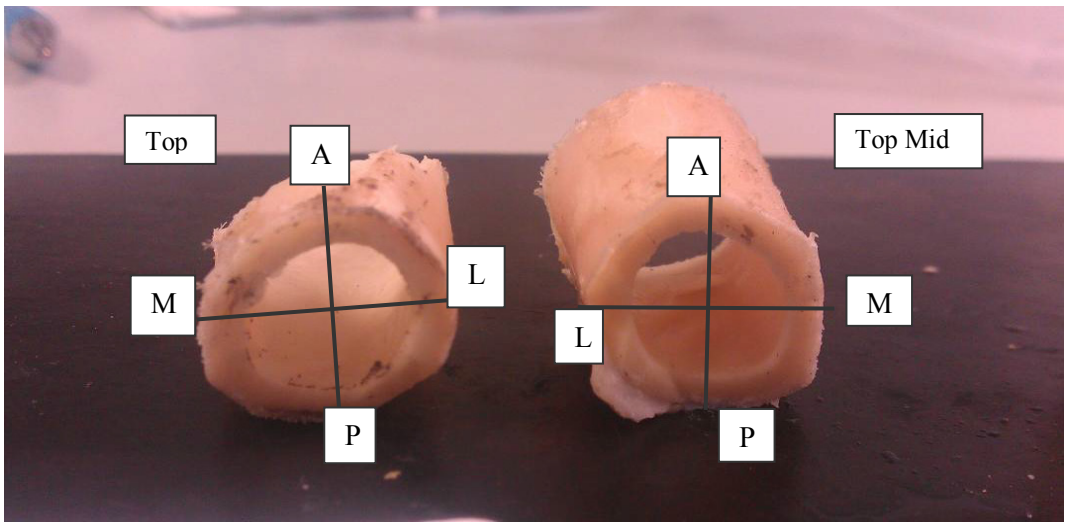

Figure 4.6: Top and Top Mid section

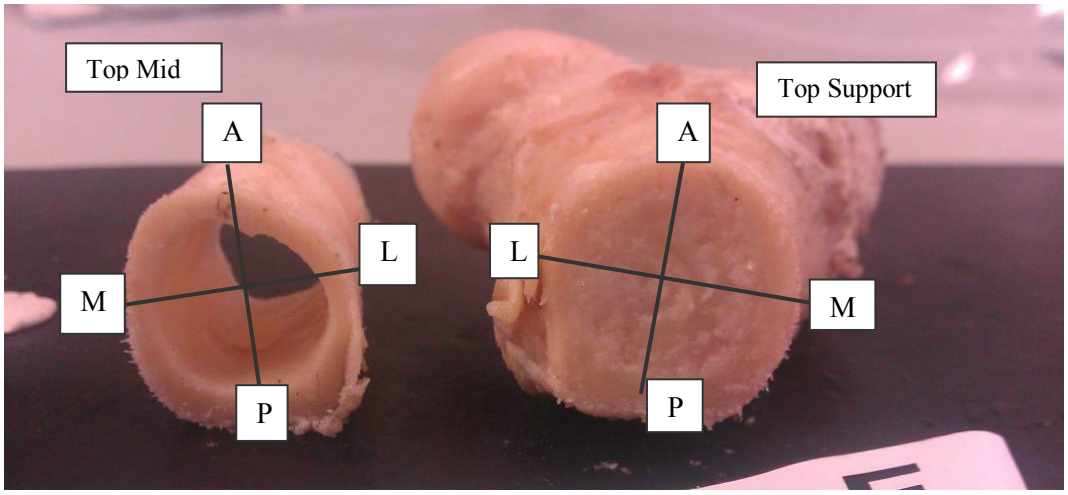

Figure 4.7: Top-Mid and Top-Support section

The orientation of the scanned image can be seen in Figure 4.8 below.

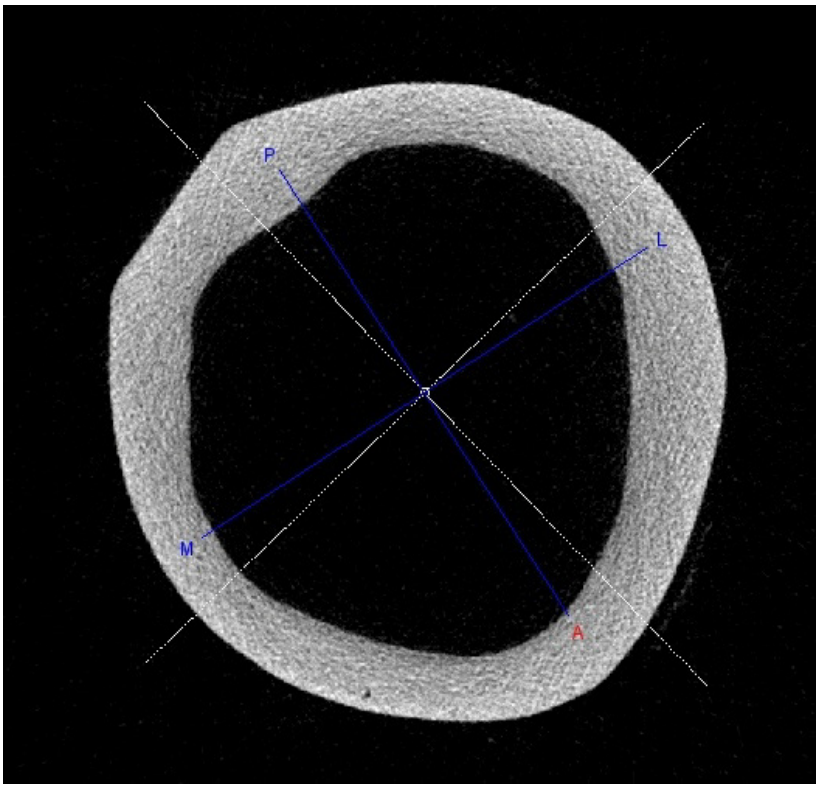

Figure 4.8: Scanned image orientated with respect to loading direction

4.4 Fracture Surface Area

In a clinical setting it would be beneficial to be able to determine an approximation of the energy involved in creating the trauma. This information could provide an indication to the potential damage suffered by the surrounding soft tissue, which has a bearing on the bone's ability to heal. Severe soft tissue damage could reduce blood flow to the injured bone and result in a delay to callus formation. Additionally, there may be further complications resulting from soft tissue damage that could require surgical intervention.

As patients undergo x-ray imaging when a fracture is suspected, a method that can utilise these radiographs to derive the surface area would be preferable, as this would mean that no additional procedures would have to be undertaken. In cases of severe trauma, where the knowledge of the energy involved and likelihood of significant soft tissue damage would be of the most use. The extra insight gained by any additional procedure would have to be

weighed against the time taken to perform the test, the extra workload this would place on the clinical care team and further discomfort for the patient.

To investigate the validity of a method of estimating the fracture surface area from radiographic images of the fracture, measurements of the newly created fracture surfaces were taken from the post testing radiographs using imageJ. An elliptical cross section was assumed for the bone, and measurements of the cortical thickness and of the major and minor axis of this cross section were taken, this is shown in Figure 4.9. The axis measurements were made to the external surfaces, allowing the area to be estimated by the following formula:

$$\boldsymbol{Area = \pi(ab - a_i b_i)} \qquad \text{Equation 4-1}$$

Where a = long axis / 2
b = short axis / 2
t = cortical thickness
a_i = a - t
b_i = b - t

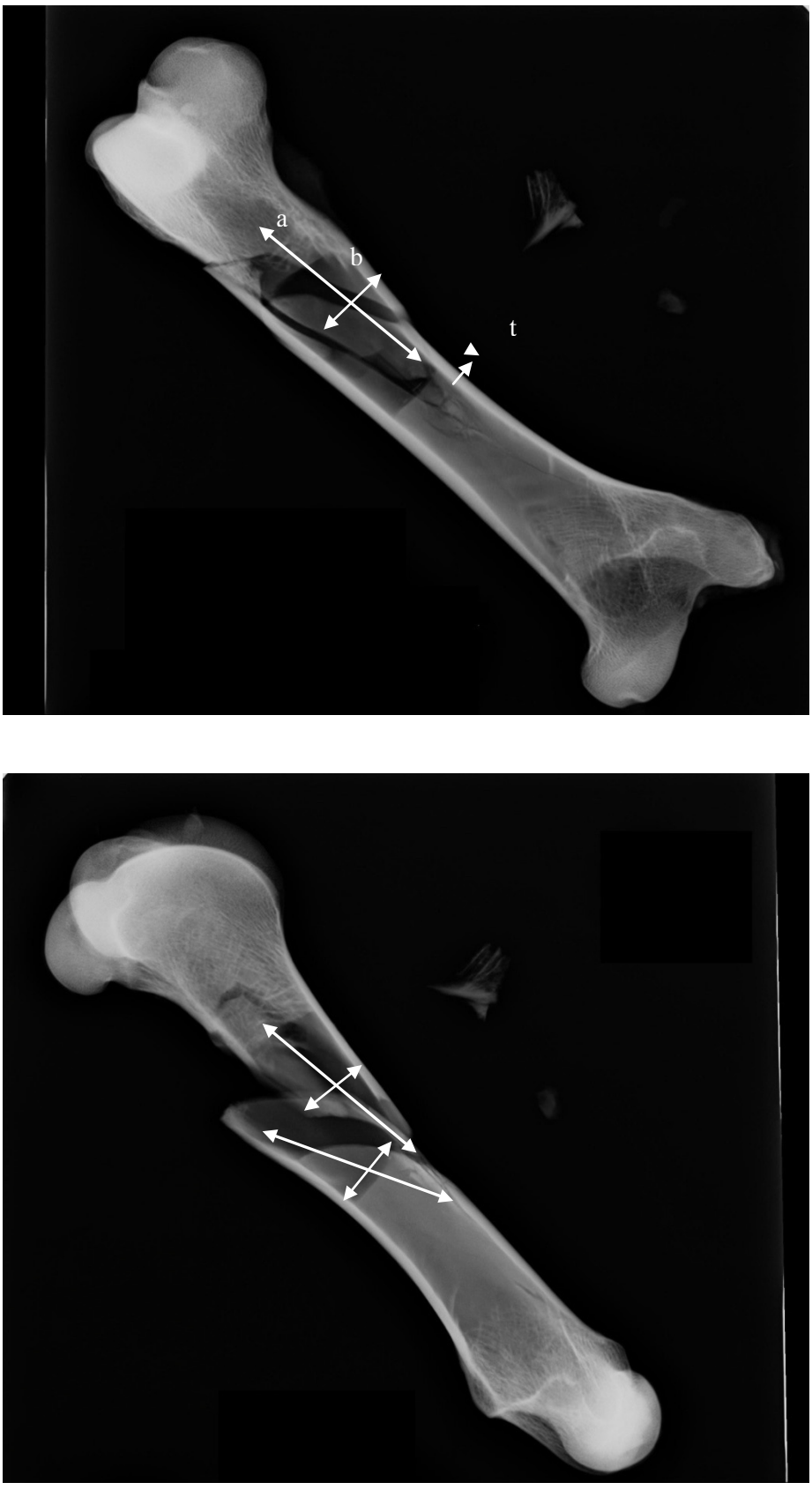

Figure 4.9: Measurements for fracture area

The mean thickness of the bone at the area of the fracture was taken as a general measure of thickness, facilitating an estimation of the fracture surface area from the measured length.

When the bone was comminuted, measurements of the fragments circumference were taken, and this was multiplied by the thickness to give an approximate fracture area for the fragment.

4.5 Measurement of Displacement

The deflection of the bone was measured from still images taken from the high speed camera footage, using the image analysis software, ImageJ (National Institute of Health. Maryland, USA). The point of contact and the onset of fracture were identified by careful examination of the images. Measurements were taken at the point of contact and for the intervening frames up to and including the onset of fracture. The distance in pixels between the side of the frame and the edge of the bone was measured. As the camera was stationary, the edge of the frame acted as a fixed reference point, therefore the reduction in this measured distance was said to be the deflection of the bone. The locations for these measurements are shown in Figure 4.10.

A point on the edge of the bone directly in line with the centre of the loading actuator was used as the location for the displacement measurement. This satisfied the requirement for the work energy relationship between force and deflection, which is only valid if the displacement at the point of loading is used (Hibbeler 1998).

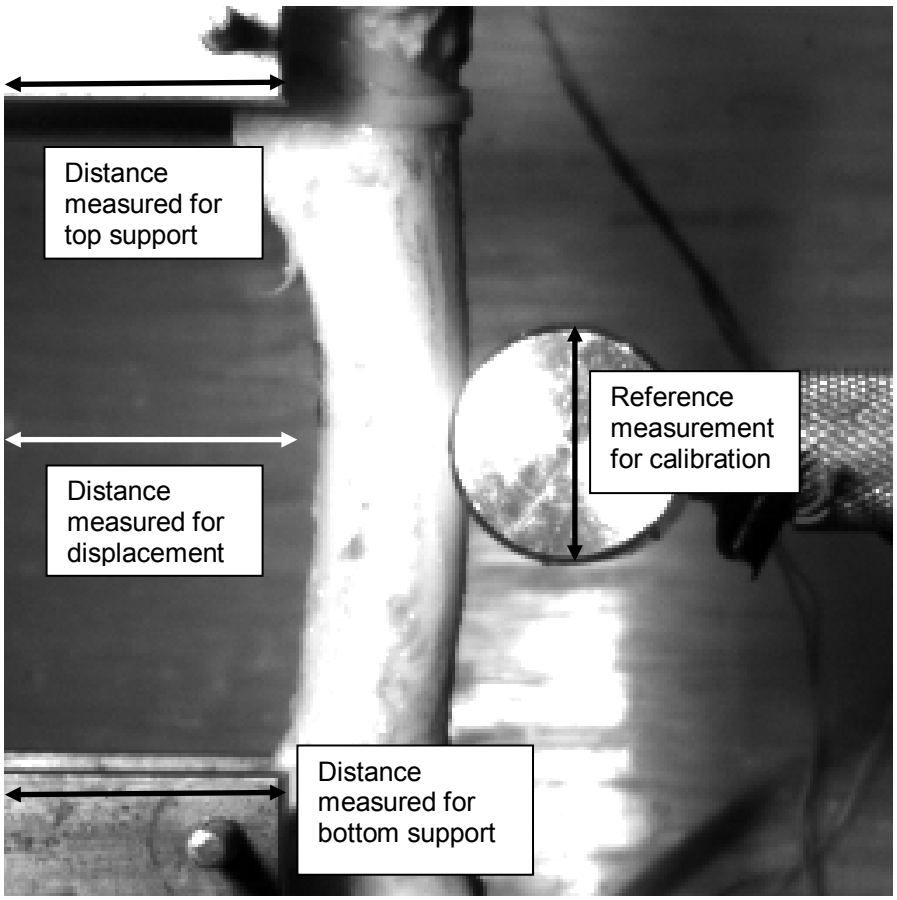

Figure 4.10: Location for displacement measurement

To ensure accuracy the measurement process was repeated and the mean value selected. If a difference greater than 3 pixels between measurements was found, a precaution against manual error was implemented and a third measurement was taken. This allowed the erroneous measurement to be identified and removed. To ensure that the measured displacement of the bone was due to bending and not from whole bone translation measurements were also taken at the support points. These were then subtracted to give the deflection of the bone due to bending.

On the camera frame at the initial point of contact, a reference measurement for the diameter of the impactor head was taken. As the diameter of this component was known it enabled a calibration of the measured displacement in pixels to a value in mm to be made.

When the measured displacement data was plotted against time, it could be seen that it was not a smooth and continuous line, but would jump between values. It was considered that this was a consequence of the minimum measurable size being one pixel on the still image.

To counteract these sources of error, a measurement algorithm was applied to the displacement data. The algorithm ensured that there was no relative backwards movement in the deflection of the bone (likely due to operator error), and that any sudden increase in displacement was averaged over nearby "frames" as during deformation the bone does not jump between positions but undergoes a graduated transition.

This process was termed the discrete displacement algorithm (DDA). This algorithm was only applicable for use before the bone fractured. After fracture, sudden large increases in displacement were not considered unusual. Figure 4.11shows an example of this effect. The graphs for all high loading rate tests can be found in Appendix D.

The use of the averaging function of the algorithm was restricted to instances where there was a large change in the displacement measured on one frame, but no such change was encountered in neighbouring frames. Taking the average deflection of these frames removed step-jumps from the displacement measurement, and the inherent error that an instantaneous change in displacement would create.

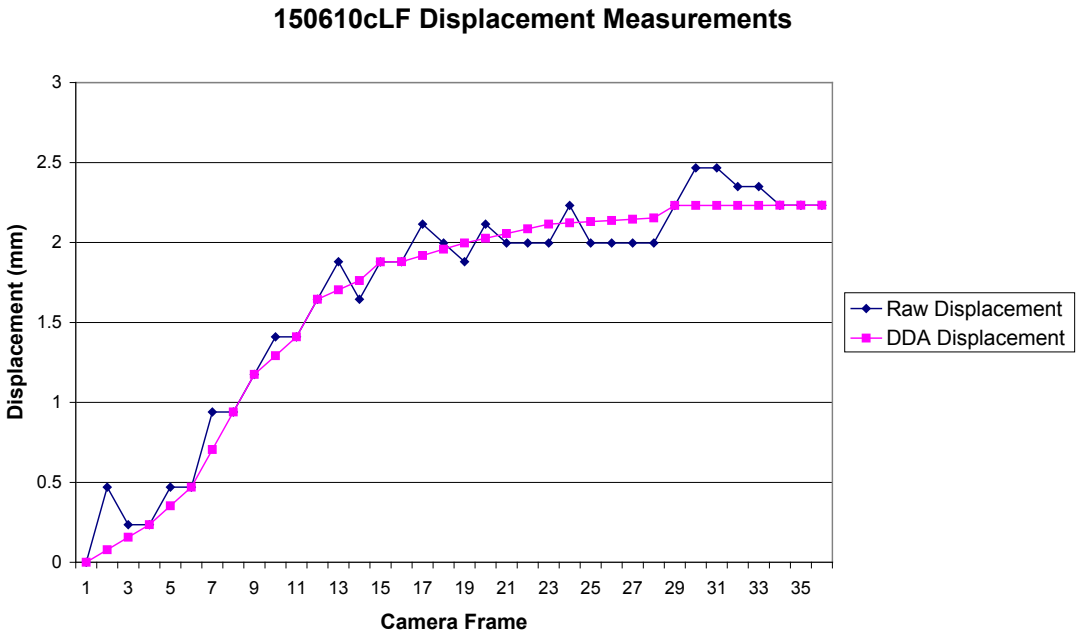

Figure 4.11: Graph comparing pre and post DDA displacement plots

4.6 Evaluation of Force data

As described in section 3.4, the data acquisition system used to record the force in this study captured the output from a dynamic force sensor at discrete time intervals. This data was extracted for each experimental run and presented graphically in the form of Force v Time.

The force data from the impact load cases was in the form of an oscillating waveform. A typical example of this waveform is shown in Figure 4.12 below. The full set of Force v Time graphs can be found in appendix E. The reason for the oscillating force waves recorded during the high loading rate experiments was thought to be due to the high stiffness of the impactor head and loading actuator, coupled with the fast response time of the force sensor. The recoded force waves were considered to be due to reflected stress waves. In order to analyse the load applied to the bone a method of filtering this data was applied. The development of this method is outlined in the following sections.

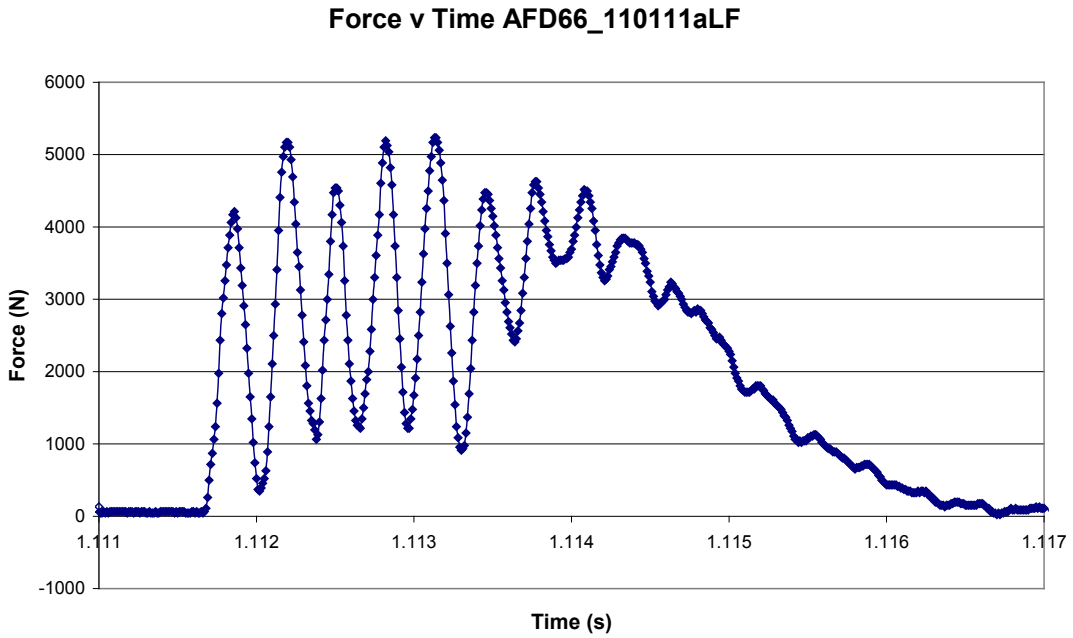

Figure 4.12: Raw Force v Time

In order to allow assessment of the loading process, it was desired that the data was converted into the form of Force v Displacement. This format facilitated the derivation of well established engineering relationships, namely Stress and Strain. Additionally, the area

under the force v displacement curve indicated the energy (work) required to cause the deformation and the toughness is found from the area under the Stress v Strain graph.
The deflection of the bone was derived from measurements made on the high speed camera images. These measurements were also in the time domain (as they were made per frame, where each frame was separated by a discrete unit of time).

As both the force and displacement were measured in the time domain they could be plotted against each other by taking values at corresponding times and plotting one against the other. Figure 4.13 below shows a plot of the measured force values against the displacement. It can be seen that the resulting graph does not lend its self to further analysis. Therefore further processing of the measured force data was required before a useful plot of Force v Deflection could be realised.

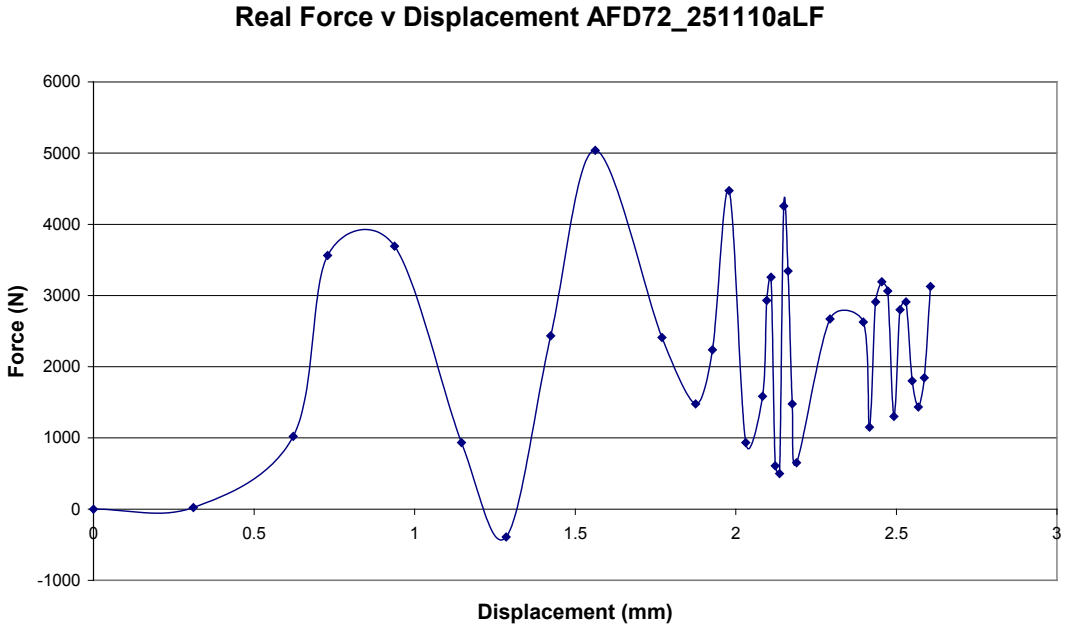

Figure 4.13: Measured Force plotted against Displacement

4.6.1 The effect of filtering

It could be seen by examining the raw force waveform that the oscillations were at a higher frequency than the main loading curve. Therefore, it was reasoned that in order to remove these oscillations a low pass filter could be applied to the data.

Upon examining which filter type to use on the force data it was decided that a Low-pass Butterworth filter met the requirement of smoothing out the oscillations above the cut-off frequency without adversely affecting the data that is wished to be preserved. A Butterworth filter was chosen as this is termed a maximally flat magnitude filter, this gives the filter a flat frequency response in the pass-band of the filter. In the low-pass filter used for this study, the pass-band is the frequencies below the cut-off frequency.

Other filter types such as a Chebyshev or Elliptic filter have a fast response between the pass band and the stop band, but there is some disruption to the signal passed through the filter as these filter types are not maximally flat. In addition to the type of filter, both the order and the cut-off frequency must also be decided. Samples of force data were input into MatLAB where different parameters of low pass Butterworth filter could be investigated. The order of the filter has an influence on the amount of phase delay and on the smoothness of the output. In traditional filter design, the order of the filter would refer to the number of components, such as capacitors or inductors, used to construct the active part of the filter. The effect of different filter orders can be seen in Figure 4.14

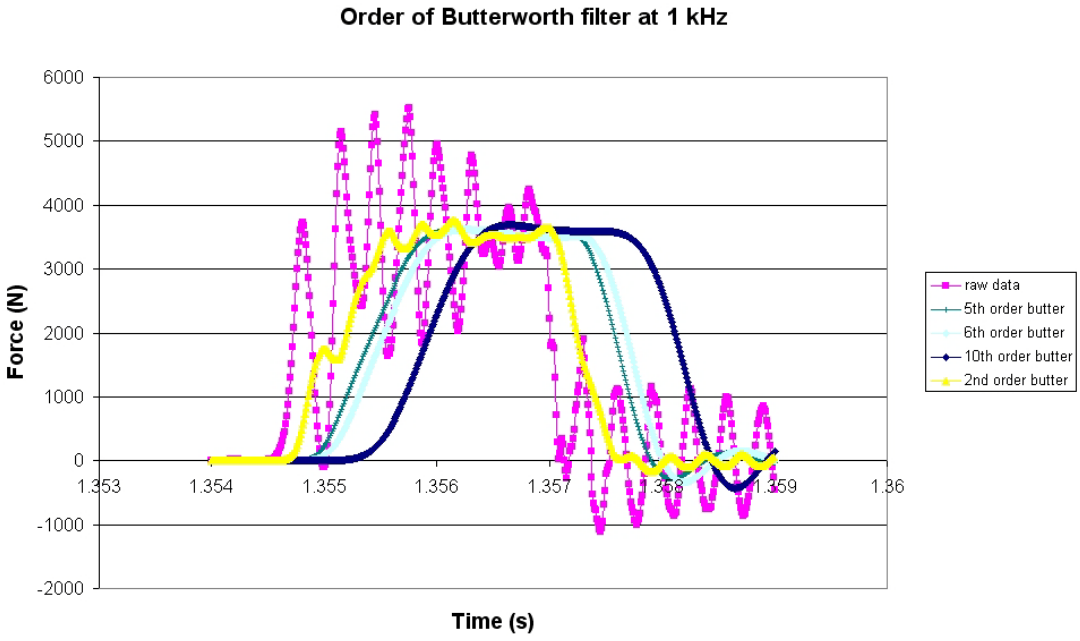

Figure 4.14: Effect of filter order

After comparing the output of filters of different orders it was decided that a 5th Order Butterworth filter met the requirement for adequately smoothing the data at the cost of introducing minimal phase delay with sufficient frequency response.

4.6.2 Filter Cut-Off Frequency

When a filter is applied to the data the will be both a smoothing effect (lead up/trail off) and a shift in phase of the output data, this is known as the frequency response of the filter. This can be seen in the output of the dynamic force sensor when a low pass filter is applied, as is shown below in Figure 4.15 for a filter frequency of 2 kHz, 1 kHz and 500 Hz. The raw force data and the polynomial line of best fit are included for comparison.

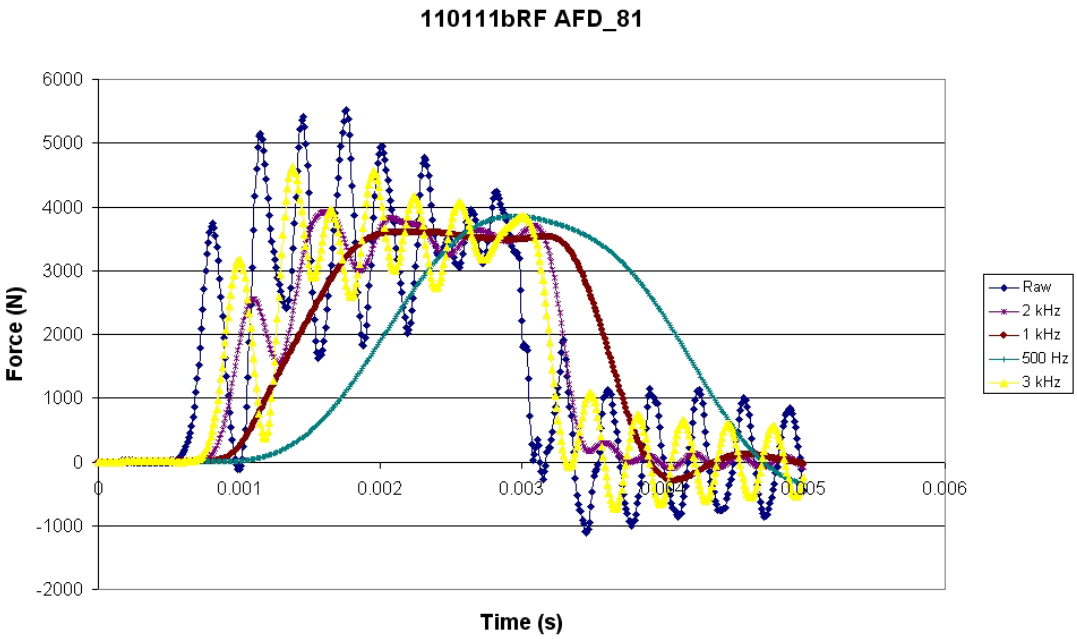

Figure 4.15: Raw and filtered data

As can be seen by observing this figure, filters with a lower cut-off frequency result in a larger phase shift and a greater degree of 'smoothing' during loading and unloading leading to more pronounced lead in and trail off effects. When the cut-off frequency was set to greater than 1 kHz, there was a large amount of fluctuation in the load waveform. As the use of a filter was to remove these oscillations, 1 kHz was selected as the filter frequency to be used for further analysis.

Figure 4.16 below shows only the raw force data and the 1 kHz filter frequency output for clarity. Figure 4.17 has had the filtered plot shifted in the time domain to account for the phase shift.

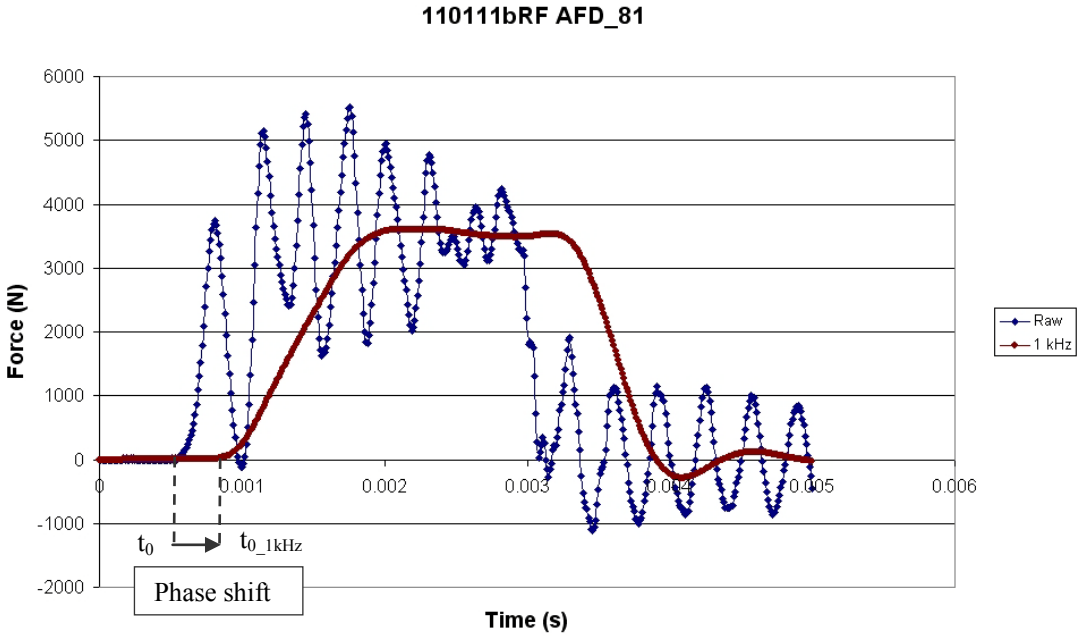

Figure 4.16: Annotated chart of 1 kHz low-pass filter

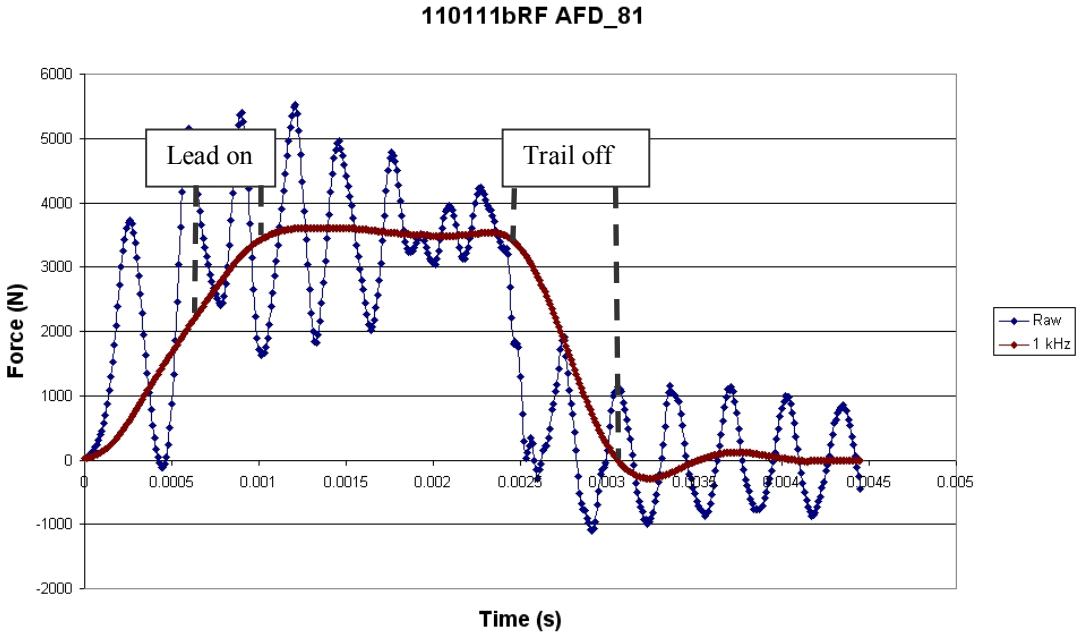

Figure 4.17: Annotated chart showing frequency response as “lead on” and “trail off”

In order to provide a closer representation of the loading, with respect to the time domain, a further phase shift was performed. Rather than targeting a common origin, the aim of this off-set was to centre the main point of the loading, where the lead in and trail off frequency responses are centred over the loading and unloading components respectively. This can be seen in Figure 4.18 below.

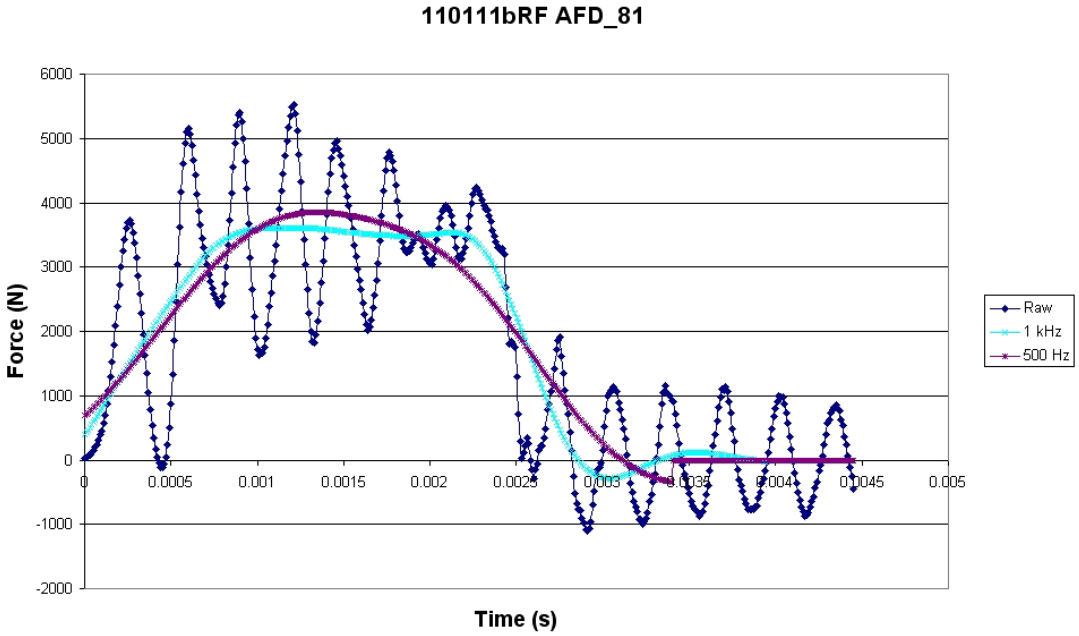

Figure 4.18: Full phase shift of filtered loading data

The more significant consequence of the effect of the frequency response occurs with the unloading section of the data. Many of the specimens suffered a rapid fracture at failure, which results in a steep drop of the raw force data. The filtered data cannot accurately represent this steep drop, resulting in a pre-drop tail off and a post drop trail on (which in turn implies the unloading gradient will not be adequately represented). This could result in an incorrect assessment of the plastic deformation, total deflection, work done and the toughness.

It was therefore considered that an alternative method of filtering the data should be employed.

4.6.3 Polynomial Line of Best fit

In was therefore required to assess the force using a technique that would eliminate these peaks and troughs from the data but still give a usable measure of the force from that experiment. Importantly, any method used to achieve these goals must allow the full duration of loading to be evaluated so as not to underestimate the toughness.This was achieved by obtaining a line of best fit of the force data and deriving the equation of this trend line.

Before deriving this line of best fit it was important that only the loading data up to the point of fracture was included. Once the bone has fractured it has lost its structural form, therefore any equation describing the loading process up to this point will not be suitable to describe the loading process after fracture has occurred.

After identifying the relevant loading region a curve fitting algorithm was employed to derive the line of best fit. It was found that a 6^{th} order polynomial equation gave consistent results and was therefore used to extract a loading equation for all the impact tests. An example of the derived line of best fit with the raw force data is shown below in Figure 4.19.

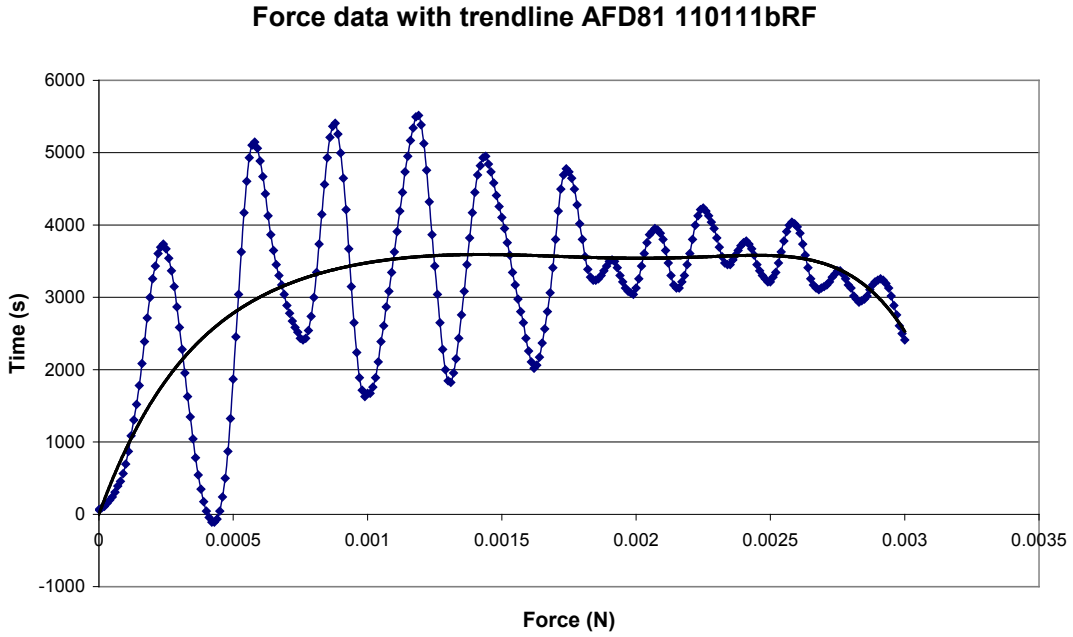

Figure 4.19 Raw force data with polynomial line of best fit

The measurement time and loading time were synchronised using the point of contact with the bone from the camera images and the start of the loading data from the data acquisition data as reference points.

The extracted polynomial equation of the force was then used to calculate the force at the time corresponding to the time of measurement. The measurement data was obtained previously by utilising the methods outlined in section 4.6, and applying the discrete displacement algorithm.

Plotting the derived polynomial force against the displacement allowed the relationship between these two parameters to be seen. This is shown below in Figure 4.20. The same test data used in the raw force v measured deflection example was used for this example (shown in, Figure 4.13). This comparison illustrates how the use of the polynomial force data created a useful relationship between force and deflection, allowing further analysis to be carried out.

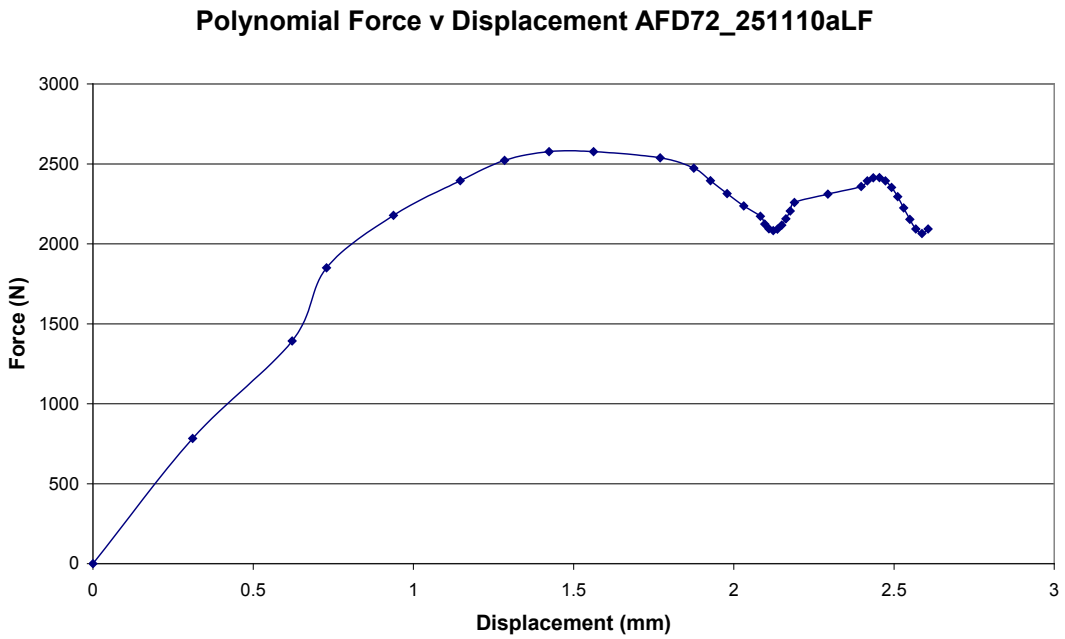

Figure 4.20: Polynomial Force v Displacement

The output from both the Low-pass Butterworth filter and the polynomial line of best fit could then be combined to facilitate analysis of the bending behaviour of the bone.

The equation for the polynomial line of best fit (which was derived directly from the raw data) can be used to define the initial start point of the loading curve. This was used to correlate the loading data with the high speed camera images. It was not considered suitable to use the filtered data to define this point of contact due to the response delay that is a consequence of the low pass filter.

The polynomial equation data can also be used to help account for the phase shift offset, and frequency response delay of the filtered data. This compensation was achieved by means of an x-axis (time) shift of the filtered data, while the y-axis (force) remained unchanged. The amount of x-axis shift was chosen so that the loading phase of the filtered data corresponded with the loading phase of the polynomial derived data.

In order to confirm that the correct offset had been applied to the data it was considered appropriate to compare the midpoints of the loaded sections. This was done manually by plotting the raw data, polynomial equation data and the filtered data were on the same graph. If the centre of the loading sections were all in agreement then the offset was considered to be correct. This is shown in Figure 4.18.

This method of phase shift compensation resulted in a non-zero force origin for the time corresponding to the point of contact (t = o). As the point of contact was used to synchronise the time measurement between the sensor data and the camera frames, and hence the displacement, it is this time point that defined the origin on both the deflection and strain axis. Intuitively, having a value for the load applied to the bone at this point does not represent the physical loading conditions experienced by the bone, as no load can be applied before contact is made.

4.6.4 Poly v filter

The compromises to the data as a result of applying a filter, are somewhat mitigated by using the polynomial equation technique. It should be noted that the Butterworth filter also utilises polynomial equations to describe the output of the function. However, the filter is required to be able to process a wide range of input data, and in the case of the low pass filter, blocking only oscillations in the input signal that are above a defined frequency. The polynomial equation provides a bespoke analysis for each loading curve.

Additionally, as the polynomial line of best fit started and ended at user defined values, it was possible to select the point where the bone fractured as the end point for the line of best fit.

Therefore, although deriving the polynomial equation and from that the force value at the time corresponding to the camera frame is a considerably more time intensive technique than applying a filter to the data, for the reasons outlined above it was considered to be more accurate and was therefore used to derive properties such as yield, work and toughness. A comparison of the respective values found for each method can be found in section 10.14.

The filtered and polynomial line of best fit derived force v time graphs can be found in Appendix E.

4.7 Energy of Bone deformation

The energy absorbed in the deflection of the bone was derived by calculating the area under the force deflection curve. The mechanical testing machine used for the slow loading tests made simultaneous measurements of force, deflection and time.

The dynamic load cases require transformation following the protocol outlined above in section 4.7.3. Once the graphs of force v deflection were obtained for all load cases the area under the curve was found by integration.

4.7.1 Accuracy of method for deriving area

The derived plot of force v displacement, and therefore the graph of stress v strain were not only utilised to give a pictorial representation of the loading process and identify maximum loading and the onset of yield. The area under these curves also yields useful information. The area under the force v deflection curve reveals the energy required to deform the bone (the work done) and the area under the stress v strain graph is known as the toughness.

To ensure that utilising a polynomial line of best fit would provide accurate results for the energy and toughness, the area under the force v time graph for both the raw force data and the calculated polynomial force curve was calculated for all 20 dynamic loading cases.

The area under the raw force v time graph and the polynomial force v time graph were then compared to give a percentage difference between these two methods. The results of this comparison can be found in Table 4.1 below.

Variable	Mean	SE Mean	StDev	Minimum	Q1	Median	Q3	Maximum
Difference in area	0.57 %	0.12%	0.55%	0.03%	0.12%	0.38%	1.03%	1.82%

Table 4.1: Difference between the area under the raw force data and the area under the polynomial line of best fit force data

As can be seen, the average difference in the measured area found by these two techniques was 0.57%, while the median difference is 0.38%. Therefore it can be said that using the polynomial line of best fit provides an accurate representation of the area enclosed by the force data.

4.7.2 Energy of Deformation

The energy due to deformation in bending can be calculated by assuming a triangular force v displacement distribution. In this method the peak force and the deflection up to failure are used and the energy is found by using the relationship:

$$Energy = 0.5 \times Force \times Displacement \qquad \text{Equation 4-2}$$

This method does not take into account any post yield or stiffening effects and therefore should only be used for calculations in the linear elastic range. Calculating the area under the load v deflection curve and the peak force, peak deflection method (Equation 4-2) were performed and the results compared by means of a paired t test.

The Fast loading - Demineralised, Slow loading – Normal quality, and Slow loading – Demineralised groups all showed significant differences (p values were; 0.01, 0.005 and 0.002 respectively). The Fast loading – Normal quality group showed no significant difference (p value = 0.211). It should be noted that even for the non-significantly different

Fast loading – Normal Quality group that the triangular energy method underestimates the work energy by 10.2%.

4.8 Second Moment of Area

The second moment of area, often referred to as the moment of inertia, can be considered as the beam's geometric contribution to the stiffness (where Young's modulus of elasticity provides the material contribution to the stiffness). It describes how the material is distributed around the cross section, and as a result the stress distribution that will result from loading.

The second moment of area in the sections tested was found by applying the parallel axis theorem to the cross section. Gere (Mechanics of Materials, 6th edition, p838) defines that parallel axis theorem as:

"The moment of inertia of an area with respect to any axis in its plane is equal to the moment of inertia with respect to a parallel centroidal axis plus the product of the area and the square of the distance between the two axis".

The moment of inertia (around the centroidal axis running X-X) is found by the integral:

$$I_{NA\_X} = \int y^2 dA \qquad \text{Equation 4-3}$$

For cross sections with commonly occurring, regular geometric shapes, such as circles and rectangles the values of the moment of inertia about the centroidal axis are known. Other less well defined shapes must be broken down into smaller elements of known cross section, and the parallel axis theorem applied to these sub elements.

Due to the shape of the cross section of bone it was required that the tested bones be subdivided into a large number of smaller elements to obtain an accurate description of the distribution of material. It was considered that calculating the centroidal moment of inertia for each of them as well as finding and multiplying by the square of the corresponding distances to the neutral axis would be a time consuming process. Therefore computational methods that could accomplish this procedure could be more efficiently were investigated. The BoneJ add on for ImageJ was used for this process.

After processing the bone following the protocol established in section 4.3, the values for I_{NA} found for the cross sections at either side of the fracture were used to derive an average cross section to represent the point of failure.

4.9 Bending stresses in the beam

The maximum force from the test data was used to derive the stress following the methods set out in this chapter. This stress should be considered the ultimate stress, and references to stress should be considered to refer to the ultimate stress, unless stated otherwise, for example, the yield stress.

When deriving the ultimate stress for the slow loading tests, the load, P, was taken as the maximum value from the output file of the TestXpert programme used to control the mechanical testing machine.

In the fast loading rate experiments, the load, P, was taken as the maximum value from the dynamic force sensor. The unfiltered results were used to derive the maximum force. The unfiltered maximum force was used because filtering the data, whether by use of a low-pass filter of a polynomial line of best fit, has the effect of smoothing out the data plot and reducing the peak stress (as discussed in section 4.7.3). It was considered that using the peak values was appropriate as following Newton's first Law of Motion the force experienced by the sensor would also be experienced by the bone.

4.9.1 Bending Moment

During three point bending of a beam, bending forces and shear forces are developed in response to the applied load. In order to calculate these stresses a free body diagram of the applied and reacted forces was created. This free body diagram facilitates the creation of a shear force diagram and a bending moment diagram from which in turn the shear force and bending moments are found. This is shown in Figure 4.21 below.

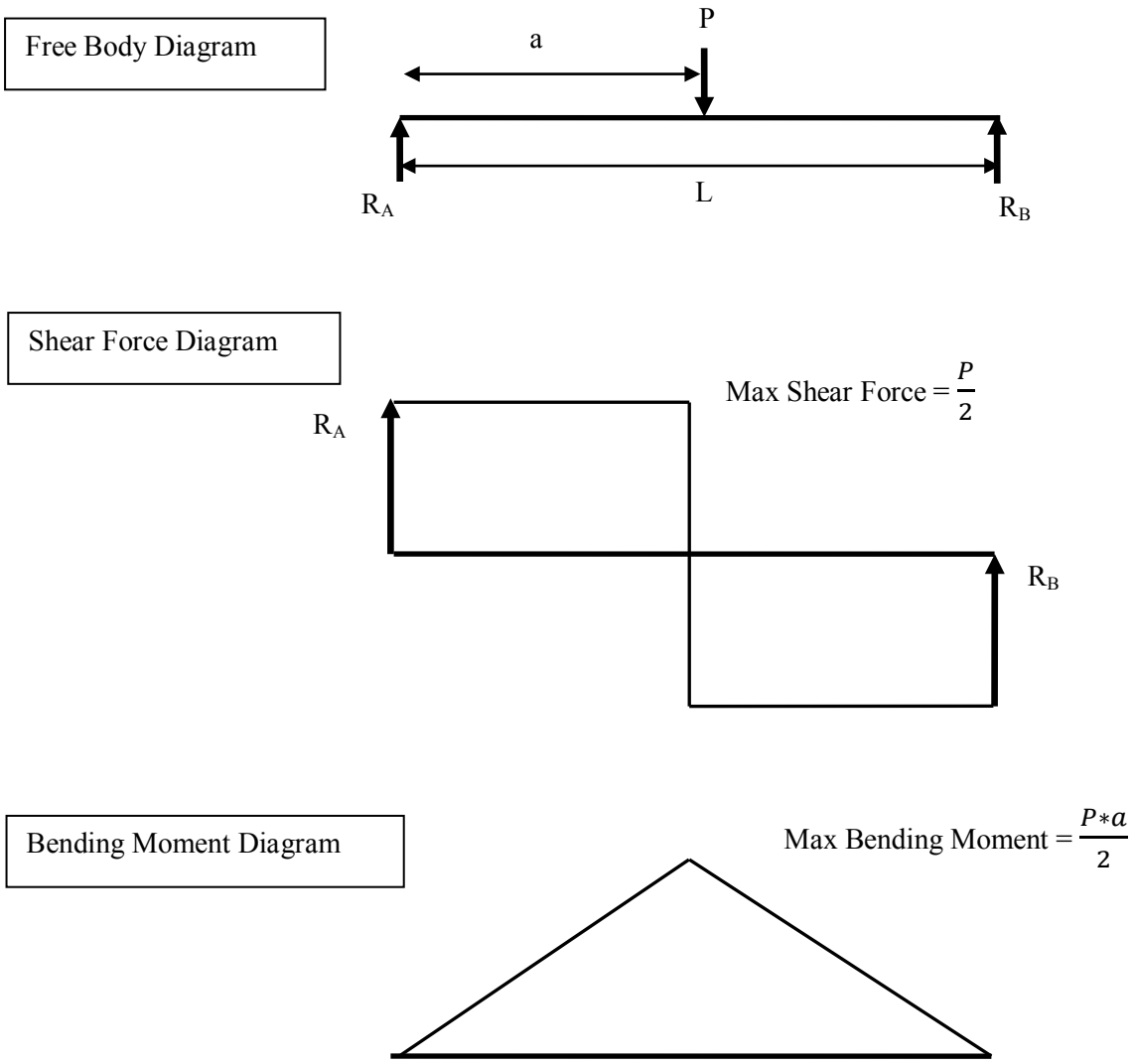

Figure 4.21: Free Body Diagram, Shear Force Diagram and Bending Moment Diagram

As can be seen in Figure 4.22, the stress due to bending is at its greatest when furthest from the neutral axis. The cross section of femoral bone, which can be approximated as an ellipse, has the neural axis at the centre of the cross section. This is unlike, for example, the tibia which is approximately triangular in cross section and as such the neutral axis is one third from the base, two thirds from the peak. Therefore, as the distance from the neutral axis to the outermost surface of the bone in the femur is the same in the tensile and compressive directions, the stress will be the same in both instances.

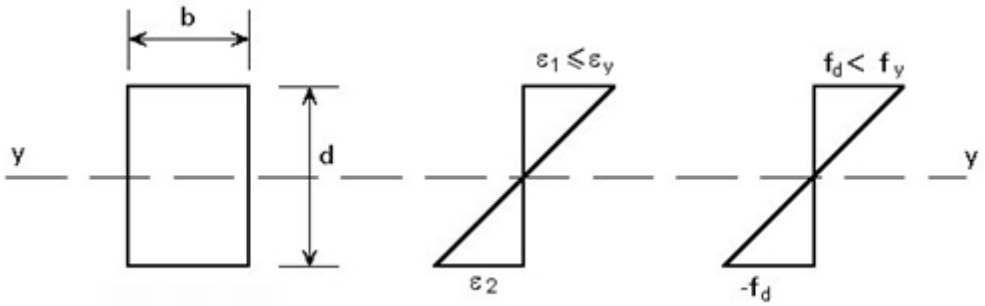

Figure 4.22: Distribution of bending stress through cross section (reproduced from http://www.fgg.uni-lj.si)

For all the tests, both at the high and low strain rates, the supports were set at a distance of 120mm from each other. As "simple support" conditions were used and the load applied at the midpoint of the span, the maximum bending moment will occur at the point of loading and has a value given by Equation 4-4, below. (Taken from "Formulas for Stresses and Strains" (Roark) p101 – case 1e)

$$\boldsymbol{M = \frac{P*L}{4}} \qquad \text{Equation -4.4}$$

Where: M - is the moment
P - is the load
l - is the length of the span

In ideal conditions, Engineers Bending Equation, shown below in Equation 4-5, can be used to find the stress due to bending.

$$\boldsymbol{\sigma_B = \frac{M * \bar{y}}{I_{NA}}} \qquad \text{Equation 4-5}$$

Where: σ_B - is the stress due to bending.

M - is the bending moment at that location.

y - is the distance from the neutral axis to the outermost point in the cross section.

I_{NA} - is the Second Moment of area around the neutral axis.

The distribution of bending stress shown in Figure 4.22 is considered to be true for elastic loading only. When the beam undergoes plastic deformation the tensile and compressive forces will be redistributed, resulting in more load applied nearer the neutral axis. This redistribution occurs when the outermost fibres reach the yield point, resulting in a reduction in Young's modulus of these fibres. As load is carried by the stiffest part of the structure, according to the principal of least work, the fibres of the beam that have not reached the yield point will be stiffer than those that have and as such will attract more load. Therefore more of the load will be transferred to the fibres immediately nearer the neutral axis. In some highly ductile materials this redistribution will continue until purely plastic bending occurs. The distribution from elastic-plastic bending to fully plastic bending is shown diagrammatically in Figure 4.23 and Figure 4.24 below (reproduced from http://www.fgg.uni-lj.si).

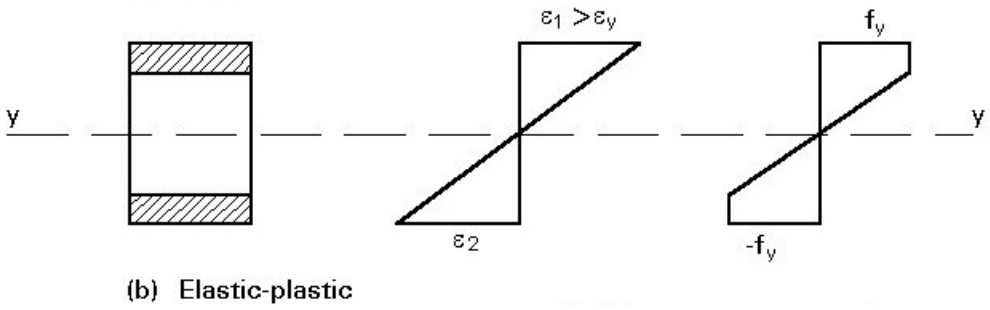

Figure 4.23: Bending stress distribution during elastic-plastic bending (reproduced from http://www.fgg.uni-lj.si)

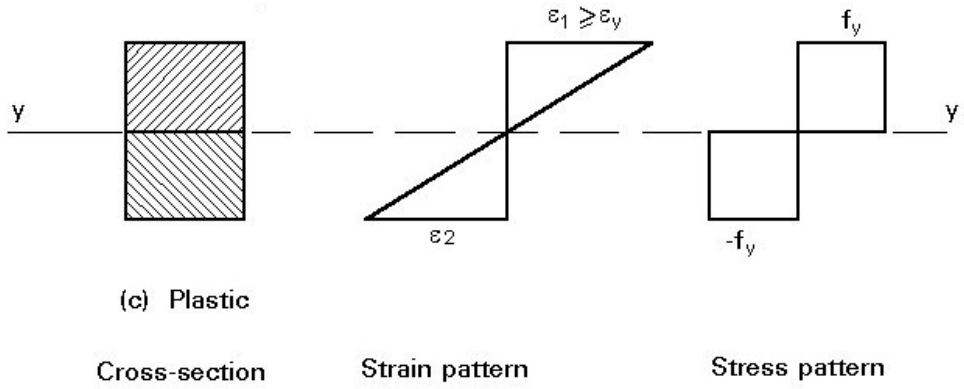

Figure 4.24: Fully plastic bending (reproduced from http://www.fgg.uni-lj.si)

4.9.2 Non-prismatic beam

It can be seen that the cross section of a femur is not constant over its entire length. The change in cross section can be simplified as two larger areas at either end that taper towards the centre. This type of beam is termed non-prismatic. In general terms, this is similar to what is seen in large civil engineering structures such as motorway bridges. Therefore, in order to calculate the material contribution to stiffness, the elastic modulus, more accurately a technique more common to civil engineering analysis was employed: the conjugate-beam method for non-prismatic beams (Hibbeler, 1999).

In civil engineering, this method is used to calculate deflections of members as well as carry-over forces from one span to the next, where there would otherwise be a statically indeterminate structure. The ability to calculate deflections accurately can be an important part of the design phase, as even if a bridge or building can comfortably carry the expected

loading with a suitable reserve factor, it is not desirable to have deflections sufficient to be noticeable.

The conjugate beam method replaces the boundary conditions of the real beam with those of the "conjugate" beam, and also replaces the real loads applied with the M/EI diagram of the real loading on the real beam. Due to the change in boundary conditions, the slope of the real beam is numerically equal to the shear at the corresponding point on the conjugate beam. Similarly, the displacement on the real beam is numerically equivalent to the moment at the corresponding point on the conjugate beam (Hibbeler, 1999). As the boundary conditions in the bones during testing at both loading rates were simple supports, the supporting condition in the conjugate beam remain the same. Simply supported (roller or pin) is the only boundary condition where the conjugate beam is modelled the same as the real beam.

A worksheet of the conjugate beam analysis was created in Microsoft Excel, this allowed the second moment of area for the bone being analysed to be input for each slice where a calculation for this property had been derived following the methods outlined in section 4.4.2. The location of the slice was found from the measurements taken of the sections of bone and the slice number of the μCT scan, as described in section 4.4.1.

In this analysis, the value for deflection was known, and the equation was used to find for Young's Modulus. This was achieved by substituting a guessed value of Young's modulus into the equation. The solver function was then used to perform a numerical iterative method to find a value for Young's Modulus that resolves the equation to give a value for deflection equal to the measured value from the experiments.

4.10 Stiffness

Bone is known to be anisotropic; therefore the material property that relates stress to stiffness, Young's Modulus, will not be constant throughout the whole bone. However, it is how the bone acts as a single structure that describes its bending behaviour. It follows that only a single value for this property can be derived from whole bone bending tests, but that this value should be accurate when describing the bending behaviour of that bone up to the elastic limit. Young's Modulus is found from Equation 4-6.

$$E = \frac{P * L^3}{48 * d * I_{NA}} \qquad \text{Equation 4-6}$$

To derive the Young's modulus, the value used for the deflection, d, should be taken from the linear region of the loading graph, as described in section 4.13 for the slow loading rate and section 4.15 for the fast loading rate.

4.10.1 Inclusion of Shear Forces

As the beam is loaded in three-point bending there will be significant shear forces acting upon it. Therefore, it cannot be said to be in pure bending, where there is only bending forces acting on the beam. In long slender beams, the contribution of this shear force is often trivial, and the beam can be treated as in pure bending, and therefore the Euler-Bernoulli bending equation will provide an accurate solution (Gere 2006)

As the experiments were carried out on whole bones, rather than machined sections, they cannot be said to satisfy the requirements for Engineers bending theory (Euler-Bernoulli equation). A requirement for the accuracy of this equation is that the beam should have a length to depth ratio of 20:1 (Roark 1989). When comparing the length of the loaded section of bone to its depth, an average ratio of 5.13 (± 0.41 SD) was found. Therefore, the effect of the shear force cannot be considered trivial. In addition to the depth to length considerations, bone has also been found to have a low shear modulus compared to the Young's Modulus. This implies that there will be an even greater contribution to displacement from the shear force. Therefore, this contribution must be taken into account.

Spatz et al (1996) carried out 3-point bending tests on machined samples of cortical bone from different species and machined to give a range of span to depth ratios between 10 and 25. From their testing they recommend a ratio of E to G of 20:1. However, this ratio would result in Poisson's ratio in excess of 0.5, therefore a ratio of shear modulus to Young's modulus of 3:1 was used, giving the maximum allowable Poisson's ratio of 0.5.

4.10.2 Timoshenko Beam Equations

The method used to account for the contribution of the shear force to the bending of bone that was used in this study was taken from Timoshenko beam theory (Timoshenko 1925). To ease distinction between the Euler-Bernoulli 'classic' beam bending equation, the method including a contribution from the shear force will be termed the Timoshenko bending method.

In order to separate the deflection due to bending and due to the action of the shear force, Timoshenko's bending theory was used in conjunction with the solutions of the Euler beam equation following the methods set out by Wang (1995). The following equations were used in this analysis:

$$\boldsymbol{Deflection = d_E + d_T} \qquad \text{Equation 4-7}$$

Where: d_E = deflection due to Euler bending and
d_T = the deflection due to the contribution from shear

The deflection due to Euler bending is found from Equation 4-8:

$$\boldsymbol{d_E = \frac{P*L^3}{48*E*I_{NA}}} \qquad \text{Equation 4-8}$$

The deflection due to shear force is found from Equation 4-9.

$$\boldsymbol{d_T = \frac{P*L}{4*G*A*k}} \qquad \text{Equation 4-9}$$

Where: P = Applied Force

L = Span Length

I_{NA} = Second Moment of Area

A = Area of cross section

E = Young's Modulus

G = Shear Modulus

k = shear factor

As both E and G were unknown, G was expressed as a ratio of E, as discussed in section 4.11.1

The measured displacement was used for the value of total deflection in Equation 4-7 and the equation was solved for Young's modulus using an iterative approach. The amount of displacement due to bending and shear were also identified.

4.11 Calculation of strain

In this project, the force and deflection were measured directly. From these measurements the strain can be calculated. It should be noted that this will therefore be a theoretical strain as it was not measured directly.

As stated in section 4.11, the total deflection of the bone is due to a combination of deflection due to bending and deflection due to shear. For clarity, the deflection due to bending will be termed normal deflection. Therefore the strain due to bending will be called normal strain. The term 'normal' is used as the stresses produced in the beam due to bending are normal (perpendicular) to the force producing them.

The deflection due to the contribution of shear force will be called deflection due to shear, therefore the strain from this deflection will be termed strain due to shear. This is distinct to the shear strain.

Strain is calculated using the following formula:

$$\in = \frac{12 * d * \bar{y}}{L^2}$$ Equation 4-10

Where d = deflection (for normal strain the bending deflection from the Timoshenko equation should be used)

$\bar{y}$ = distance from neutral axis to outer fibres of the bone

L = length of span

The bending stress v normal strain plots for all the tests can be found in Appendix G.

4.12 Yield

The yield point, or elastic limit, can be defined as the point to which loading can occur without causing permanent deformation in the structure. A standard value of strain is taken, normally 0.2% and a line of equal gradient to the linear portion of the stress strain curve is drawn. Where this line intersects the stress strain curve is termed the yield point. The corresponding stress is termed the yield stress and the value in the strain axis, the yield strain.

Due to the complex nature of the construction of bone, and theory on the formation of microcracks as the stimulus for the remodelling of bone (Burr 1996, Vashishth and Tanner 2003), bone cannot be considered to suffer no permanent effects from loading to just before the yield point. In fact, many fatigue or creep studies have been carried out (Burr 1985. Bruce, 2003. O'brien 2003) that show bone does suffer a change in its mechanical properties from loading at sub yield levels. However, it was considered that the widely used 0.2% strain criteria was suitable to be used as the definition of the yield point in these single tests to failure.

4.12.1 Slow loading tests

In order to define the yield in the slow loading tests, a plot of the stress v strain was used. As can be seen in Figure 4.25, there was an initial loading phase where a large deflection is produced from a relatively low load. This was due to small movements of the bone on the supports and as such does not give a true representation of the bending behaviour of the bone. This area of the stress strain graph is termed the "toe-in region". It should be stated

that the strains shown on this graph were calculated for the total deflection and as such is not representative of the normal strain due to bending.

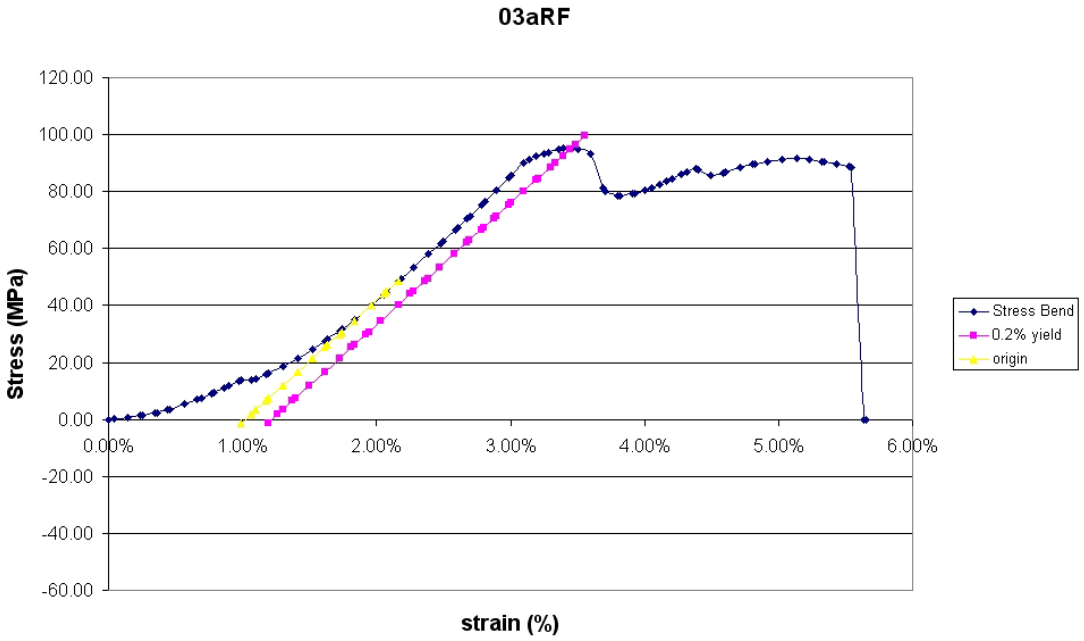

Figure 4.25: Stress v Strain plot with toe in region

A linear section of the stress strain graph was chosen, this was above the toe-in region and before the onset of plastic deformation. From this linear section, the gradient of the loading line can be determined. This allowed the linear section of the loading line to be interpolated back to the x-axis to find a representative origin for the loading, thus negating the effect of this toe-in region from further calculations, such as deriving the toughness of the bone or the strain at yield and failure.

A yield line was plotted on the graph. This had its origin on the x-axis, 0.2% along from the representative origin derived using the method outlined above. This line followed the same gradient as the linear portion of the stress strain curve and was continued until it intersected the stress strain curve. This point of intersection is known as the yield point. The yield stress and yield strain are found by reading off the corresponding axis at this point. This is shown in Figure 4.26 below. The strain shown on this graph is the normal strain due to bending.

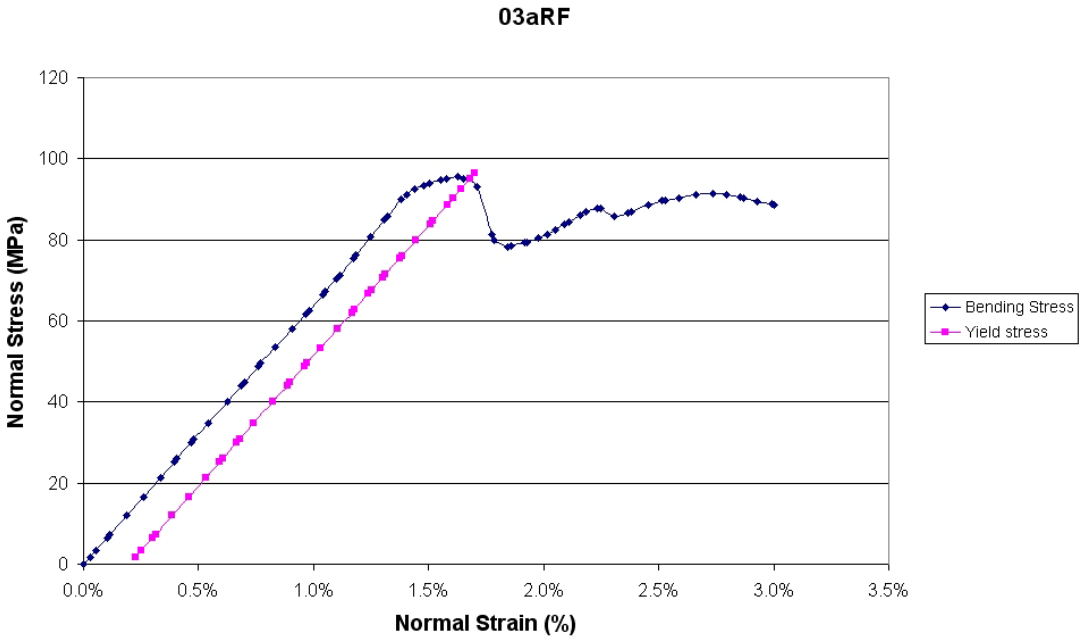

Figure 4.26: Stress v normal strain, toe in region removed

Deformation after the yield point was termed plastic deformation. The total amount of plastic strain could then be derived by subtracting the yield strain from the strain at failure.

4.13 Dynamic yield

In order to determine the linear portion of the loading curve in the fast strain rate tests a combination of techniques were utilised. This approach was used for two principal reasons. Firstly, the force data was recorded in the time domain, therefore the procedure detailed in section 4.7 was required before any analysis of the force v displacement data could be carried out. In addition to this, the force data was not in the form of a smooth loading curve. The following techniques were carried out on the force waveform to facilitate further analysis.

4.13.1 Data Filtering

The output from applying the 1 kHz low-pass Butterworth filter and the 6th order polynomial line of best fit were used to establish a yield point for the high strain rate tests. As the polynomial line of best fit was used for the majority of the analysis conducted on the high

loading rate test it was considered appropriate that the Young's modulus derived from this data should be used.

Values were derived using the filtered data and a comparison between these and those found from the polynomial line of best fit can be found in section 10.15.

The force data for the polynomial line of best fit and 1 kHz filtered data were plotted along with the raw force data against time. The filtered data was centred with respect to the raw data to account for the effects of phase shift and lead on described in section 4.7.1. The following protocol was observed to derive the Young's modulus.

- The initial linear loading point of the filtered and polynomial force plots were identified
- The time points of linear loading noted.
- Corresponding time points on the camera time used
- Previously derived stress strain values were then used to derive the slope/gradient for the identified beginning and end of the linear loading region.

4.13.2 Numerical value of high loading rate yield

In the slow loaded tests, yield occurred at an identifiable point. The yield point on the high strain rate experiments was not simple to determine. This lack of identifiable yield point on the high strain rate experiments impedes comparison between the two sets of data.

Any inaccuracies would be compounded by the difficulties in extracting a load deflection curve for the high speed data. A line of best fit or a low pass filter was required to be applied to the force data to allow it to be plotted against displacement.

A consequence of the line of best fit or applying a filter was that the maximum force values are not captured by either of these methods. Therefore, the yield stress calculated from the graphical data is lower than predicted from examination of the maximum stress. In order to circumvent this problem a ratio was applied to the values for yield stress read from the graph. The ratio was found by dividing the maximum force from the raw data by the maximum force from the polynomial line of best fit. This equation was calculated for each specimen.

4.14 Derived Bending Toughness

Toughness can be considered a material property, therefore values of this parameter can be directly compared with other specimens, by they of different size, a different species or even different materials.

While it may be easier to visualise the loading process with concepts of applied force and absorbed energy, as these can be more easily related to normal experience, they are less useful when it comes to structural analysis. It is not the amount of force that will determine whether a structure suffers yield or failure, but rather the stress that this force produces in the material. During axial loading, the force and stress are proportionally related by the area over which the force is acting, as stress is equal to force divided by area. However, this proportionality does not hold for all types of loading. The distribution of the material in the loaded structure becomes highly significant during bending and torsion loads, where it would no longer be accurate to relate the force to the stress using the cross sectional area of the loaded specimen.

Therefore it is preferable to discuss the strength of materials in terms of stress than in terms of force, as stress can be transferred to different shapes and distributions of material and facilitates comparison between different types of materials.

Toughness is defined as the energy absorbed before failure per unit volume of material and is expressed in the SI system of units as Joules per cubic meter (J/m^3). As toughness is derived from the area under the stress strain curve it includes the effect of the specimen geometry, material stiffness, boundary conditions and the loading type. Therefore, toughness is to energy, as stress is to force.

Consequently, while it may be more natural to think in terms of the energy absorbed by the bone, it is more useful from a structural strength point of view to use toughness, as this allows direct comparison between different specimens.

The area up to the yield point is known as the modulus of resilience, as it is assumed that all energy imparted up to this point will be recovered when the load is removed. As has been discussed in section 4.13 not all of the energy will be recovered from bone if it is loaded to

the yield point. However, it was considered that a distinction between the "elastic" and "plastic" deformation contributions to the toughness should be made.

A value of strain for all points of deflection must be derived before this can be worked out. As it was desired to evaluate the response to the bending load, the toughness was derived from the area under the plot of normal stress v normal (theoretical) strain. The normal stress was plotted against the theoretical normal strain occurring at these measured deflections, giving a plot of bending stress v strain. The area under this graph is the toughness of the bone in bending.

4.15 Shear stress

The shear stress in a beam is found using the following formula:

$$\tau = \frac{V*Q}{I_{NA}*b} \qquad \text{Equation 4-11}$$

Where: V = Shear force
Q = First moment of area
I_{NA} = Second moment of area about the neutral axis
b = width of beam

As was shown in Figure 4.21, the maximum shear force in 3-point bending is equal to half the applied load. When the beam is hollow, as is the case in bone, the value for b in Equation 4-11 is taken as the thickness of the solid sections.

The first moment of area is found by multiplying the area above the point where the first moment of area is to be calculated by the distance from the centroid of that area to the neutral axis.

This is represented by the following integral:

$$Q = \int_{y_1}^{\bar{y}} y\, dA \qquad \text{Equation 4-12}$$

Where: $\bar{y}$ is the distance from the neutral axis to the outermost fibres of the beam

y_1 is the distance from the neutral axis to the point of interest

This is illustrated in Figure 4.27 for a rectangular cross section:

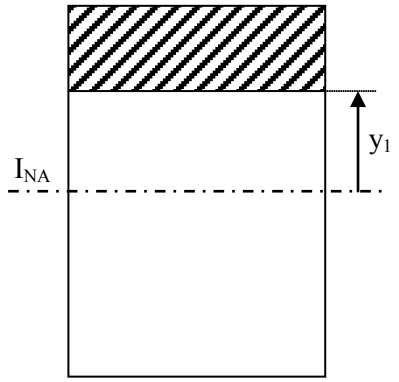

Figure 4.27: First moment of area for shaded section

Therefore, the first moment of area will be at a maximum at the neural axis and will be zero when at the outermost fibres. It follows that the shear stress will also be at a maximum at the neutral axis and zero at the outermost fibres.

4.15.1 Shear stress distribution in bone

An elliptical cross section was assumed to analyse the shear stress in the femur, as shown below in Figure 4.28

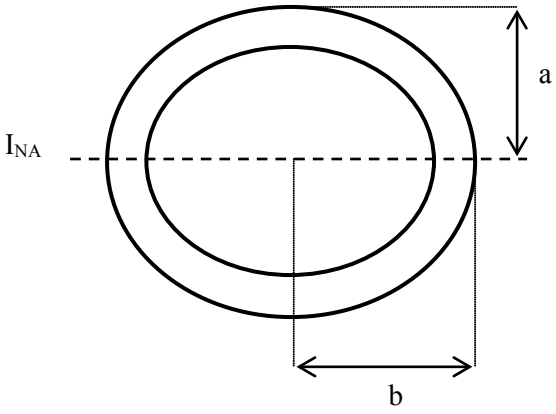

Figure 4.28: Cross section of bone as a hollow ellipse

The scanned μCT data (section 4.4.2) was used and measurements of the outer and inner dimensions were taken using ImageJ.

The maximum shear stress is found by taking the first moment of area at the neutral axis. The area, and centroid, of half an ellipse is therefore required. The area of half an ellipse is found by Equation 4-13

$$\boldsymbol{A = \frac{\pi * (a * b)}{2}} \qquad \text{Equation 4-13}$$

As the bone is hollow, the area of the cortical bone was found by deriving half the area of a solid ellipse, with dimensions equal to the outer dimensions of the bone, and subtracting the area found for half a solid ellipse with the inner dimensions.

The centroid of this half ellipse is found by Equation 4-14:

$$\boldsymbol{c = \frac{4 * b}{3 * \pi}} \qquad \text{Equation 4-14}$$

To find the area of the half an ellipse above a given location, y, on the cross section, Equation 4-15 was used.

$$\boldsymbol{A_Q = a * b * \sin^{-1}\left(\frac{y}{a}\right) + \frac{b * y}{a} * \sqrt{a^2 - y^2}} \qquad \text{Equation 4-15}$$

4.15.2 Example calculation for a tested bone

It was considered that an example calculation would be the most appropriate way to demonstrate the methods presented in section 4.17.1. The dimensions and forces from a slow loading, normal quality bone (Bone ID 110111bLF) were used.

To illustrate the distribution of the Shear stress through the cross section, the stress was derived at the following locations:

- neutral axis (maximum shear stress)
- midpoint between the neutral axis and the outer surface of the bone
- a point ¾ from the neutral axis

The dimensions shown in Table 4.2 were found for this bone:

external	b	0.014425
	a	0.01409
internal	b	0.011016
	a	0.011342
cortical thickness	y = o	0.006195
	y = 1/2 a	0.006041
	y = 3/4 a	0.008991

Table 4.2: Dimensions (m) for shear stress analysis

This bone was subjected to a maximum load of 4791N. A second moment of area of 1.48022E-08 m^4 was found using the methods detailed in section 4.3. The shear and bending stresses for the locations of y given in Table 4.2 are presented in Table 4.3 below (all values in MPa), The total stress at that location is due to a combination of shear stress and bending stress and is calculated by Pythagoras theorem.

location	Shear	Bending	Total
Ina	27.1	0	27.1
y = 1/2 a	21.7	68.4	71.7
y = 3/4 a	8.7	102.6	103.0
y = a	0	136.8	136.8

Table 4.3: Distribution of stress (MPa) through cross section

5 Small animal study

Prior to conducting the main body of experimentation, the method of decalcification was verified and the effect that the decalcification process has on the mechanical strength of bone was evaluated. To achieve these goals an experimental study using rat bones was carried out. The rat was selected for this model as it is relatively available and the smaller volume of bone (compared with ovine bone) would result in a quicker response to the decalcification medium.

Forty rat tibias were harvested, in accordance with the Animals (Scientific Procedures) Act 1986, and subjected to a bending load. This bending load was applied by means of a four point bend test to eliminate the effect of shear forces and also to provide a constant bending force in the centre section of the bone.

The bones were split into 4 batches containing 10 tibias in each. These were labelled cohorts A to D. Sonification has been shown to speed up the decalcification process without affecting the structural or biological properties of the bone beyond the effects of the removal of the calcium (Thorpe 1963, Milan 1981, and Shah 1995). It was this method that was used to increase the rate of decalcification in this study.

Cohort A acted as a control of the decalcification process and was therefore not subjected to EDTA immersion or sonification. Cohort B underwent 7 hours of sonification in an EDTA solution. Cohort C underwent 14 hours of sonification submerged in EDTA and Cohort D underwent 21 hours of sonification in EDTA. The rat bones were placed in individual glass vials and covered with a 10% solution of ethylene diaminetetra acetic acid (EDTA). The vials containing rat bones were then placed in an ultrasonic bath (Kerry Ultrasonics, KC3 ultrasonic cleaning tank) containing water and were subjected to sonification. Placing the bones into glass vials ensured that each bone could be individually labelled and tracked. The high stiffness of glass makes it a good transmitter of ultrasonic energy, and it was therefore felt that this would not prevent the action of the ultrasonic tank on the decalcification process. In order to evaluate the proposed increase in decalcification rate, a control bone was placed in a glass vial and submerged in EDTA solution in the same manner as the other specimens. This control bone was radiographed every 48 hours to monitor the demineralization that occurred.

The ultrasonic stimulation produces cavities in the fluid, this cavitation process transmits energy to the fluid and therefore the temperature of this fluid will increase. This was confirmed during trial operation of the apparatus. A thermometer was placed in the bath before experimentation, giving a reading for the water temperature of 20°C. After 1 hour of sonification the temperature in the bath was 33°C, after 2 hours the temperature was 40°C and after 3 hours the temperature was 44°C. The machine was switched off during temperature measurement to ensure that it was the temperature of the fluid that was measured and not a direct effect of ultrasonic stimulation. In order to prevent excessive temperature rise during decalcification the transmission medium, in this case the water around the vials, was changed on an hourly basis.

5.1 X ray imaging

Radiographs were taken of all the samples before testing to provide a reference for the amount of mineral present. Further radiographs of the samples were taken at the end of each 7 hour decalcification session. This provided an opportunity to change the EDTA the bones were submerged in. The EDTA in the non-ultrasonically assisted decalcification control specimen was also changed after x-ray. The testing cohort specimens were stored in Phosphate Buffered Saline (PBS) solution between decalcification periods, the control bone was kept in EDTA at all times. A sample x-ray picture can be seen below in Figure 5.1.

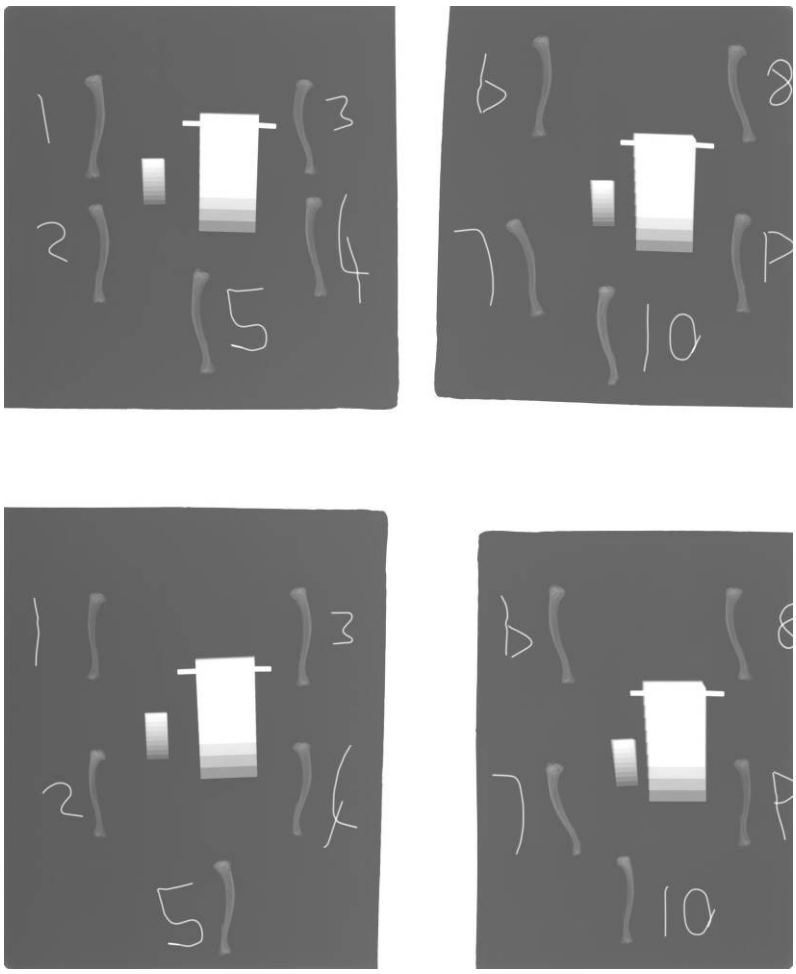

Figure 5.1: X-ray of decalcified rat tibias with calibration wedge

As can be seen in the images a stepped aluminium wedge was placed in the exposure to facilitate calibration. The grey level of the bones was measured from the radiographs and was expressed in terms of equivalent aluminium thickness. The thickness of each bone was also taken into account to allow the amount of decalcification between bones to be compared. This process is described in detail in section 3.5.3

It can be seen in Figure 5.2 below, that the decalcification process is non linear. It was found that the best fit for the data gathered was a logarithmic curve. As the largest amount of decalcification occurs during the first few hours of the process, using ultrasonic agitation to accelerate decalcification by EDTA is a very useful method to allow the study of the mechanical effects of bone diseases such as Osteomalacia where partial demineralisation of the bone is the goal.

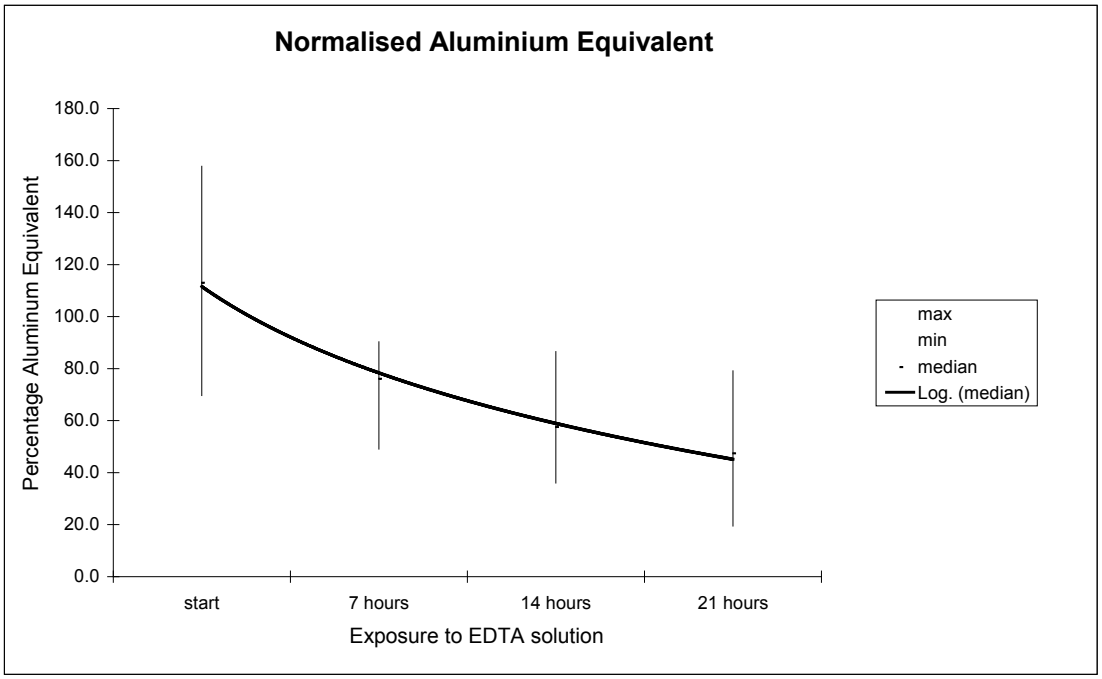

Figure 5.2: Graph of x-ray density V EDTA exposure

Figure 5.3 below shows the rate of decalcification between the ultrasonically assisted bones and the control bone exposed to EDTA alone. It can be seen that the action of ultrasound increased the rate of decalcification dramatically. Similar levels of mineral reduction were found after 14 hours of ultrasonically assisted decalcification in EDTA as achieved by 144 hours of EDTA exposure alone. This duration represented an approximate 60% reduction in the equivalent aluminium thickness.

This experiment demonstrated the potential of sonification to increase the rate of decalcification, and therefore its suitability for use in the main body of experiments using ovine bone.

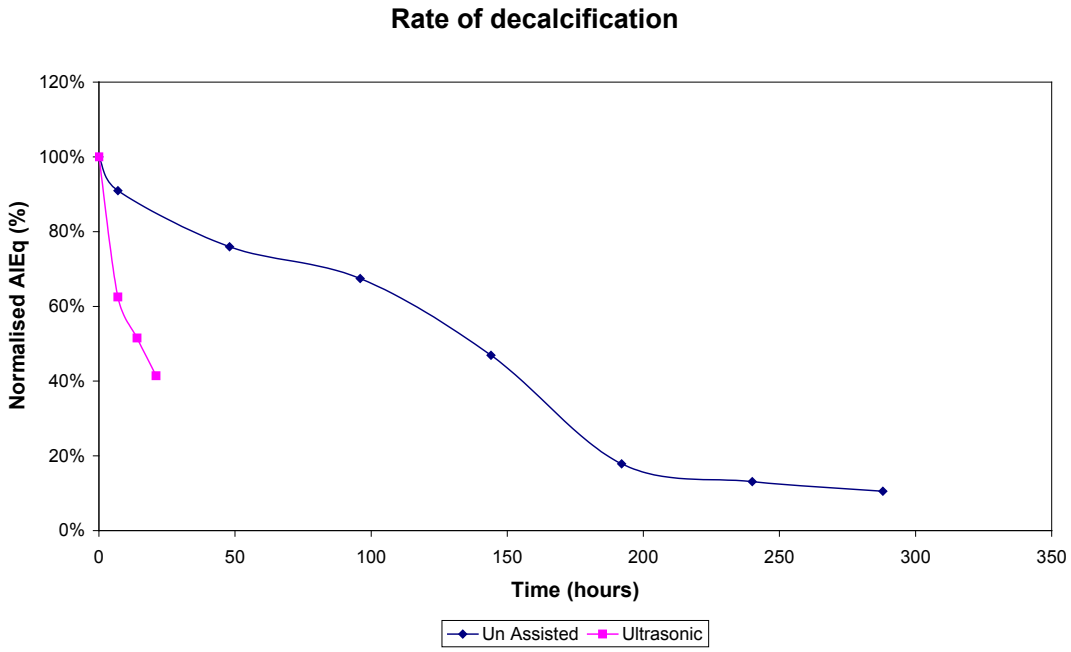

Figure 5.3: Control v Ultrasonic Decalcification

5.2 Mechanical Testing

The tibias were loaded in four point bending by a Zwick/Rowell z005 mechanical testing machine at a rate of 1N per second. The loading and defection data are captured from the Zwick by the TestXpert computer programme that is used to control the mechanical testing machine. Data from this programme is extracted for use by Microsoft Excel to facilitate analysis and presentation of the results. A rat bone ready for testing can be seen in Figure 5.4.

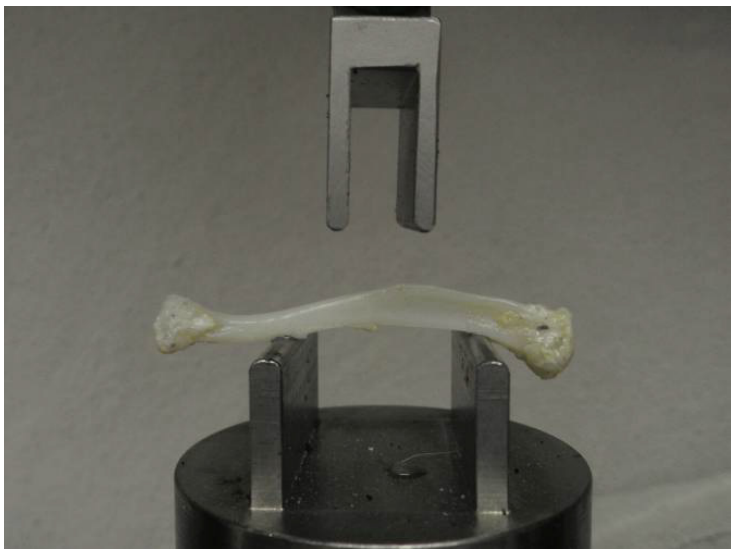

Figure 5.4: Rat tibia in four point bending rig

External and internal measurements of the tibias were taken either side of the fracture to determine the size of the bone at the fracture site. These measurements were then used to calculate a second moment of area for the bone at the fracture site. A triangular shape was assumed for this model of the rat tibias to facilitate calculation.

It was not always possible to take internal measurements of all the bones, for example when no fracture occurred internal measurements could not be made. In order to provide an estimate of the second moment of area for these specimens an approximation must be made. An average ratio of external to internal dimensions was found from all the specimens where internal measurement was possible. This ratio was then used to gain an estimate of the internal cavity and allow a second moment of area, and thus the stress in the bone, to be derived for all specimens.

It was felt that for calculation involving the rat bones that taking the height and width measurements and applying an assumed geometric shape would provide a suitable level of accuracy to derive the stress at failure and therefore validate the structural effects of decalcification. However, when testing the ovine bone the assumption of a geometric cross section could not be made, as depending on the area of fracture an eclipse or circular profile was found. The methods for deriving the cross sectional distribution and thus the second moment of area for the ovine bones was detailed in section 4.3.

5.3 Mechanical Testing Results

The applied force from the Zwick testing machine was used along with Engineers Bending Theory to calculate the stresses present in the bone. Engineers bending theory states that the stress due to bending can be derived by the following formula:

$$\sigma_B = \frac{M * y}{I_{NA}} \qquad \text{Equation 5-1}$$

Where: σ_B is the stress due to bending.

M is the bending moment at that location.

y is the distance from the neutral axis to the outermost point in the cross section (due to the triangular cross section of the rat tibia this distance is not the same for the compressive and tensile side).

I_{NA} is the Second Moment of area around the neutral axis.

As the rat tibia is loaded in four-point bending the maximum bending moment is found between the two central loading points. This bending moment will be constant between these points.

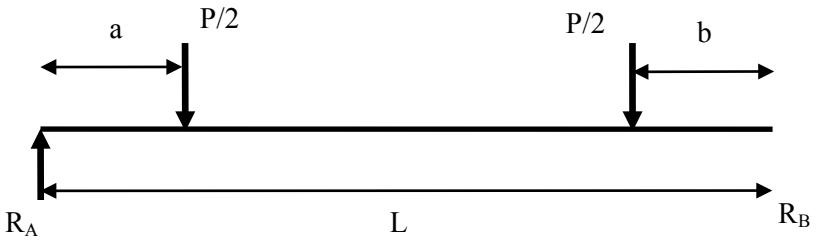

Figure 5.5: Four point bending

Table 5.1, containing the maximum, minimum and average stress in the bone at failure (N/mm^2) for each cohort can be found below.

Cohort	Mean	Max	Min
A (0 hours)	224.3	321.4	154.6
B (7 hours)	53.9	107.8	24.1
C (14 hours)	37.2	62.9	18.8
D (21 hours)	11.1	37.1	1.8

Table 5.1: Stress (MPa) at Failure for each group split by demineralisation time

Figure 5.6 displays the inter-quartile ranges of the cohorts for all 40 test specimen. A connecting line highlights the change in trend of the median of these groups.

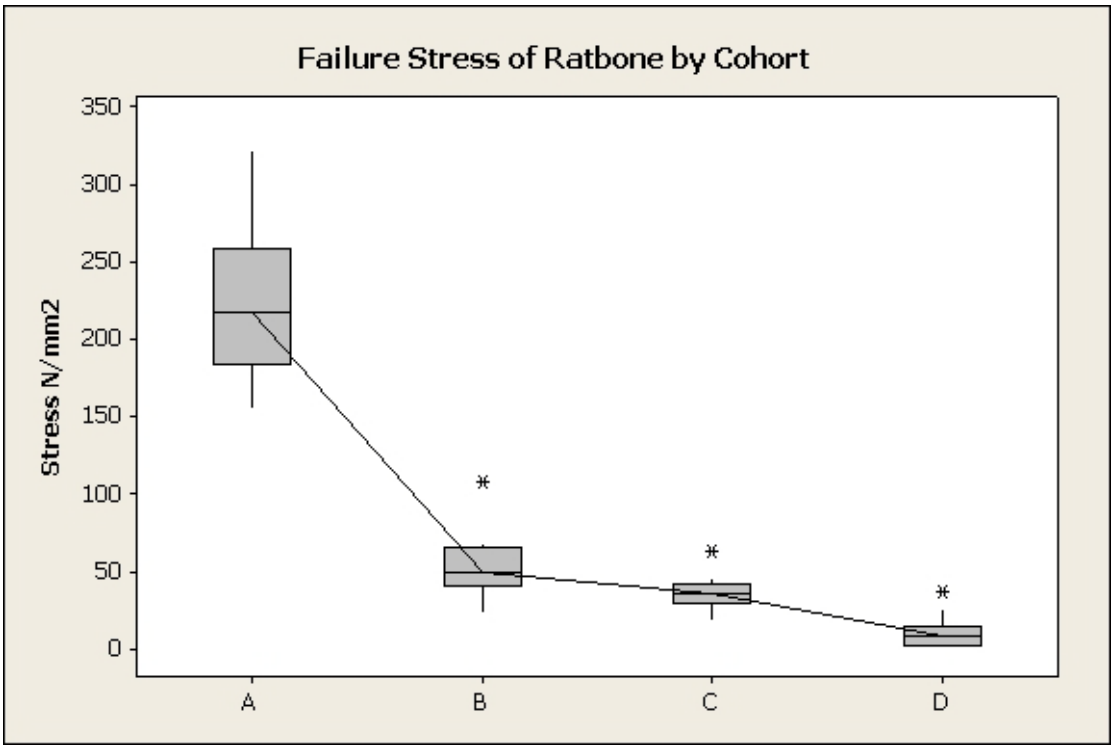

Figure 5.6: Graph of failure stress for rat tibias where A = 0 hours, B = 7 hours, C = 14 hours and D = 21 hours demineralisation

5.4 Ash weighting

After structural testing, the ash weight of 20 of the tibias was determined to evaluate the amount of demineralisation that took place. Five bones were selected from each group at random. To determine the ash weight the bones were weighed when wet then subjected to 24 hours in a kiln at 110ºC to remove the water content before being weighed again to establish a dry mass. The bones were then placed back into the kiln at a temperature of 450ºC for 48 hours. This secondary exposure at the higher temperature removed the organic component from the bone, leaving the mineral in the form of ash. This was then weighed allowing the percentage of mineral to be derived. The correlation of ash weight to derived aluminium thickness is shown in

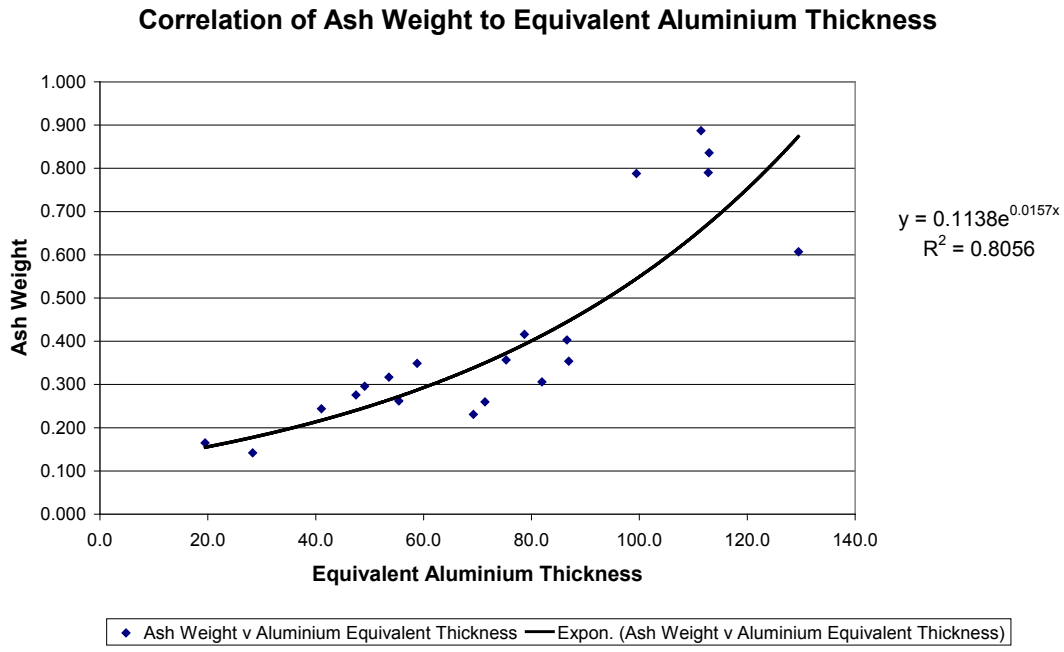

Figure 5.7: Ash v aluminium thickness value

5.5 Discussion of results

As could be seen in Figure 5.6, there was a strong relationship between the stress at failure and the amount of demineralisation. It should be noted that the degree of demineralisation undergone by cohorts C and D, (14 and 21 hours of ultrasonically assisted decalcification respectively) was greater than would be expected to be found physiologically. Specimen in these cohorts had so little stiffness that they provided very little resistance to deformation. As such, failure was defined when a deflection of 5 mm was reached unless fracture had occurred before this point.

It was therefore decided that these high levels of decalcification would not be required to be repeated in the main body of the experiments involving ovine bone. A target for the demineralisation of the ovine bone was set to be representative to the amount of mineral expected to be found in a 75 year old female. This was equivalent to a 20% loss in the value of the equivalent aluminium thickness measured from the radiograph.

6 Fresh v Frozen

As it is not practical to test all specimens when they have been freshly harvested. Storage methods such as freezing and embalming have shown that the mechanical properties can be conserved by these means (Haaren et al 2008). The above studies were conducted at pseudo-static strain rates. This study examines the influence of loading rate on the bending behaviour of bone. Therefore, it was considered that it should first be established that storage does not affect the mechanical properties of bone at higher strain rates.

5 pairs of tibias were harvested at the same time as the corresponding femurs. The soft tissue was removed before wrapping each bone in gauze soaked with 1M PBS solution to prevent the bones from drying out. The tibias were then allocated at random to either the fresh or frozen test group, with the contralateral limb assigned to the other group. 5 bones were allocated at random to be the fresh testing group. The contralateral pairs of these bones were frozen in accordance with the protocol used for the femurs in the main body of experimentation. Contralateral pairs of limbs were used to reduce variability between the compared specimens, allowing a direct comparison to be made. Testing was carried out on the specimens in the fresh group and the results of which were saved for analysis after all the testing of the frozen group was completed. This allowed all the analysis to be carried out at the same time, preventing any experimental bias.

The peak force and deflection at failure of these bones were used to examine the effect of storage. After comparison of these values it was not felt necessary to examine the bending behaviour in greater detail at this time.

6.1 Results

The following values for maximum force (values in N) were observed.

Variable	Mean	SE mean	St Dev	Minimum	Median	Maximum
Fresh	5390	183	449	4713	5560	5842
Frozen	5289	241	590	4365	5353	5864

Table 6.1: Maximum force (N) in fresh v frozen tests of ovine tibias

The distribution of the maximum force is shown graphically in Figure 6.1 below

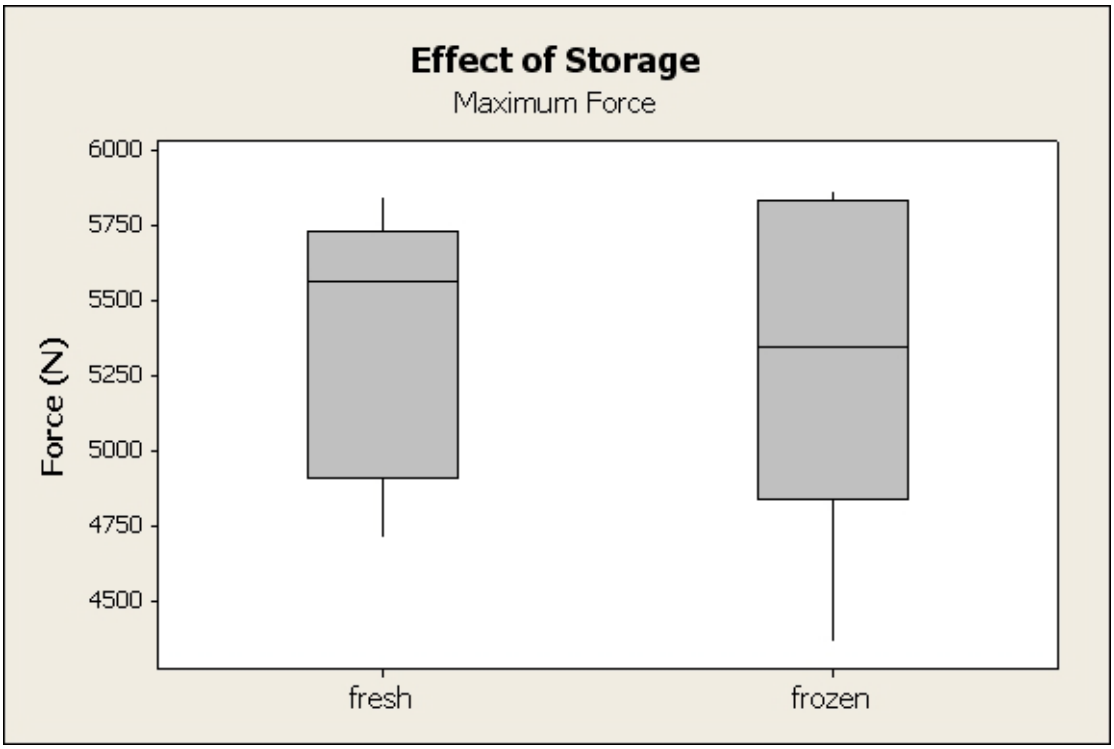

Figure 6.1: Box-plot of maximum force in ovine tibias

The following values for deflection at failure (values in mm) were observed.

Variable	Mean	SE mean	St Dev	Minimum	Median	Maximum
Fresh	3..370	0. 276	0. 618	2. 349	2. 832	3..519
Frozen	3. 624	0. 284	0. 635	2. 786	3. 176	3. 594

Table 6.2: Deflection at failure (mm) for fresh v frozen tests of ovine tibias

The distribution of the displacement at failure is shown graphically in Figure 6.2 below

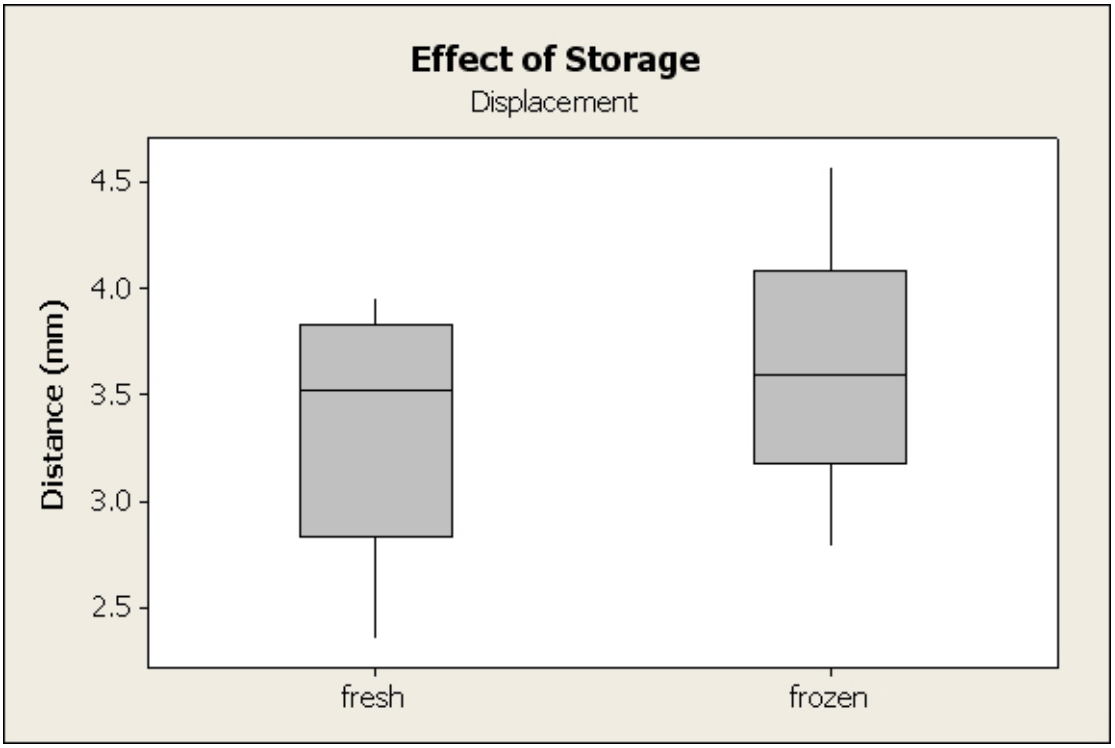

Figure 6.2: box-plot of displacement at failure for ovine tibias

Statistical significance of the results was examined by means of a paired t-test. No statistically significant differences were found between the two groups:

Force	P = 0.758
Displacement	P = 0.473

From this study it was concluded that freezing is a suitable means of storage for testing at high strain rates.

7 Accelerometer data

As discussed in section 3.3, an accelerometer was mounted on the femoral head of the bones during testing at high loading rates. It was considered that the dominant frequency of vibration recorded would give further insight into the fracture of the bone. As can be seen in Figure 7.1 below, the amplitude of the recorded vibration was far greater at fracture than at the point of load application. In order to aid recognition of these points, the unfiltered force plot is included on the graph.

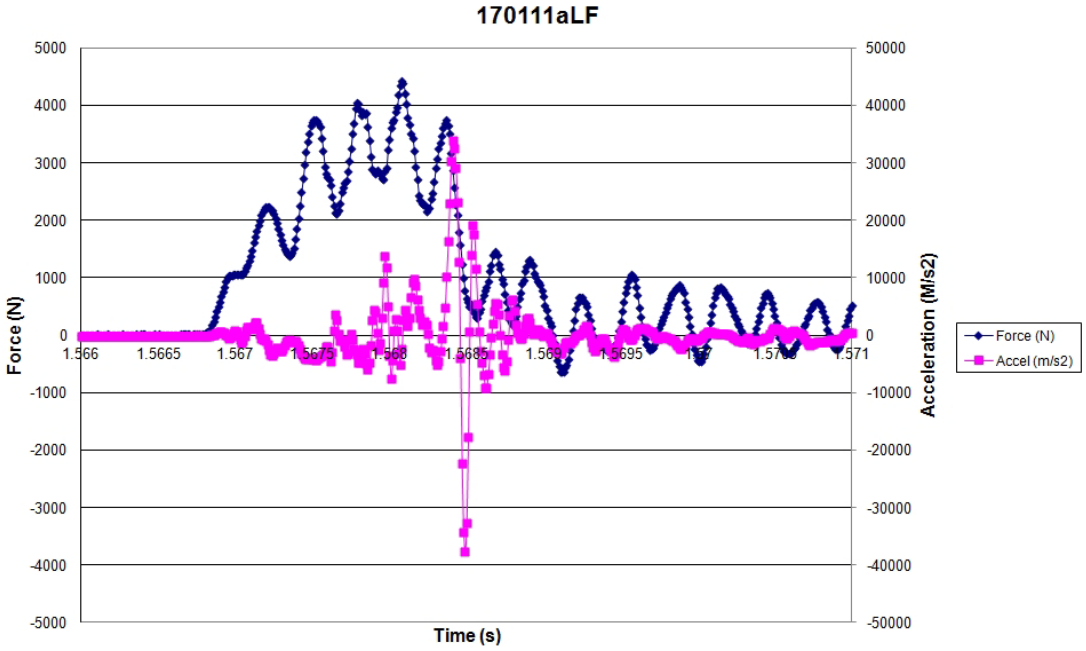

Figure 7.1: Example of accelerometer output during high loading rate fracture on ovine femurs

It was decided that the focus of this analysis should be on the frequency of the output at the point of failure. The frequency was chosen over the amplitude because it was considered that the amplitude of the output would be strongly influenced by the whole bone movement of the entire proximal section of the bone when this section of bone was released after fracture. If the proximal section had a small mass, such as would be found if the bone suffered an oblique fracture near the proximal end, then it would be expected to accelerate faster for a given fracture release energy than would be found if the proximal bone section had a relatively larger mass, such as would be found if the bone suffered a distal oblique fracture.

Therefore it was decided that the frequency of the output from the accelerometer during fracture should be compared. It was hypothesised that a high frequency would imply a faster, more brittle fracture. A slower, more ductile fracture would result in a lower frequency.

The output from the accelerometer is in the time domain (acceleration v time). In order to extract frequency from this data a Fourier Transform was carried out on the data. The points of highest amplitude could then be located in the frequency domain and the corresponding frequency identified. These frequencies were collated and compared by means of a 2-sample t-test with respect to bone quality. A paired t-test was also carried out on the specimens in the Fast Loading, Demineralised Quality (quality compared) and the Fast Loading, Normal Quality (quality compared) sub groups. Table 7.1 presents the results found for this analysis. Due to connection issues with the sensor, where a short circuit was created during the test, data from one test at each bone quality could not be extracted. This did not affect the paired tests. A graphical representation of the data is presented in Figure 7.2 below

Quality	N	Mean	SE Mean	St Dev	Minimum	Q1	Median	Q3	Maximum
Demineralised	9	4677	711	2134	2637	3027	3809	6201	8984
Normal	9	7444	796	2387	4102	5078	8398	9570	10547

Table 7.1: Frequency (Hz) at maximum amplitude during high loading rate testing on ovine femurs

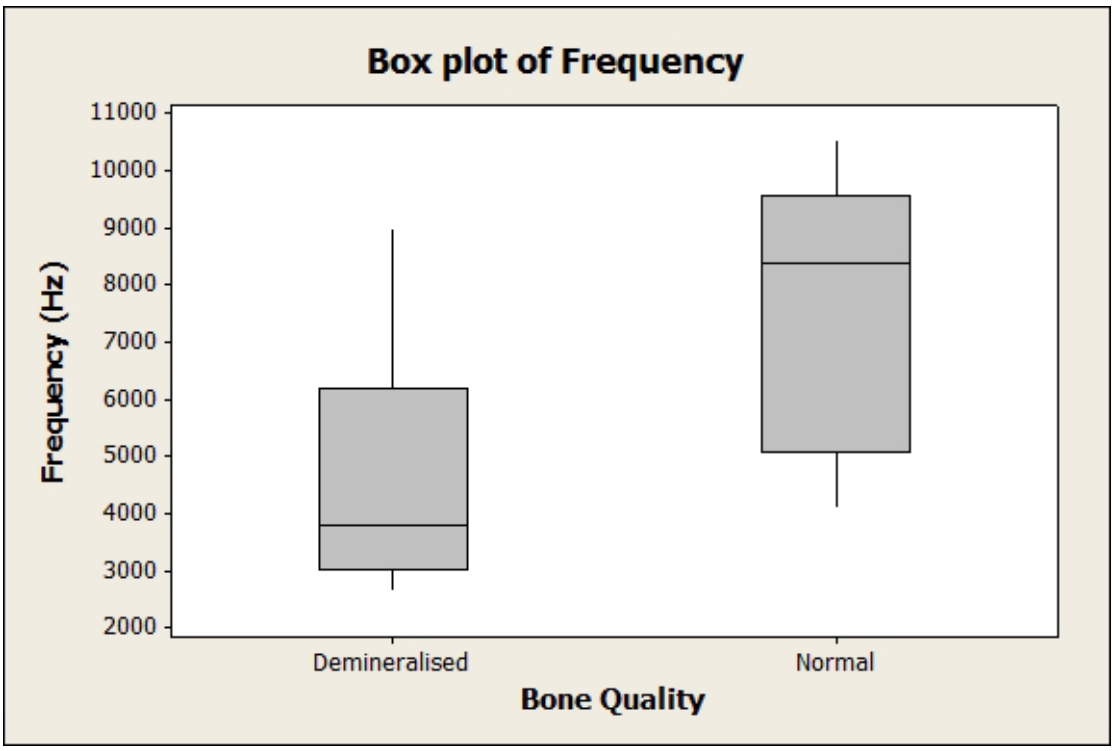

Figure 7.2: Box-plot of frequency data from accelerometer mounted on ovine femurs

7.1.1 Statistical significance

A 2-sample t-test showed that there was a statistically significant difference between the two groups with a p value of 0.020. The paired t-test confirmed this significant difference with a p value of 0.043. The frequency range in the contra-lateral specimens is shown in Table 7.2 below.

Group	Mean Frequency (Hz)	Standard Deviation
Fast Demineralised – quality paired (FDq)	4434	2587
Fast Normal – quality paired (FNq)	8594	2043
Difference	-4160	3175

Table 7.2: Range of frequency in paired examples (ovine femurs)

8 Fracture Area

It was desired to compare the newly created surface area of the fractured bone with the loading rate fracture energy, mineral content and toughness. The fracture length and area were calculated following the method set out in section 4.5

As discussed in Chapter 9, Radiographic fracture correlation, one of the specimens in the fast loading rate, normal quality group of bones suffered a fracture that did not propagate through the entire bone. As a consequence, the extent of the fracture was not easily identified in the radiograph of the fractured bone. This is shown below in Figure 8.1 alongside a photograph of the bone for comparison

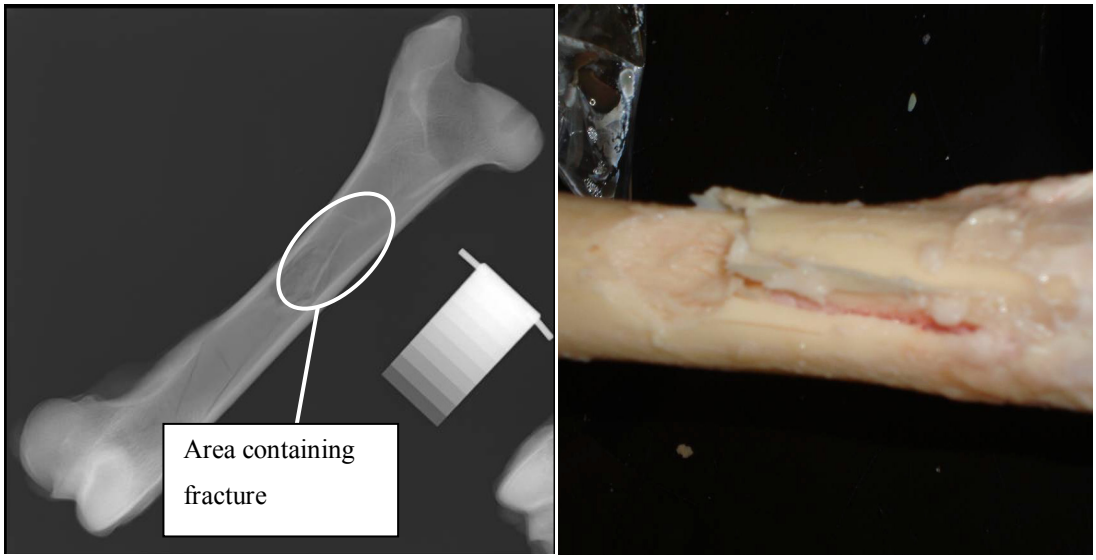

Figure 8.1: Radiograph and photograph of cracked ovine femur

8.1.1 All data

The data was initially analysed by comparing all specimen together. The distribution of data shown in Table 8.1 was recorded when loading rate was used as the variable. Table 8.2 shows the distribution of data when quality was used as the variable. All values are in mm^2.

Rate	N	Mean	SE Mean	StDev	Minimum	Q1	Median	Q3	Maximum
Fast	19	877	143	662	260	572	678	1009	3085
Slow	20	558	56	251	219	397	502	599	1178

Table 8.1: Fracture surface area (mm^2) of ovine femur split by loading rate

Quality	N	Mean	SE Mean	StDev	Minimum	Q1	Median	Q3	Maximum
Demineralised	20	632	46	205	351	471	596	756	1178
Normal	19	799	154	671	219	382	572	1087	3085

Table 8.2: Fracture surface area (mm^2) of ovine femur split by bone quality

Statistical significance was examined for loading rate and quality by means of a 2-sample t-test. A statistically significant difference was found for the groups split by loading rate, indicated by a p value of 0.049.When quality was used as the variable between the two groups a p value of 0.310 was found indicating no statistically significant difference.

8.1.2 Split by loading rate

Isolating the tests performed at the different loading rates and performing a 2-sample t-test with quality as the variable gave a p value of 0.264 for the high loading rate group. At the slow loading rate a p value of 0.971 was found. Therefore no statistically significant difference was found for either group, although it should be noted that the difference in fracture area between the two bone qualities at the slow loading rate was minimal.

8.1.3 Split by bone quality

The results were grouped together by quality to allow the effect of loading rate to be examined by means of a 2-sample t-test. In the normal quality bones loading rate was found to have no statistically significant effect on the fracture surface, as indicated by a p value of 0.134. In the demineralised bones a p value of 0.1 was found, indicating no statistically significant difference.

Although no statistically significant difference was found, it could be seen that the specimen tested at the fast loading rate yielded a larger fracture surface area. The distribution between the groups is represented graphically in Figure 8.2 below.

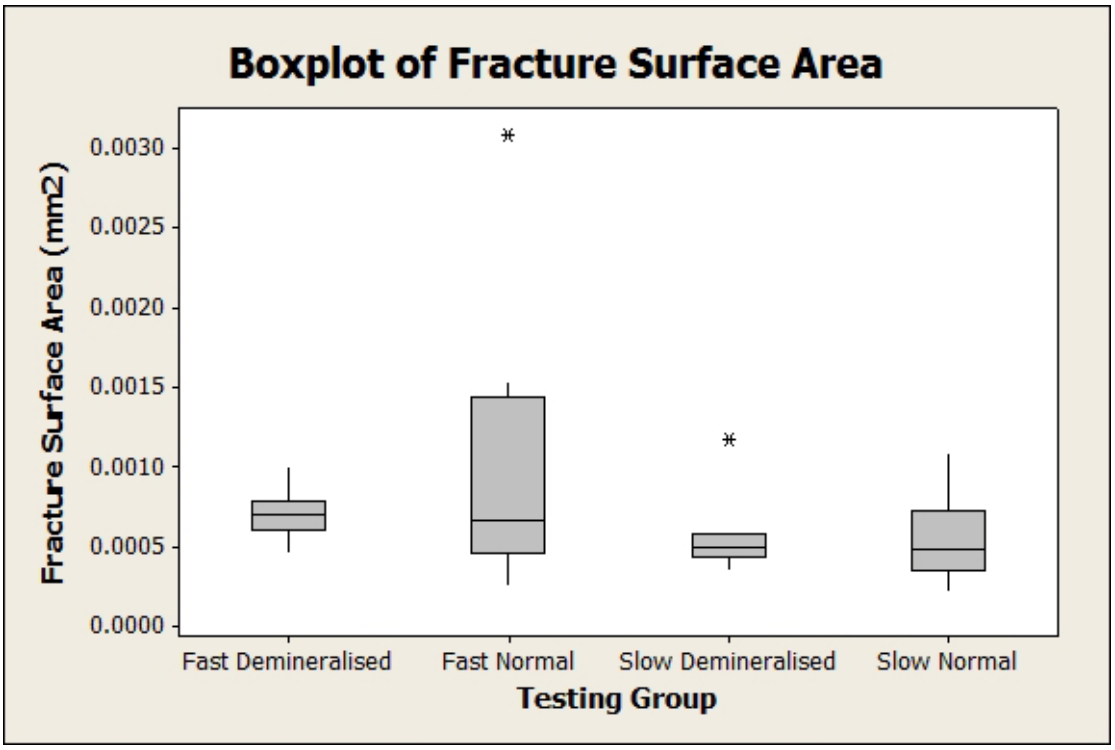

Figure 8.2: Distribution of fracture surface area of ovine femur between testing groups

Performing a paired t-test on the respective groups revealed the statistical significances shown in Table 8.3.

Pairing	P value
FNr – SNr	0.193
FNq – FDq	0.615
FDr – SDr	0.042
SNq – SDq	0.657

Table 8.3: Paired statistical tests of fracture surface area

To determine if information about the energy or stresses involved during the fracture can be determined from the fracture surface area, correlations between this parameter and the calculated values for force, stress, displacement, toughness, work and Young's modulus (as

derived by utilizing the method for non-prismatic beams and accounting for shear using Timoshenko beam theory, as described in section 4.10.3, were carried out using the method for Pearson product-moment correlation coefficient. The correlation coefficients, with the p values in parenthesis, are presented in Table 8.4 below.

Variable	All	Fast	Slow	Demineralised	Normal
Force	0.426 (0.007)	0.347 (0.146)	0.235 (0.318)	0.191 (0.420)	0.149 (0.542)
Displacement	-0.447 (0.004)	-0.483 (0.036)	-0.100 (0.676)	-0.065 (0.786)	0.144 (0.557)
Work	-0.382 (0.016)	0.383 (0.105)	-0.205 (0.386)	-0.398 (0.082)	-0.202 (0.408)
Stress	0.240 (0.141)	0.179 (0.463)	-0.072 (0.761)	0.100 (0.676)	-0.018 (0.941)
Flexural Modulus	0.801 (0.000)	0.873 (0.000)	0.330 (0.156)	0.280 (0.231)	0.069 (0.778)
Toughness	-0.407 (0.010)	-0.452 (0.052)	-0.388 (0.145)	-0.453 (0.045)	-0.296 (0.218)
Density	0.251 (0.123)	0.218 (0.371)	0.204 (0.389)	0.206 (0.383)	0.181 (0.459)

Table 8.4: Table of Correlation Co-efficients (p-value) on ovine femurs

These results are discussed further in section 11.11 but the high correlation with Young's modulus in the "all data" and fast loading rate groups should be highlighted as is the poor correlation with all variables in the "normal" group.

9 Radiographic fracture correlation

Testing with whole bone enabled a comparison to be made between the lab created fractures and fractures retrieved from patient data. The aim of this comparison was to validate the experimental method by relating the type of fracture resulting from loading at a high strain rate in the laboratory, to the type of physiological fractures resulting from what had been termed in the patient notes as "high energy impacts".

In order to examine the radiographs in detail, access to the hospital wide PACS and Trak systems was required. An honorary NHS contract was granted for this purpose. The NHS Trak database was investigated to identify suitable fractures for this comparison. This involved the examination of over 1000 adult femoral fractures. These were identified by examining patient data where femoral surgical intervention was required. These cases were reduced by applying lower and upper age bounds of 18-55 years of age respectively. This age range was applied in order to limit the comparison to adult bone of normal quality. Therefore, only the radiographs of experiments involving normal quality bone, loaded at the high loading rate were used for comparison. Cases of surgery for non trauma reasons and those involving a non diaphyseal fracture were removed. Of those remaining only instances where the method of injury was detailed in the case notes were put forward for further examination.

In order to select cases involving high energy trauma the following selection criteria, adapted from (RTAC Trauma Triage Plan - 2004) were applied:

- Motorbike accident at 20 mph or greater
- Car accident at 30 mph or greater
- Pedestrian hit by vehicle at 15 mph or greater
- Fall from more than 7m

This process yielded 33 suitable instances of high energy fracture in the diaphyseal of the femur. It is recognised that other activities such as skiing, mountain biking or indeed contact sports could provide cases of impact loading that could be termed high energy. However, many fractures from these activities occur as a result of a bad landing or due to a combination of loading. As it would be impossible to know the exact circumstances at the

time of injury, fractures resulting from these activities were excluded from the comparison. Injuries resulting from ballistic trauma, such as a gunshot or explosion, were not included as these represent loading rates far in excess of those created in (high energy blunt trauma) the lab and were therefore not relevant to this study. This restriction acts as an upper bound on the range defined as "high speed loading". Amongst the identified 13 oblique and 14 transverse high energy fractures, there were 4 severely comminuted and 2 with butterfly fragments.

The hospital database was scanned by an orthopaedic trainee, who also assisted in the classification process. To prevent bias in this analysis the trainee was only shown the x-rays of the laboratory created fractures after the classification process outlined above was completed.

9.1 Laboratory Experiments

Of the 10 high speed fractures in healthy bone created in the lab the following distribution of fracture classifications was found: 3 transverse, 4 oblique, 2 Comminuted and 1 with a large longitudinal crack but no transverse fracture. This is shown in Table 9.1 below.

The bone with the longitudinal crack was the only example where no full fracture was achieved in either the fast or slow loading rate tests. While this was surprising, examination of the bone did reveal that the crack, which measured approximately 62mm and extended through the extent of the cortex, clearly represented severe structural weakening of the bone. It offered little resistance to opening up under torsion and it was believed that if it was placed under compressive or bending loads total failure would be reached at a significantly lower stress than when in the pre fractured state and therefore no further mechanical testing was performed on the specimen.

Fracture Type	Patient x-ray		Experimental	
Comminuted / Butterfly	6	18%	2	22%
Transverse	14	42%	3	33%
Oblique	13	39%	4	44%

Table 9.1: Fracture type distribution

When comparing the respective percentages of each fracture types within the groups it can be seen that the laboratory produced fractures had a similar rate of occurrence to those that were found in the real data. Indicating that the types of fracture produced in the laboratory experiments were representative of those that were found in clinical practice.

9.2 Pictorial Comparison

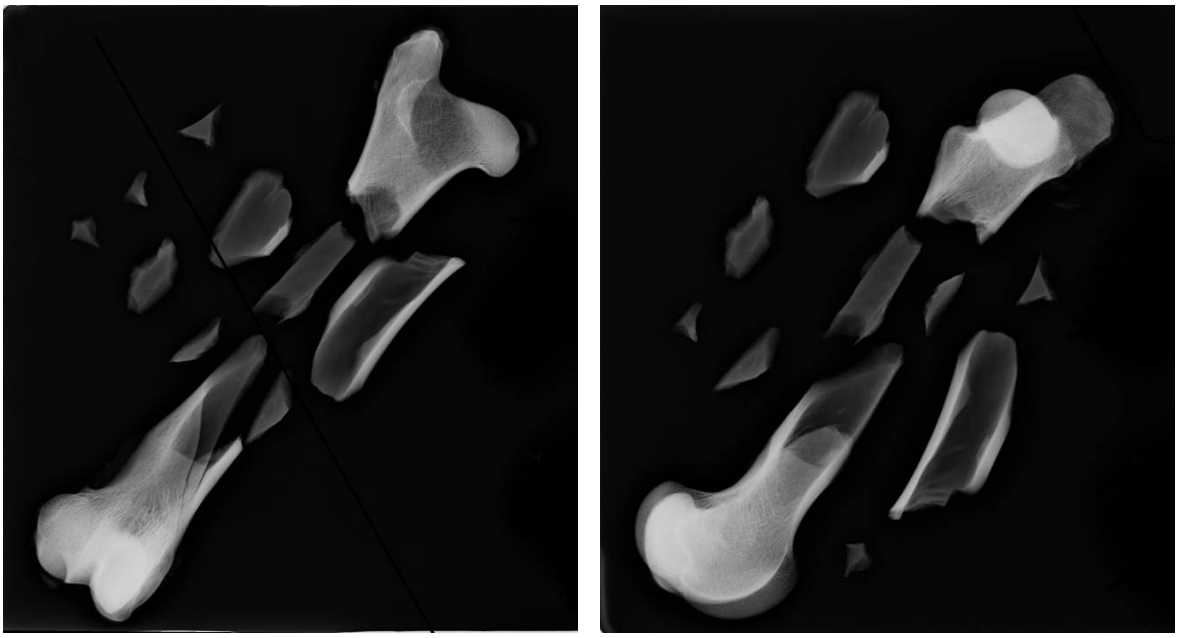

Figure 9.1: Example of comminuted fracture of ovine femur created in the lab

Figure 9.2: Comminuted fracture from patient radiograph

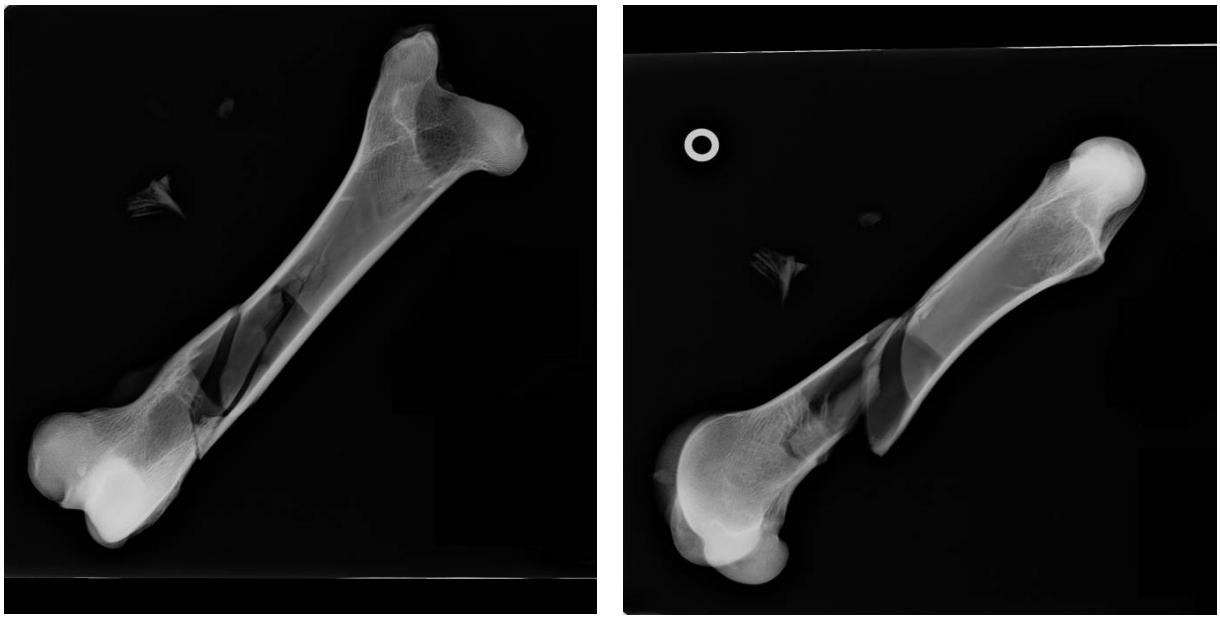

Figure 9.1: Example of Oblique fracture on ovine femur created in the laboratory

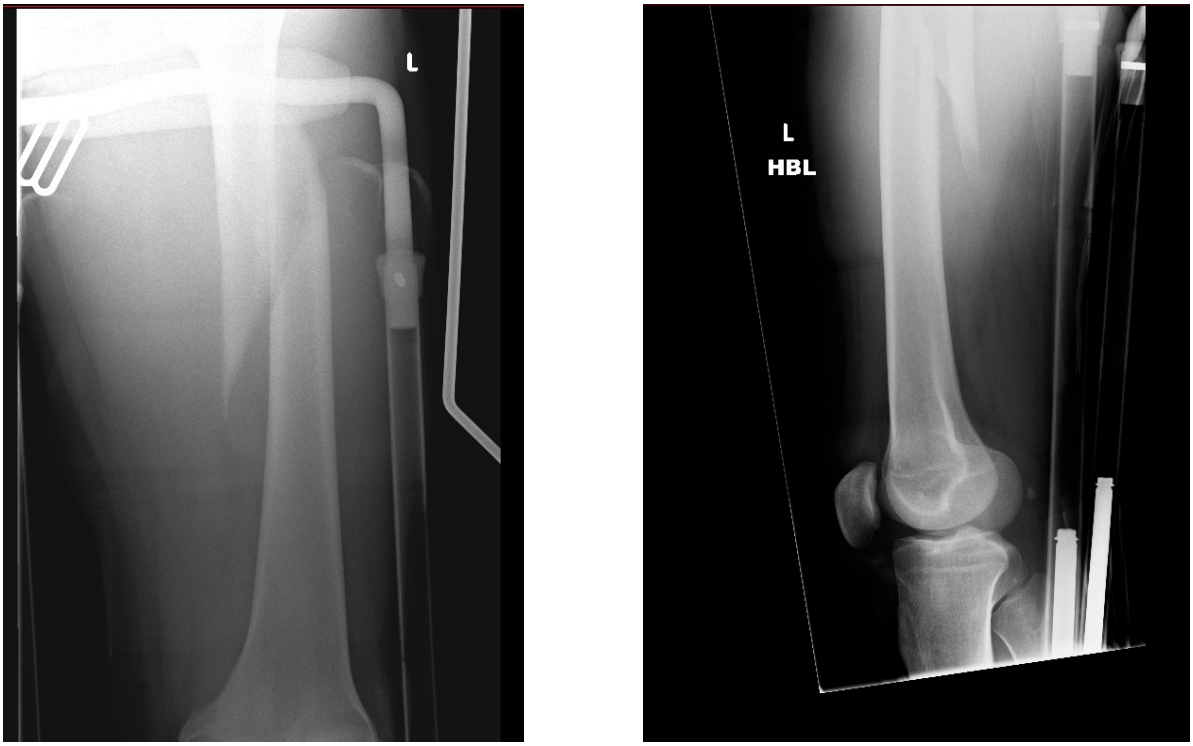

Figure 9.2: Oblique fracture from patient radiograph

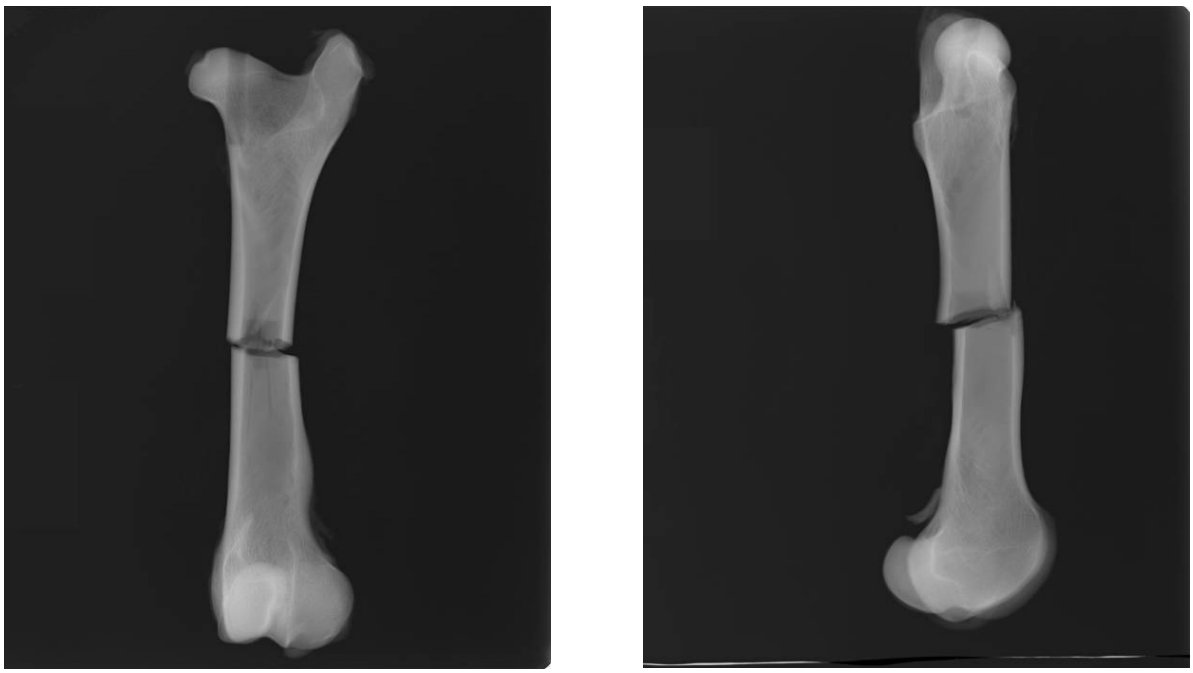

Figure 9.5: Example of transverse fracture of ovine femur created in the laboratory

Figure 9.6: Transverse fracture from patient radiograph

10 Results

The aim of this study was to evaluate the effect of both strain rate and bone quality. To meet this goal the femurs were allocated into groups denoting both rate and quality, this resulted in 4 distinct groupings; Fast-Normal (FN), Fast-Demineralised (FD), Slow-Normal (SN), Slow-Demineralised (SD). It was desirable that contralateral pairs of limbs be used where possible. To achieve this objective, the 4 main groupings were further split with respect to comparison between paired limbs, to give 8 sub groups as follows: FNr, FNq, FDr, FDq, SNr, SNq, SDr, SDq where:

- F = Fast Loading
- S = Slow Loading
- N = Normal Bone
- D = Demineralised Bone.
- r = rate compared
- q = quality compared

The results of the analysis were collated to allow statistical analysis to be performed. For ease of presentation the order of these results follows the format of:

- All specimen data – rate compared (n = 20)
- All specimen data – quality compared (n = 20)

Each testing group were also independently collated

- Fast Loading, Normal Quality (n = 10)
- Fast Loading, Demineralised (n = 10)
- Slow Loading, Normal Quality (n = 10)
- Slow Loading, Demineralised (n = 10)

Where n = number of specimen in each group

As there was more than one experimental factor, and many response variables, an analysis of variance (ANOVA) was performed on all the data sets to investigate the influence of the

factors Loading Rate and Bone Quality on the response variables Force, Stress, Yield Stress, Young's Modulus, Displacement, Work Energy, Resilience, Toughness, yield Strain and Failure Strain. The ANOVA enables the investigation of both the main effects of factors and of any interaction effect.

The results of this analysis are shown in table 10.1 below. F denotes the result of the F-test where a higher value indicates a greater level of significance to the result and a p-value equal to or less than 0.05 gives evidence of a real effect, less than 0.01 provides strong evidence of a real effect and less than 0.001 shows very strong evidence of a real effect. Interaction plots giving a visual representation of the data can be found in Appendix H.

	Loading Rate		**Bone Quality**		**Interaction**	
	F	p-value	F	p-value	F	p-value
Force	25.37	<0.0005	47.07	<0.0005	11.34	0.002
Stress	15.07	<0.0005	22.18	<0.0005	9.89	0.003
Yield Stress	0.56	0.459	1.21	0.279	2.57	0.118
Young's Modulus	37.79	<0.0005	4.01	0.053	3.58	0.067
Displacement	6.19	0.018	12.65	0.001	0.47	0.498
Work Energy	21.67	<0.0005	0.71	0.406	1.52	0.226
Resilience	44.43	<0.0005	0.04	0.847	1.45	0.236
Toughness	16.91	<0.0005	2.33	0.135	2.23	0.144
Yield Strain	88.5	<0.0005	0.26	0.613	0.46	0.504
Failure Strain	19	<0.0005	0.87	0.357	1.48	0.232

Table 10.1 ANOVA of dependent variables

Box-plots, such as Figure 10.1, were used to give a visual comparison of means and the spread of variation both in, and between, the groups, where the box denotes Q1, median and Q3 ranges and the whiskers show max min values. Outliers are denoted by an asterix.

Histograms of the data sets, split by variable, were created to check for normality of the data. After discussion with a statistician it was agreed that the data was distributed with sufficient normality to allow parametric testing to be used for further statistical analysis.

Statistical analysis was performed on the 4 groups, (FD, FN, SD and SN) split by the experimental factors of loading rate and bone quality, by means of the Tukey simultaneous

test. This test is mathematically similar to the students t-test, but takes into account the whole data set when determining statistical significance. This method reduces the likelihood of a Type I error (false positive), assessing the true statistical significance between the groups and therefore can be considered a more robust method of statistical analysis where there are multiple groups than the students t-test.

The use of contralateral pairings, where only one variable was altered between the pairs, created normal controlled groups within the specimens. This facilitated additional statistical testing to be performed by means of a paired t-test. As contralateral pairs were used the number of specimen in each group dropped from 10 to 5. While it is recognised that this is at the lower end of group size that allows for conclusions to be drawn it was considered to be suitable, especially when taken as a part of the further analysis outlined above.

10.1 Force

10.1.1 All Data – Loading Rate Compared

The following analysis was carried out on all 40 specimens. Loading rate was selected as the variable for comparison, resulting in 20 specimens in each group.

The fast loading rate group had a mean value for maximum force of 4585 N (± 1293 SD). The slow loading rate group had a mean value for maximum force of 3530 N (± 712 SD). A two-sample t-test indicated a statistically significant difference between the groups with a p value of 0.003.

Figure 10.1 below shows the distribution of stress results for each group in the form of a box-plot.

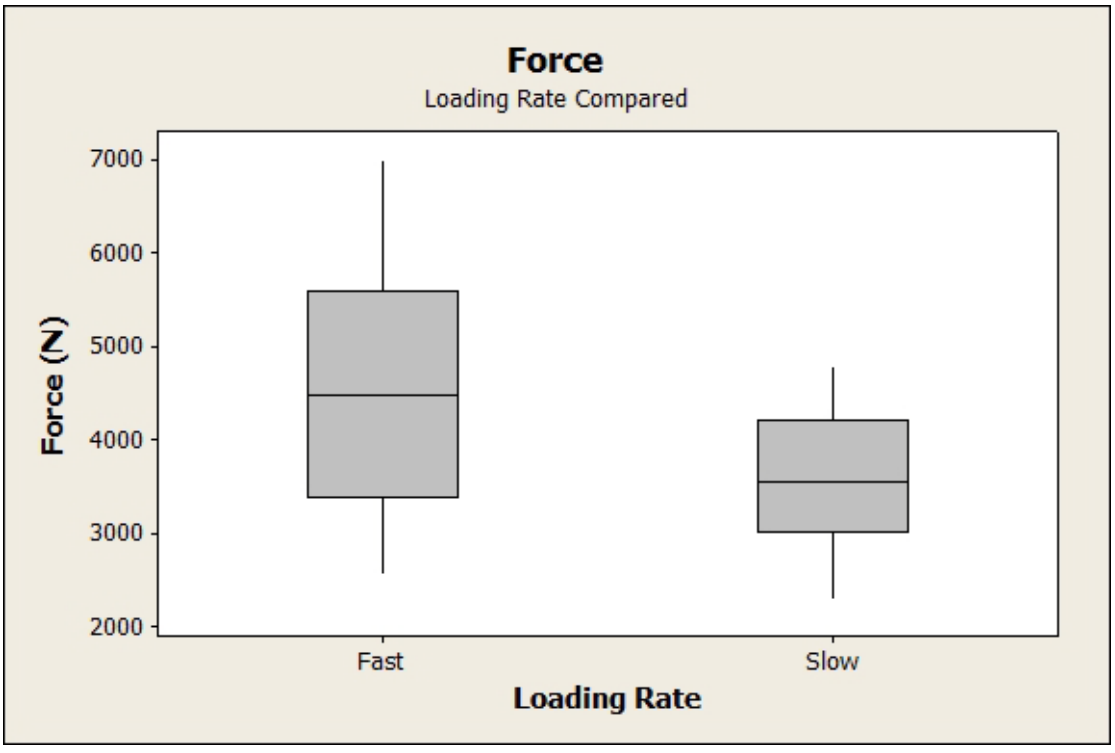

Figure 10.1: Box-plot of Peak Force by loading rate on ovine femurs

10.1.2 All Data – Bone Quality Compared

The normal quality bones had a mean value of maximum force of 4776 N (± 1143 SD). The mean value of maximum force for the demineralised bones was 3339 N (± 609 SD). A two-sample t-test revealed a statistically significant difference between the groups ($p<0.0005$).

Figure 10.2 below shows the distribution of peak force values for each group in the form of a box-plot.

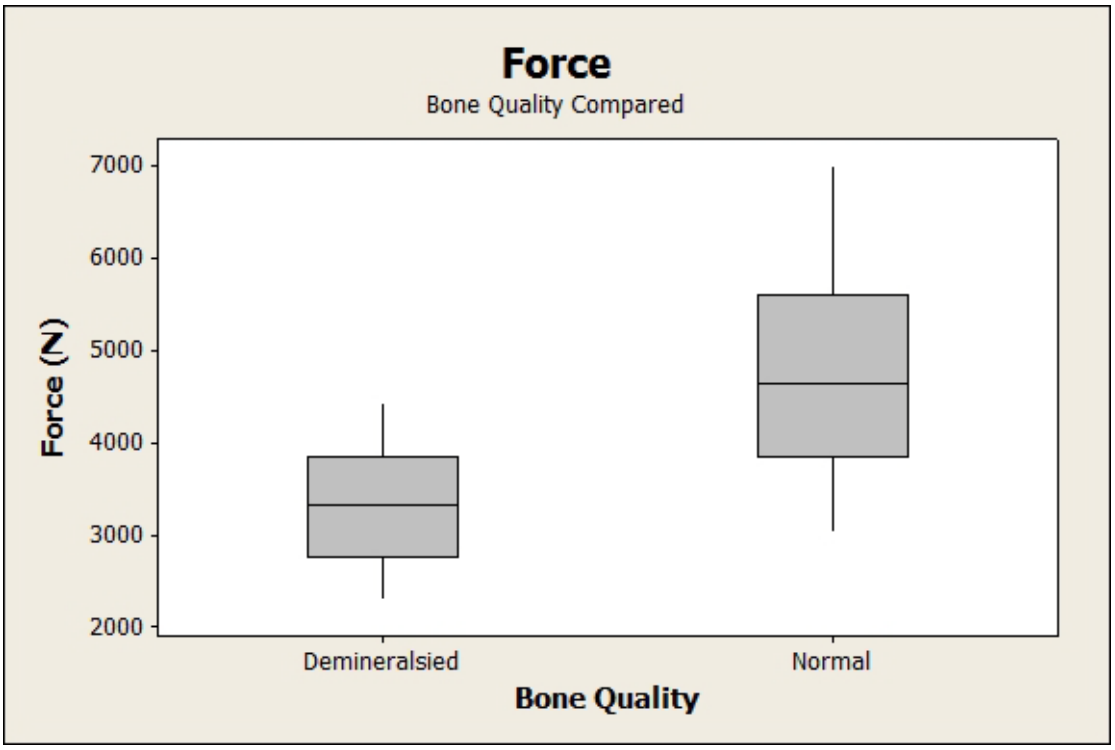

Figure 10.2: Box-plot of Peak Force by bone quality on ovine femurs

10.1.3 Force – by subgroup

The mean values for maximum force in each testing group are shown in Table 10.2

Testing Group	Force (N)	± SD
Fast Loading, Normal Quality	5656	795
Fast Loading, Demineralised	3514	591
Slow Loading, Normal Quality	3896	637
Slow Loading, Demineralised	3165	605

Table 10.2: Mean values of Force by testing group (ovine femurs)

This distribution of maximum force values in the above testing groups is shown in Figure 10.3 below.

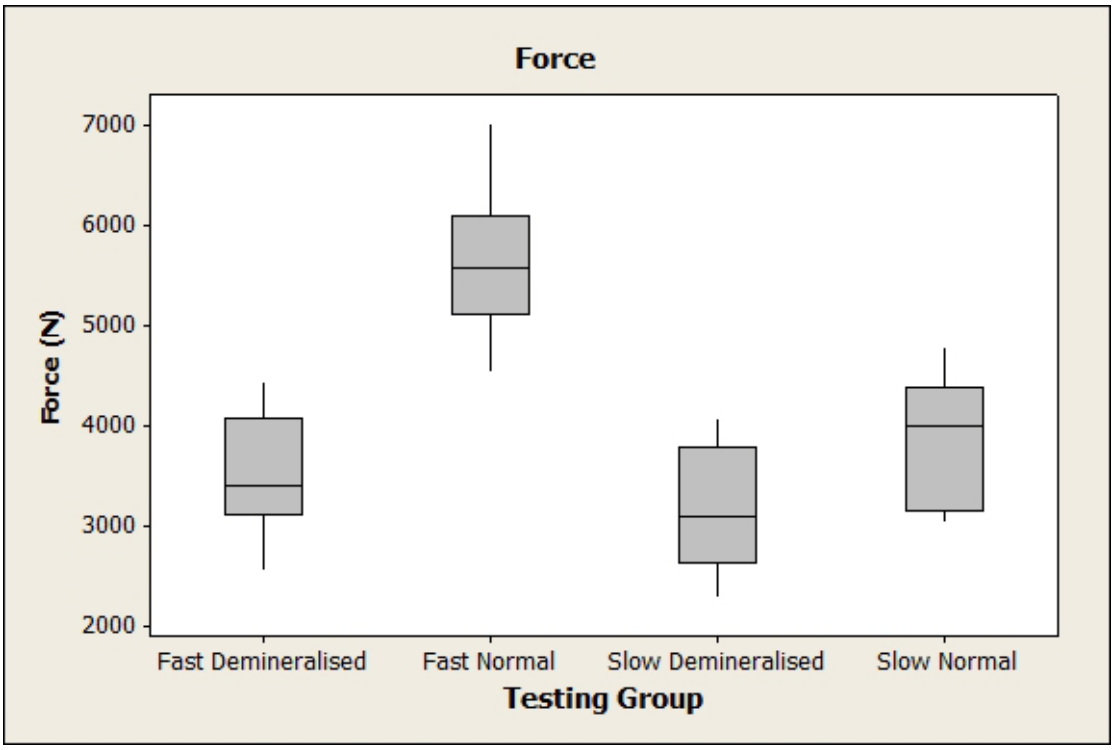

Figure 10.3: Box-plot of peak force values for each testing group (ovine femurs)

A Tukey simultaneous test was used to test for statistically significant differences in the force between the groups. The results of this statistical analysis are presented in Table 10.3.

Groups Compared (Force)	p-value	Significant
Normal Quality – Rate Compared (FN v SN)	<0.00005	Yes
Demineralised – Rate Compared (FD v SD)	0.6429	No
Fast Loading – Quality Compared (FN v FD)	<0.00005	Yes
Slow Loading – Quality Compared (SN v SD)	0.0821	No
Fast Normal v Slow Demineralised (FN v SD)	<0.00005	Yes
Fast Demineralised v Slow Normal (FD v SN)	0.5754	No

Table 10.3: Tukey simultaneous test of Force on ovine femurs

Statistically significant differences were found for force in all cases involving normal quality bone loaded at the fast loading rate No further statistical differences were observed between the groups.

A paired t-test was performed on the contralateral pairings of the specimens. The results of this analysis are presented in Table 10.4.

Contralateral Pairs (Force)	p-value	Significant
Normal Quality – Rate Compared (FNr v SNr)	0.015	Yes
Demineralised – Rate Compared (FDr v SDr)	0.109	No
Fast Loading – Quality Compared (FNq v FDq)	0.005	Yes
Slow Loading – Quality Compared (SNq v SDq)	0.012	Yes

Table 10.4: Paired t-test of force between contralateral ovine femurs

Statistically significant differences were found for all paired tests (Normal quality - rate compared, demineralised quality – rate compared and slow loading – quality compared) except when comparing the effect of loading rate on demineralised bones.

10.2 Stress

10.2.1 All data – Loading Rate Compared

The following analysis was carried out on all 40 specimens. Loading rate was selected as the variable for comparison, resulting in 20 specimens in each group.

The specimens in the fast loading rate group had a mean bending stress of 171.2 MPa (± 35.7 SD). The slow loading rate group had a mean bending stress of 141.7 MPa (± 28.3 SD).

A two-sample t-test was performed on these groups. This indicated a statistically significant difference between the stress result of the groups (p=0.006).

Figure 10.4 below shows the distribution of stress results for each group in the form of a box-plot.

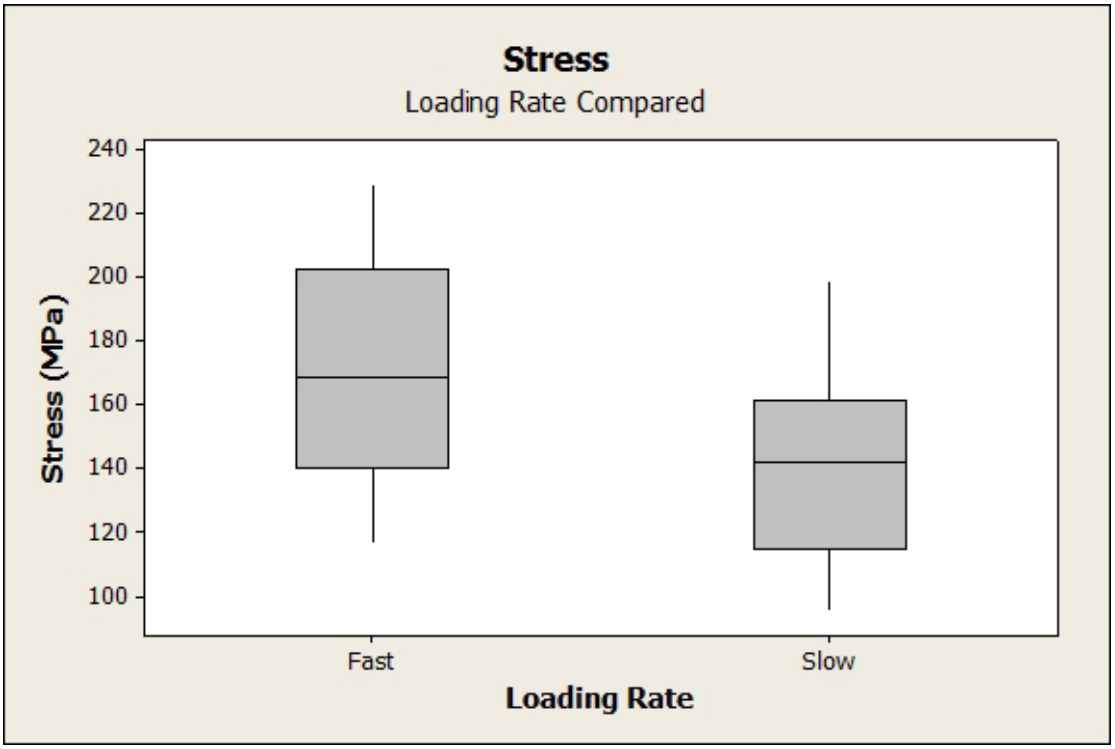

Figure 10.4: Box-plot of Bending Stress by loading rate on ovine femurs

10.2.2 All Data – Bone Quality Compared

The mean of the maximum bending stress for all the specimens of normal bone quality was 174.4 MPa (± 37.8 SD). Collating together the maximum stresses for the demineralised bones gave a mean value of 138.6 MPa (± 20.4 SD).

A two-sample t-test was performed on these groups. This indicated a statistically significant difference between the stress result of the groups (p=0.001).

Figure 10.5 below shows the distribution of stress results for each group in the form of a box-plot.

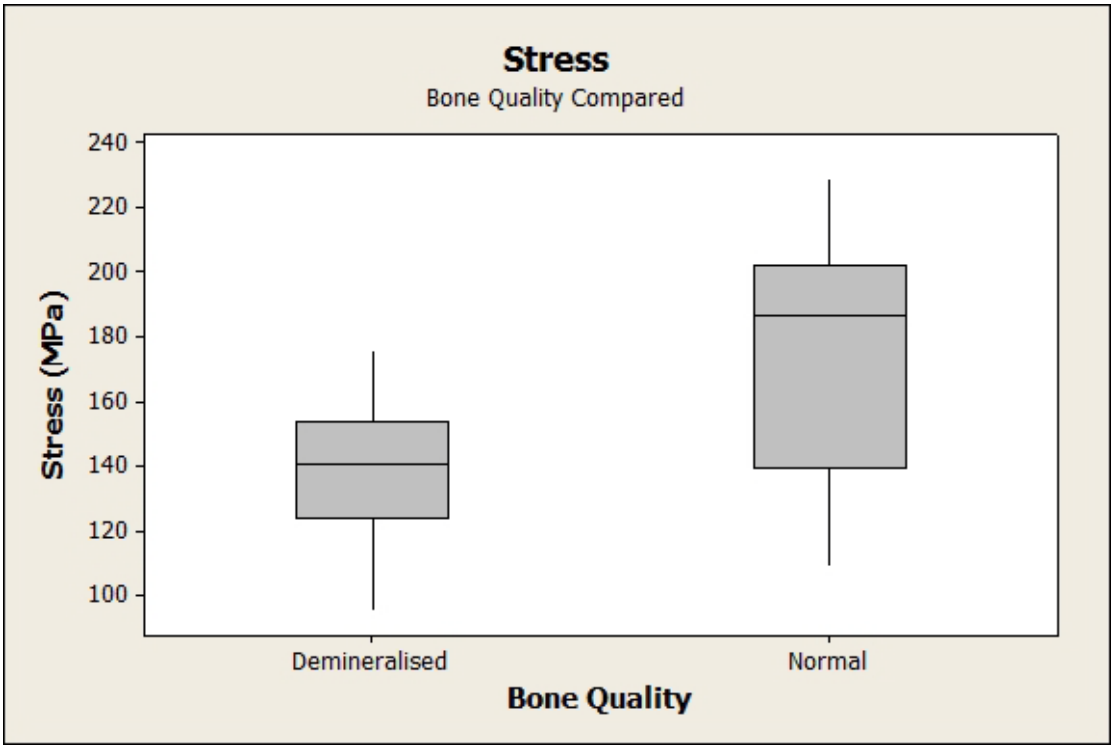

Figure 10.5: Box-plot of Bending Stress by bone quality on ovine femurs

10.2.3 Stress – by subgroup

The mean values for maximum stress in each testing group are shown in Table 10.5.

Testing Group	Stress (MPa)	± SD
Fast Loading, Normal Quality	201.08	19.88
Fast Loading, Demineralised	141.36	19.88
Slow Loading, Normal Quality	147.6	23.87
Slow Loading, Demineralised	135.75	23.87

Table 10.5: Mean values of Stress by testing group (ovine femurs)

This distribution of maximum stress values in the above testing groups is shown in Figure 10.6

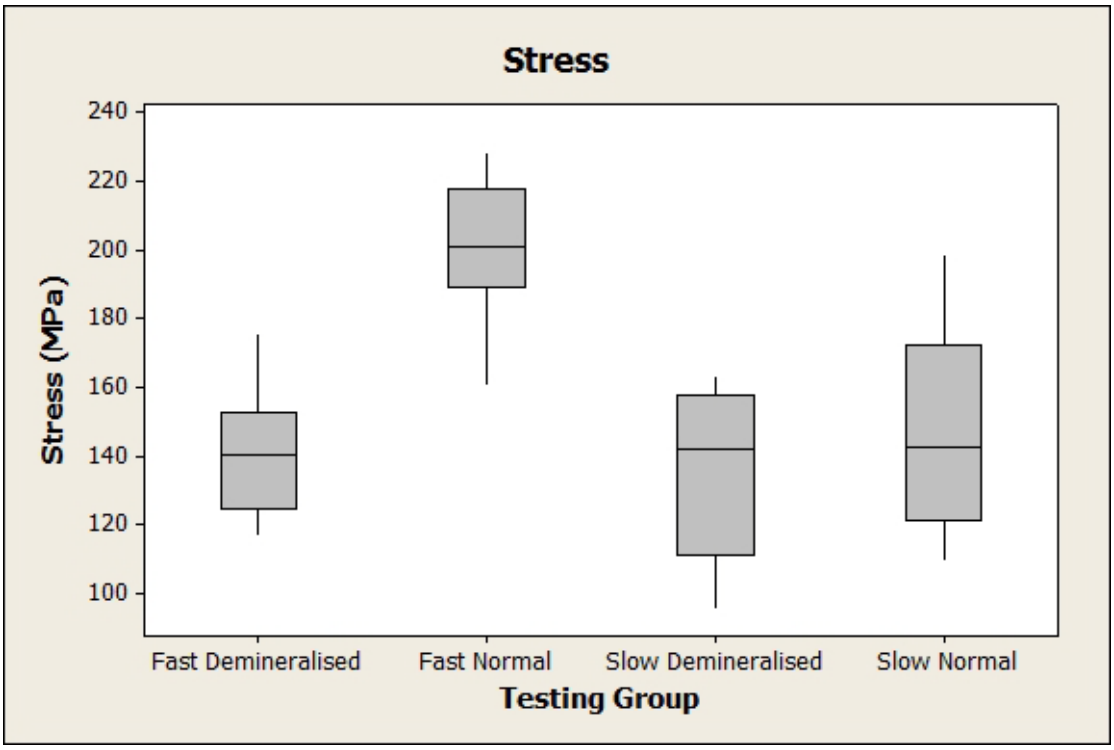

Figure 10.6: Box-plot of peak stress values for each testing group (ovine femurs)

A Tukey simultaneous test was used to check for statistically significant differences in the value for stress between the groups. The results of this analysis are presented in Table 10.6.

Groups Compared (Stress)	p-value	Significant
Normal Quality – Rate Compared (FN v SN)	0.0001	Yes
Demineralised – Rate Compared (FD v SD)	0.9532	No
Fast Loading – Quality Compared (FN v FD)	<0.00005	Yes
Slow Loading – Quality Compared (SN v SD)	0.6879	No
Fast Normal v Slow Demineralised (FN v SD)	<0.00005	Yes
Fast Demineralised v Slow Normal (FD v SN)	0.9361	No

Table 10.6: Tukey simultaneous test of Stress on ovine femurs

Statistically significant differences were observed between the fast loading, normal quality group and all other groups. No statistically significant results were found between the other groups

A paired t-test was performed on the contralateral limbs. The results of this analysis are presented in Table 10.7.

Contralateral Pairs (Stress)	p-value	Significant
Normal Quality – Rate Compared (FNr v SNr)	0.01	Yes
Demineralised – Rate Compared (FDr v SDr)	0.153	No
Fast Loading – Quality Compared (FNq v FDq)	0.003	Yes
Slow Loading – Quality Compared (SNq v SDq)	0.007	Yes

Table 10.7: Paired t-test of stress between contralateral ovine femurs

Statistically significant differences were found for all paired tests except when comparing the effect of loading rate on demineralised bones.

10.3 Yield Stress

The results presented in this section use the factored value for the fast loading rate yield stress as discussed in section 4.13.2

10.3.1 All Data – Loading Rate Compared

The following analysis was carried out on all 40 specimens. Loading rate was selected as the variable for comparison, resulting in 20 specimens in each group.

When the yield stress was considered the fast loading rate group had a mean stress at yield of 112.9 MPa (±42.5 SD), the slow loading rate group had a mean stress at yield of 121.0 MPa (± 25.0 SD).

A two-sample t-test was performed on these groups. This indicated no statistically significant difference between the stress result of the groups (p=0.470).

Figure 10.7 below shows the distribution of yield stress in each group in the form of a box-plot.

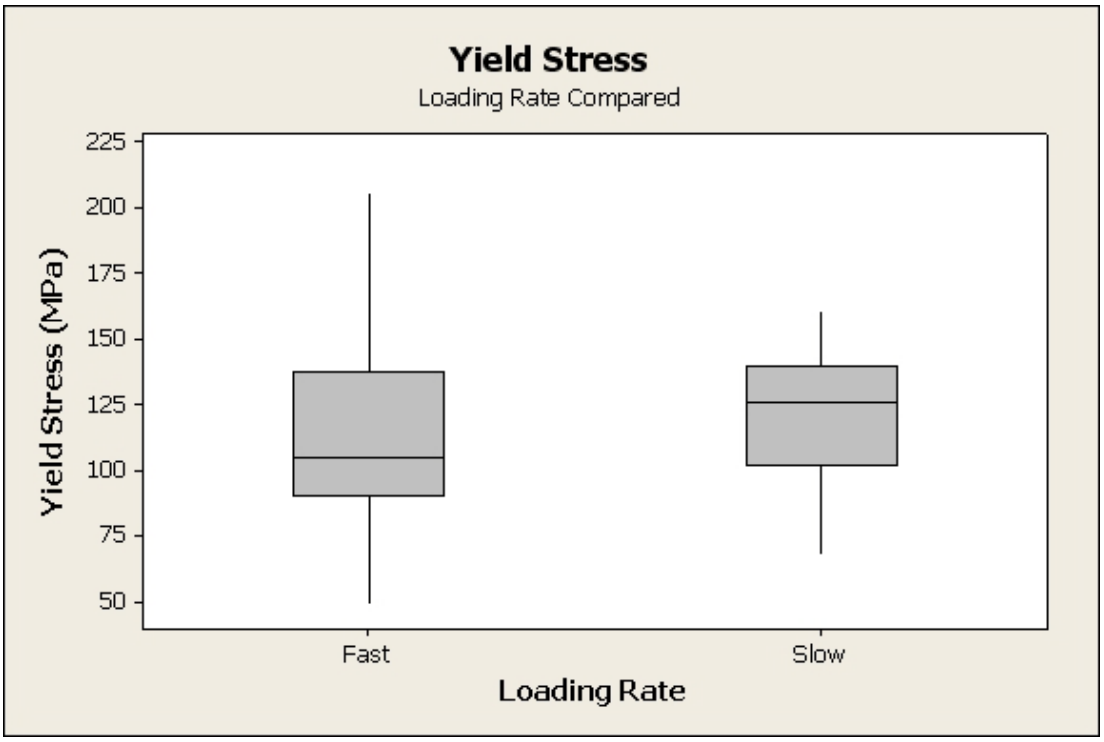

Figure 10.7: Box-plot of Yield Stress by loading rate on ovine femurs

10.3.2 All data – Quality Compared

When the yield stress was considered the normal quality group had a mean stress of 122.9 MPa (± 32.8 SD), the demineralised group had a mean stress of 111.1 MPa (± 36.2 SD).

A two-sample t-test was performed on these groups. This indicated no statistically significant difference between the yield stress results of the groups (p=0.286).

Figure 10.8 below shows the distribution of stress results for each group in the form of a box-plot.

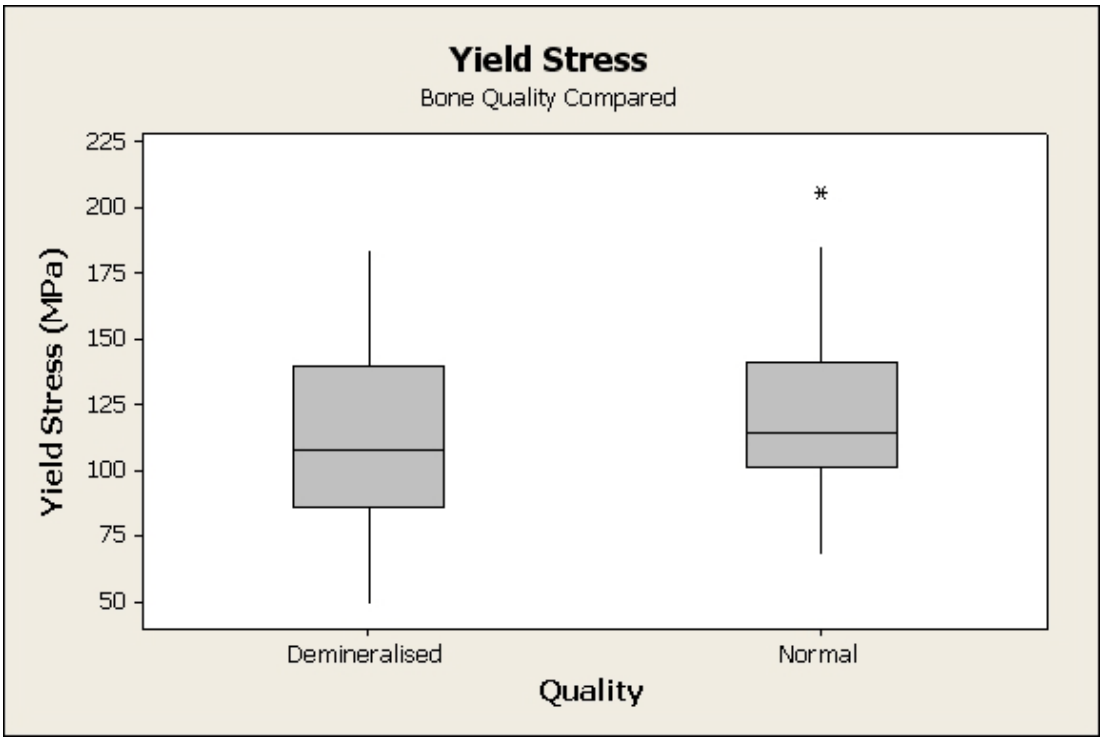

Figure 10.8: Box-plot of Yield Stress by bone quality on ovine femurs

10.3.3 Yield Stress – by subgroup

The mean values for yield stress in each testing group are shown in Table 10.8.

Testing Group	Yield Stress (MPa)	± SD
Fast Loading, Normal Quality	127.5	39.1
Fast Loading, Demineralised	98.4	42.5
Slow Loading, Normal Quality	118.3	26.3
Slow Loading, Demineralised	123.7	24.6

Table 10.8: Mean values of Yield Stress by testing group (ovine femurs)

This distribution of yield stress values in the above testing groups is shown in Figure 10.9

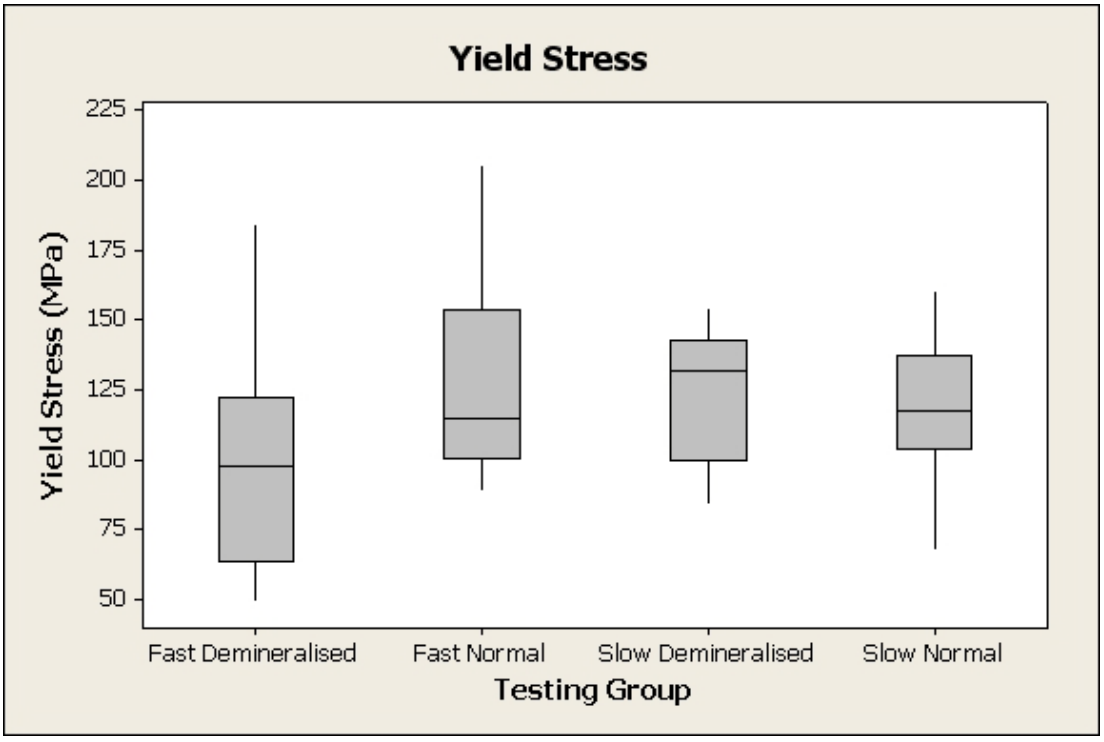

Figure 10.9: Box-plot of yield stress for each testing group (ovine femurs)

A Tukey simultaneous test was used to check for statistically significant differences in the yield stress between the groups. The results of this statistical analysis are presented in Table 10.9.

Groups Compared (Yield Stress)	p-value	Significant
Normal Quality – Rate Compared (FN v SN)	0.9302	No
Demineralised – Rate Compared (FD v SD)	0.3577	No
Fast Loading – Quality Compared (FN v FD)	0.2417	No
Slow Loading – Quality Compared (SN v SD)	0.9842	No
Fast Normal v Slow Demineralised (FN v SD)	0.9946	No
Fast Demineralised v Slow Normal (FD v SN)	0.5648	No

Table 10.9: Tukey simultaneous test of Yield Stress on ovine femurs

No statistically significant differences were observed between the groups compared.

A paired t-test was performed on the contralateral pairings within these groups. The results of this analysis are presented in Table 10.10.

Contralateral Pairs (Yield Stress)	p-value	Significant
Normal Quality – Rate Compared (FNr v SNr)	0.927	No
Demineralised – Rate Compared (FDr v SDr)	0.082	No
Fast Loading – Quality Compared (FNq v FDq)	0.2	No
Slow Loading – Quality Compared (SNq v SDq)	0.072	No

Table 10.10: Paired t-test of Yield Stress between contralateral ovine femurs

No statistically significant differences were found for the paired tests. The contralateral limbs comparing loading rate on demineralised bones and the slow loading rate tests comparing bone quality were close to statistical significance.

10.4 Young's Modulus of Elasticity

The results in the following section refer to the Flexural Modulus calculated by the non-prismatic beam method and the Timoshenko beam equation. The methods for these techniques can be found in section 4.9.2 and 4.10.2 respectively.

10.4.1 All data – Loading Rate Compared

When evaluating the non-prismatic calculation of Young's modulus the fast loading rate group had a mean value of 25.7 GPa (± 14.2 SD), the slow loading rate group had a mean value of 7.26 GPa (± 2.29 SD).

A two-sample t-test was performed on these groups. This indicated a statistically significant difference between the stress result of the groups ($p<0.0005$).

Figure 10.10 below shows the distribution of results for each group in the form of a box-plot.

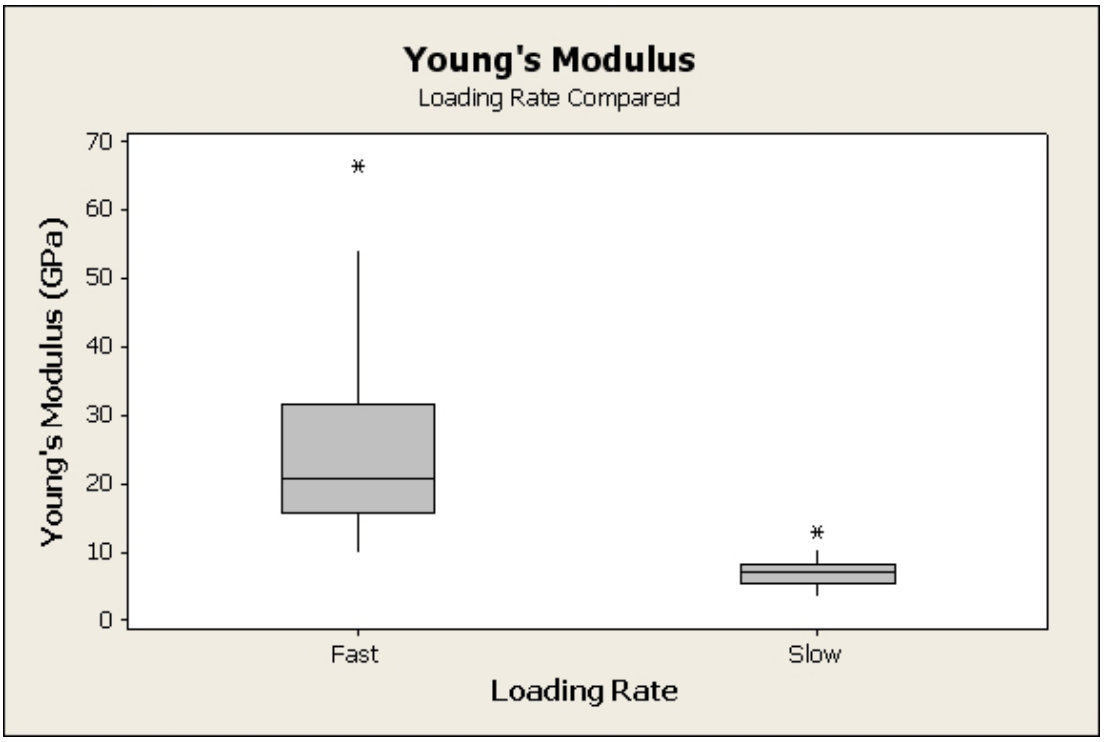

Figure 10.10: Box-plot of Young's Modulus by loading rate on ovine femurs

10.4.2 All data – Quality Compared

When the non-prismatic beam derived value for Young's modulus was compared the normal quality group had a mean value of 19.5 GPa (± 16.9 SD), the demineralised group had a mean value of 13.47 GPa (± 8.94 SD).

A two-sample t-test was performed on these groups. This indicated no statistically significant difference between the yield stress results of the groups (p=0.172).

Figure 10.11 below shows the distribution of values in each group in the form of a box-plot.

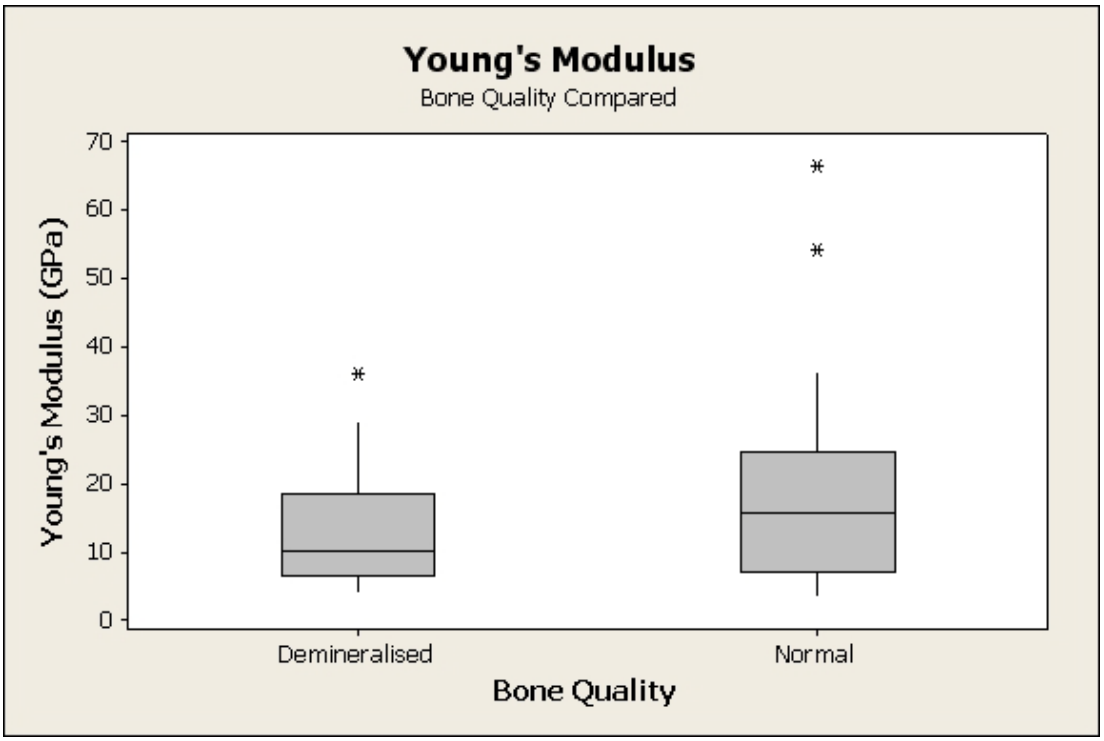

Figure 10.11: Box-plot of Young's Modulus by bone quality on ovine femurs

10.4.3 Young's Modulus – by subgroup

The mean values for Young's modulus in each testing group are shown in Table 10.11.

Testing Group	Young's Modulus (GPa)	± SD
Fast Loading, Normal Quality	31.5	16.6
Fast Loading, Demineralised	19.85	8.60
Slow Loading, Normal Quality	7.42	2.58
Slow Loading, Demineralised	7.09	2.10

Table 10.11: Mean values of Young's modulus by testing group (ovine femurs)

This distribution of values for the non-prismatic Timoshenko beam derived Young's modulus in the above testing groups are displayed in Figure 10.12.

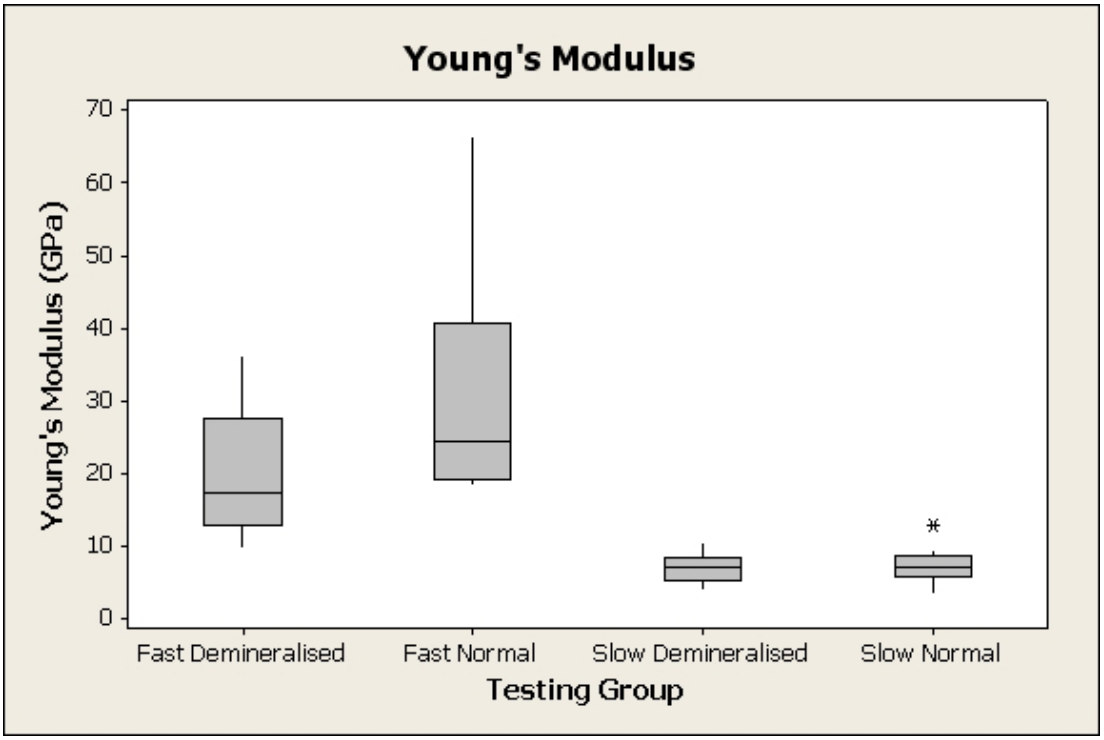

Figure 10.12: Box-plot of Young's modulus for each testing group (ovine femurs)

A Tukey simultaneous test was used to check for statistically significant differences between the Young's Modulus in the groups. The results of this statistical analysis are presented in Table 10.12.

Groups Compared (Young's Modulus)	p-value	Significant
Normal Quality – Rate Compared (FN v SN)	<0.00005	Yes
Demineralised – Rate Compared (FD v SD)	0.0236	Yes
Fast Loading – Quality Compared (FN v FD)	0.0435	Yes
Slow Loading – Quality Compared (SN v SD)	0.9998	No
Fast Normal v Slow Demineralised (FN v SD)	<0.00005	Yes
Fast Demineralised v Slow Normal (FD v SN)	0.0285	Yes

Table 10.12: Tukey simultaneous test of Young's Modulus on ovine femurs

Statistically significant differences were found between all groups except when evaluating the effect of bone quality at the slow loading rate.

A paired t-test was performed on the contralateral pairings of the specimens. The results of this analysis are presented in Table 10.13.

Contralateral Pairs (Young's Modulus)	p-value	Significant
Normal Quality – Rate Compared (FNr v SNr)	0.045	Yes
Demineralised – Rate Compared (FDr v SDr)	0.022	Yes
Fast Loading – Quality Compared (FNq v FDq)	0.329	No
Slow Loading – Quality Compared (SNq v SDq)	0.998	No

Table 10.13: Paired t-test of Young's modulus between contralateral ovine femurs

The contralateral testing showed statistically significant differences when comparing the effect of loading rate on both qualities of bone. However no statistical differences were seen when examining the effect of bone quality at either loading rate.

10.5 Displacement

10.5.1 All data – Loading Rate Compared

The following analysis was carried out on all 40 specimens. Loading rate was selected as the variable for comparison, resulting in 20 specimens in each group.

It was found that taking all the bones loaded at the fast loading rate resulted in a mean displacement value of 2.816 mm (± 0.802 SD). The slow loading rate group had a mean displacement of 3.308 mm (± 0.605 SD).

A two-sample t-test was performed on these groups, indicating a statistically significant difference between the groups (p=0.035).

Figure 10.13 below shows the distribution of results for each group in the form of a box-plot.

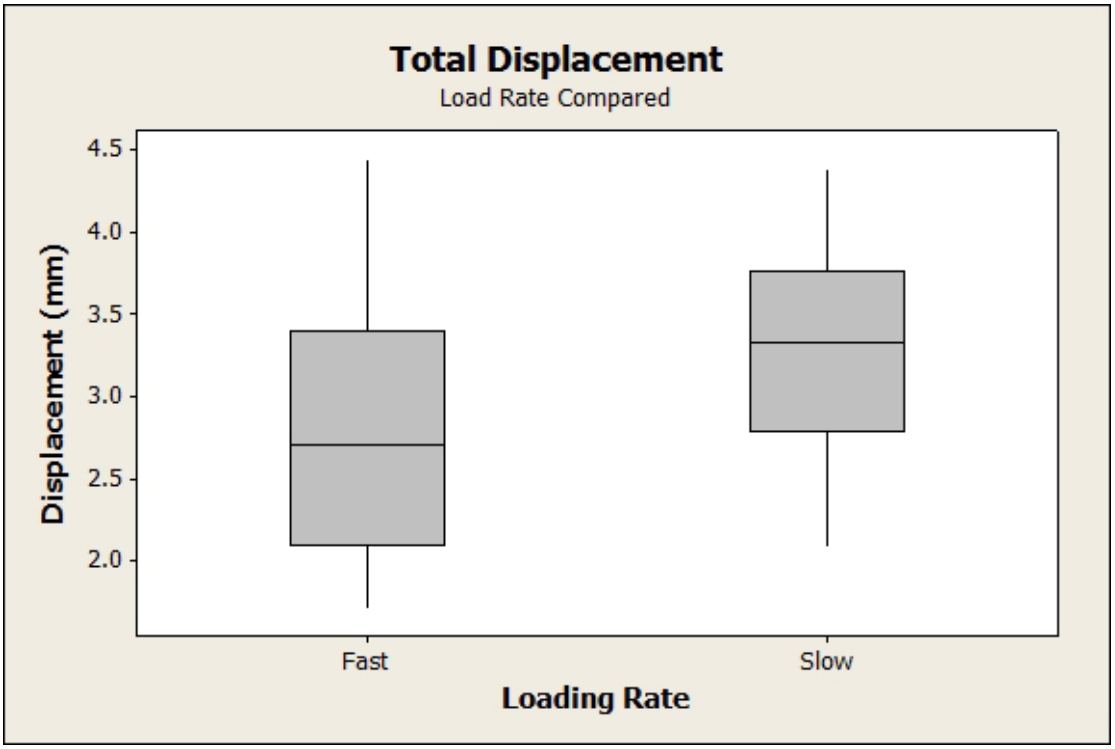

Figure 10.13: Box-plot of total displacement by loading rate on ovine femurs

10.5.2 All Data – Bone Quality Compared

The mean of the maximum displacement for all the specimens of normal bone quality was 2.711 mm (± 0.653 SD). Collating together the maximum displacements for the demineralised bones gave a mean value of 3.414 (± 0.671 SD).

A two-sample t-test was performed on these groups. This indicated a statistically significant difference between the results of the groups (p=0.002).

Figure 10.14 below shows the distribution of displacements for each group in the form of a box-plot.

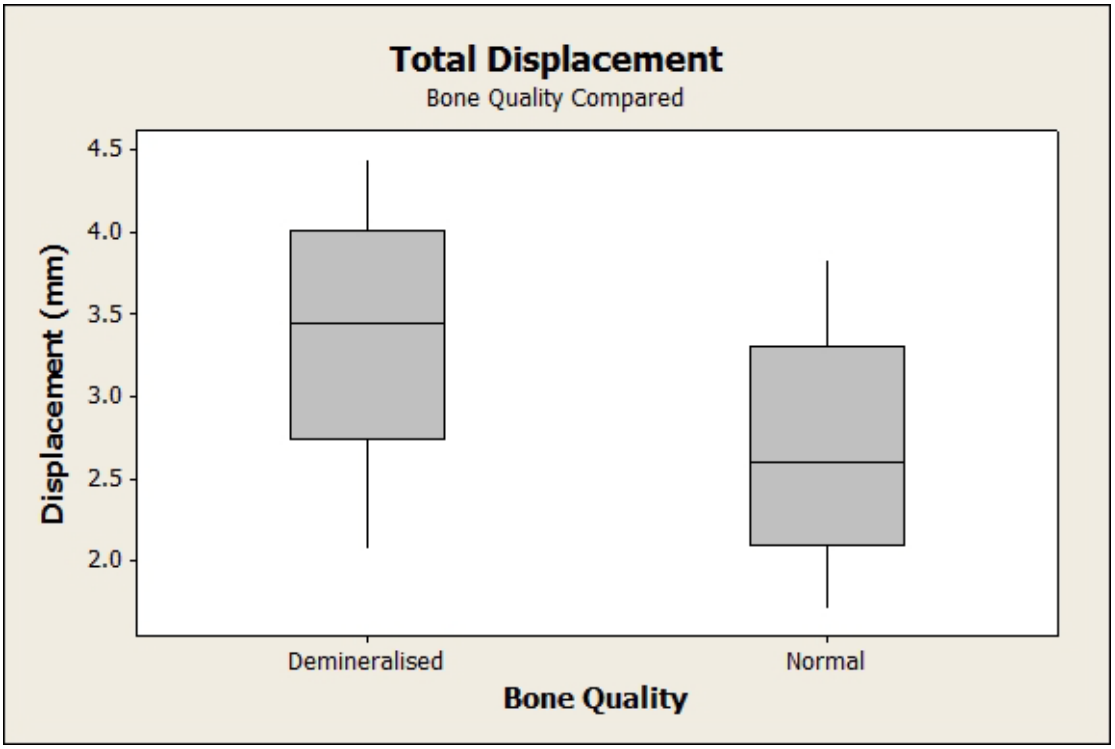

Figure 10.14: Box-plot of displacement by bone quality on ovine femurs

10.5.3 Displacement – by subgroup

The mean values of maximum displacement in each testing group are shown in Table 10.14.

Testing Group	Displacement (mm)	± SD
Fast Loading, Normal Quality	2.397	0.604
Fast Loading, Demineralised	3.325	0.777
Slow Loading, Normal Quality	3.024	0.562
Slow Loading, Demineralised	3.592	0.526

Table 10.14: Mean values of displacement by testing group (ovine femurs)

This distribution of maximum displacement values in the above testing groups is shown in Figure 10.15.

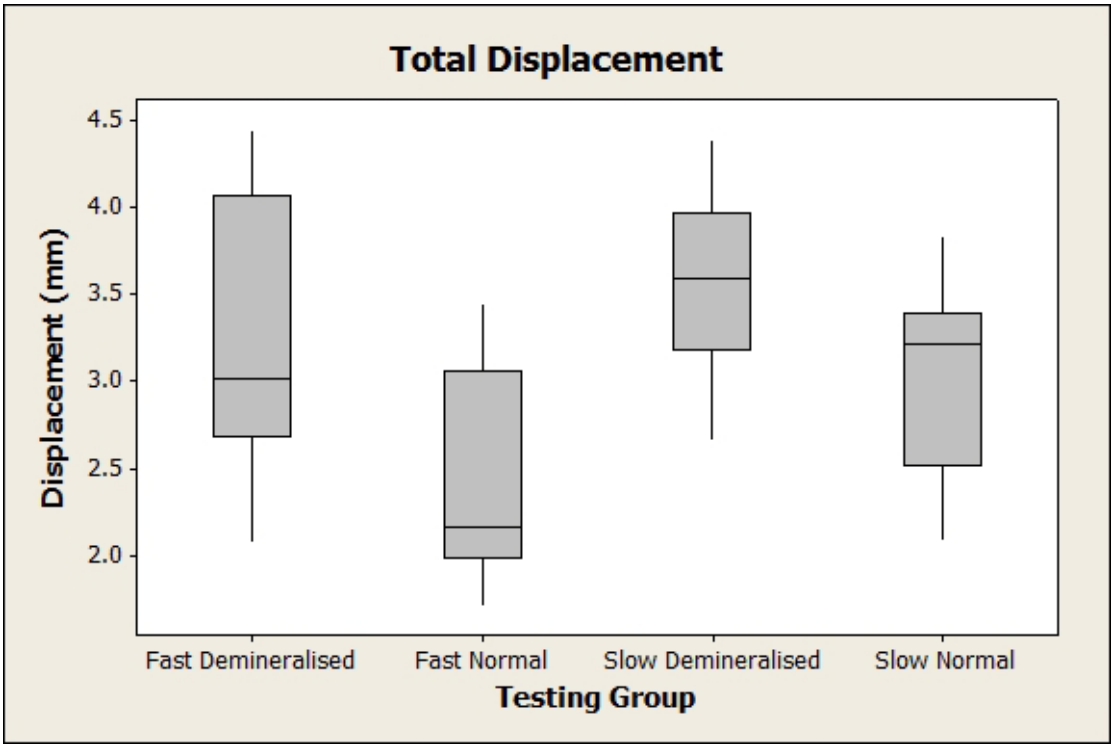

Figure 10.15: Box-plot of displacement values for each testing group (ovine femurs)

Statistically significant differences between the measured displacement at failure of the specimen were assessed by use of a Tukey simultaneous test. The results of this statistical analysis are presented in Table 10.15.

Groups Compared (Displacement)	p-value	Significant
Normal Quality – Rate Compared (FN v SN)	0.1312	No
Demineralised – Rate Compared (FD v SD)	0.5841	No
Fast Loading – Quality Compared (FN v FD)	0.0242	Yes
Slow Loading – Quality Compared (SN v SD)	0.1955	No
Fast Normal v Slow Demineralised (FN v SD)	0.0008	Yes
Fast Demineralised v Slow Normal (FD v SN)	0.8734	No

Table 10.15: Tukey simultaneous test of displacement on ovine femurs

Statistically significant differences were found when comparing the effect of normal quality, fast loading rate specimen on demineralised bones at both loading rates. No other statistically significant differences were found.

A paired t-test was performed on the contralateral limbs. The results of this analysis are presented in Table 10.16.

Contralateral Pairs (Displacement)	p-value	Significant
Normal Quality – Rate Compared (FNr v SNr)	0.061	No
Demineralised – Rate Compared (FDr v SDr)	0.355	No
Fast Loading – Quality Compared (FNq v FDq)	0.392	No
Slow Loading – Quality Compared (SNq v SDq)	0.152	No

Table 10.16: Paired t-test of displacement between contralateral ovine femurs

No statistically significant differences were observed for the paired tests. However, it should be noted that the result comparing loading rate between contralateral limbs of normal quality was nearly significant.

10.6 Work Energy

10.6.1 All Data – Loading Rate Compared

The following analysis was carried out on all 40 specimens. Loading rate was selected as the variable for comparison, resulting in 20 specimens in each group.

It was found that taking the calculated values for work for all the bones loaded at the fast loading rate gave a mean value of 5.92 J (± 1.54 SD). The slow loading rate group had a mean value of 8.88 J (± 2.42 SD).

A two-sample t-test was performed on these groups, indicating a statistically significant difference between the groups ($p < 0.0005$).

Figure 10.16 below shows the distribution of results for each group in the form of a box-plot.

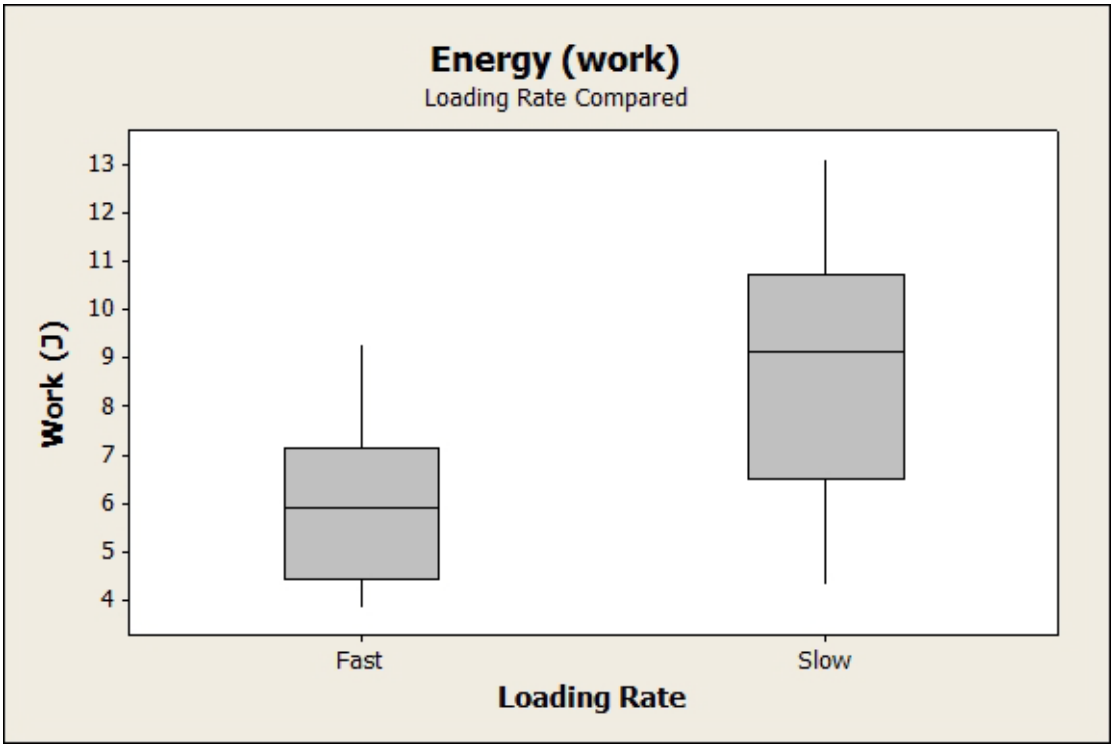

Figure 10.16: Box-plot of total work by loading rate on ovine femurs

10.6.2 All Data – Bone Quality Compared

The mean of the maximum work for all the specimens of normal bone quality was 7.68 J (± 2.70 SD). Collating together the values for work for the demineralised bones gave a mean value of 7.12 J (± 2.32 SD).

A two-sample t-test was performed on these groups. This indicated no statistically significant difference between the results of the groups (p=0.490).

Figure 10.17 below shows the distribution of the calculated values for work for each group in the form of a box-plot.

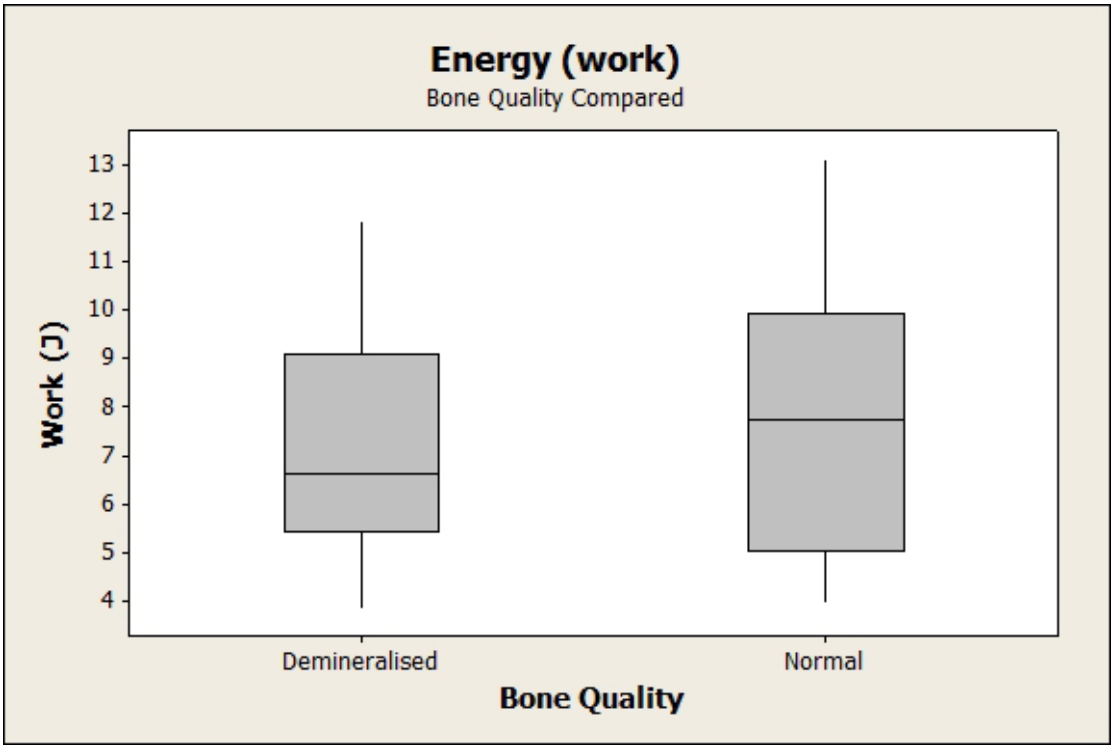

Figure 10.17: Box-plot of work by bone quality on ovine femurs

10.6.3 Work – by subgroup

The mean values of the work done in each testing group are shown in Table 10.17.

Testing Group	Work (J)	± SD
Fast Loading, Normal Quality	5.813	1.479
Fast Loading, Demineralised	6.030	1.666
Slow Loading, Normal Quality	9.545	2.340
Slow Loading, Demineralised	8.219	2.434

Table 10.17: Mean values of work by testing group (ovine femurs)

This distribution of the maximum work values in the above testing groups is shown in Figure 10.18.

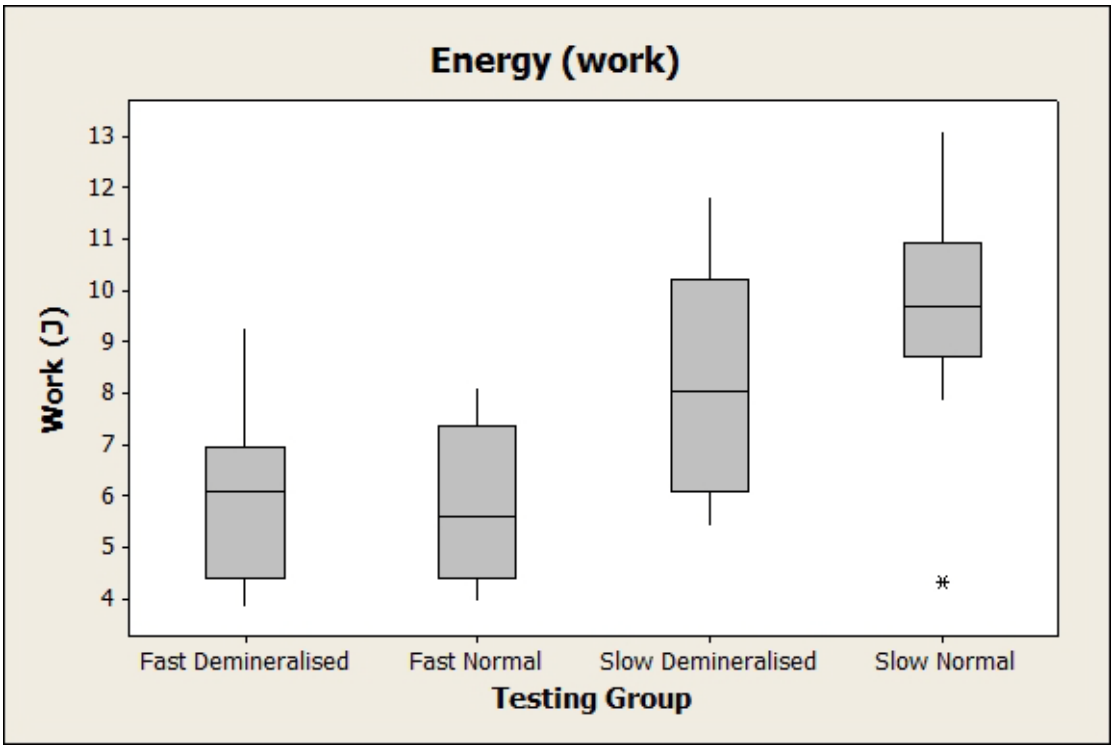

Figure 10.18: Box-plot of work for each testing group (ovine femurs)

A Tukey simultaneous test was used to check for statistically significant differences in the energy of deflection between the groups. The results of this statistical analysis are presented in Table 10.18.

Groups Compared (Work)	p-value	Significant
Normal Quality – Rate Compared (FN v SN)	0.0010	Yes
Demineralised – Rate Compared (FD v SD)	0.0911	No
Fast Loading – Quality Compared (FN v FD)	0.9925	No
Slow Loading – Quality Compared (SN v SD)	0.4683	No
Fast Normal v Slow Demineralised (FN v SD)	0.0495	Yes
Fast Demineralised v Slow Normal (FD v SN)	0.0023	Yes

Table 10.18: Tukey simultaneous test of work energy on ovine femurs

Statistically significant differences were found when comparing normal quality bone loaded at the high loading rate with slow loaded bone of both qualities. A statistically significant difference was also found between the groups comparing fast loading, demineralised bone and slow loaded normal quality bone.

A paired t-test was performed on the contralateral limbs within these groups. The results of this analysis are presented in Table 10.19.

Contralateral Pairs (Work)	p-value	Significant
Normal Quality – Rate Compared (FNr v SNr)	0.013	Yes
Demineralised – Rate Compared (FDr v SDr)	0.114	No
Fast Loading – Quality Compared (FNq v FDq)	0.928	No
Slow Loading – Quality Compared (SNq v SDq)	0.493	No

Table 10.19: Paired t-test of work between contralateral ovine femurs

A statistically significant difference was observed when comparing contralateral limbs of normal quality tested at different loading rates. The lack of the expected statistical significance in the difference between the groups comparing loading rate in the demineralised bones could possibly be explained by the large range covered by these values.

10.7 Toughness at Yield (Resilience)

10.7.1 All data – Loading Rate Compared

The following analysis was carried out on all 40 specimens. Loading rate was selected as the variable for comparison, resulting in 20 specimens in each group.

It was found that taking the value for toughness at the yield point for all the bones loaded at the fast loading rate gave a mean value of 547 J/m^3 (± 279 SD). The slow loading rate group had a mean value of 1415 J/m^3 (± 5007 SD).

A two-sample t-test was performed on these groups, indicating a statistically significant difference between the groups ($p < 0.0005$).

Figure 10.19 below shows the distribution of results for each group in the form of a box-plot.

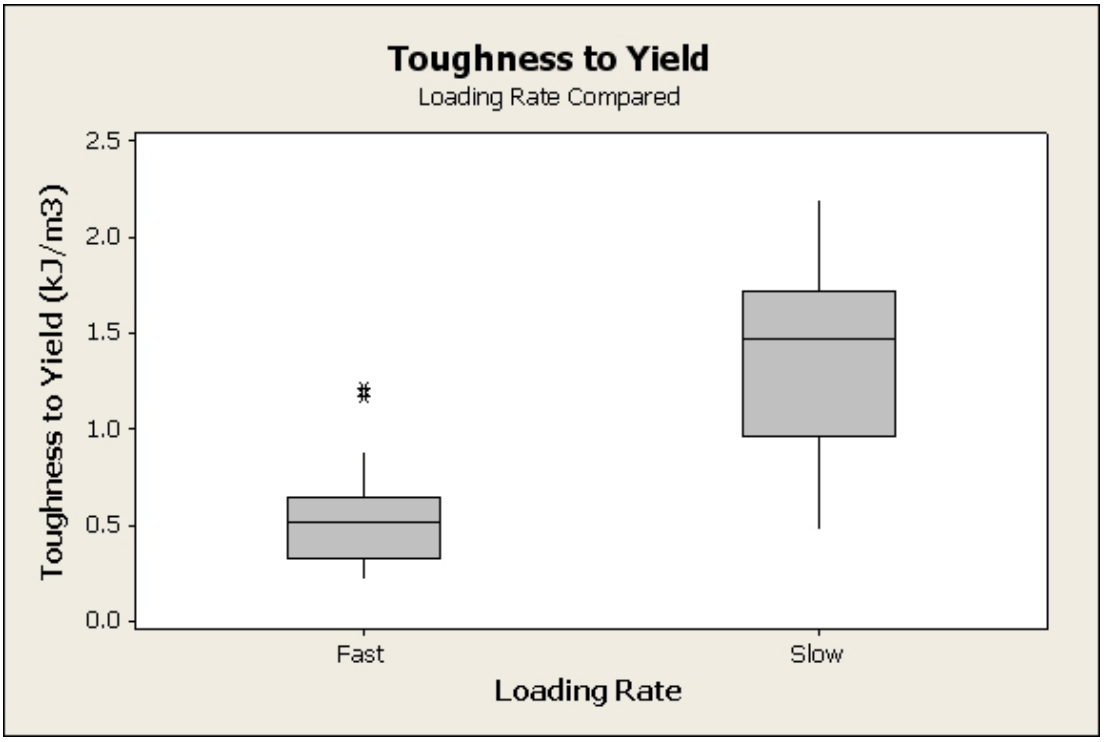

Figure 10.19: Box-plot of toughness at yield grouped by loading rate on ovine femurs

10.7.2 All Data – Bone Quality Compared

The mean of the toughness at yield values for all the specimens of normal bone quality was 968 J/m^3 (± 514 SD). Collating together the values of yield toughness for the demineralised bones gave a mean of 994 J/m^3 (± 684 SD).

A two-sample t-test was performed on these groups. This indicated no statistically significant difference between the results of the groups (p=0.896).

Figure 10.20 below shows the distribution of the calculated values for yield toughness in each group used above in the form of a box-plot.

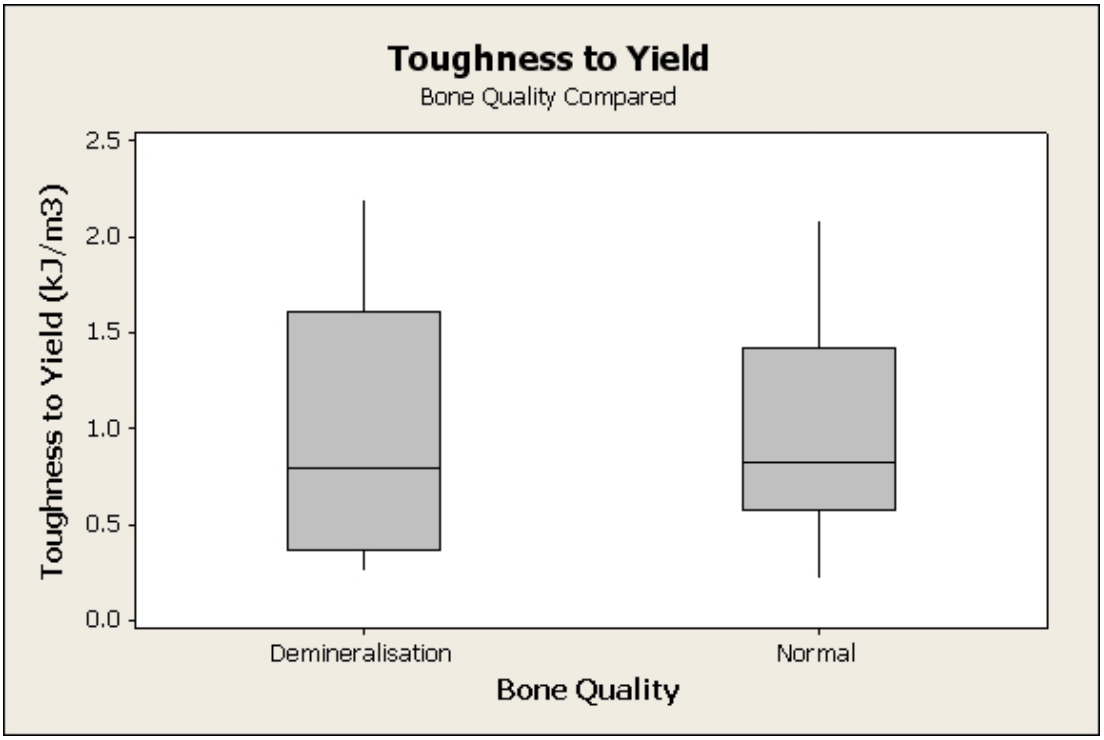

Figure 10.20: Box-plot of yield toughness by bone quality on ovine femurs

10.7.3 Yield Toughness – by subgroup

The mean values of the toughness measured at the yield point in each testing group are shown in Table 10.20.

Testing Group	Toughness (J/m^3)	± SD
Fast Loading, Normal Quality	613	279
Fast Loading, Demineralised	481	278
Slow Loading, Normal Quality	1324	446
Slow Loading, Demineralised	1507	570

Table 10.20: Mean values of yield toughness by testing group (ovine femurs)

This distribution of the values for toughness at yield used in the above testing groups is shown in Figure 10.21.

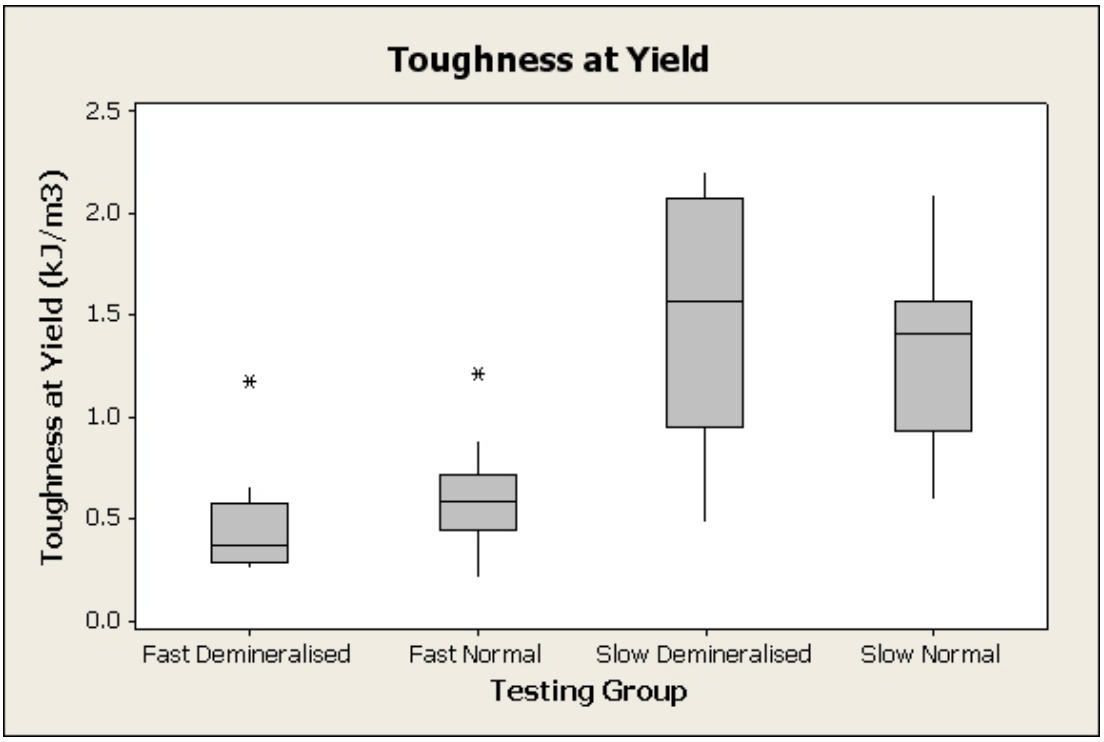

Figure 10.21: Box-plot of values for each testing group (ovine femurs)

A Tukey simultaneous test was used to check for statistically significant differences in the value for toughness at yield between the groups. The results of this statistical analysis are presented in Table 10.21.

Groups Compared (Toughness of Yield)	p-value	Significant
Normal Quality – Rate Compared (FN v SN)	0.0024	Yes
Demineralised – Rate Compared (FD v SD)	<0.00005	Yes
Fast Loading – Quality Compared (FN v FD)	0.8907	No
Slow Loading – Quality Compared (SN v SD)	0.7569	No
Fast Normal v Slow Demineralised (FN v SD)	0.0001	Yes
Fast Demineralised v Slow Normal (FD v SN)	0.0003	Yes

Table 10.21: Tukey simultaneous test of toughness at yield on ovine femurs

Statistically significant differences were found when comparing the effect of loading rate at both bone qualities and for the interactions between loading rates and bone qualities. No significant differences were found when comparing the effect of quality at either loading rate.

The results for the toughness at yield between contralateral limbs were examined by means of a paired t-test. The results of this analysis are presented in Table 10.22.

Contralateral Pairs (Toughness at Yield)	p-value	Significant
Normal Quality – Rate Compared (FNr v SNr)	0.03	Yes
Demineralised – Rate Compared (FDr v SDr)	0.027	Yes
Fast Loading – Quality Compared (FNq v FDq)	0.077	No
Slow Loading – Quality Compared (SNq v SDq)	0.644	No

Table 10.22: Paired t-test of toughness at yield between contralateral ovine femurs

A statistically significant difference was observed when comparing loading rate with contralateral limbs of both bone qualities. This is in agreement with that found in the larger testing groups.

The fast loading rate contralateral pairs of different bone quality did not display a statistically significant difference. However, the p value of 0.077 does indicate that the values were close to being statistically significant.

10.8 Toughness at Failure

10.8.1 All data – Loading Rate Compared

The following analysis was carried out on all 40 specimens. Loading rate was selected as the variable for comparison, resulting in 20 specimens in each group.

It was found that taking the maximum toughness for all the bones loaded at the fast loading rate gave a mean value of 2034 J/m^3 (± 546 SD). The slow loading rate group had a mean value of 3230 J/m^3 (± 1220 SD).

A two-sample t-test was performed on these groups, indicating a statistically significant difference between the groups ($p < 0.0005$).

Figure 10.22 below shows the distribution of results for each group in the form of a box-plot.

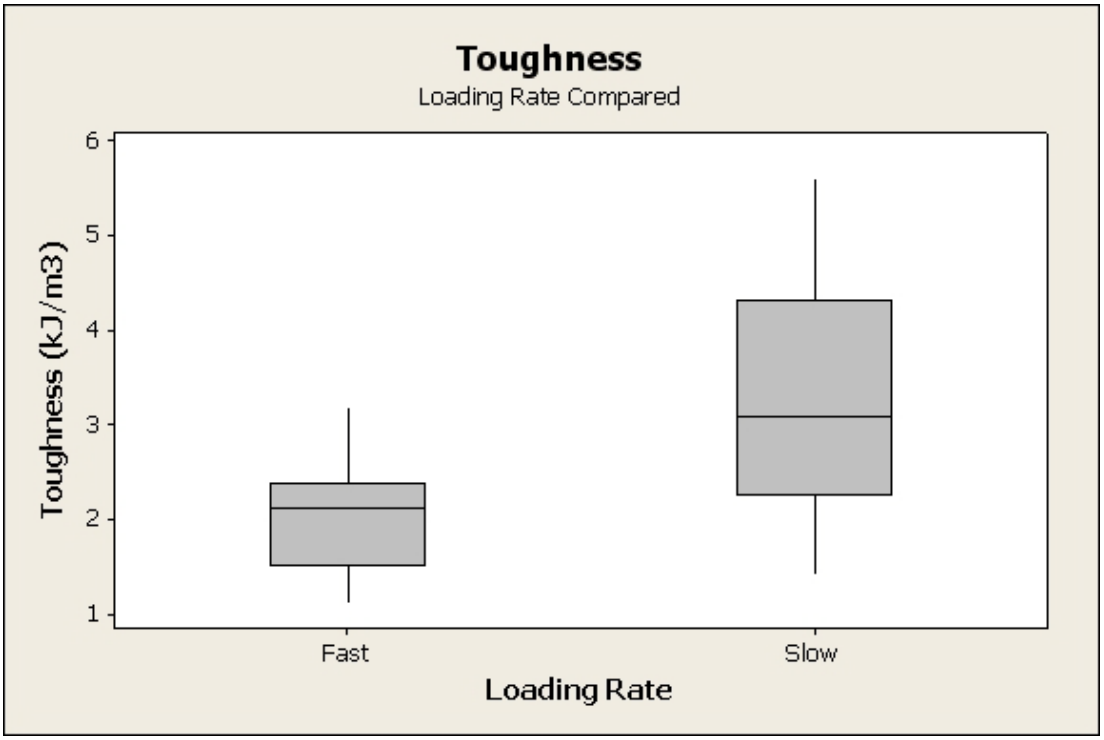

Figure 10.22: Box-plot of toughness grouped by loading rate on ovine femurs

10.8.2 All Data – Bone Quality Compared

The mean of the toughness values for all the specimens of normal bone quality was 2850 J/m^3 (± 1310 SD). Collating together the values of toughness for the demineralised bones gave a mean of 2409 kJ/m^3 (± 844 SD).

A two-sample t-test was performed on these groups. This indicated no statistically significant difference between the results of the groups (p=0.214).

Figure 10.23 below shows the distribution of the values for toughness in the groups used above in the form of a box-plot.

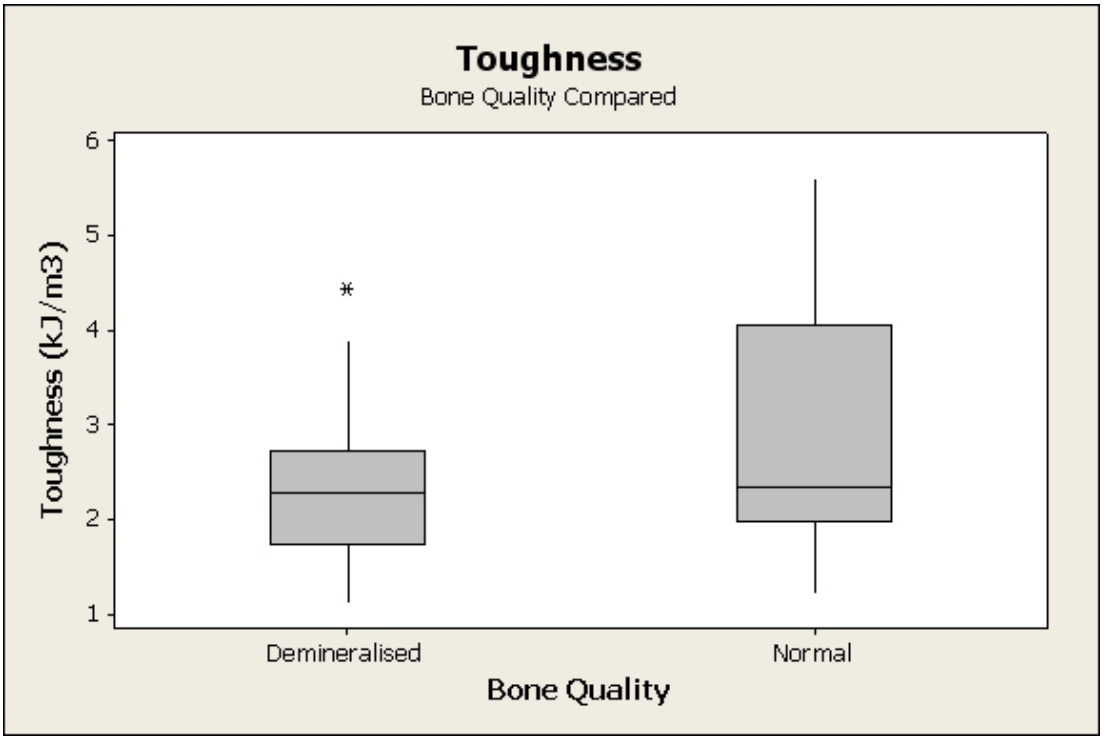

Figure 10.23: Box-plot of toughness by bone quality on ovine femurs

10.8.3 Toughness – by subgroup

The mean values of calculated toughness values in each testing group are shown in Table 10.23.

Testing Group	Toughness (kJ/m^3)	± SD
Fast Loading, Normal Quality	2039	584
Fast Loading, Demineralised	2030	538
Slow Loading, Normal Quality	3660	1360
Slow Loading, Demineralised	2789	946

Table 10.23: Mean values of toughness by testing group (ovine femurs)

This distribution of the values of toughness for the above testing groups is shown in Figure 10.24.

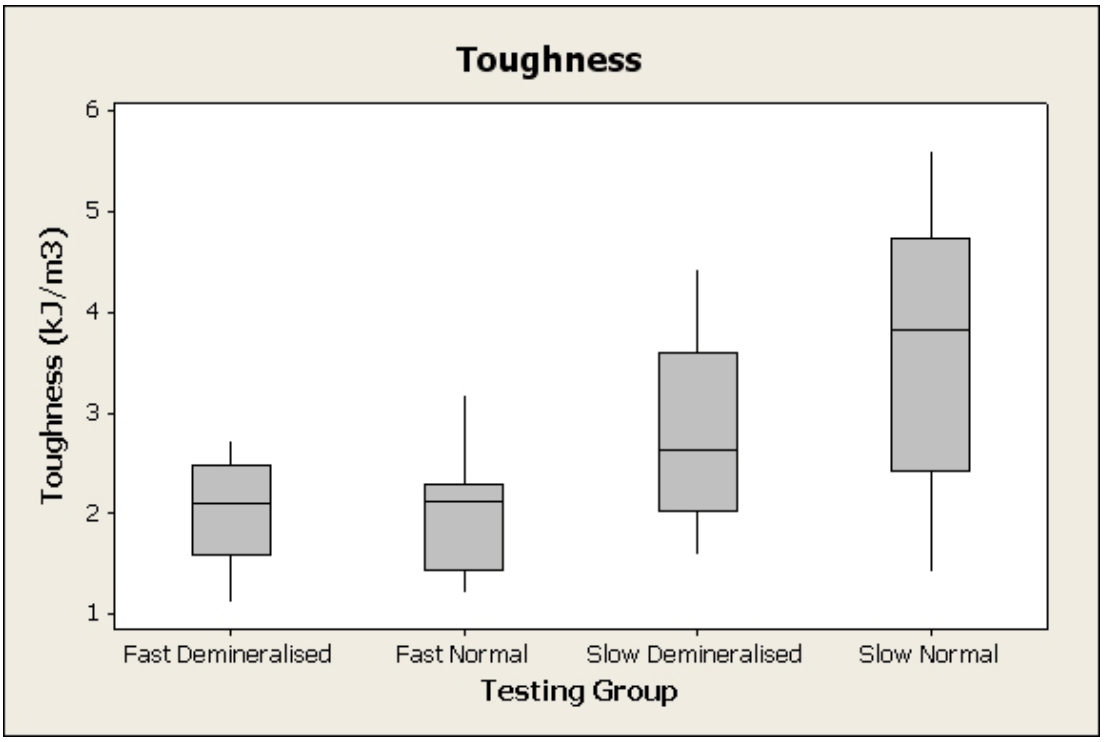

Figure 10.24: Box-plot of values for each testing group (ovine femurs)

A Tukey simultaneous test was used to assess statistically significant differences for toughness between the groups. The results of this statistical analysis are presented in Table 10.24.

Groups Compared (Toughness)	p-value	Significant
Normal Quality – Rate Compared (FN v SN)	0.0018	Yes
Demineralised – Rate Compared (FD v SD)	0.2668	No
Fast Loading – Quality Compared (FN v FD)	1.0000	No
Slow Loading – Quality Compared (SN v SD)	0.1611	No
Fast Normal v Slow Demineralised (FN v SD)	0.2775	No
Fast Demineralised v Slow Normal (FD v SN)	0.0017	Yes

Table 10.24: Tukey simultaneous test of toughness on ovine femurs

Statistically significant differences were found when comparing the effect of loading rate at normal bone quality. A statistically significant difference was also found between the fast loading, demineralised quality and the slow loading, normal quality groups. No other statistical differences were found.

A paired t-test was performed on the contralateral limbs within these groups. The results of this analysis for toughness are presented in Table 10.25.

Contralateral Pairs (Toughness)	p-value	Significant
Normal Quality – Rate Compared (FNr v SNr)	0.013	Yes
Demineralised – Rate Compared (FDr v SDr)	0.135	No
Fast Loading – Quality Compared (FNq v FDq)	0.056	No
Slow Loading – Quality Compared (SNq v SDq)	0.814	No

Table 10.25: Paired t-test of contralateral ovine femurs

A statistically significant difference was found when comparing the effect of loading rate at normal bone quality, this is in agreement with the results found in the larger testing groups. The effect of bone quality on the pairs loaded at a high loading rate was very nearly significant.

10.9 Normal Strain

As described in section 4.11, Timoshenko's beam theory was used to isolate the deflection due to bending and the deflection due to shear. The following analysis uses the calculated value of deflection due to bending to derive "normal strain". It is these normal strain values that are used in the following analysis.

10.9.1 All Data – Loading Rate Compared

The following analysis was carried out on all 40 specimens. Loading rate was selected as the variable for comparison, resulting in 20 specimens in each group.

The fast loading rate group had a mean value for strain at yield of 0.726 % (± 0.289 SD), the slow loading rate group had a mean value for the strain at yield of 1.896 % (± 0.464 SD). A two-sample t-test confirmed a statistically significant difference ($p<0.0005$).

Figure 10.25 below shows the distribution of yield strain in each group in the form of a box-plot.

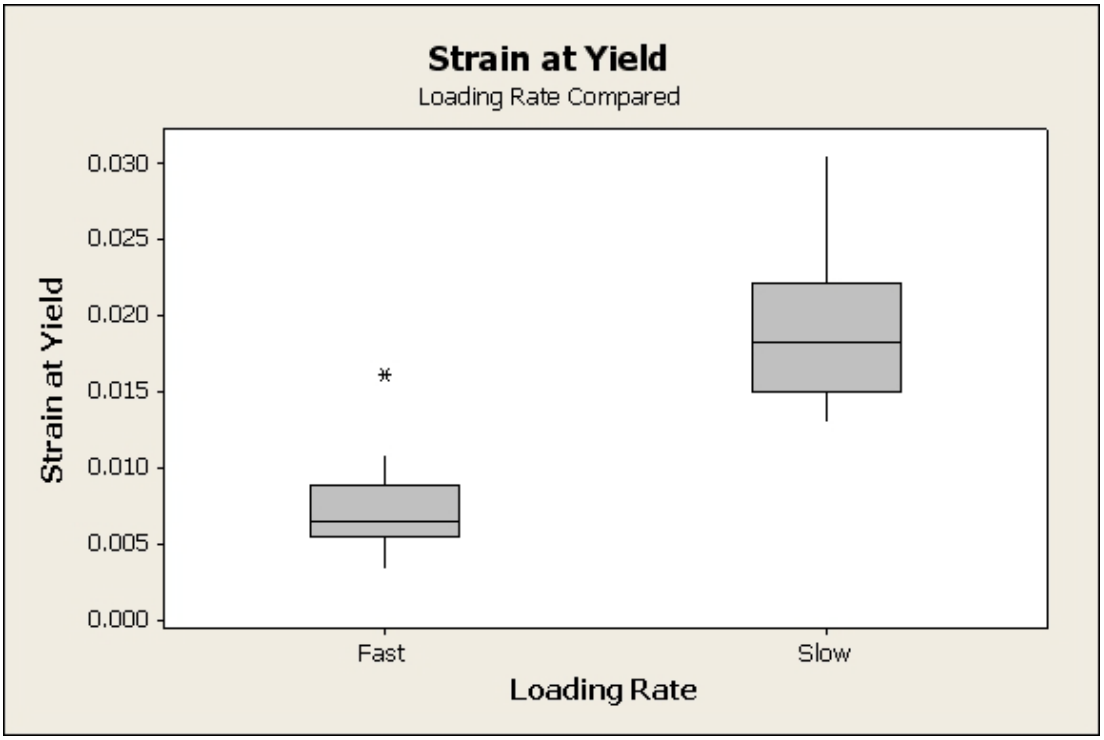

Figure 10.25: Box-plot of Yield Strain by loading rate on ovine femurs

10.9.2 All data – Quality Compared

When the yield strain was considered, the normal quality specimens had a mean value of 1.279 % (± 0.694 SD), the demineralised specimens had a mean value of 1.343 % (± 0.731 SD).

A two-sample t-test was performed on these groups. This indicated that there was no statistically significant difference between the results of the groups (p=0.780).

Figure 10.26 below shows the distribution of results for each bone quality in the form of a box-plot.

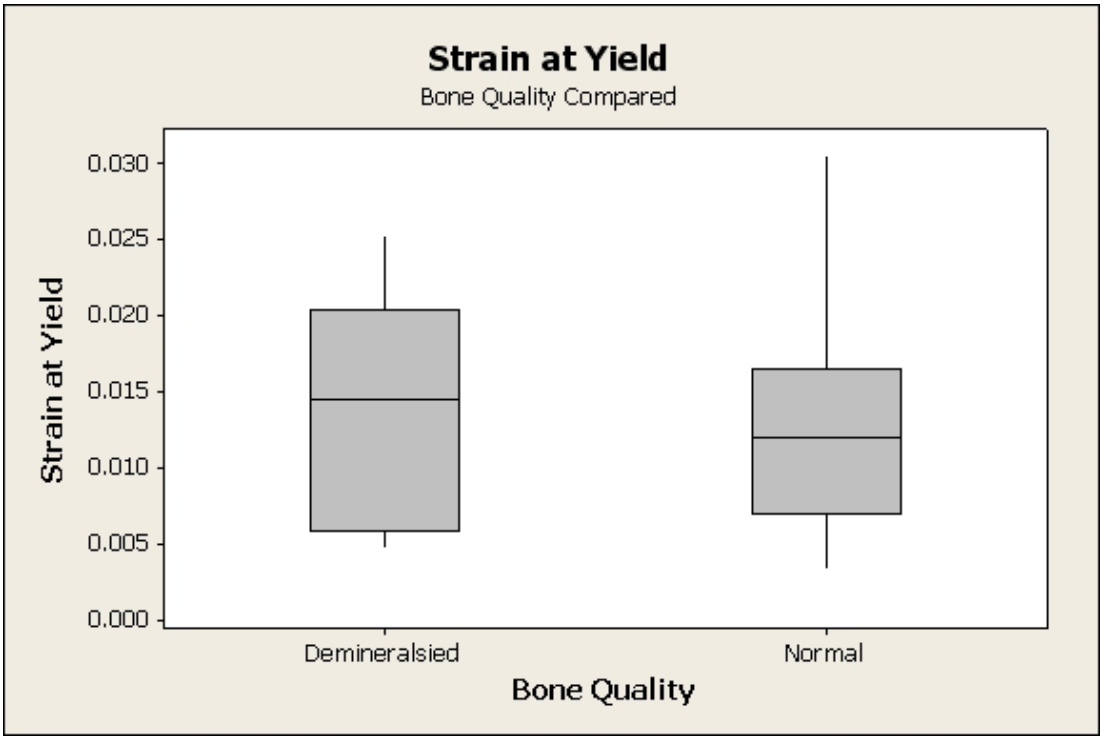

Figure 10.26: Box-plot of Yield Strain by bone quality on ovine femurs

10.9.3 Yield Strain – by subgroup

The mean values for yield strain in each testing group are shown in Table 10.26.

Testing Group	Strain (%)	± SD
Fast Loading, Normal Quality	0.736	0.251
Fast Loading, Demineralised	0.716	0.335
Slow Loading, Normal Quality	1.822	0.547
Slow Loading, Demineralised	1.970	0.379

Table 10.26: Mean values of Yield Strain by testing group (ovine femurs)

The distribution of yield strains in the above testing groups is shown in Figure 10.27

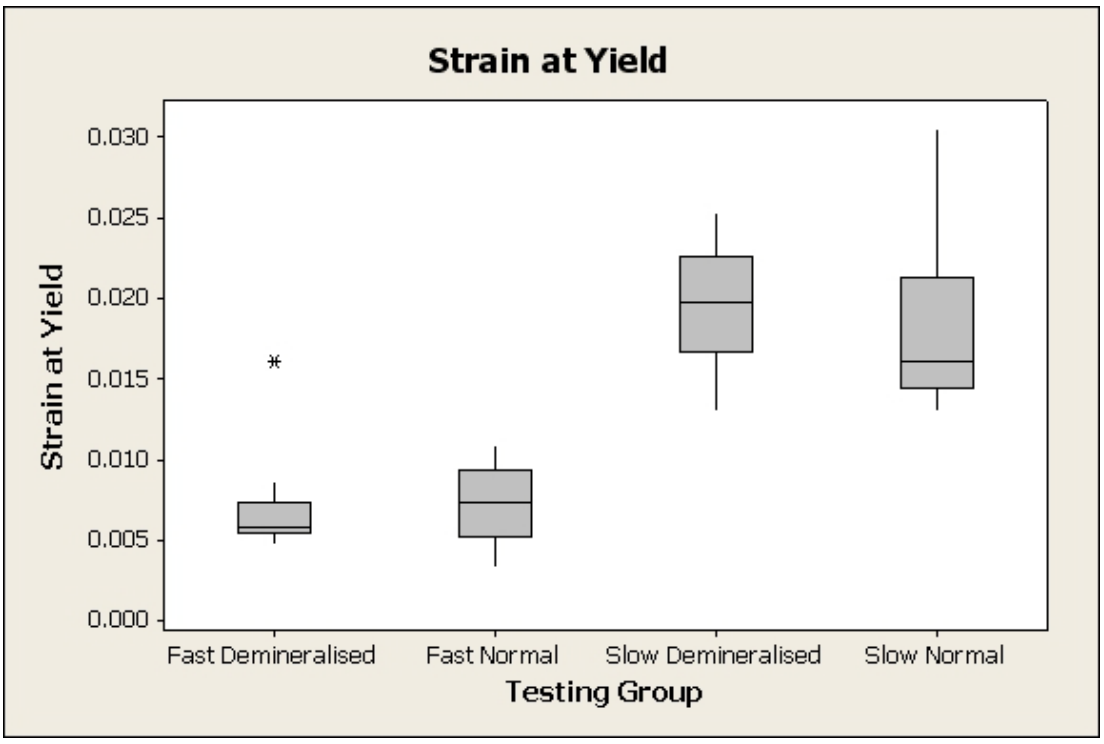

Figure 10.27: box-plot of yield strain for each testing group (ovine femurs)

A Tukey simultaneous test was used to check for statistically significant differences in the yield strain between the groups. The results of this statistical analysis are presented in Table 10.27.

Groups Compared (Yield Strain)	p-value	Significant
Normal Quality – Rate Compared (FN v SN)	<0.00005	Yes
Demineralised – Rate Compared (FD v SD)	<0.00005	Yes
Fast Loading – Quality Compared (FN v FD)	0.9994	No
Slow Loading – Quality Compared (SN v SD)	0.8362	No
Fast Normal v Slow Demineralised (FN v SD)	<0.00005	Yes
Fast Demineralised v Slow Normal (FD v SN)	<0.00005	Yes

Table 10.27: Tukey simultaneous test of Yield Strain on ovine femurs

Statistically significant differences were observed in both qualities of bone when loading rate was compared.

A paired t-test was performed on the contralateral pairings within these groups. The results of this analysis are presented in Table 10.28.

Contralateral Pairs (Yield Strain)	p-value	Significant
Normal Quality – Rate Compared (FNr v SNr)	0.023	Yes
Demineralised – Rate Compared (FDr v SDr)	0.017	Yes
Fast Loading – Quality Compared (FNq v FDq)	0.206	No
Slow Loading – Quality Compared (SNq v SDq)	0.157	No

Table 10.28: Paired t-test of contralateral ovine femurs

The findings for the contralateral limbs confirmed the results seen in the larger testing groups: Statistically significant differences were found when comparing loading rate in both qualities of bone.

10.10 Normal Strain at Failure

As in the preceding section, the strains used in the following analysis are the normal strains due to bending.

10.10.1 All Data – Loading Rate Compared

The following analysis was carried out on all 40 specimens. Loading rate was selected as the variable for comparison, resulting in 20 specimens in each group.

The fast loading rate group had a mean value for strain at failure of 2.344 % (± 0.608 SD).
The slow loading rate group had a mean value for strain at failure of 3.670 % (± 0.122 SD).
A two-sample t-test confirmed statistically significant difference between the groups was found ($p<0.0005$).

Figure 10.28 below shows the distribution of failure strain in each group in the form of a box-plot.

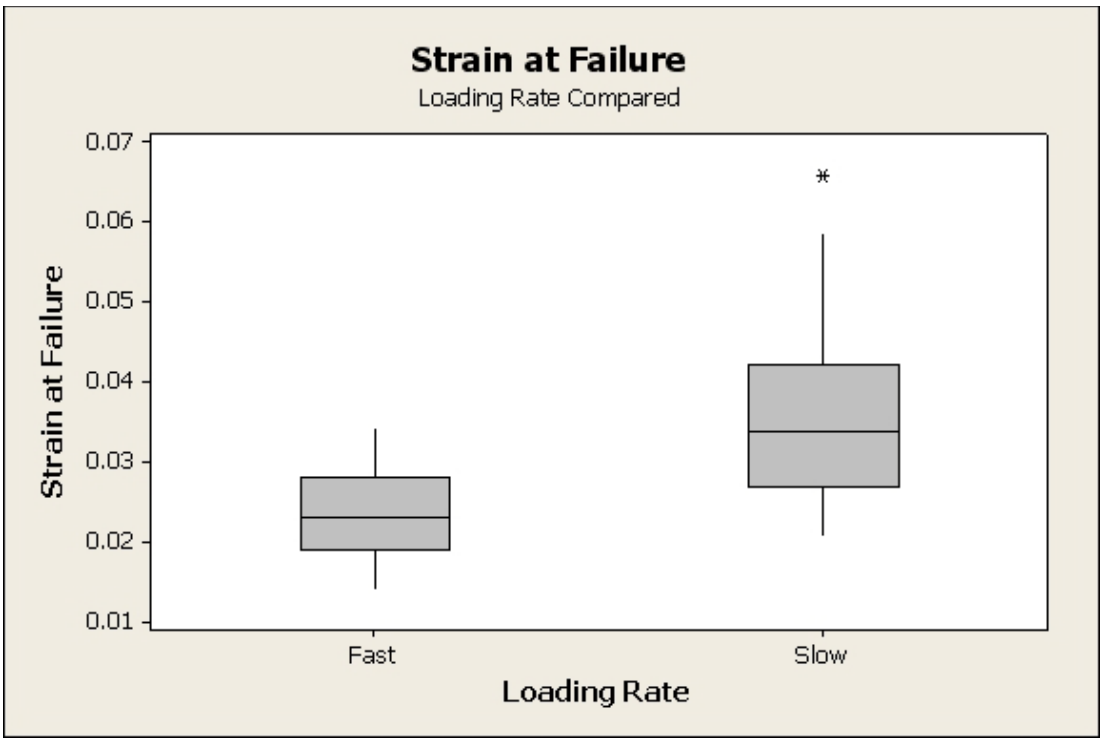

Figure 10.28: Box-plot of Strain at failure by loading rate on ovine femurs

10.10.2 All data – Quality Compared

Collating together the strain at failure for all the normal quality specimens presented a mean value of 3.150 % (± 1.41 SD), the demineralised specimens had a mean value of 2.864 % (± 0.864 SD).

A two-sample t-test was performed on these groups. This indicated that there was no statistically significant difference between the groups (p=0.450).

Figure 10.29 below shows the distribution of results for each bone quality in the form of a box-plot.

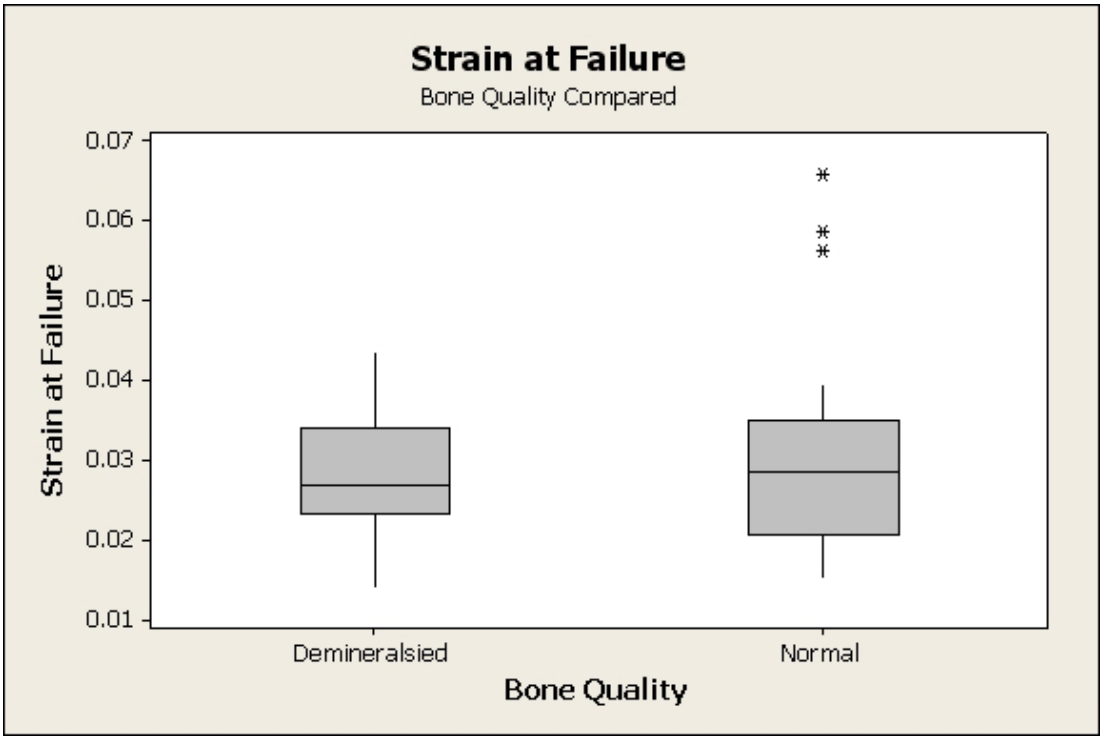

Figure 10.29: Box-plot of Strain by bone quality on ovine femurs

10.10.3 Strain – by subgroup

The mean values for strain at failure in each testing group are shown in Table 10.29.

Testing Group	Strain (%)	± SD
Fast Loading, Normal Quality	2.301	0.577
Fast Loading, Demineralised	2.387	0.666
Slow Loading, Normal Quality	3.990	1.510
Slow Loading, Demineralised	3.341	0.790

Table 10.29: Mean values of Strain at failure by testing group (ovine femurs)

The distribution of strain at failure in the testing groups is displayed in Figure 10.30

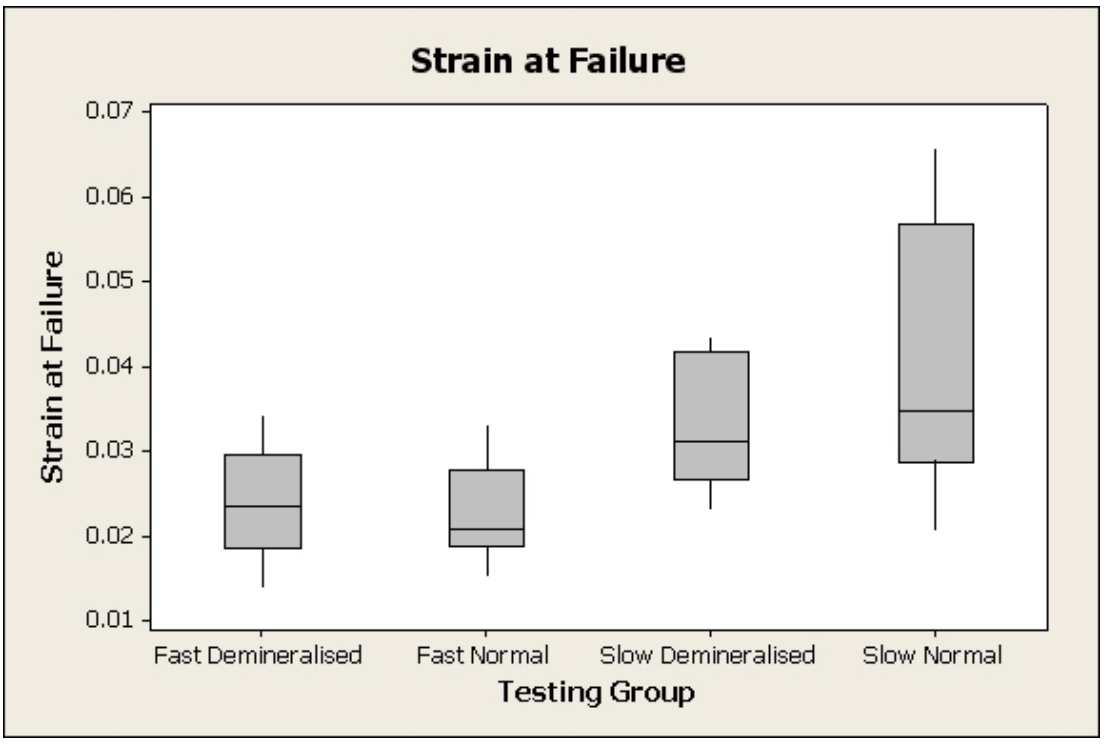

Figure 10.30: Box-plot of strain at failure for each testing group (ovine femurs)

A Tukey simultaneous test was used to check for statistically significant differences in strain at failure between the groups. The results of this statistical analysis are presented in Table 10.30.

Groups Compared (Strain)	p-value	Significant
Normal Quality – Rate Compared (FN v SN)	0.0019	Yes
Demineralised – Rate Compared (FD v SD)	0.1366	No
Fast Loading – Quality Compared (FN v FD)	0.9971	No
Slow Loading – Quality Compared (SN v SD)	0.4369	No
Fast Normal v Slow Demineralised (FN v SD)	0.0908	No
Fast Demineralised v Slow Normal (FD v SN)	0.0034	Yes

Table 10.30: Tukey simultaneous test of Strain at failure on ovine femurs

A statistically significant difference was observed in the slow loaded bones of normal quality when compared to the fast loaded bones of both qualities. No other statistically significant results were found.

A paired t-test was performed on the contralateral pairings within these groups. The results of this analysis for the strain at failure are presented in Table 10.31.

Contralateral Pairs (Strain)	p-value	Significant
Normal Quality – Rate Compared (FNr v SNr)	0.023	Yes
Demineralised – Rate Compared (FDr v SDr)	0.017	Yes
Fast Loading – Quality Compared (FNq v FDq)	0.206	No
Slow Loading – Quality Compared (SNq v SDq)	0.157	No

Table 10.31: Paired t-test of strain at failure between contralateral ovine femurs

The findings for the contralateral limbs showed statistically significant differences when comparing loading rate in both qualities of bone. No statistically significant differences were found when comparing bone quality at either loading rate.

10.11 Strain Rate

The strain rate for each test was found using the calculated values for normal strain at three distinct points, the time corresponding to these points was extracted from the loading data. The areas of interest were the yield point (Table 10.32), point of maximum loading (Table 10.33) and the failure point (Table 10.34).

Testing Group	Strain rate (s^{-1})	± SD
Fast Loading, Normal Quality	26.8	20.6
Fast Loading, Demineralised	15.39	5.88
Slow Loading, Normal Quality	7.94×10^{-3}	9.51×10^{-4}
Slow Loading, Demineralised	7.80×10^{-3}	2.84×10^{-4}

Table 10.32: Normal strain rate up to yield point on ovine femurs

Testing Group	Strain rate (s^{-1})	± SD
Fast Loading, Normal Quality	15.34	8.59
Fast Loading, Demineralised	18.34	5.84
Slow Loading, Normal Quality	9.642×10^{-3}	2.15×10^{-3}
Slow Loading, Demineralised	8.178×10^{-3}	6.48×10^{-4}

Table 10.33: Normal strain rate to max load on ovine femurs

Testing Group	Strain rate (s^{-1})	± SD
Fast Loading, Normal Quality	12.3	6.00
Fast Loading, Demineralised	16.09	6.66
Slow Loading, Normal Quality	1.04×10^{-2}	2.39×10^{-3}
Slow Loading, Demineralised	9.04×10^{-3}	2.77×10^{-3}

Table 10.34: normal strain rate to failure on ovine femurs

10.12 Differences between yield and fail point

The amount of post yield strain found for the samples was compared. The results for each testing group can be found in Table 10.35. These results were compared by means of a two-sample t-test. The results of this analysis are presented in Table 10.36

Testing Group	Post Yield Strain (%)	± SD
Fast Loading, Normal Quality	1.074	0.316
Fast Loading, Demineralised	1.415	0.353
Slow Loading, Normal Quality	1.316	0.835
Slow Loading, Demineralised	0.958	0.549

Table 10.35: Post yield strain on ovine femurs

Groups Compared (plastic strain)	p-value	Significant
Normal Quality – Rate Compared (FN v SN)	0.464	No
Demineralised – Rate Compared (FD v SD)	0.886	No
Fast Loading – Quality Compared (FN v FD)	0.994	No
Slow Loading – Quality Compared (SN v SD)	0.230	No
Fast Normal v Slow Demineralised (FN v SD)	0.966	No
Fast Demineralised v Slow Normal (FD v SN)	0.623	No

Table 10.36: Tukey simultaneous test of plastic strain on ovine femurs

The results from this analysis indicate that there were no statistically significant results between the groups.

10.13 Euler v Timoshenko Beam

The Young's modulus for all the tested femurs was found using both the Euler beam equation and the Timoshenko beam equation. A comparison of the results from these analytical methods is presented in Table 10.37.

Groups Compared	Mean Value	St Dev
Euler Young's Modulus	11.40	8.02
Timoshenko Young's Modulus	12.63	8.84
Difference	-1.234	0.847

Table 10.37: Euler v Timoshenko stiffness for ovine femurs

A paired t-test revealed a statistically significant difference with a p-value of <0.005.

10.14 Idealised v Non-prismatic beam

A method for incorporating the changing cross section of bone was employed in order to calculate the Young's modulus of elasticity of the bone more accurately. This was the conjugate beam method for non-prismatic beams as described in section 4.9.2. Before accounting for deflections due to shear by utilizing Timoshenko beam theory (section 4.10.2) values of Young's modulus were calculated using the entire measured deflection using both Engineers Bending theory (Euler beam method) and the conjugate beam method for non-prismatic beams. The results of these two analyses were compared using a paired t-test, the results of which as shown in Table 10.38 below.

Groups Compared	Mean Value (GPa)	St Dev
Euler derived Young's Modulus	11.40	8.02
Non-prismatic derived Young's Modulus	14.91	12.40
Difference	-3.51	6.35

Table 10.38: Paired comparison of beam stiffness for ovine femurs: Euler bending v non-prismatic Euler bending

This represented a statistically significant difference with a p value of 0.001.

This analysis was also completed using the predicted component of deflection from the Timoshenko beam equation, for both an assumed continuous cross section and by utilising the conjugate beam method for non-prismatic beams. The results of these two analyses were compared using a paired t-test, the results of which as shown in below.

Groups Compared	Mean Value (GPa)	St Dev
Timoshenko derived Young's Modulus	12.63	8.84
Timoshenko non-prismatic derived Young's Modulus	16.47	13.69
Difference	-3.84	6.93

Table 10.39: Paired comparison of beam stiffness for ovine femurs: Timoshenko v Timoshenko Non-prismatic

This represented a statistically significant difference with a p value of 0.001

10.15 Polynomial line of best fit v filtered data

In section 4.6 two methods of post processing of the fast loading rate data were discussed; A Butterworth low pass filter and the polynomial line of best fit. In the following section the respective results found by each method are compared.

10.15.1 Polynomial line of best fit v filtered data: Young's Modulus

A comparison of the values found for Young's modulus as found each method is presented in Table 10.40 for the normal quality bone and Table 10.41 for the demineralised bone. Statistical analysis was carried out by means of a paired t-test. The values of Young's modulus quoted were calculated using the bending deflection derived from the Timoshenko beam equation and analysed with the conjugate beam method for non-prismatic beams.

Groups Compared	Mean Value (GPa)	St Dev
Polynomial derived Young's Modulus	31.52	16.57
Butterworth filter derived Young's Modulus	10.54	3.60
Difference	20.98	14.01

Table 10.40: Effect of filtering on fast loading rate, normal quality ovine femurs

Groups Compared	Mean Value (GPa)	St Dev
Polynomial derived Young's Modulus	19.85	8.60
Butterworth filter derived Young's Modulus	9.13	2.90
Difference	10.72	7.41

Table 10.41: Effect of filtering on fast loading rate, demineralised ovine femurs

A paired t-test was performed on the date giving a p value of 0.001 for the normal quality comparison and a p value of 0.001 for the demineralised comparison indicating a statistically significant difference in both cases.

10.15.2 Polynomial line of best fit v filtered data: Toughness at yield

The toughness values found by calculating the area under the stress v normal strain graphs at the yield point for the polynomial line of best fit and the filtered data were compared for the normal quality bone in Table 10.42 and the demineralised bone in Table 10.43.

Groups Compared	Mean Value (J/m^3)	St Dev
Polynomial derived yield toughness	613	279
Butterworth filter derived yield toughness	1391	541
Difference	-778	564

Table 10.42: Effect of filtering on toughness at Yield for normal quality ovine femurs

Groups Compared	Mean Value (J/m^3)	St Dev
Polynomial derived yield toughness	481	278
Butterworth filter derived yield toughness	1371	576
Difference	-890	657

Table 10.43: Effect of filtering on toughness at Yield for demineralised ovine femurs

This represents a statistically significant difference for both bone qualities with a paired t-test giving a p value of 0.002 for the normal quality bone and a p value of 0.002 for the demineralised bones.

The reason for this significant difference was considered to be due to the smaller value for Young's modulus found by using the filtered data. This would result in the yield point being defined at a greater amount of strain than with the polynomial method.

10.15.3 Polynomial line of best fit v filtered data: Toughness at failure

The values for toughness found by calculating the area under the whole stress v normal strain graphs for the polynomial line of best fit and the filtered data were compared for the normal quality bone in Table 10.44 and the demineralised bone in Table 10.45.

Groups Compared	**Mean Value (J/m^3)**	**St Dev**
Polynomial derived toughness	2039	584
Butterworth filter derived toughness	1960	588
Difference	80	236

Table 10.44: Effect of filtering on toughness values for normal quality ovine femurs

Groups Compared	**Mean Value (J/m^3)**	**St Dev**
Polynomial derived toughness	2030	538
Butterworth filter derived toughness	1940	527
Difference	90	162

Table 10.45: Effect of filtering on toughness values for demineralised ovine femurs

A p value of 0.313 was found for the normal group, and a value of 0.114 was found for the demineralised group when compared using a paired t-test, indicating no statistically significant differences for the measurement of toughness with the polynomial equation or the filtered data.

11 Discussion

11.1 Experimental testing issues

Testing of any biological material can be subject to a number of complications that are not encountered when testing a traditional engineering material. The most significant of these is the repeatability (accuracy) of each test, as natural biological variations could produce results with a wide range of values. These problems are magnified when, as in this thesis, the material tested is the whole bone. In addition to variations in the construction of the components that make up the structure, there is likely to be variations in the size and shape of the whole bone.

The first of these issues could not be addressed by any testing methodology, in fact, it is the range of these variations that are desired to be studied. There are many approaches to the issue of the size of test specimen. Firstly, care should be taken to select animals that are of similar age and size. However, even with this approach, a range of size and shapes was seen on the femurs tested. Initially, it was proposed that the supports could be moved to provide fixation at the same anatomical site for each specimen. While this initially proved to be an appealing solution, the complexity of allowing small adjustments to the support locations on the high loading rate apparatus encouraged a different approach. Applying a fixed distance between the supports facilitated simplification when performing the stress analysis on the bones. As the range of sizes between the ovine femurs had been minimised by selecting animals of a similar height, it was possible to chose a fixed distance between the supports and have the bones attached at a similar location, so that only the diaphysis of the bone was stressed during loading. It was felt that this was an appropriate solution to the problem.

11.2 Data filtering

The experimental apparatus used for the testing in this thesis was subject to a system of continual improvement up to the point when the main body of experiments was conducted. One of the issues that could not be engineered out of the set up was the formation of an oscillating waveform from the dynamic force sensor. As discussed in section 4.6, this was considered to be due to the nature of the high loading rate experiments and the location of

the sensor. It was therefore necessary to remove these oscillations from the loading curve using a form of filtering.

Two different approaches to filtering the data were investigated. The first of these was a digital representation of a Butterworth type filter that was optimised for filter frequency and order. Even though a "flat response" filter type was used, the data plot was altered by a lead in/trail off phase response. This was shown to have a significant effect on the mechanical properties of stiffness and yield (as shown in section 10.15), in addition to introducing obstacles to accurate synchronisation with the displacement measurements.

The delay to the onset of the loading curve, and the reduction in gradient was shown to be a consequence of both the filter order and filtering frequency. Therefore this was considered to be an unavoidable function of applying a direct filter to the data.

Therefore a second method of smoothing the data was employed, using a line of best fit equation, and as such an individual equation was created for each loading curve. The line of best fit was achieved using a 6^{th} order polynomial equation. Applying this filtering method to the data was a more time consuming process, but it was considered to provide a better representation of the loading curve and was also not affected by the previously mentioned filtering phenomena meaning there were no further complications involved to synchronise the force data with the displacement data. Therefore this was demonstrated to be the most suitable approach to proceed with for the analysis.

11.3 Stress at traumatic loading rates

No statistically significant difference was found for demineralised bone when comparing peak stress between the two loading rates, with either the Tukey simultaneous test (ANOVA) of all the demineralised bones ($p = 0.9532$) or in the paired tests on contralateral limbs ($p = 0.153$). This was considered to be a very interesting finding.

The strain rate was shown to have a large effect on the stress at failure when all tested specimen were grouped for comparison and also when only the normal quality bones were compared. In the comparison between all the testing groups the fast loaded, normal quality group demonstrated a significant difference in failure stress to all other groups. It should be noted that for demineralised bone, the high strain rate experiments did show an increase in

the mean value of maximum stress with increasing strain rate but that this increase was not statistically significant (Fast Demineralised v Slow Demineralised $p = 0.6429$).

These results show that bone has an ability to withstand high stresses for a short period of time and that this ability is reduced with demineralisation. Studies by Hansen (2008) with compressive loading over similar rates of strain found in this study and by Ferreira (2006) using the split Hopkinson pressure bar applying tension at rates of strain in excess of those used in this study, showed that there was an increase in the stress required to cause failure. Both of these investigations of the effect of strain rate were performed on idealised sections of bone.

This large reduction in shock loading capacity that was found to occur with demineralisation could offer some explanation as to why low mineral density bone can suffer failure at stresses not much higher than found in physiological activity, i.e. in a trip or fall situation where the impact force is large, but not excessively so. It should also be stated that other factors such as increased microcracking, poor quality collagen and a reduced cross sectional area will also be contributing factors to bone fracture in the instance of a trip or fall with aged or diseased bone, but that these factors remained constant between the tests performed in this study. Therefore these results can be said to isolate the effect of mineral at high strain rate.

Therefore, it can be said that that the ability to withstand higher stresses at a higher rate of strain transfers to whole bone and that this ability is lost by reducing the mineral content alone. This finding was considered to answer one of the main research questions of this study.

11.4 Stress at slow loading rate

It was found that the effect of demineralisation on both the yield stress and the stress at failure of the bone was minimal at low strain rates, as the Tukey simultaneous tests performed on all the data did not show a significant difference for either yield stress or stress at failure.. However the contralateral pairs comparing failure stress at a slow loading rate with normal and demineralised bone did show a significant difference ($p = 0.007$). The fact that the slow loading, quality altered contralateral pairs did show a significant difference in the stress at failure confirms that the mineral plays an important role in bone strength.

The lack of a statistically significant difference in the stress at failure when comparing bone quality between all the slow loaded specimens could be explained by variability in the biological samples: even if the stress at failure was reduced by demineralisation it may still be in the region of values found for some of the specimens with normal bone quality. This confirms the importance of utilizing the contralateral samples to facilitate a more meticulous form of statistical testing, especially when testing biological materials. Intuitively, one would expect a comparison of like with like (or before and after) to provide a better basis for comparison. The principal drawback of using contralateral specimen is the large amount of animals that are required to perform tests, especially if more than one primary variable is investigated, as there was in this study.

It should be noted that expected trends of stress increasing with strain rate and mineral content were found, even where the difference was not statistically significant.

11.4.1 Pre-yield displacement of the loading graph

It was observed on 13 out of 20 of the slow loaded tests that there was a point on the loading curve where there was an increase in displacement for no additional force. After a brief translation, the loading curve continued as it had before, where force and deflection increased. This was termed slide/slip-displacement. The presence of this slide/slip-displacement in some, but not all of the slow loading tests presented a problem when determining the yield point of these tests.

An example of the slide/slip displacement can be seen in Figure 11.1 below.

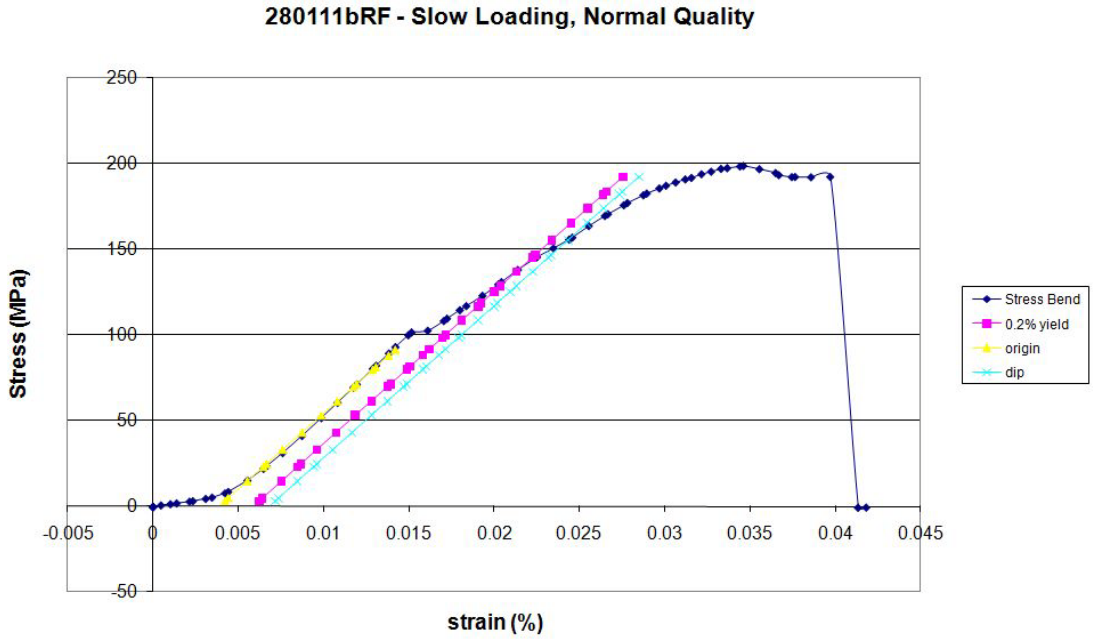

Figure 11.1 Example of slide/slip in normal quality bone

It was considered that if the slip / displacement occurred in the initial stages of loading (to around 50% of maximum load) then the likely cause of this was a movement of the bone on the supports. This was not considered to be representative of the true load / deflection curve of the bone and therefore inclusion of this no-load translation would not give an accurate representation of mechanical properties such as yield or stiffness.

If the no-load translation (translation for no extra added load) occurred above the point used to define a movement on the supports then it was considered that this may be due to a failure at the loading point of the bone. As this was considered to be the onset of failure of the bone then the indicated location for yield was considered to be valid. It should be noted that the calculated value for the Young's modulus of the bone would not be affected by this translation of the stress-strain curve.

It is recognised that there is uncertainty in the cause of the no-load translation. The primary reason for this uncertainty was due to the inability to closely observe all the aspects of the experiment at the same time. Watching the actual test live, along with the curve of load v deflection gave competing interests for the observer. Additionally, the actual displacement that occurred was very slight. It is unlikely that even with close observation the cause could

be identified in the live test. Therefore the post test classification of this phenomena was considered to be appropriate.

11.5 Yield Stress

In the slow loaded tests, yield occurred at an identifiable point. The yield point on the high strain rate experiments was not simple to determine accurately due to the effects of filtering the data. This lack of identifiable yield point on the high strain rate experiments impedes comparison between the two sets of data. These results would suggest that further work is carried out to improve the accuracy of both identifying the yield point in high strain rate tests and deriving a value for the stress at this location.

11.5.1 Effect of Quality at slow loading rate

The slowly loaded demineralised specimen displayed a higher yield stress than the slow loaded normal specimen. This was thought to be due to the lower value of Young's modulus in these specimen, resulting in the intercept between the 0.2% offset stiffness line and the stress plot occurring further into the loading process and therefore resulting in a higher value of stress.

11.6 Young's Modulus

In the Tukey simultaneous tests performed on the results for Young's modulus, a statistically significant difference was found for all comparisons except when examining the effect of bone quality at the slow loading rate. When the data from the contralateral paired limbs was examined by means of a paired t-test, statistically significant differences were observed when examining the effect of loading rate on both qualities of bone, but not when examining the effect of bone quality in either fast or slow rates of loading. Therefore it can be concluded that the loading rate was the dominant influence on stiffness.

It is recognised that evaluating the Young's modulus of bone from bending tests is more difficult compared to tensile or compressive tests. However, as traumatic loading is often the form of a bending load, calculating the Young's modulus from tests performed in bending can have physiological relevance for situations involving trauma. Additionally, traumatic

fracture occurs at a rate of strain significantly higher than that normally used in laboratory testing protocols. Therefore testing bone in bending at high loading rates more closely represents the physiological types of loading that would cause failure to occur.

This study found a mean value of 7.4 GPa for the slow loaded tests on ovine femur of normal quality. When compared to the values of 16.7 GPa and 19.7 GPa found for human femur and bovine tibia extracted from tension testing in Currey (2002, p130) or the value of 10.1 GPa taken compression tests performed by Reilly and Burstien (1975) it can be seen that the Young's modulus for the femurs used in this study are lower than examples found in the literature.

A potential reason for this discrepancy could be due to extracting the Young's modulus from bending tests on whole bone. The examples quoted above were extracted from testing conducted on idealised sections of bone. It was considered that the fact that these tests derive a local measure for the Young's modulus compared to an overall value for the whole bone as was found by the testing conducted in this study could be responsible for some of the variation. In addition to the above, a further source of error could have been introduced by the shear modulus, which was an unknown property and was estimated as a ratio of 3:1(as discussed in section 4.10.1) for this study. As this value is used to derive the normal strain in accordance with Timoshenko's bending theory an erroneous value would lead to an incorrect normal strain, which in turn would lead to errors in the Young's modulus. When testing with long, thin sections of bone the contribution from shear, and therefore the importance of the shear modulus is not as great as when the comparably short and deep whole bones are used for bending tests. As these sources of error apply to all the ovine femurs tested in this research the conclusions derived regarding comparisons between the groups were considered to be appropriate, but care should be taken when comparing absolute values between different studies.

The hierarchical composite nature of bone was considered to be a likely reason for the wide range of calculated Young's modulus values found for the high loading rate tests. Local areas of higher than average mineralization could provide a stiffer response, while an area of local microcracking could give rise to a less stiff response. This issue would not influence the slow loading tests to the same degree as there would be sufficient loading time to allow redistribution of the load over areas differing in local stiffness. There may be insufficient

time for this to occur in the higher loading rate tests, giving the wide spread of stiffness values found.

In addition to the physiological reasons outlined above, the method of measuring the displacement from the high speed camera images, as well as the effect of smoothing the data could be contributory factors for the outliers in the data.

11.6.1 Influence of Non-prismatic cross section

It was shown that analysing the bone as a nonprismatic beam made a significant difference to the calculated value of Young's modulus. It is recognised that finite element modelling is used in much of the analysis that is carried out on bone, which will by the nature of the models, take the effect of changing geometry into account. However, accurate results from this technique depend on accurate models, usually requiring full CT scanning of the bone.

The significance of this finding could have relevance to testing performed with animal models where there is often not the resources to implement a full scaled, detailed modelling approach. Furthermore, there is the possibility of applying these methods to existing studies where a constant cross section was presumed in order to increase the accuracy of these results. In addition to this, radiographic data could be used to approximate the change in cross section. If this is combined with density assessment, such as DEXA scanning or a calibrated step wedge, accurate analysis could be conducted with patient data without the need for more intensive procedures such as a CT scan.

11.7 Displacement

The measured values of displacement at fracture provided interesting results as no statistically significant differences were found between the contralateral pairs although the paired test comparing loading rate between normal quality specimens was nearly significant ($p = 0.061$).

This contrasted with the findings from the ANOVA derived Tukey simultaneous tests where all the specimens in the testing groups were collated for assessment. In these tests, statistically significant differences were found for the Fast Loading, Normal Quality bones

when comparing them to demineralised bone at both loading rates. This implies that the amount of deflection before failure in bone of reduced mineral content is not dependant on loading rate.

11.8 Work

It was observed that strain rate was the dominant variable for the energy to deflect the bone.

The majority of the findings in this study show a trend of increasing values with an increase in strain rate. This was not demonstrated by the work of deformation, the slower loading rate resulted in a significantly larger area under the force deformation curve as indicated by the p-value of 0.001 when comparing the effect of loading rate on normal quality bone, a p-value of 0.0495 for the comparison between Fast Normal and Slow Demineralised and a p-value of 0.0023 for the comparison between Fast Demineralised and Slow Normal in the Tukey simultaneous tests (ANOVA).

11.9 Toughness

A similar pattern of results was found for toughness as was observed in the energy of deformation: results were significantly different for strain rate and it was the slow loading tests that resulted in the higher values. This similarity between energy and toughness would be expected as both parameters area taken from the area under a graph representing deformation due to an external stimulus. The findings for toughness also take into account the geometry of the samples under investigation.

If microcracking is the primary toughening mechanism then this finding would imply that during a traumatic loading event there is insufficient time for the microcracking process to fully take place. At lower strain rates energy can be dissipated in the form of microcracks.

This division between the strain rates was even more pronounced at the yield point, highly significant differences were found when comparing all combinations of bone qualities loaded at different loading rates (FD v SD, FD v SN, FN v SD, FN v SN). Further analysis on the contralateral paired limbs showed significant differences when loading rate was altered for both qualities of bone, but not when quality was altered for either high or slow rates of loading.

When the toughness at failure was considered, statistically significant differences were observed for the Tukey simultaneous tests only when comparing slow loaded bones of normal quality with fast loaded bone of both normal and demineralised qualities. The analysis on the contralateral limbs revealed a statistically significant difference only when loading rate was compared between bones of normal quality. It is recognised that as there was a degree of uncertainty in determining the yield point at the higher loading rate these results may not be conclusive, but as they are supported by the findings at failure they are at least indicative.

11.10 Ultimate strain

When the effect of shear deflections had been accounted for by applying the Timoshenko beam equation the resulting mean values for normal strain at failure were found to agree with those predicted by tensile testing in the literature.

It was expected that the comparison of results for strain between the groups would give similar findings to the results for displacement. However, the results for strain at failure showed a stronger influence of the loading rate at both qualities. This was evident in the comparison between the testing groups and the contralateral limbs. No significance was found when comparing bone quality at either loading rate. When the effect of loading rate was compared the fast loading rate was found to produce significantly less strain before failure for both bone qualities.

11.11 Shear Modulus

The Timoshenko bending equation requires values for the Young's Modulus, E, and the Shear Modulus, G. As both of these values are unknown, it was required to take an initial value for one of these properties from the literature. The behaviour of the bone due to bending was the main focus of this study, therefore it was considered more appropriate that the value for the shear modulus should be inferred from the literature. This would allow the Timoshenko beam equation to derive a value for the young's modulus in addition to attributing the total measured deflection between the contributions from bending and shear.

It was recognised that the choice of G would have an influence on the amount of deflection attributed to bending and hence the values for normal strain and stiffness. Bones, like all biological structures, are subject to variability's in their mechanical properties far in excess of those encountered in traditional structural materials. With this in mind it was considered appropriate that the shear modulus should be expressed as a ratio of the Young's modulus. This would allow some degree of compensation for the variability of stiffness between samples, as any variability in one modulus would be proportionally reflected in the other. If a fixed value for the shear modulus was used it would likely have a disproportionate effect on the spread of results. Applying the ratio of 3:1 for the elastic modulus to shear modulus resulted in the values of shear modulus shown in Table 11.1 below.

Testing Group	Shear Modulus (GPa)	± SD
Fast Loading, Normal Quality	7.82	3.14
Fast Loading, Demineralised	5.00	2.83
Slow Loading, Normal Quality	2.37	0.65
Slow Loading, Demineralised	1.93	0.42

Table 11.1: Shear modulus in cortical bone of ovine femur

When considering the reasons why such a high ratio of 3:1 exists between the two moduli one must consider the hierarchical nature of bones construction. In addition to this, the directional nature of this hierarchy must also be taken into account. The fibres, osteons and lamella that make up the structure of bone have been shown to run in the longitudinal direction of long bone. This is an advantage as the bone will be stronger in the regular loading direction, and as this axis is also the direction of bone growth, having the components of the structure orientated in this direction will not encumber growth. A possible explanation for the larger than expected gap between moduli could be due to these structural features being less bound in the non preferential direction which in turn may provide less resistance to deformation, and hence a lower modulus of stiffness.

The implication of bone having a low shear modulus for transverse loading is that it endows the bone with the ability to endure greater deformation when subjected to an out of plane load than would be predicted from its Young's modulus. This is a direct effect of the composite structure of bone bestowing a beneficial property of impact protection.

11.11.1 Effect of demineralisation on the shear modulus

There is no evidence to predict what affect strain rate or partial demineralisation would have on the ratio of Young's modulus to shear modulus. The assumption that a proportional relationship between these two variables would remain at both different strain rates and different bone qualities was considered to be the most logical path to take. Further work is required to test that this hypothesis was correct.

It is not known if the ratio of E to G will remain the same, or even remain proportional after partial demineralisation. In the absence of evidence, it was considered appropriate that the ratio should remain unchanged as no grounds could be given for modifying it one way or the other. It is proposed that the effect of partial demineralisation on the shear modulus be investigated after completion of this study.

11.12 Fracture surface area

The fracture surface area analysis revealed a strong correlation between the newly created fracture surface and the Young's modulus of the bone. In addition, it was observed that the specimen with the highest value for Young's modulus was the specimen that suffered the greatest comminution. Reducing the level of mineral in the bone resulted in less comminution, although oblique fractures were obtained. This could provide an interesting basis for further study (section 13.1)

While no strong correlation was revealed with the other variables, there was a correlation in the fast loading rate tests between fracture surface area, displacement and toughness. Additionally, there was a slight correlation for the fracture surface area with both the force and stress. For the other three testing groups, slow, normal and demineralised the best correlation was with toughness. These early findings do show potential that a more detailed analysis might reveal further insight.

In this study, no distinction was made between the direction of the fractured surfaces. It has been demonstrated that the energy required to propagate a fracture in the transverse direction

is greater than that required to propagate a longitudinal crack. When considering the structural elements of bone, this would be expected as a transverse crack is required to pass through features such as osteons and across the prevailing direction of the fibrils that make up cortical bone, while a crack in the longitudinal direction can run parallel to these elements. This should be considered as a direct effect of the directionally dependant composite of a composite structure that makes up bone.

Additionally, this study did not account for surface roughness. When examined in detail the undulations encountered in a rough fracture surface could add considerably to the true surface area created by the fracture process and therefore the energy required to create that surface. In order to derive the surface area imaging techniques like scanning electron microscopy (SEM) could be employed. If two images are taken of the same surface, but at different angles, the height of any features on that surface can then be derived. It is hoped that by incorporating these two additional analysis methods a better representation of the fracture surface area and of the energy required to create this new surface area can be realised and that this will provide a stronger correlation with the strain rate and the energy of deformation in the bone.

11.13 Variation of Results

It can be seen from the results presented in Chapter 10, that there is a large range of values covering the calculated stiffness of the bones, especially when considering the high loading rate experiments. The hierarchical composite structure of the bone can explain some of this variation, as even the contralateral paired bones will have variation as the scale length decreases. These variations, coupled with the previously discussed effects of filtering the data, were reasoned to be responsible for most of this variation. However, the act of applying a large load in a few milliseconds could add in further variation to the results as the load will initially be carried by the stiffer sections of bone. In a slowly loaded specimen there will be time for the load to be redistributed throughout the structure, especially as yield is approached. If there was insufficient time for this redistribution of load to occur the specimen could be in a state of loading where more of the load is carried by stiffer sections, such as any highly mineralised sections, this could be indicated by the stiff initial response to loading. This uneven loading could promote crack formation and growth, leading to the occurrence of a rapid fracture, which would be indicated by a reduced measure of toughness.

Additionally, other features, such as osteons, will not be evenly distributed throughout the structure. The distribution of holes, voids and dislocations that have the potential to act as both crack stoppers and crack initiation points could have an influence on the perceived toughness of the bone and on the fracture pattern that results when failure occurs.

11.14 Microcracking process

As discussed in section 2.7, bone displays a microcracking response to overloading. These very small cracks form in isolation to each other. This provides the opportunity for maximum toughening before a full thickness fracture occurs. The formation of these cracks around the tip of a large crack also show that there is a "damage zone" (Vashishth and Tanner 2003) ahead of the progression of a major crack. The range and distribution of these microcracks show the localised area of the bone that is subjected to a stress greater or equal to the yield stress, or microcracking initiation stress. The energy required to form these microcracks can be considered to have been removed from the energy supplied to grow the main crack, thus increasing the toughness of the bone.

This can be thought of as a direct effect of the hierarchical structure of bone, as there are toughening mechanisms at work on each level of the hierarchy, through protein unravelling and collagen fibril bridging at smaller end of the hierarchy to microcracking and fracture path diversion at the level of whole bone. These effects, and the differing scales that they are involved on, are thought to be responsible for the differing fracture patterns that were found between repeated tests In fact, it was considered that even if the same bone (or one identical at all levels) was loaded in exactly the same way, it would not be guaranteed to result in exactly the same fracture pattern on both instances.

11.15 Fracture Pattern

It was observed that the higher loading rate tests produced fractures with varying degrees of comminution. This range of comminution was not seen in the slow loaded tests. The reasons discussed above in section 11.14 can explain the variation in fracture pattern, but the comminution that was seen only in the high loading rate tests was considered to be due to influence of the structure at the larger end of the hierarchical scale. In the slow loading tests, there will be time for any crack growing and crack stopping process to occur. In the high

loading tests this assumption cannot be made. Therefore, it follows that more than one crack would be grown; where in the slow tests the fracture would be encouraged to propagate along one path

11.16 Effect of Demineralisation

The research conducted in the main body of this thesis isolated the role of mineral content to act as a variable for bone quality. It is recognised that there are many other contributing factors to the overall quality of bone, but none of these other factors, such as the number of and distribution of microcracks, and the elasticity of collagen could be assessed in a patient clinic setting. The most used assessment method is that of bone mineral content and as such it was considered appropriate that it was the mineral content alone that was used as a variable for this study.

The process of removing only the mineral from the bone, while keeping all other aspects of the structure unchanged is perhaps not representative of how under mineralised bone would occur in nature, where the bone would form without sufficient mineral there. The intricacies of this formation and the influence this would have on the mechanical properties of the whole bone structure was beyond the scope of this thesis. Never the less, one should be mindful of the differences between naturally occurring bone of low mineral content and that created in the lab.

12 Conclusions

Cortical bone has an ability to withstand much greater stresses if these stresses are applied fast and for a short duration, such as would happen in a fall or accident. When the quality of bone is reduced by demineralisation this ability is lost.

However, demineralisation does not have a significant effect at the high loading rate on the toughness of the bone. As this property has been shown to be negatively affected with age, these negative effects are not realised as a singular result of the mineral loss that occurs with aging. It is believed that in addition to the loss of mechanical strength that occurs with mineral loss, a combination of a build up of microcracks that occurs in old bone and a reduction in the quality of collagen present in the matrix of the bone is responsible for the increase in fracture risk that occurs with age.

A greater amount of post yield deformation, or strain hardening, was found in the bones tested at a high loading rate. This could appear as a contradiction to the findings that the slow loaded bone is tougher, as it would be expected that a higher failure stress coupled with more strain hardening would produce the greatest values for toughness. However, as Burr (1985) and Bruce (2003) have shown, microcracking acts as a stimulus for bone remodelling. This implies that microcracking occurs below the yield stress. Therefore there is likely an additional form of plastic deformation occurring that constitutes the viscoelastic behaviour of bone when a high loading rate is applied that accounts for this strain hardening.

It could be considered that normal quality bone has an ability to withstand traumatic blows as a higher stress was required to cause failure. This ability was reduced when the mineral was reduced, as indicated by the lower stress required to cause failure. This could show one of the symptoms of why poor quality bone is more susceptible to fracture due to falls, or is more severely damaged in a high energy type impact. The normally present ability to cope with a temporarily high state of stress is no longer there, leading to a far lower critical stress to cause fracture.

In addition to the demonstrated reduction in failure stress occurring at high loading rates due to mineral loss, there could be an even greater decline in the failure stress of aged or diseased bone due to a build up of microcracks and a reduction in the quality of the collagen matrix that have been shown to occur with age.

The findings from the fracture surface area experiments indicate that inferring the energy of injury from the degree of comminution seen on a radiograph must be done with caution unless the degree of mineralisation is also known.

13 Future Work

13.1 Fracture surface area

One of the aspects of this study that would benefit from further investigation is the correlation of fracture surface area to trauma energy. This study demonstrated that there was a correlation between the loading rate and the newly created fracture surface, but this was in some ways a simplistic analysis. The principal simplification was to treat all newly created fracture surfaces the same.

The research carried out in this study should be expanded by a detailed examination of the surface roughness. This information may shed more light on the amount of energy that was involved in propagating the crack and if a correlation between the surface roughness and fracture energy is established for the specimens used in this study then a more detailed analysis could be conducted

This study found a correlation between fracture surface and stiffness and that the stiffer, more mineralised specimens suffered comminution as a result of traumatic loading. This could have implications on the prescription of bisphosphonates as a treatment for osteoporosis. It the bones become more mineralised, but are otherwise structurally poor, then a more serious fracture could result from minor trauma.

13.2 Optical Strain Measurement

The attempt to implement an optical method of measuring strain was not successful in this study. However, it has been used successfully by other researchers (Thurner et al 2007, Barak et al 2009), albeit at a greatly reduced rate of strain.

If the requirements for a high resolution, high speed camera can be met, then the use of this technique could provide a very useful method for investigating the strains developing at all points on the bone during deformation. Additionally, the strain rates at various points in the loading process can also be found using this technique. It is hoped that this may show when

certain areas of the bone have begun plastic deformation, while others are still in the elastic region.

It should be noted that there are currently high speed high definition cameras that could be used to achieve these goals. The downside is at the present moment the relative cost of these devices would dissuade against speculative investigation of this technique.

13.3 Other loading modes

The testing apparatus for high loading rate was designed to be able to accommodate a large range of bone sizes. With suitable ethical approval, this equipment could be used to study high loading rate effects in whole human bone. This could allow the direct study of the viscoelastic effects on osteoporotic bone.

In addition to this, the bone holder tower could be repositioned on the base plate facilitate the application of torque to the bone. As torsion produces shear loading in the bone, the effects of shear at a high loading rate could be studied.

13.4 Effect of storage

Further analysis could be carried to examining the effect of storage at traumatic loading rates. Other loading types, such as torsion, compression and tension should be investigated before publication of these findings in a peer reviewed journal, although it is recognised that a greater number of tests would be required before publication could be achieved.

13.5 Finite Element Analysis

The results found in this study, particularly for the demineralised bone, provide an interesting set of properties that could be applied to a finite element model. It is recognised that to fully replicate the bending behaviour a non-linear analysis should be applied to these models which will increase not only the accuracy but also the complexity. If sufficient resources can be allocated to such a study the viscoelastic effects should also me modelled. It would therefore be prudent to construct the model from a detailed CT scan in order to fully represent the geometrical features of the bone.

14 Appendices

14.1 Appendix A: Data sheets

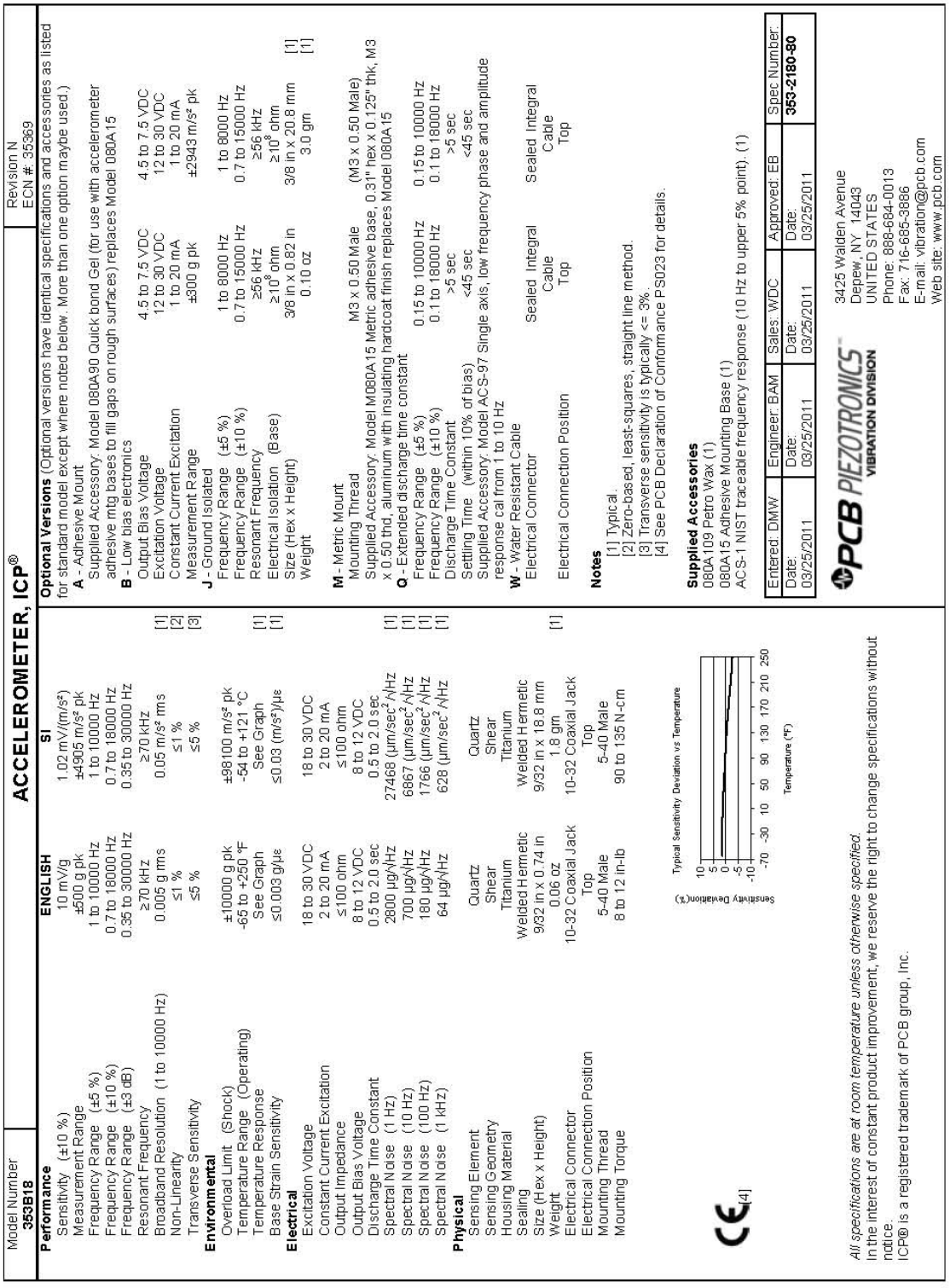

Model Number 353B18

ACCELEROMETER, ICP®

Revision N
ECN # 35369

	ENGLISH	SI	
Performance			
Sensitivity (±10 %)	10 mV/g	1.02 mV/(m/s²)	
Measurement Range	±500 g pk	±4905 m/s² pk	
Frequency Range (±5 %)	1 to 10000 Hz	1 to 10000 Hz	
Frequency Range (±10 %)	0.7 to 18000 Hz	0.7 to 18000 Hz	
Frequency Range (±3 dB)	0.35 to 30000 Hz	0.35 to 30000 Hz	
Resonant Frequency	≥70 kHz	≥70 kHz	
Broadband Resolution (1 to 10000 Hz)	0.005 g rms	0.05 m/s² rms	[1]
Non-Linearity	≤1 %	≤1 %	[2]
Transverse Sensitivity	≤5 %	≤5 %	[3]
Environmental			
Overload Limit (Shock)	±10000 g pk	±98100 m/s² pk	
Temperature Range (Operating)	-65 to +250 °F	-54 to +121 °C	
Temperature Response	See Graph	See Graph	[1]
Base Strain Sensitivity	≤0.003 g/με	≤0.03 (m/s²)/με	[1]
Electrical			
Excitation Voltage	18 to 30 VDC	18 to 30 VDC	
Constant Current Excitation	2 to 20 mA	2 to 20 mA	
Output Impedance	≤100 ohm	≤100 ohm	
Output Bias Voltage	8 to 12 VDC	8 to 12 VDC	
Discharge Time Constant	0.5 to 2.0 sec	0.5 to 2.0 sec	
Spectral Noise (1 Hz)	2800 µg/√Hz	27468 (µm/sec²)/√Hz	[1]
Spectral Noise (10 Hz)	700 µg/√Hz	6867 (µm/sec²)/√Hz	[1]
Spectral Noise (100 Hz)	180 µg/√Hz	1766 (µm/sec²)/√Hz	[1]
Spectral Noise (1 kHz)	64 µg/√Hz	628 (µm/sec²)/√Hz	[1]
Physical			
Sensing Element	Quartz	Quartz	
Sensing Geometry	Shear	Shear	
Housing Material	Titanium	Titanium	
Sealing	Welded Hermetic	Welded Hermetic	
Size (Hex x Height)	9/32 in x 0.74 in	9/32 in x 18.8 mm	
Weight	0.06 oz	1.8 gm	[1]
Electrical Connector	10-32 Coaxial Jack	10-32 Coaxial Jack	
Electrical Connection Position	Top	Top	
Mounting Thread	5-40 Male	5-40 Male	
Mounting Torque	8 to 12 in-lb	90 to 135 N-cm	

CE [4]

Typical Sensitivity Deviation vs Temperature

Sensitivity Deviation (%)

10
5
0
-5
-10

-70 -30 10 50 90 130 170 210 250

Temperature (°F)

All specifications are at room temperature unless otherwise specified.
In the interest of constant product improvement, we reserve the right to change specifications without notice.
ICP® is a registered trademark of PCB group, Inc.

Optional Versions (Optional versions have identical specifications and accessories as listed for standard model except where noted below. More than one option maybe used.)

A - Adhesive Mount
Supplied Accessory: Model 080A90 Quick bond Gel (for use with accelerometer adhesive mtg bases to fill gaps on rough surfaces) replaces Model 080A15

B - Low bias electronics

Output Bias Voltage	4.5 to 7.5 VDC	4.5 to 7.5 VDC
Excitation Voltage	12 to 30 VDC	12 to 30 VDC
Constant Current Excitation	1 to 20 mA	1 to 20 mA
Measurement Range	±300 g pk	±2943 m/s² pk

J - Ground Isolated

Frequency Range (±5 %)	1 to 8000 Hz	1 to 8000 Hz
Frequency Range (±10 %)	0.7 to 15000 Hz	0.7 to 15000 Hz
Resonant Frequency	≥56 kHz	≥56 kHz
Electrical Isolation (Base)	$\geq 10^8$ ohm	$\geq 10^8$ ohm
Size (Hex x Height)	3/8 in x 0.82 in	3/8 in x 20.8 mm [1]
Weight	0.10 oz	3.0 gm [1]

M - Metric Mount

Mounting Thread	M3 x 0.50 Male	(M3 x 0.50 Male)

Supplied Accessory: Model M080A15 Metric adhesive base, 0.31" hex x 0.125" thk, M3 x 0.50 tnd, aluminum with insulating hardcoat finish replaces Model 080A15

Q - Extended discharge time constant

Frequency Range (±5 %)	0.15 to 10000 Hz	0.15 to 10000 Hz
Frequency Range (±10 %)	0.1 to 18000 Hz	0.1 to 18000 Hz
Discharge Time Constant	≥5 sec	≥5 sec
Settling Time (within 10% of bias)	<45 sec	<45 sec

Supplied Accessory: Model ACS-97 Single axis, low frequency phase and amplitude response cal from 1 to 10 Hz

W - Water Resistant Cable

Electrical Connector	Sealed Integral	Sealed Integral
	Cable	Cable
Electrical Connection Position	Top	Top

Notes
[1] Typical.
[2] Zero-based, least-squares, straight line method.
[3] Transverse sensitivity is typically <= 3%.
[4] See PCB Declaration of Conformance PS023 for details.

Supplied Accessories
080A109 Petro Wax (1)
080A15 Adhesive Mounting Base (1)
ACS-1 NIST traceable frequency response (10 Hz to upper 5% point). (1)

Entered: DMW	Engineer: BAM	Sales: WDC	Approved: EB	Spec Number:
Date: 03/25/2011	Date: 03/25/2011	Date: 03/25/2011	Date: 03/25/2011	353-2180-80

PCB PIEZOTRONICS
VIBRATION DIVISION

3425 Walden Avenue
Depew, NY 14043
UNITED STATES
Phone: 888-684-0013
Fax: 716-685-3886
E-mail: vibration@pcb.com
Web site: www.pcb.com

Model Number	ACCELEROMETER, ICP®, SHOCK	Revision E
350B23		ECN #: 28655

Performance	**ENGLISH**	**SI**	
Sensitivity (±30 %)	0.5 mV/g	0.05 mV/(m/s²)	
Measurement Range	±10000 g pk	±98000 m/s² pk	
Frequency Range (±1 dB)	0.4 to 10000 Hz	0.4 to 10000 Hz	
Frequency Range (-3 dB)	0.2 to 25000 Hz	0.2 to 25000 Hz	[2]
Electrical Filter Corner Frequency (-3 dB)	13 kHz	13 kHz	[1][3]
Mechanical Filter Resonant Frequency	23 kHz	23 kHz	[1][4]
Resonant Frequency	≥100 kHz	≥100 kHz	
Broadband Resolution (1 to 10000 Hz)	0.04 g rms	0.39 m/s² rms	[1]
Non-Linearity	≤2.0 %	≤2.0 %	
Transverse Sensitivity	≤7 %	≤7 %	
Environmental			
Overload Limit (Shock)	±50000 g pk	±490000 m/s² pk	
Temperature Range (Operating)	0 to +150 °F	-18 to +66 °C	
Temperature Range (Storage)	-40 to +200 °F	-40 to +93 °C	
Temperature Response	See Graph	See Graph	[1]
Base Strain Sensitivity	0.002 g/με	0.02 (m/s²)/με	[1]
Electrical			
Excitation Voltage	20 to 30 VDC	20 to 30 VDC	
Constant Current Excitation	2 to 20 mA	2 to 20 mA	
Output Impedance	≤200 ohm	≤200 ohm	
Output Bias Voltage	8 to 14 VDC	8 to 14 VDC	
Discharge Time Constant	1.0 to 2.0 sec	1.0 to 2.0 sec	[1]
Settling Time (within 10% of bias)	<10 sec	<10 sec	
Electrical Isolation (Case)	>1000000 ohm	>1000000 ohm	
Physical			
Sensing Element	Ceramic	Ceramic	
Sensing Geometry	Shear	Shear	
Housing Material	Titanium	Titanium	
Sealing	Hermetic	Hermetic	
Size (Hex x Height)	0.375 in x 0.75 in	9.5 mm x 19.1 mm	
Weight	0.16 oz	4.5 gm	[1]
Electrical Connector	Integral Cable	Integral Cable	
Cable Length	10 ft	3.05 m	
Cable Type	031 Twisted Pair	031 Twisted Pair	
Mounting Thread	1/4-28 Male	1/4-28 Male	

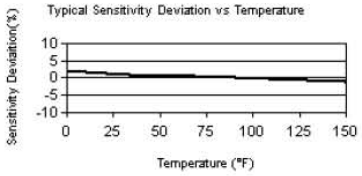

Optional Versions (Optional versions have identical specifications and accessories as listed for standard model except where noted below. More than one option maybe used.)

M - Metric Mount

Mounting Thread	M6 x 0.75 Male	(M6 x 0.75 Male)

Notes

[1] Typical.
[2] Typical corner frequency for coupled electrical and mechanical filters.
[3] Electrical filter is a second order filter.
[4] Amplitude at resonance is +9 dB.
[5] See PCB Declaration of Conformance PS023 for details.

Supplied Accessories

ACS-22 NIST Traceable frequency response (100Hz to ±1 dB point) (1)

Entered: BLS	Engineer: BAM	Sales: WDC	Approved: JJB	Spec Number:
Date: 04/23/2008	Date: 04/23/2008	Date: 04/23/2008	Date: 04/23/2008	**11670**

PCB PIEZOTRONICS VIBRATION DIVISION
3425 Walden Avenue
Depew, NY 14043
UNITED STATES
Phone: 888-684-0013
Fax: 716-685-3886
E-mail: vibration@pcb.com

Model Number	ICP® FORCE SENSOR	Revision G
208C05		ECN #: 17909

Performance	**ENGLISH**	**SI**	
Sensitivity (±15 %)	1 mV/lb	224.82 mV/kN	
Measurement Range (Compression)	5000 lb	22.24 kN	
Measurement Range (Tension)	500 lb	2.224 kN	
Maximum Static Force (Compression)	8000 lb	35.59 kN	
Maximum Static Force (Tension)	500 lb	2.224 kN	
Broadband Resolution (1 to 10000 Hz)	0.05 lb-rms	0.222 N-rms	[1]
Low Frequency Response (-5 %)	0.0003 Hz	0.0003 Hz	[2]
Upper Frequency Limit	36 kHz	36 kHz	[3]
Non-Linearity	≤1 % FS	≤1 % FS	[4]
Environmental			
Temperature Range	-65 to +250 °F	-54 to +121 °C	
Temperature Coefficient of Sensitivity	≤0.05 %/°F	≤0.09 %/°C	
Electrical			
Discharge Time Constant (at room temp)	≥2000 sec	≥2000 sec	
Excitation Voltage	20 to 30 VDC	20 to 30 VDC	
Constant Current Excitation	2 to 20 mA	2 to 20 mA	
Output Impedance	≤100 ohm	≤100 ohm	
Output Bias Voltage	8 to 14 VDC	8 to 14 VDC	
Spectral Noise (1 Hz)	0.00168 lb/√Hz	0.00750 N/√Hz	[1]
Spectral Noise (10 Hz)	0.00112 lb/√Hz	0.00501 N/√Hz	[1]
Spectral Noise (100 Hz)	0.000459 lb/√Hz	0.00205 N/√Hz	[1]
Spectral Noise (1000 Hz)	0.000133 lb/√Hz	0.000592 N/√Hz	[1]
Output Polarity (Compression)	Positive	Positive	
Physical			
Stiffness	6 lb/µin	1.05 kN/µm	[1]
Size (Hex x Height x Sensing Surface)	0.625 in x 0.625 in x 0.500 in	15.88 mm x 15.88 mm x 12.7 mm	
Weight	0.80 oz	22.7 gm	
Housing Material	Stainless Steel	Stainless Steel	
Sealing	Hermetic	Hermetic	
Electrical Connector	10-32 Coaxial Jack	10-32 Coaxial Jack	
Electrical Connection Position	Side	Side	
Mounting Thread	10-32 Female	Not Applicable	
Mounting Torque (Recommended)	16 to 20 in-lb	181 to 226 N-cm	

CE[0]

All specifications are at room temperature unless otherwise specified.
In the interest of constant product improvement, we reserve the right to change specifications without notice.
ICP® is a registered trademark of PCB group, Inc.

Optional Versions (Optional versions have identical specifications and accessories as listed for standard model except where noted below. More than one option maybe used.)

N - Negative Output Polarity		
Output Polarity (Compression)	Negative	Negative
W - Water Resistant Cable		

Notes
[1] Typical.
[2] Calculated from discharge time constant.
[3] Estimated using rigid body dynamics calculations.
[4] Zero-based, least-squares, straight line method.

Supplied Accessories
080A81 Thread Locker (1)
081B05 Mounting Stud (10-32 to 10-32) (2)
084A03 Impact Cap (1)

Entered: LAB	Engineer: LAB	Sales: JJM	Approved: DMB	Spec Number:
Date: 07/09/2003	Date: 07/09/2003	Date: 07/09/2003	Date: 07/09/2003	**8369**

PCB PIEZOTRONICS
FORCE / TORQUE DIVISION
Address: 3425 Walden Avenue
Depew, NY 14043
UNITED STATES
Phone: 888-684-0004
Fax: 716-684-8877

Switches

Type Reed	Solid state	Voltage V a.c.	V d.c.	Current max.	Temperature °C	LED	Features	Cable/ Connector length	Cable type	Cable with Connector	Datasheet
M/50/LSU/*V	–	10 to 240	10 to 170	180 mA	-20 to +80	•	–	2, 5, 10 m	PVC 2 x 0,25	–	N/UK **4.3**.005
M/50/LSU/5U	–	10 to 240	10 to 170	180 mA	-20 to +80	•	–	5 m	PUR 2 x 0,25	–	N/UK **4.3**.005
TM/50/RAU/2S	–	10 to 240	10 to 170	180 mA	-20 to +150	–	–	2 m	Silicone 2 x 0,25	–	N/UK **4.3**.005
M/50/RAC/5V	–	10 to 240	10 to 170	180 mA	-20 to +80	–	Changeover	5 m	PVC 3 x 0,25	–	N/UK **4.3**.005
M/50/LSU/CP	–	10 to 60	10 to 75	180 mA	-20 to +80	•	Plug M8x1	5 m	PVC 3 x 0,25	M/P73001/5	N/UK **4.3**.005
–	M/50/EAP/*V	–	10 to 30	150 mA	-20 to +80	•	PNP	2, 5, 10 m	PVC 3 x 0,25	–	N/UK **4.3**.007
–	M/50/EAP/CP	–	10 to 30	150 mA	-20 to +80	•	PNP, Plug M8x1	5 m	PVC 3 x 0,25	M/P73001/5	N/UK **4.3**.007
–	M/50/EAP/CC	–	10 to 30	150 mA	-20 to +80	•	PNP, Plug M12x1	5 m	PVC 3 x 0,25	M/P34614/5	N/UK **4.3**.007
–	M/50/EAN/*V	–	10 to 30	150 mA	-20 to +80	•	NPN	2, 5, 10 m	PVC 3 x 0,25	–	N/UK **4.3**.007
–	M/50/EAN/CP	–	10 to 30	150 mA	-20 to +80	•	NPN, Plug M8x1	5 m	PVC 3 x 0,25	M/P73001/5	N/UK **4.3**.007

* Please insert cable length
Further information (technical data, cable material, dimensions) see datasheet.

Theoretical forces, cushion, air consumption

Type	Cylinder Ø	Theoretical forces (N) at 6 bar outstroke	instroke	Cushion length (mm)	Initial cushion volume (cm³)	Air consumption (l/cm stroke) at 6 bar outstroke	instroke
PRA/182032/.	32	482	414	19	12,3	0,056	0,048
PRA/182040/.	40	754	633	22	20,7	0,088	0,074
PRA/182050/.	50	1178	990	24	36	0,137	0,114
PRA/182063/.	63	1870	1680	24	64	0,218	0,195
PRA/182080/.	80	3016	2722	27	116	0,35	0,32
PRA/182100/.	100	4710	4416	34	242	0,55	0,51
PRA/182125/.	125	7363	6882	41	451	0,86	0,79

Basic dimensions

PRA/182000, PRA/182000/M – Standard cylinder

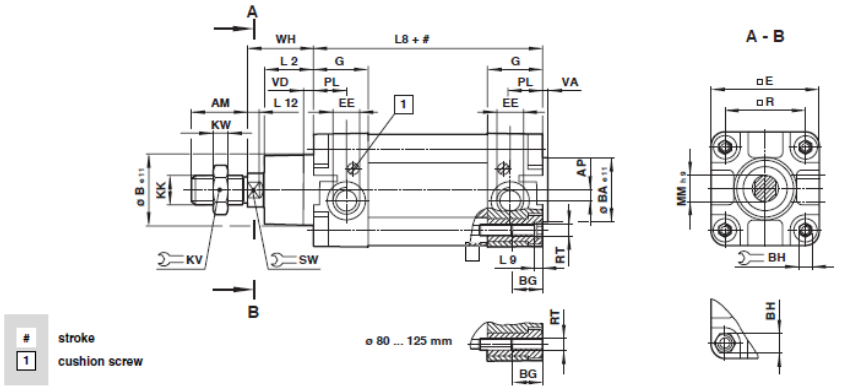

stroke
1 cushion screw

Type	Ø	AM	AP	Ø Be 11	Ø BAe 11	BG	BH	E	EE	G	KK	KV	KW	L2
PRA/182032/.	32	22	3,5	30	30	18	6	47	G 1/8	27,5	M10x1,25	17	5	20
PRA/182040/.	40	24	4,5	35	35	18	6	53	G 1/4	32	M12x1,25	19	6	22
PRA/182050/.	50	32	6	40	40	18	8	65	G 1/4	31	M16x1,5	24	8	27
PRA/182063/.	63	32	10	45	45	17,5	8	75	G 3/8	33	M16x1,5	24	8	29
PRA/182080/.	80	40	8,5	45	45	21,5	19	95	G 3/8	33	M20x1,5	30	10	33
PRA/182100/.	100	40	9	55	55	21,5	19	115	G 1/2	37	M20x1,5	30	10	36
PRA/182125/.	125	54	10	60	60	32	24	140	G 1/2	46	M27x2	41	13,5	45

Type	Ø	L8	L9	L12	Ø MMh 9	PL	R	RT	SW	VA	VD	WH	at 0 mm	per 25 mm
PRA/182032/.	32	94	4	6	12	13	32,5	M 6	10	3	6	26	0,51 kg	0,06 kg
PRA/182040/.	40	105	4	6,5	16	15	38	M 6	13	3,5	6	30	0,80 kg	0,08 kg
PRA/182050/.	50	106	5	8	20	18,5	46,5	M 8	17	3,5	6	37	1,33 kg	0,12 kg
PRA/182063/.	63	121	5	8	20	19	56,5	M 8	17	4	6	37	1,80 kg	0,13 kg
PRA/182080/.	80	128	–	10	25	19	72	M 10	22	4	6	46	3,25 kg	0,20 kg
PRA/182100/.	100	138	–	10	25	18	89	M 10	22	4	6	51	4,81 kg	0,23 kg
PRA/182125/.	125	160	–	13	32	20	110	M 12	27	6	15,5	65	8,00 kg	0,33 kg

14.2 Appendix B: Experimental Data Summary

Bone ID	Group	Force (N)	Stress (MPa)	scaled yield stress	Disp (mm)	density
110111aRF	FDq	4213	154	56	3.54	1.82
110111cLF	FDq	3714	123	121	2.08	1.98
251110aRF	FDq	3193	117	107	2.80	1.93
261110aRF	FDq	3301	140	188	4.45	2.08
270111dLF	FDq	3366	125	74	2.69	2.13
060111aRF	FDr	2563	141	111	2.66	2.04
060111bLF	FDr	3453	151	144	4.11	1.89
100111aRF	FDr	4040	152	58	3.24	1.80
150610bRF	FDr	2867	135	101	4.06	2.15
170111aLF	FDr	4431	176	72	2.73	1.82
110111aLF	FNq	5234	199	152	2.13	2.62
110111cRF	FNq	6863	229	211	3.24	3.25
251110aLF	FNq	5430	200	198	2.08	2.56
261110aLF	FNq	4735	192	126	2.20	2.45
270111dRF	FNq	5777	222	94	3.01	2.01
110111bRF	FNr	5517	161	100	1.90	2.90
150610cLF	FNr	5625	203	115	2.23	2.03
170111bLF	FNr	7015	207	100	1.71	2.75
170810cRF	FNr	5821	216	116	3.45	2.18
270111bLF	FNr	4539	181	111	2.02	2.92
03a_R_F	SDq	2624	96	94	2.67	1.85
280111aLF	SDq	2742	111	105	3.15	1.90
280111bLF	SDq	3438	156	140	3.63	1.71
280111dLF	SDq	2647	110	96	3.36	1.85
280111eRF	SDq	3764	162	162	3.88	1.71
060111aLF	SDr	2295	125	116	4.28	1.83
060111bRF	SDr	3164	143	143	3.19	1.57
100111aLF	SDr	3886	149	142	4.39	1.99
150610bLF	SDr	3016	141	139	3.81	1.69
170111aRF	SDr	4070	164	156	3.57	1.45
03a_L_F	SNq	4323	158	116	3.19	2.55
280111aRF	SNq	3138	125	118	2.44	2.44
280111bRF	SNq	4280	199	180	3.26	1.74
280111dRF	SNq	3669	148	148	2.55	2.29
280111eLF	SNq	4535	197	155	2.64	1.74
110111bLF	SNr	4791	137	80	3.58	2.79
150610cRF	SNr	3039	110	104	3.34	2.00
170111bRF	SNr	3712	109	103	2.08	2.70
170810cLF	SNr	4315	164	138	3.32	2.38
270111bRF	SNr	3157	129	116	3.84	3.08

Bone ID	Group	strain at yield	strain at max	strain at failure	strain rate yield	strain rate max force	strain rate fail
110111aRF	FDq	0.45%	1.95%	2.00%	16.9	17.0	16.9
110111cLF	FDq	0.63%	0.71%	0.94%	10.2	7.8	7.2
251110aRF	FDq	0.46%	0.48%	1.21%	11.0	11.5	13.2
261110aRF	FDq	0.44%	1.54%	1.57%	6.3	16.8	5.9
270111dLF	FDq	0.46%	1.34%	1.56%	9.3	11.3	10.7
060111aRF	FDr	0.39%	1.08%	0.94%	6.9	8.8	8.2
060111bLF	FDr	1.08%	2.03%	2.16%	11.8	6.6	4.4
100111aRF	FDr	0.53%	1.73%	1.75%	19.8	15.1	14.8
150610bRF	FDr	0.54%	1.26%	1.52%	10.0	11.0	10.5
170111aLF	FDr	0.43%	1.45%	1.52%	16.0	10.8	9.9
110111aLF	FNq	0.38%	1.26%	1.41%	10.9	5.1	4.7
110111cRF	FNq	0.75%	1.73%	1.79%	18.8	7.2	7.1
251110aLF	FNq	0.66%	0.70%	1.15%	19.1	13.1	5.8
261110aLF	FNq	0.82%	0.96%	2.09%	23.8	4.4	9.1
270111dRF	FNq	0.45%	1.33%	1.73%	29.2	13.3	9.8
110111bRF	FNr	0.66%	1.60%	2.04%	16.5	12.7	8.9
150610cLF	FNr	0.49%	1.15%	1.34%	14.2	9.4	6.2
170111bLF	FNr	0.28%	0.77%	0.94%	10.5	11.8	11.2
170810cRF	FNr	0.64%	1.75%	1.91%	55.9	21.8	16.1
270111bLF	FNr	0.68%	1.16%	1.33%	7.4	4.6	3.6
03a_R_F	SDq	1.52%	1.47%	2.72%	0.0062	0.00545	0.01104
280111aLF	SDq	1.66%	1.66%	1.66%	0.0093	0.00522	0.00522
280111bLF	SDq	1.24%	2.03%	2.76%	0.0051	0.00553	0.00555
280111dLF	SDq	1.37%	1.66%	1.66%	0.0043	0.00490	0.00490
280111eRF	SDq	1.47%	1.48%	1.48%	0.0067	0.00444	0.00444
060111aLF	SDr	1.76%	2.19%	2.94%	0.0058	0.00512	0.00518
060111bRF	SDr	1.21%	1.77%	1.77%	0.0059	0.00552	0.00552
100111aLF	SDr	1.31%	2.55%	2.57%	0.0041	0.00574	0.00574
150610bLF	SDr	1.30%	2.08%	2.08%	0.0037	0.00537	0.00537
170111aRF	SDr	1.62%	2.03%	2.03%	0.0055	0.00560	0.00560
03a_L_F	SNq	1.16%	1.65%	1.65%	0.0065	0.00510	0.00510
280111aRF	SNq	1.40%	1.39%	1.39%	0.0057	0.00571	0.00571
280111bRF	SNq	1.34%	1.89%	2.20%	0.0060	0.00573	0.00574
280111dRF	SNq	1.38%	1.55%	2.74%	0.0058	0.00596	0.00939
280111eLF	SNq	1.20%	2.37%	2.38%	0.0061	0.00603	0.00603
110111bLF	SNr	0.92%	2.56%	3.88%	0.0060	0.00712	0.00604
150610cRF	SNr	1.62%	3.15%	3.53%	0.0049	0.00927	0.00909
170111bRF	SNr	1.20%	1.09%	2.15%	0.0062	0.00518	0.00802
170810cLF	SNr	1.09%	1.91%	1.91%	0.0050	0.00571	0.00571
270111bRF	SNr	2.30%	2.86%	4.13%	0.0074	0.00684	0.00686

Bone ID	Group	Euler E (GPa)	Timo E (GPa)	non pris timo E (GPa)	prop filter timo (GPa)	G (GPa)
110111aRF	FDq	9.8	11.0	9.8	4.0	3.7
110111cLF	FDq	10.9	12.3	15.0	9.0	4.1
251110aRF	FDq	10.4	11.7	21.4	13.6	3.9
261110aRF	FDq	9.5	10.6	12.1	7.7	3.5
270111dLF	FDq	12.1	13.3	29.2	13.4	4.4
060111aRF	FDr	34.7	38.0	36.2	8.5	12.7
060111bLF	FDr	7.5	8.3	14.7	9.4	2.8
100111aRF	FDr	9.9	11.1	13.2	6.5	3.7
150610bRF	FDr	15.6	17.1	19.6	9.1	5.7
170111aLF	FDr	14.8	16.5	27.2	10.1	5.5
110111aLF	FNq	31.3	34.1	54.1	14.4	11.4
110111cRF	FNq	15.4	16.9	19.4	7.6	5.6
251110aLF	FNq	14.6	16.4	24.7	11.1	5.5
261110aLF	FNq	25.8	28.3	24.2	5.1	9.4
270111dRF	FNq	19.2	21.1	18.5	8.1	7.0
110111bRF	FNr	18.3	21.0	32.4	8.7	7.0
150610cLF	FNr	21.7	24.3	36.5	11.9	8.1
170111bLF	FNr	38.7	43.5	82.9	16.8	14.5
170810cRF	FNr	12.6	13.9	18.7	8.5	4.6
270111bLF	FNr	14.1	15.2	20.2	13.3	5.1
03a_R_F	SDq	4.3	4.7	4.1	0.0	1.6
280111aLF	SDq	5.0	5.6	8.1	0.0	1.9
280111bLF	SDq	3.3	3.6	5.4	0.0	1.2
280111dLF	SDq	4.7	5.3	9.7	0.0	1.8
280111eRF	SDq	7.3	8.1	7.7	0.0	2.7
060111aLF	SDr	4.6	5.1	8.2	0.0	1.7
060111bRF	SDr	6.3	7.0	10.5	0.0	2.3
100111aLF	SDr	5.4	6.0	5.4	0.0	2.0
150610bLF	SDr	5.4	5.9	5.3	0.0	2.0
170111aRF	SDr	6.1	6.7	6.3	0.0	2.2
03a_L_F	SNq	6.8	7.6	7.0	0.0	2.5
280111aRF	SNq	6.0	6.7	5.9	0.0	2.2
280111bRF	SNq	9.0	9.9	9.4	0.0	3.3
280111dRF	SNq	8.0	8.7	6.5	0.0	2.9
280111eLF	SNq	8.1	8.8	8.1	0.0	2.9
110111bLF	SNr	4.9	5.5	8.4	0.0	1.8
150610cRF	SNr	4.1	4.6	5.2	0.0	1.5
170111bRF	SNr	6.1	6.8	13.0	0.0	2.3
170810cLF	SNr	7.8	8.6	7.2	0.0	2.9
270111bRF	SNr	3.6	3.9	3.5	0.0	1.3

14.3 Appendix C: Bone Section Measurements

All measurements in mm

Bone ID	D supp B	B mid	Bottom	Top	Top Mid	D Supp T
03a_L_F	20	22	14	24	19	21
03a_R_F	19	24	20	17	18	22
060111aLF	10	30	28	20	0	32
060111aRF	8	39	0	39	6	28
060111bLF	10	28	32	25	20	5
060111bRF	10	27	24	24	22	13
100111aLF	19	16	26	35	0	24
100111aRF	0	29	14	10	27	40
110111aLF	20	0	30	32	28	10
110111aRF	20	22	25	15	22	16
110111bLF	21	24	37	18	0	20
110111bRF	22	0	27	17	29	25
110111cLF	12	23	22	12	35	16
110111cRF	20	0	45	15	10	30
150610bLF	17	25	17	27	22	12
150610bRF	7	0	42	19	28	24
150610cLF	0	28	30	32	25	5
150610cRF	1	28	24	22	25	20
170111aLF	14	24	20	32	30	0
170111aRF	15	29	21	20	22	13
170111bLF	10	27	24	0	30	29
170111bRF	10	27	24	0	30	29
170810cLF	15	29	21	20	22	13
170810cRF	10	28	24	0	31	27
251110aLF	25	0	47	12	25	11
251110aRF	10	0	10	55	24	21
261110aLF	15	22	51	0	24	8
261110aRF	20	24	13	37	0	26
270111bLF	10	27	26	24	23	10
270111bRF	10	26	25	28	22	9
270111dLF	0	21	26	11	33	29
270111dRF	10	26	21	16	27	20
280111aLF	15	0	44	13	25	23
280111aRF	14	27	17	26	24	12
280111bLF	10	27	22	24	27	10
280111bRF	15	29	21	20	22	13
280111dLF	20	27	20	19	21	13
280111dRF	20	28	0	46	0	26
280111eLF	18	23	21	16	23	19
280111eRF	25	28	15	20	32	0

14.4 Appendix D: DDA Graphs

14.4.1 Fast Loading, Normal Quality

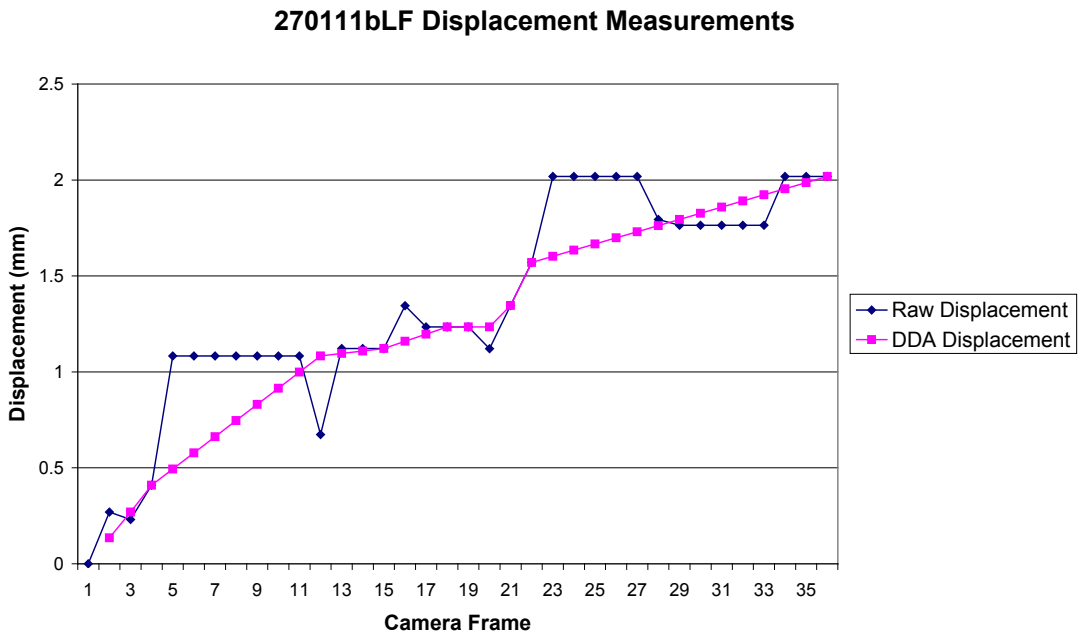

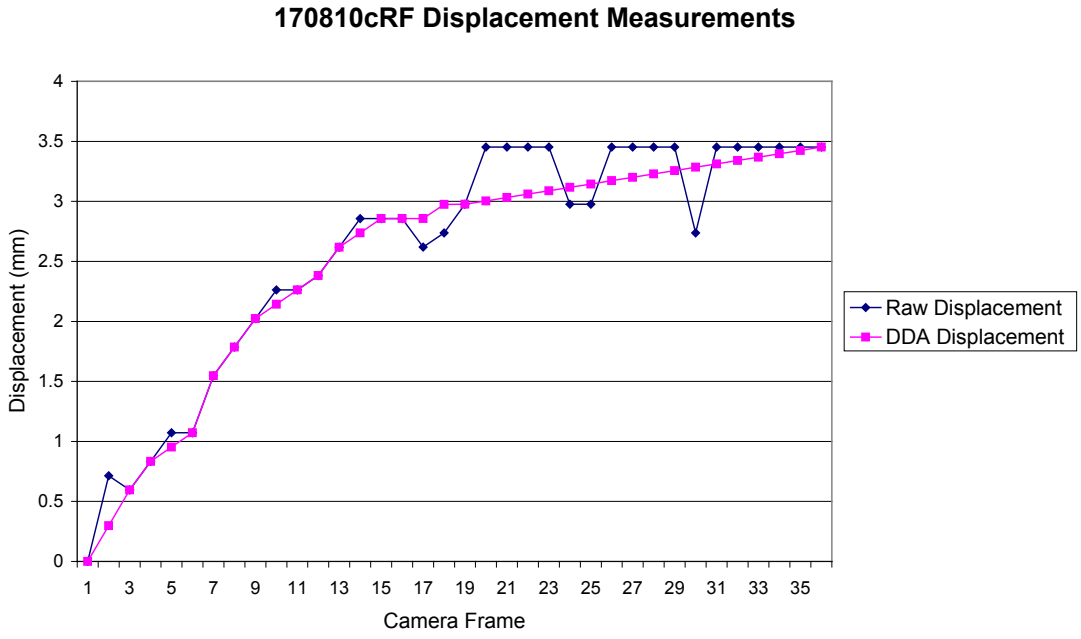

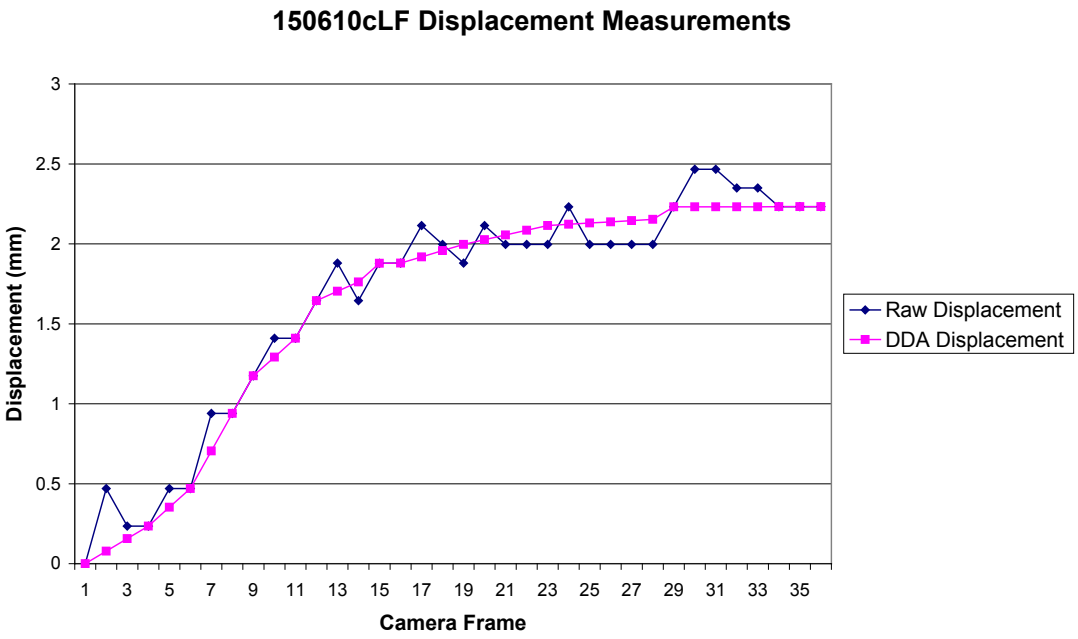
150610cLF Displacement Measurements
Displacement (mm)
3
2.5
2
1.5
1
0.5
0
1 3 5 7 9 11 13 15 17 19 21 23 25 27 29 31 33 35
Camera Frame
Raw Displacement
DDA Displacement

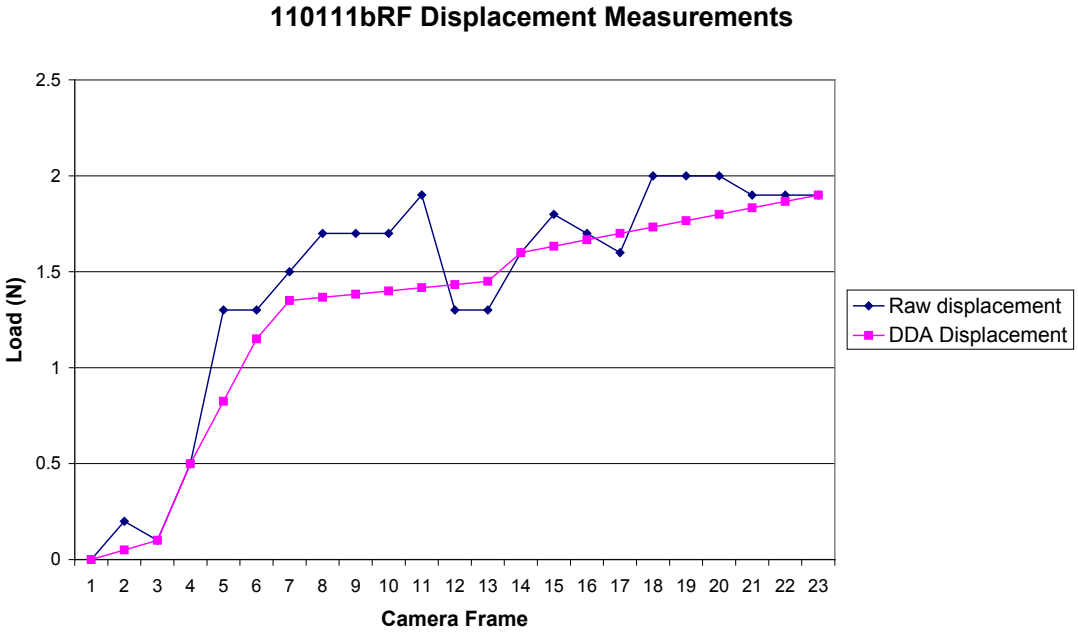
110111bRF Displacement Measurements
Load (N)
2.5
2
1.5
1
0.5
0
1 2 3 4 5 6 7 8 9 10 11 12 13 14 15 16 17 18 19 20 21 22 23
Camera Frame
Raw displacement
DDA Displacement

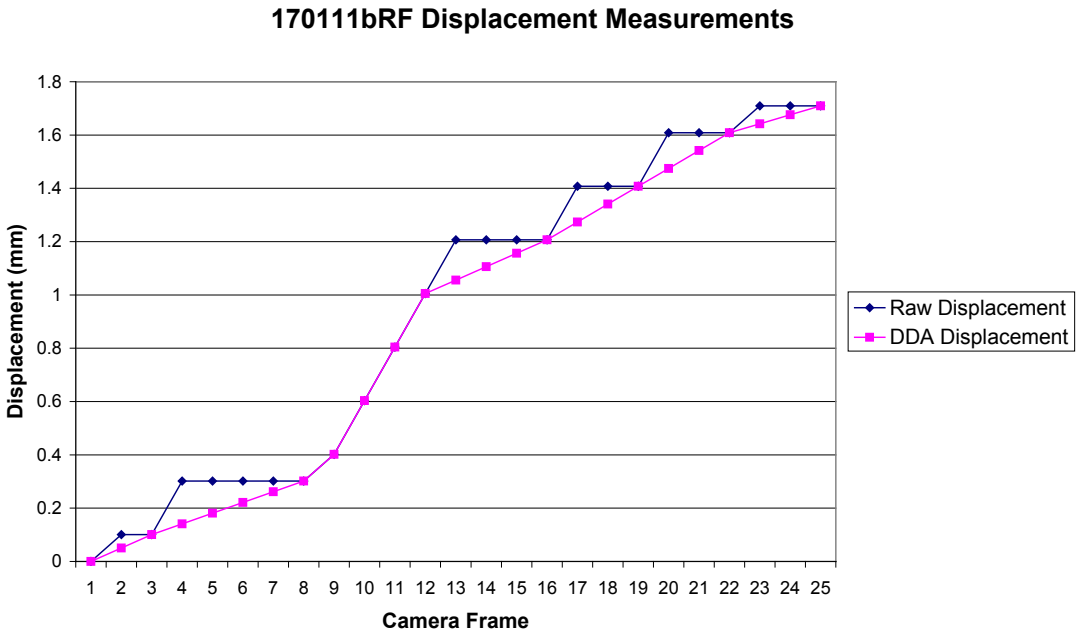
170111bRF Displacement Measurements
Displacement (mm)
1.8
1.6
1.4
1.2
1
0.8
0.6
0.4
0.2
0
1 2 3 4 5 6 7 8 9 10 11 12 13 14 15 16 17 18 19 20 21 22 23 24 25
Camera Frame
Raw Displacement
DDA Displacement

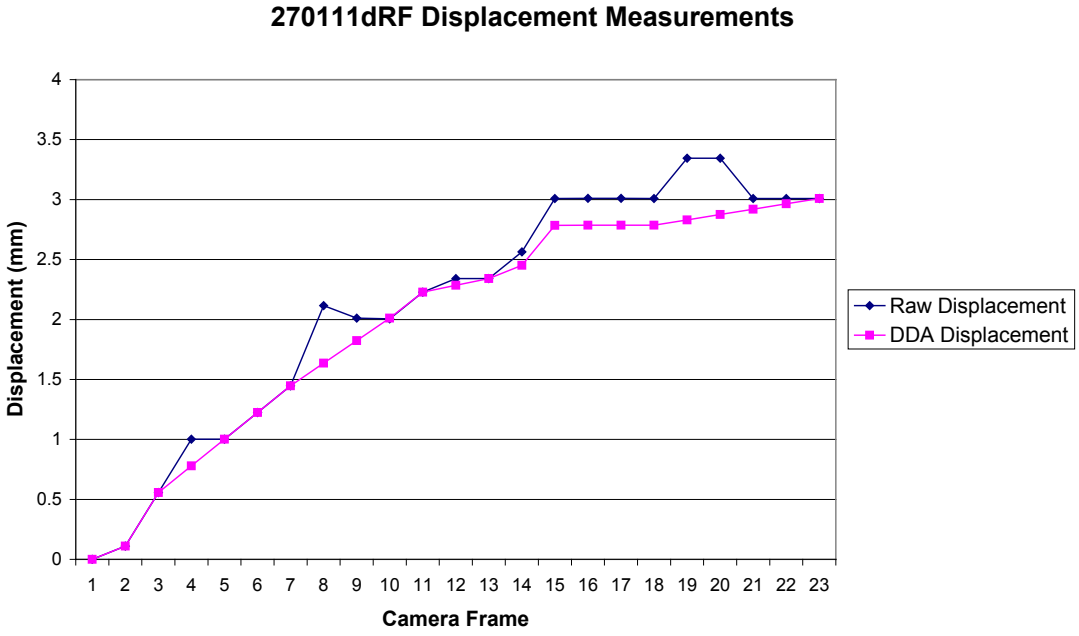
270111dRF Displacement Measurements
Displacement (mm)
4
3.5
3
2.5
2
1.5
1
0.5
0
1 2 3 4 5 6 7 8 9 10 11 12 13 14 15 16 17 18 19 20 21 22 23
Camera Frame
Raw Displacement
DDA Displacement

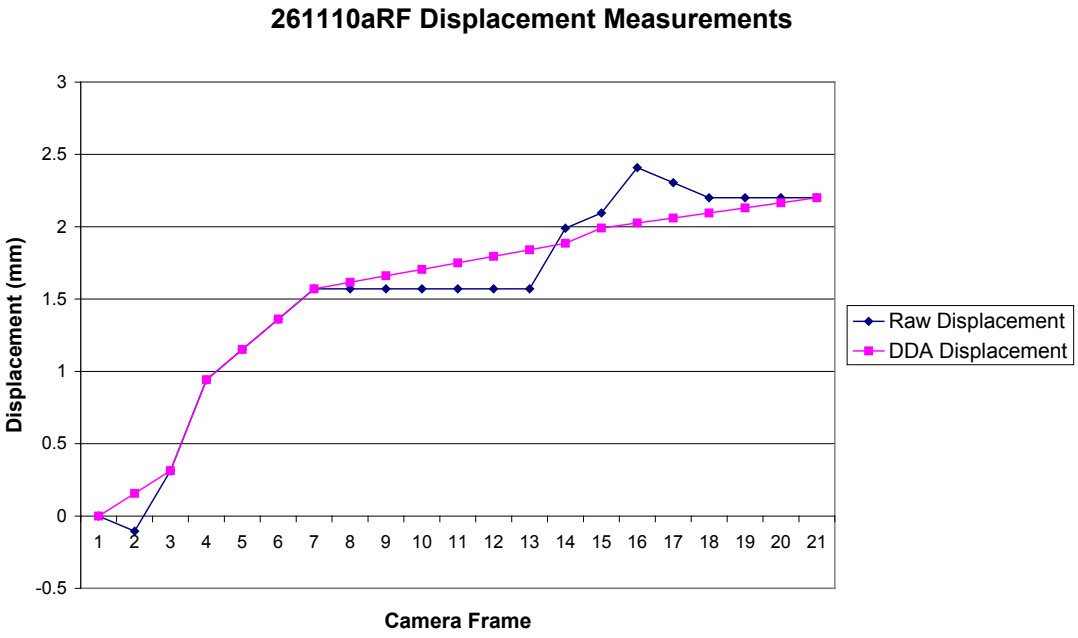
261110aRF Displacement Measurements
Displacement (mm)
3
2.5
2
1.5
1
0.5
0
-0.5
1 2 3 4 5 6 7 8 9 10 11 12 13 14 15 16 17 18 19 20 21
Camera Frame
Raw Displacement
DDA Displacement

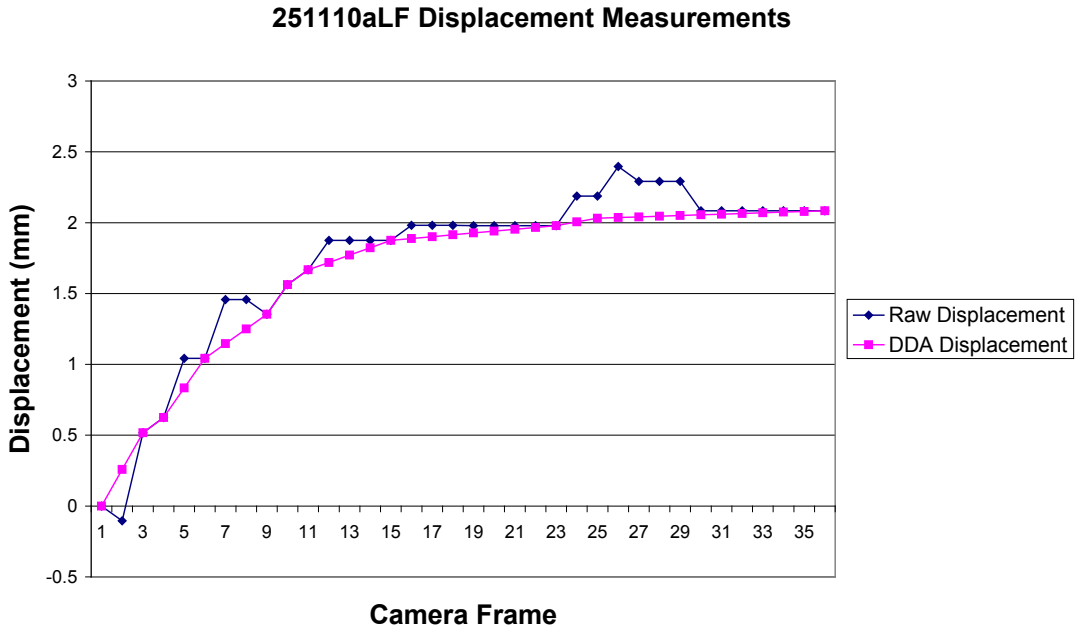
251110aLF Displacement Measurements
Displacement (mm)
3
2.5
2
1.5
1
0.5
0
-0.5
1 3 5 7 9 11 13 15 17 19 21 23 25 27 29 31 33 35
Camera Frame
Raw Displacement
DDA Displacement

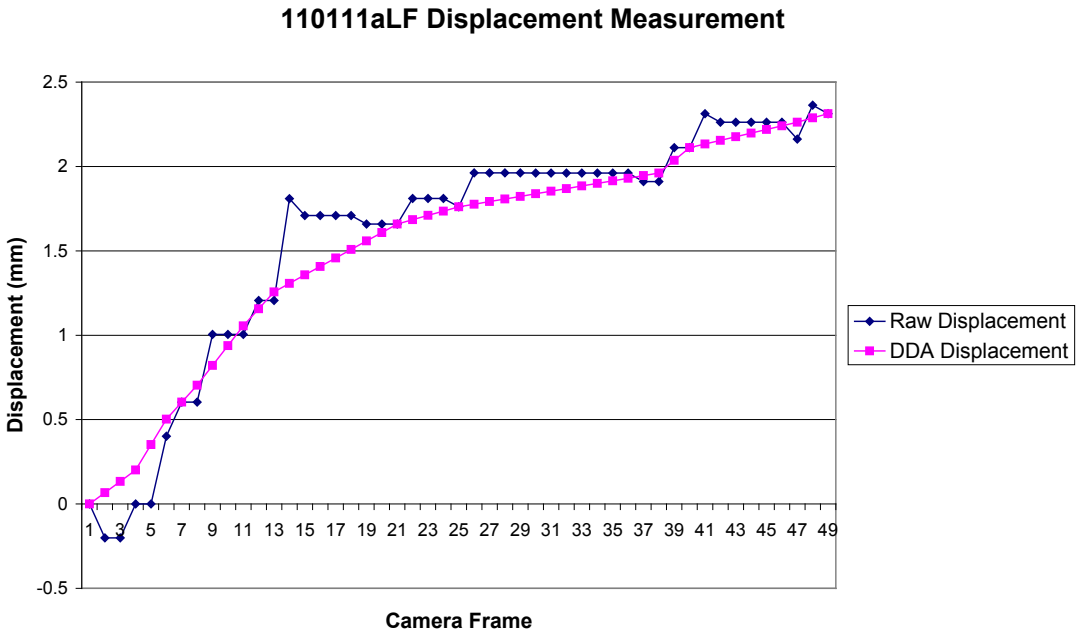
110111aLF Displacement Measurement
Displacement (mm)
2.5
2
1.5
1
0.5
0
-0.5
1 3 5 7 9 11 13 15 17 19 21 23 25 27 29 31 33 35 37 39 41 43 45 47 49
Camera Frame
Raw Displacement
DDA Displacement

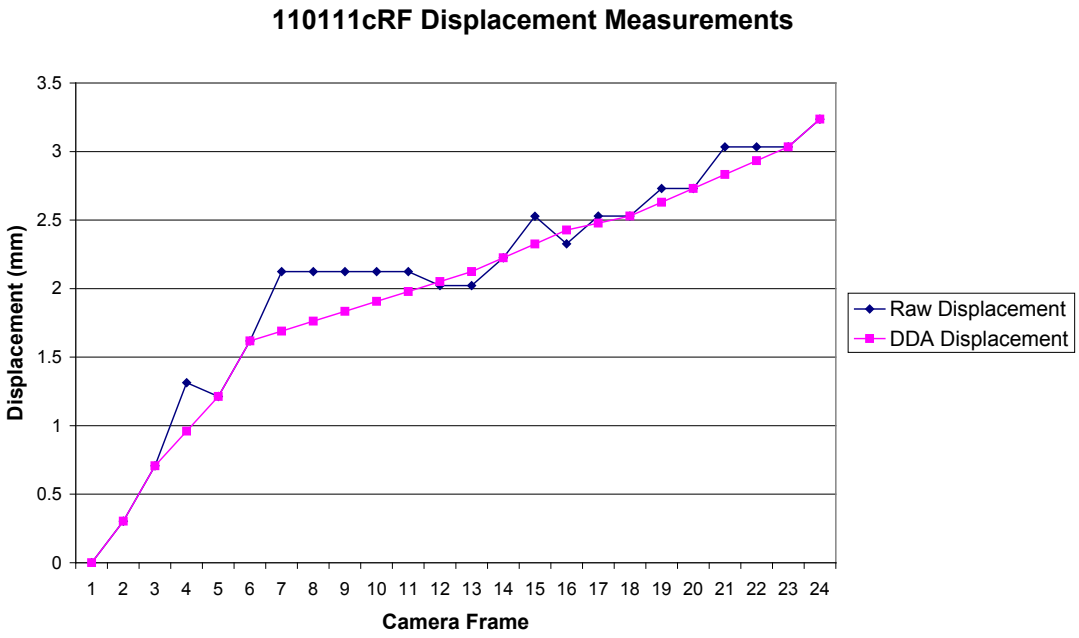
110111cRF Displacement Measurements
Displacement (mm)
3.5
3
2.5
2
1.5
1
0.5
0
1 2 3 4 5 6 7 8 9 10 11 12 13 14 15 16 17 18 19 20 21 22 23 24
Camera Frame
Raw Displacement
DDA Displacement

14.4.2 Fast Loading, Decalcified Quality

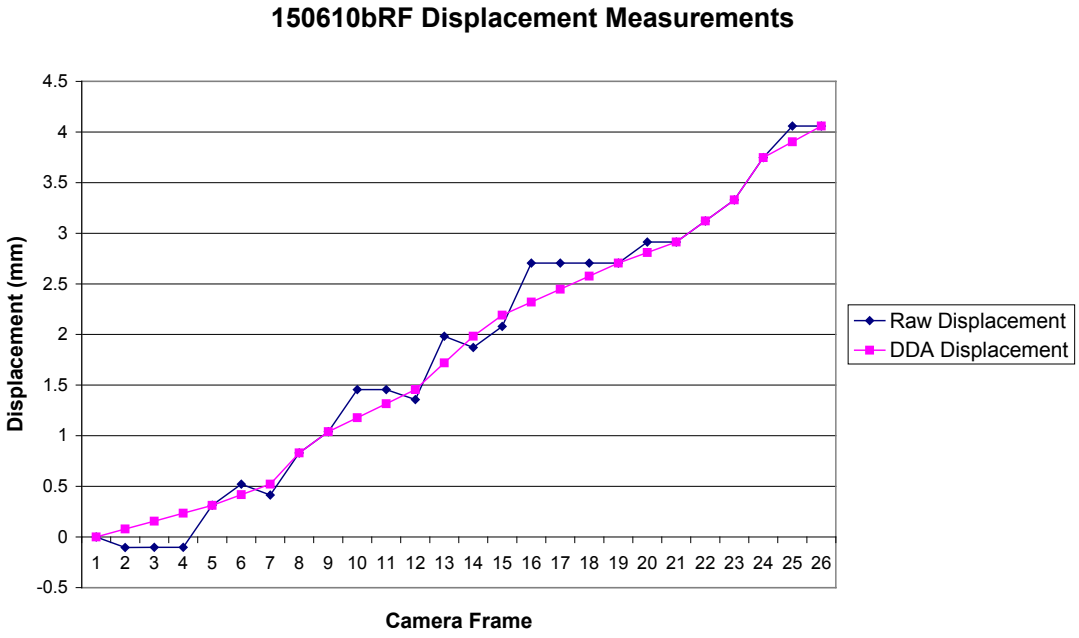

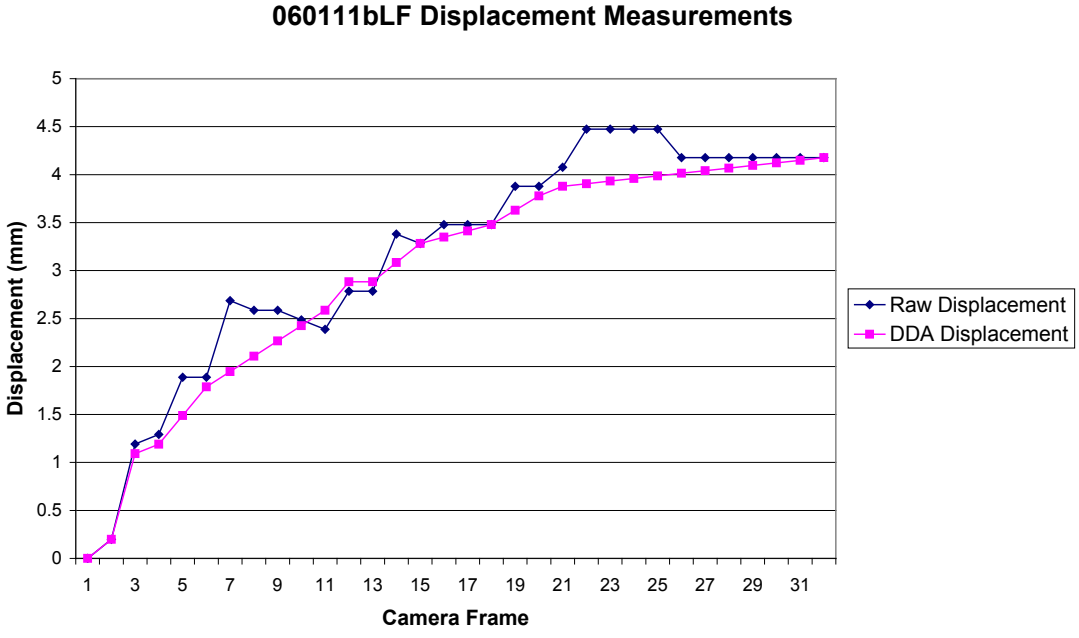

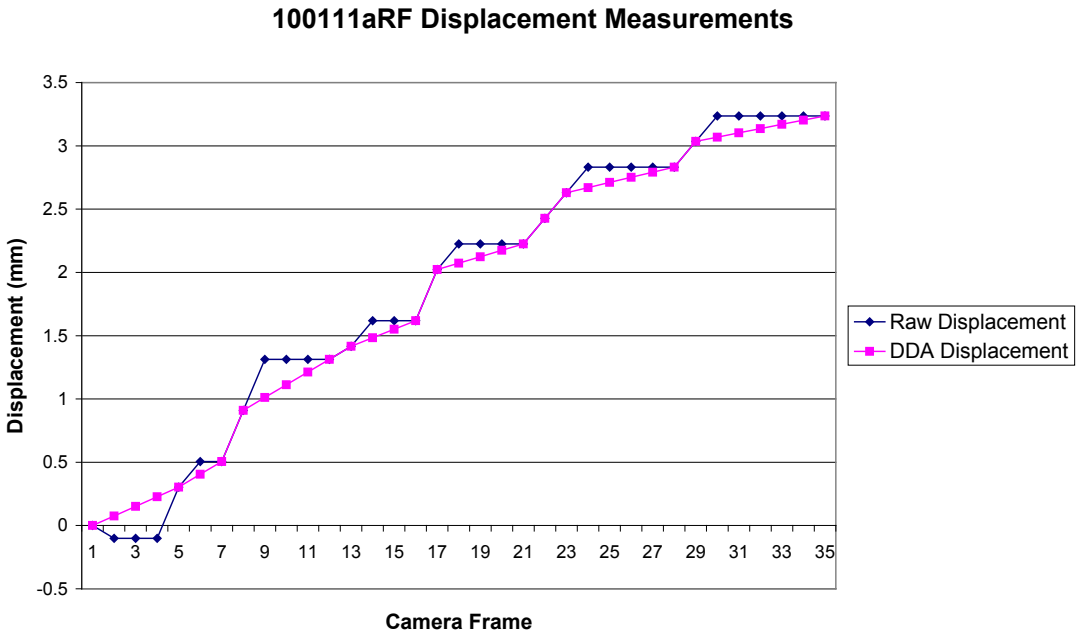
100111aRF Displacement Measurements
Displacement (mm)
3.5
3
2.5
2
1.5
1
0.5
0
-0.5
1 3 5 7 9 11 13 15 17 19 21 23 25 27 29 31 33 35
Camera Frame
Raw Displacement
DDA Displacement

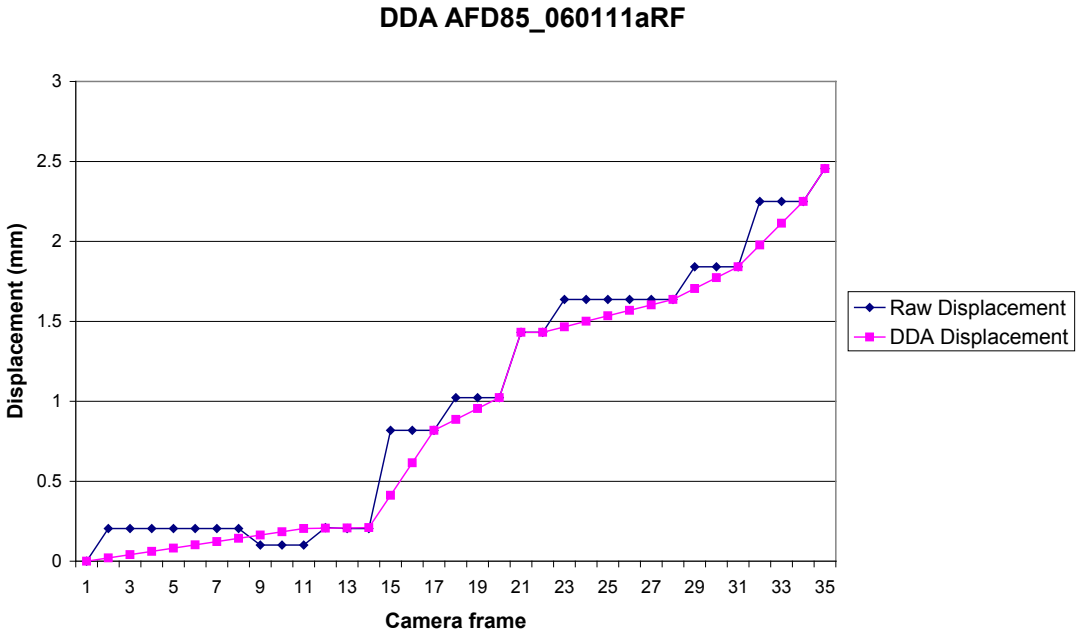
DDA AFD85_060111aRF
Displacement (mm)
3
2.5
2
1.5
1
0.5
0
1 3 5 7 9 11 13 15 17 19 21 23 25 27 29 31 33 35
Camera frame
Raw Displacement
DDA Displacement

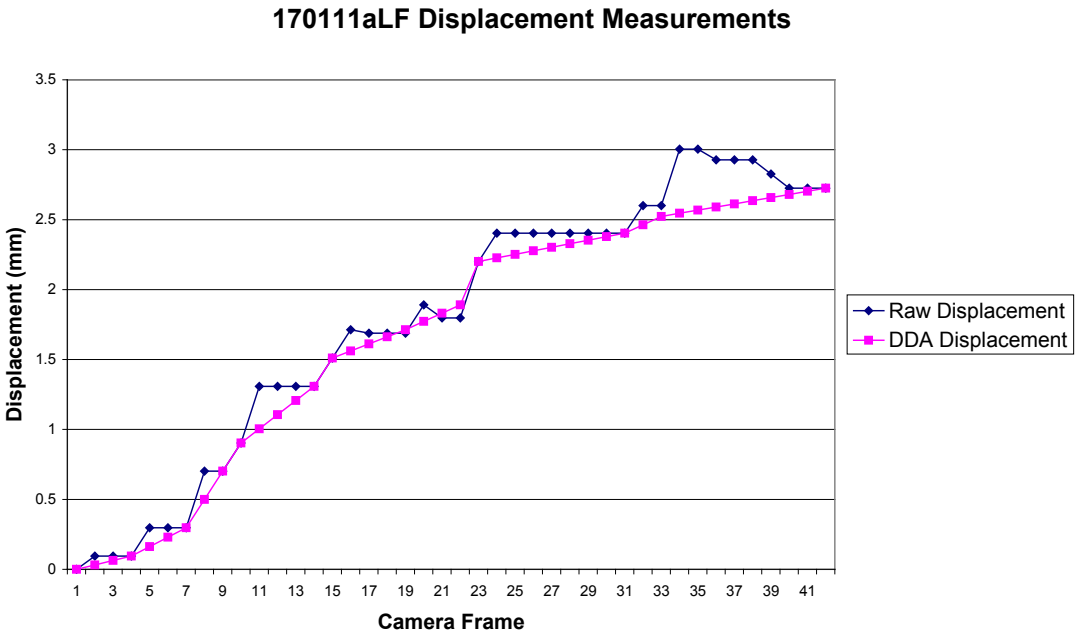
170111aLF Displacement Measurements
Displacement (mm)
3.5
3
2.5
2
1.5
1
0.5
0
1 3 5 7 9 11 13 15 17 19 21 23 25 27 29 31 33 35 37 39 41
Camera Frame
Raw Displacement
DDA Displacement

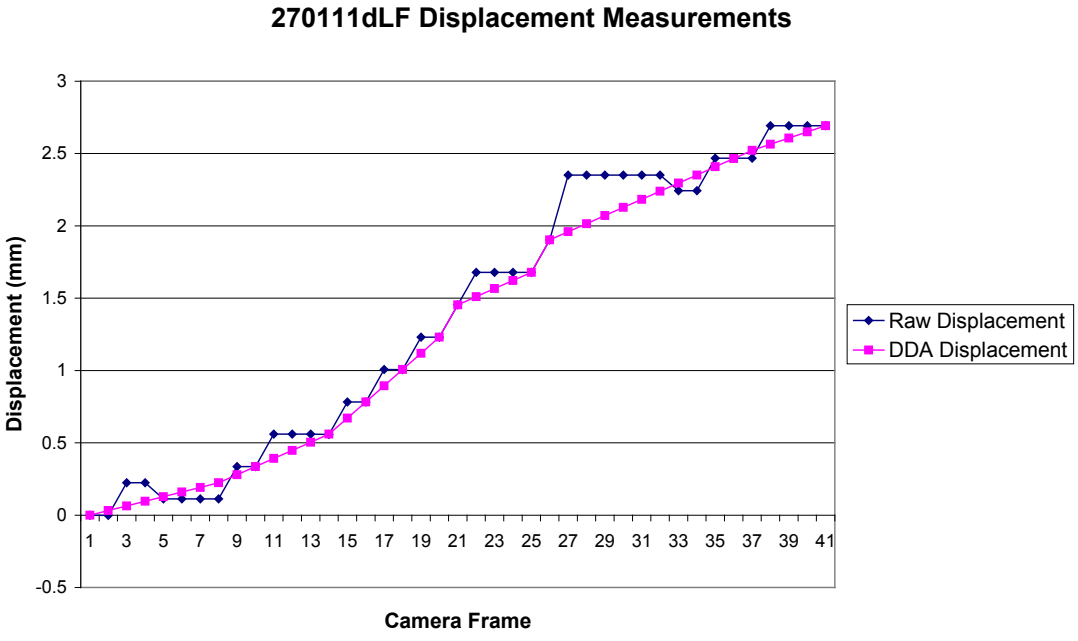
270111dLF Displacement Measurements
Displacement (mm)
3
2.5
2
1.5
1
0.5
0
-0.5
1 3 5 7 9 11 13 15 17 19 21 23 25 27 29 31 33 35 37 39 41
Camera Frame
Raw Displacement
DDA Displacement

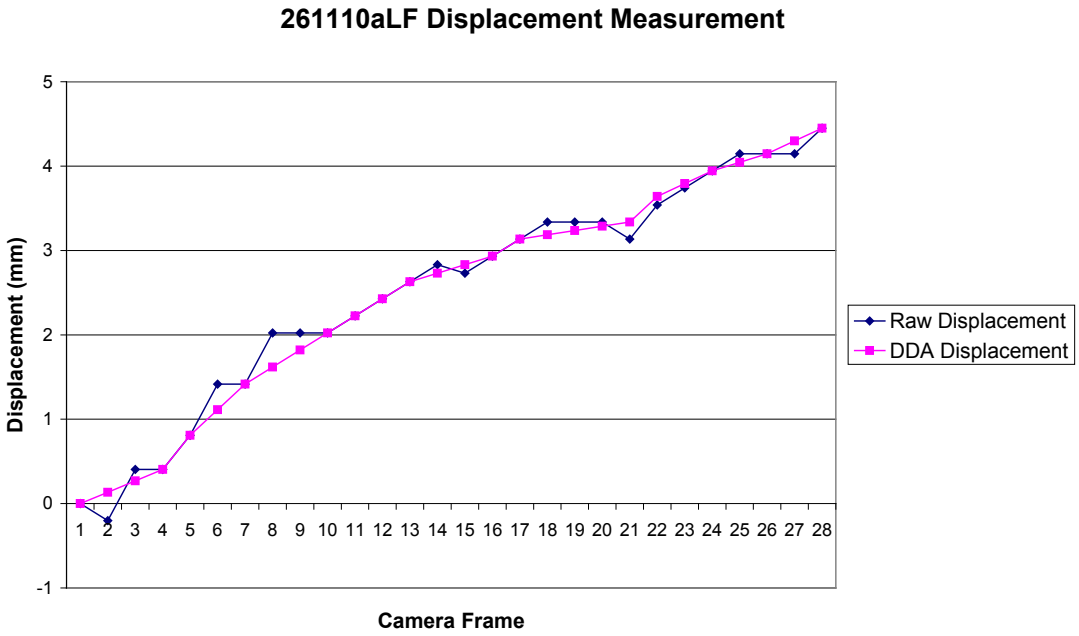
261110aLF Displacement Measurement
Displacement (mm)
5
4
3
2
1
0
-1
1 2 3 4 5 6 7 8 9 10 11 12 13 14 15 16 17 18 19 20 21 22 23 24 25 26 27 28
Camera Frame
Raw Displacement
DDA Displacement

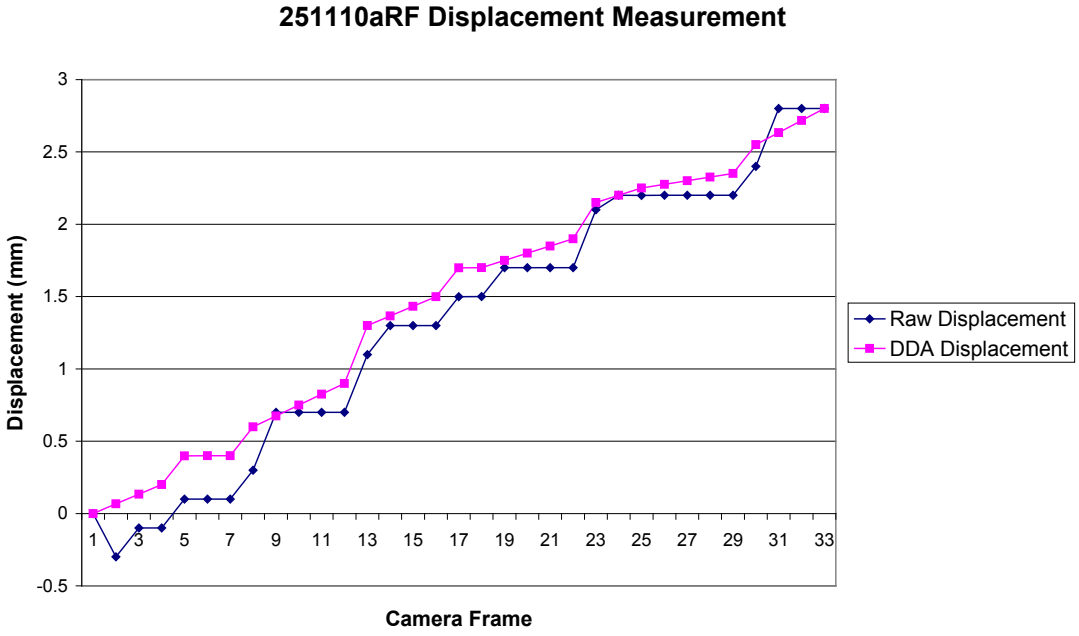
251110aRF Displacement Measurement
Displacement (mm)
3
2.5
2
1.5
1
0.5
0
-0.5
1 3 5 7 9 11 13 15 17 19 21 23 25 27 29 31 33
Camera Frame
Raw Displacement
DDA Displacement

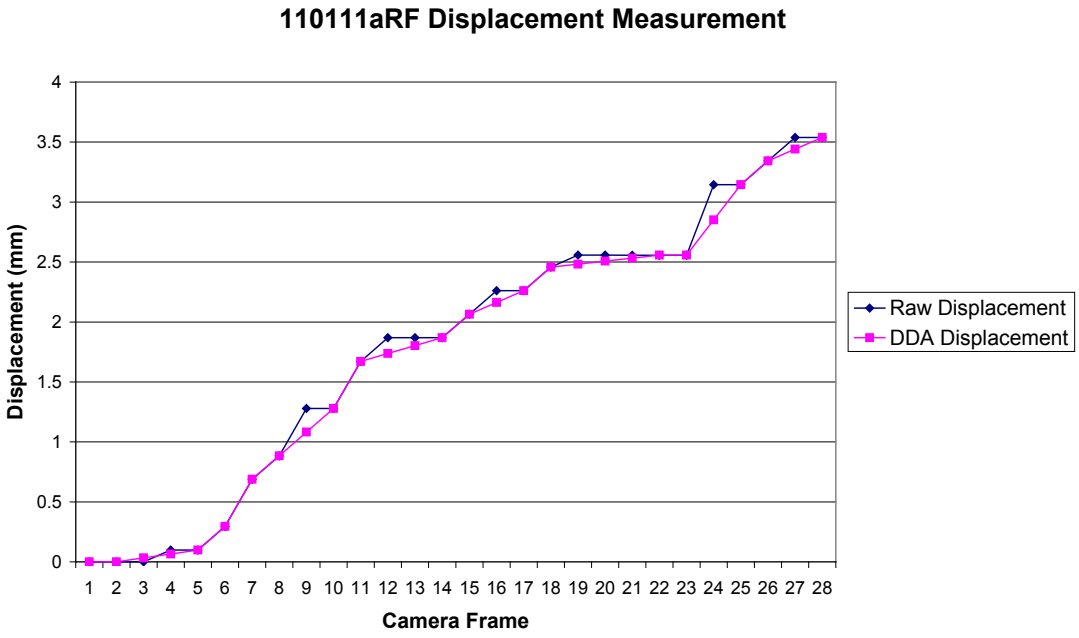
110111aRF Displacement Measurement
Displacement (mm)
4
3.5
3
2.5
2
1.5
1
0.5
0
1 2 3 4 5 6 7 8 9 10 11 12 13 14 15 16 17 18 19 20 21 22 23 24 25 26 27 28
Camera Frame
Raw Displacement
DDA Displacement

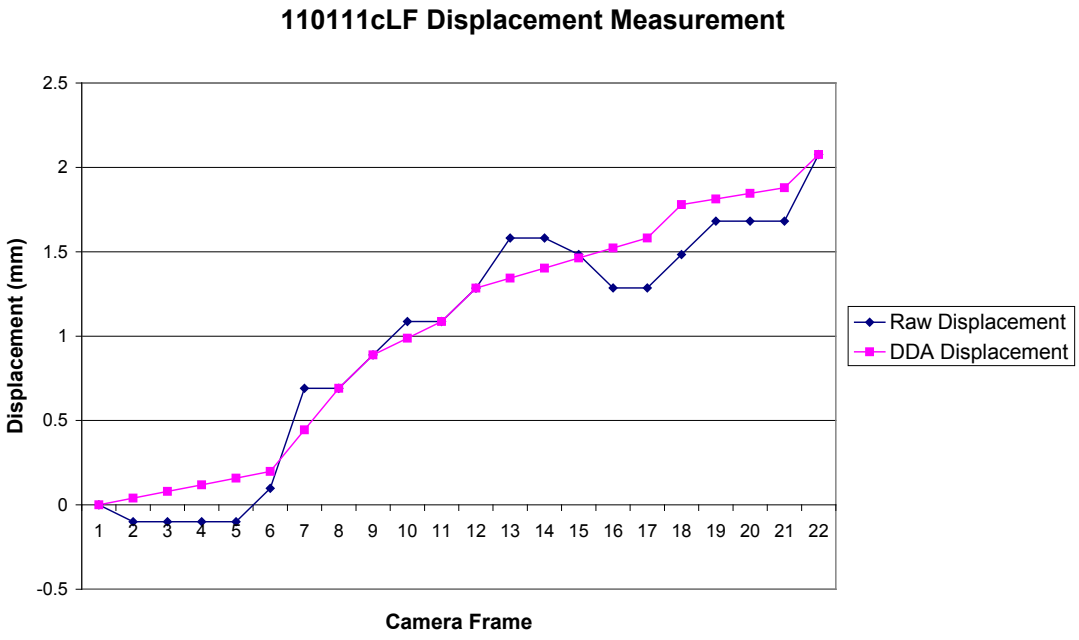
110111cLF Displacement Measurement
Displacement (mm)
2.5
2
1.5
1
0.5
0
-0.5
1 2 3 4 5 6 7 8 9 10 11 12 13 14 15 16 17 18 19 20 21 22
Camera Frame
Raw Displacement
DDA Displacement

14.5 Appendix E: Raw, Polynomial and Filtered force v Time Graphs

14.5.1 Demineralised bones

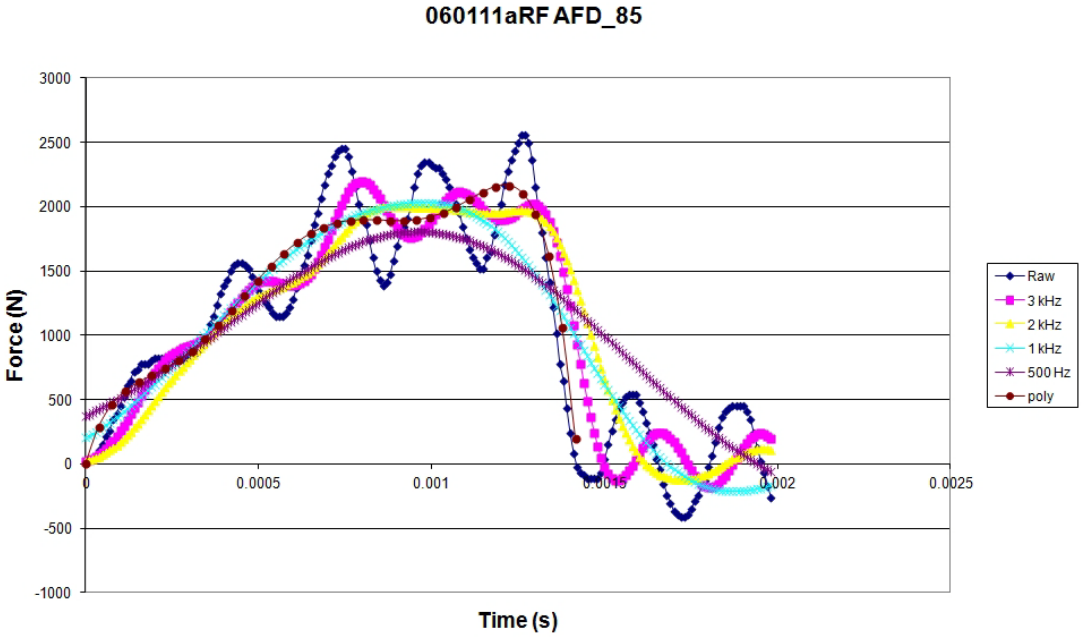

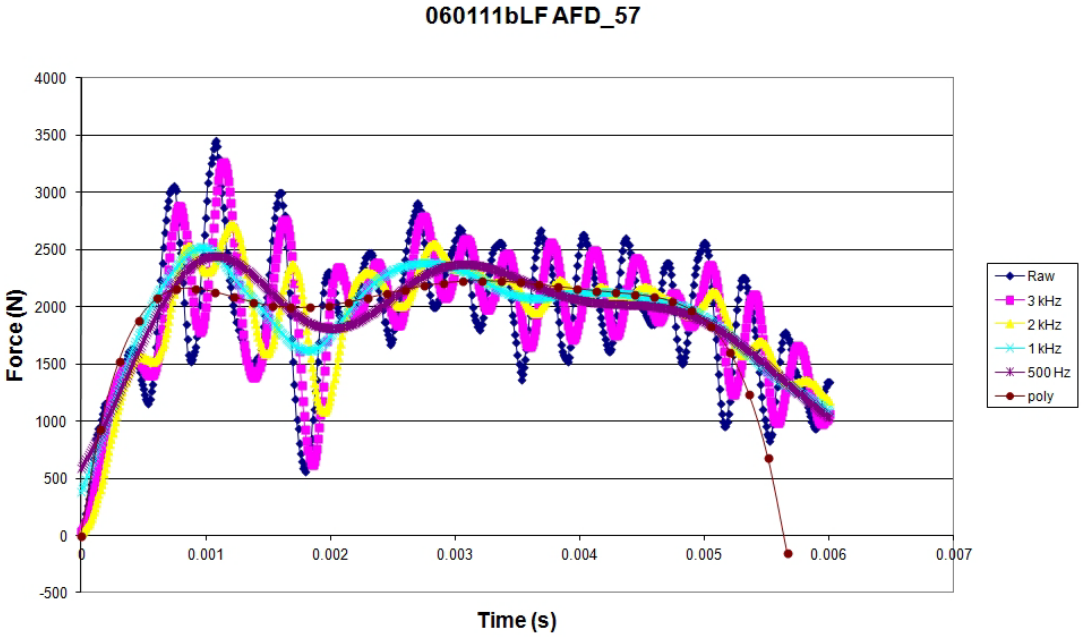

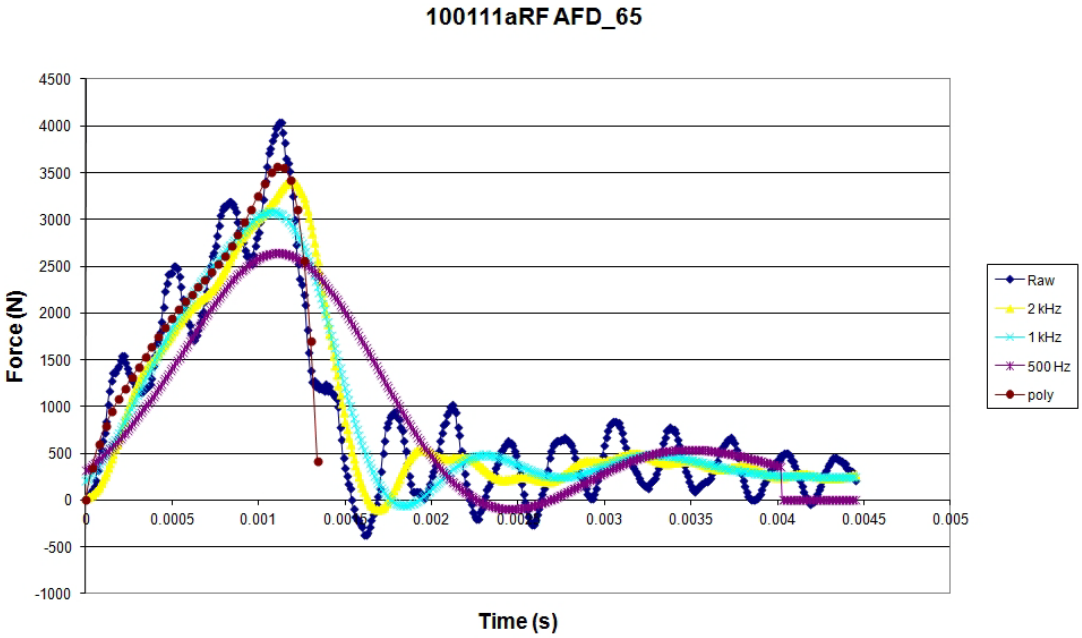
100111aRF AFD_65
Force (N)
Time (s)
Raw
2 kHz
1 kHz
500 Hz
poly

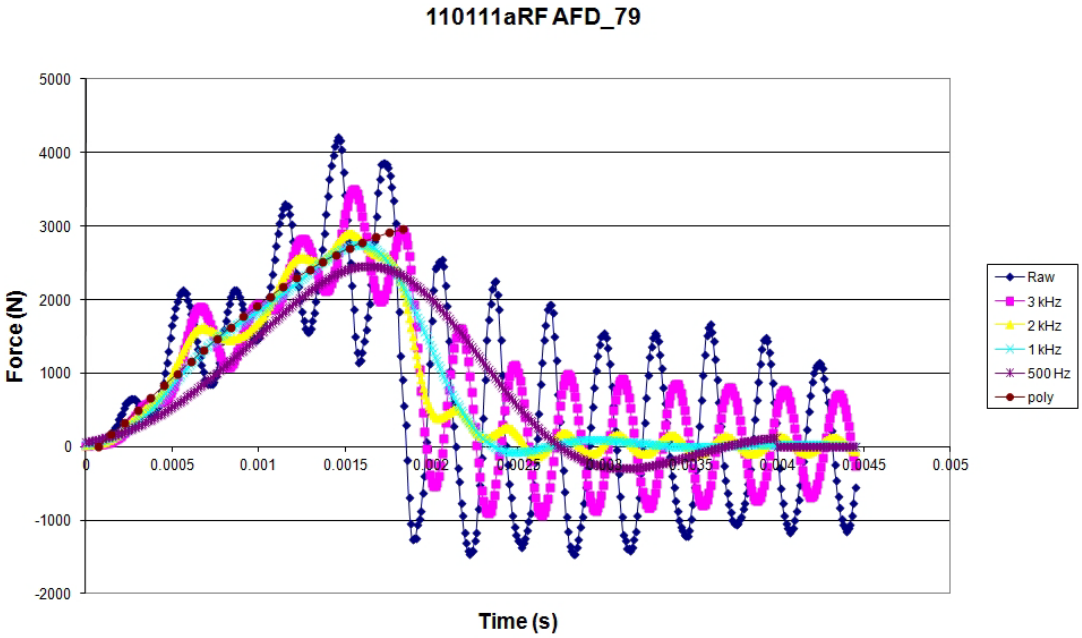
110111aRF AFD_79
Force (N)
Time (s)
Raw
3 kHz
2 kHz
1 kHz
500 Hz
poly

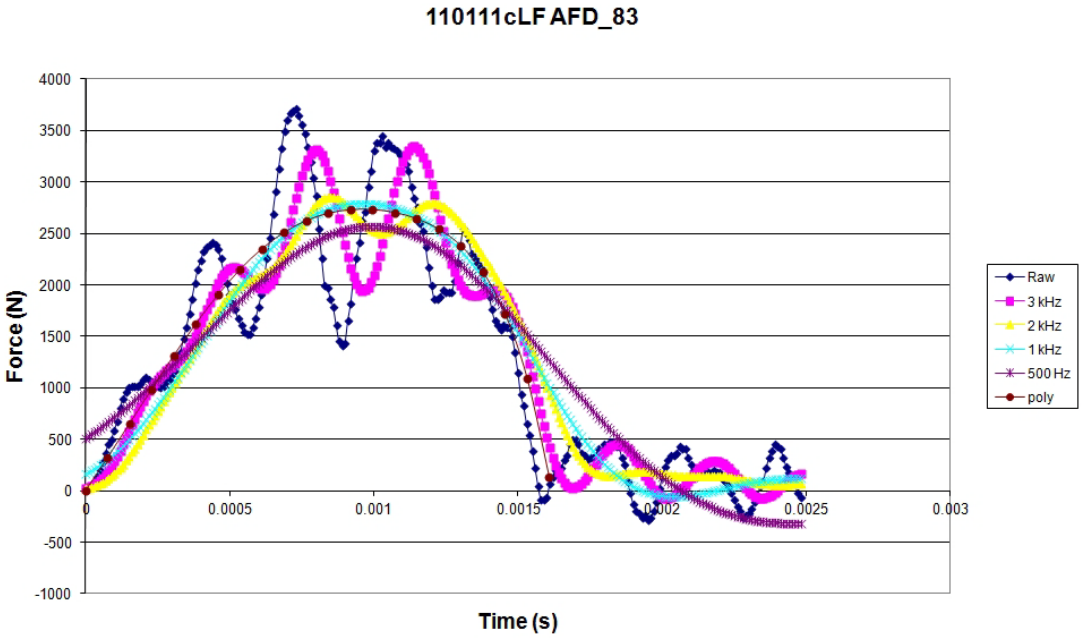
110111cLF AFD_83
Force (N)
Time (s)
Raw
3 kHz
2 kHz
1 kHz
500 Hz
poly

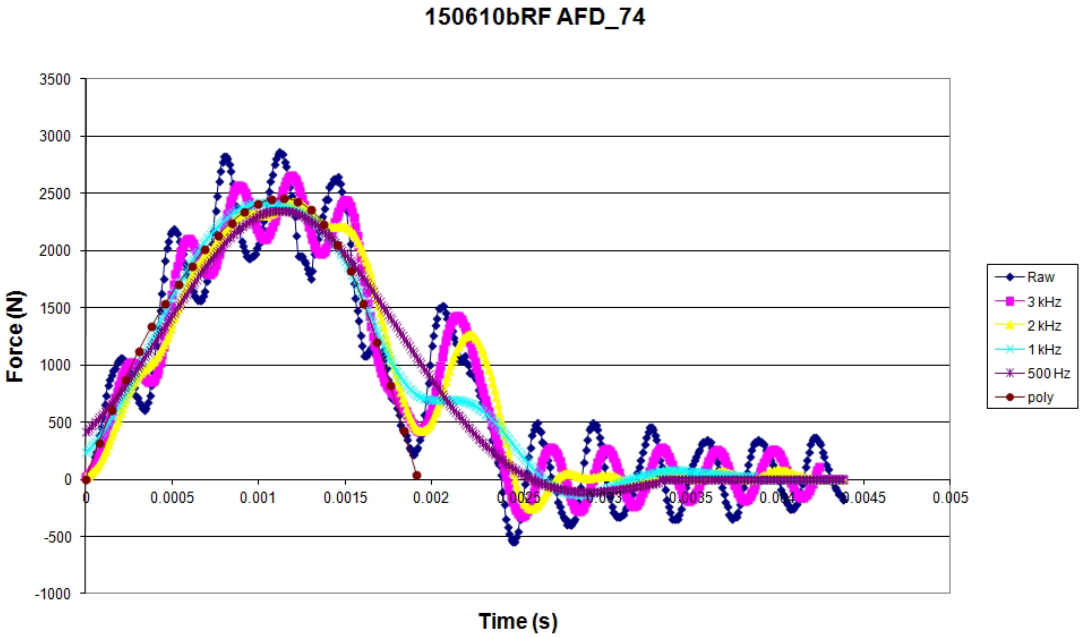
150610bRF AFD_74
Force (N)
Time (s)
Raw
3 kHz
2 kHz
1 kHz
500 Hz
poly

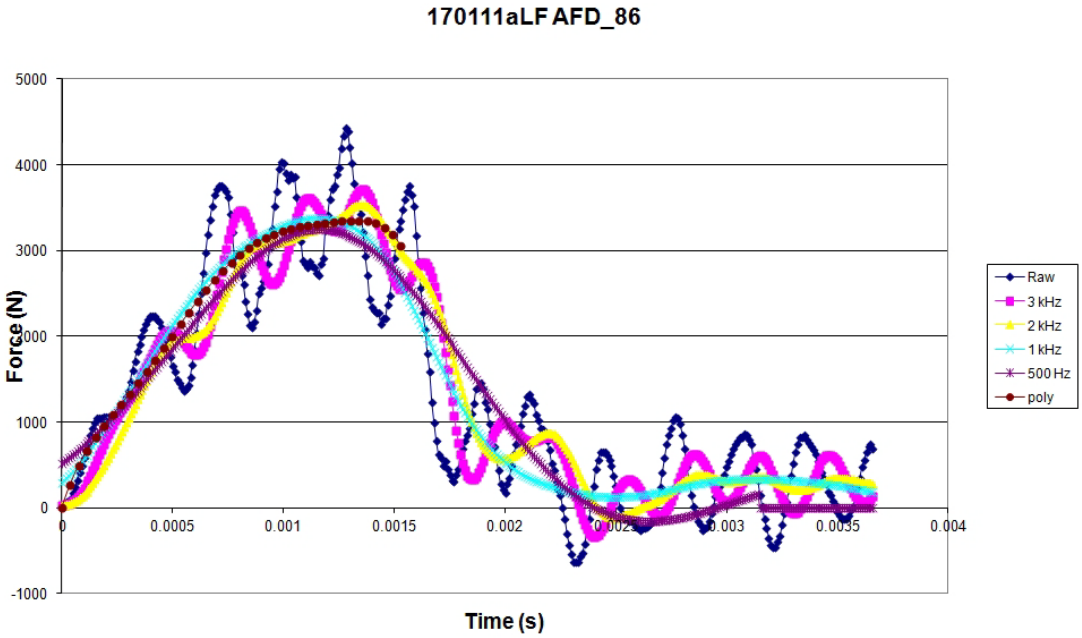
170111aLF AFD_86
5000
4000
3000
2000
1000
0
-1000
Force (N)
0
0.0005
0.001
0.0015
0.002
0.003
0.0035
0.004
Time (s)
Raw
3 kHz
2 kHz
1 kHz
500 Hz
poly

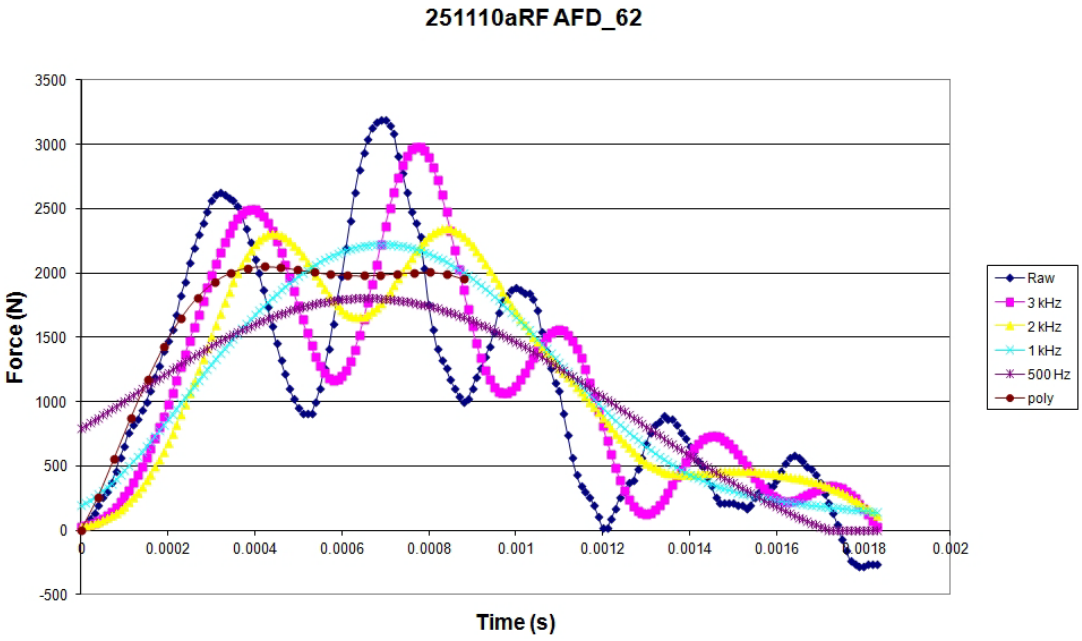
251110aRF AFD_62
3500
3000
2500
2000
1500
1000
500
0
-500
Force (N)
0
0.0002
0.0004
0.0006
0.0008
0.001
0.0012
0.0014
0.0016
0.0018
0.002
Time (s)
Raw
3 kHz
2 kHz
1 kHz
500 Hz
poly

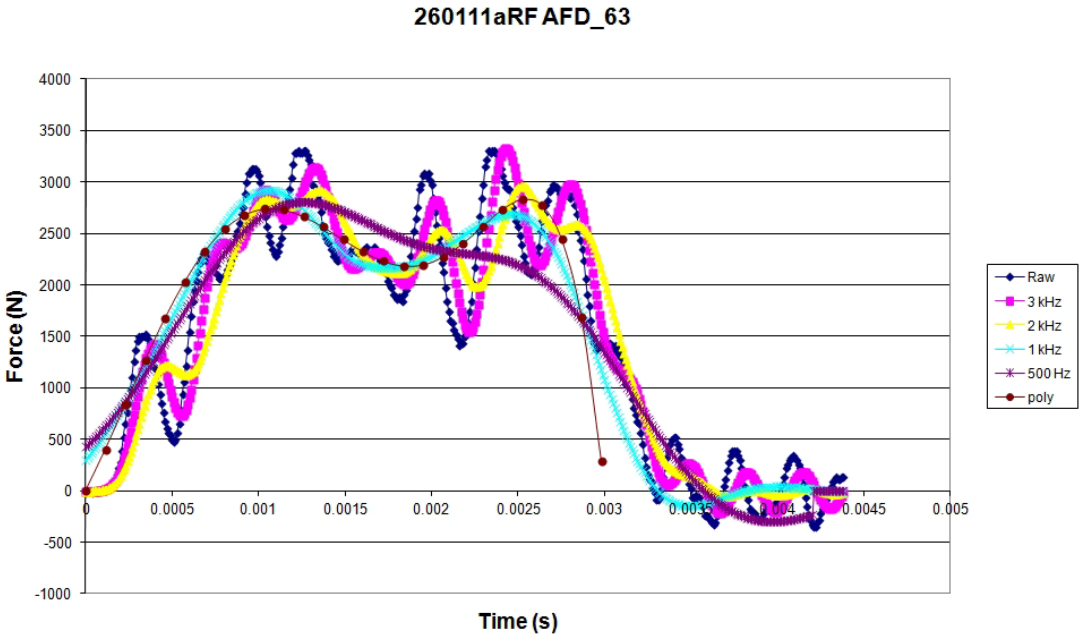
260111aRF AFD_63
Force (N)
Time (s)
Raw
3 kHz
2 kHz
1 kHz
500 Hz
poly

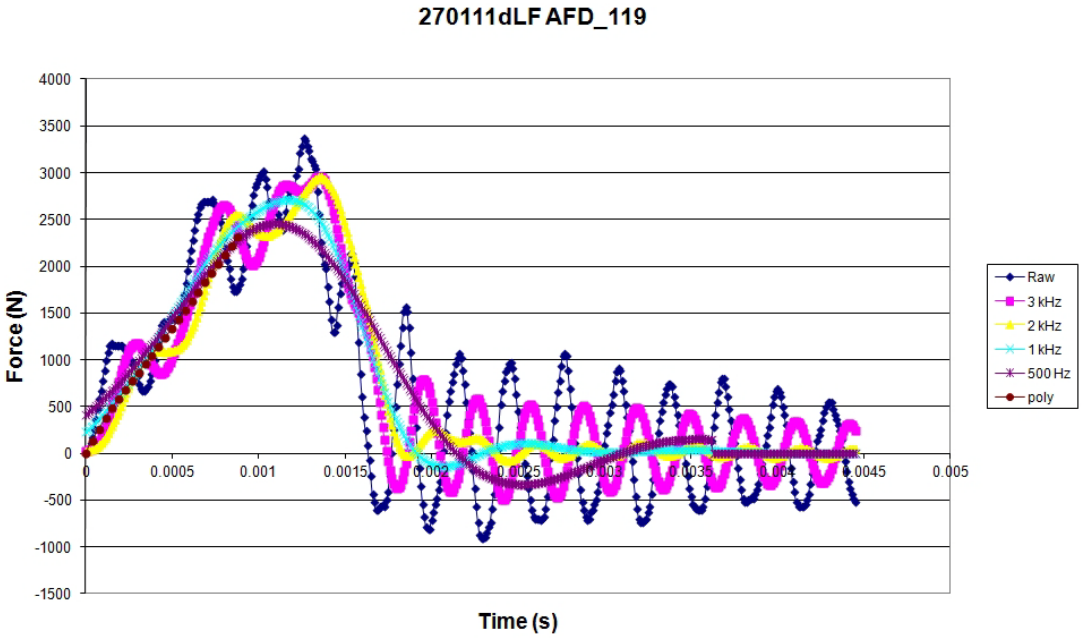
270111dLF AFD_119
Force (N)
Time (s)
Raw
3 kHz
2 kHz
1 kHz
500 Hz
poly

14.5.2 Normal Bone Quality

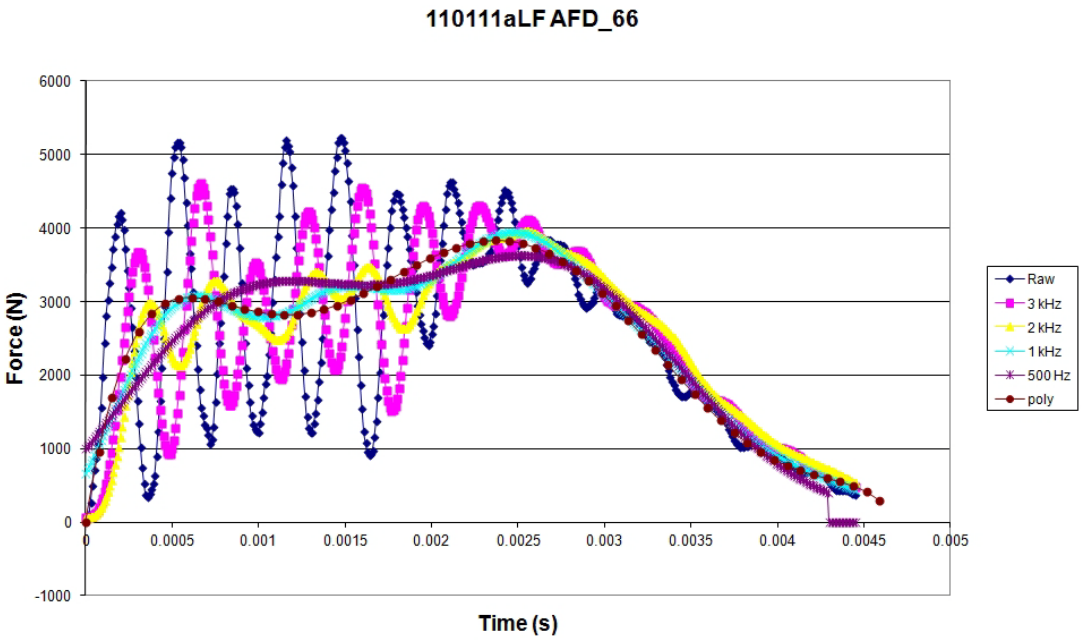

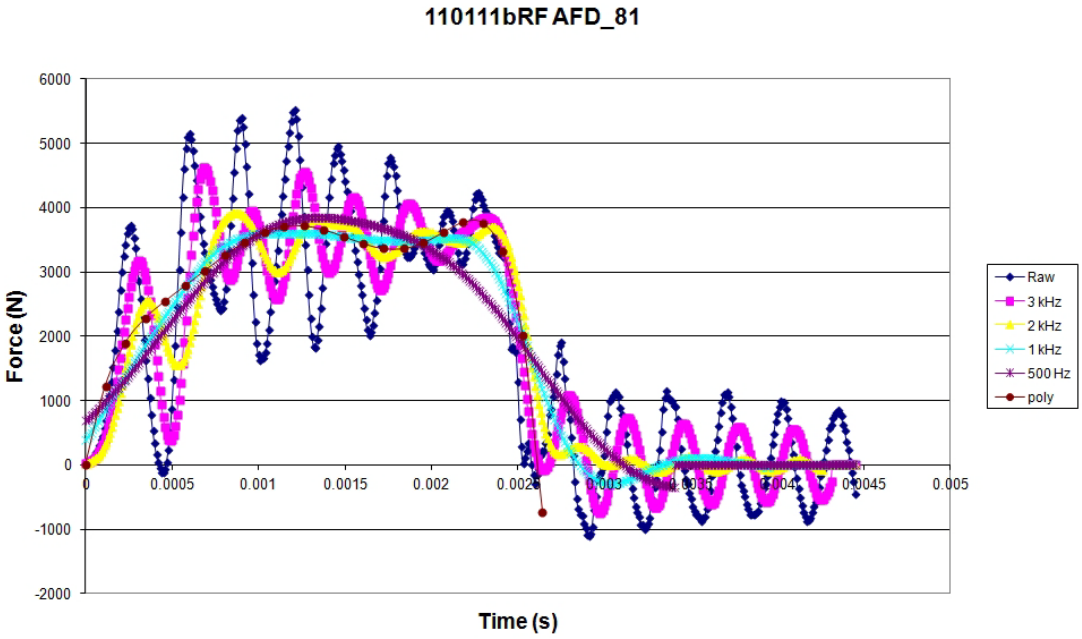

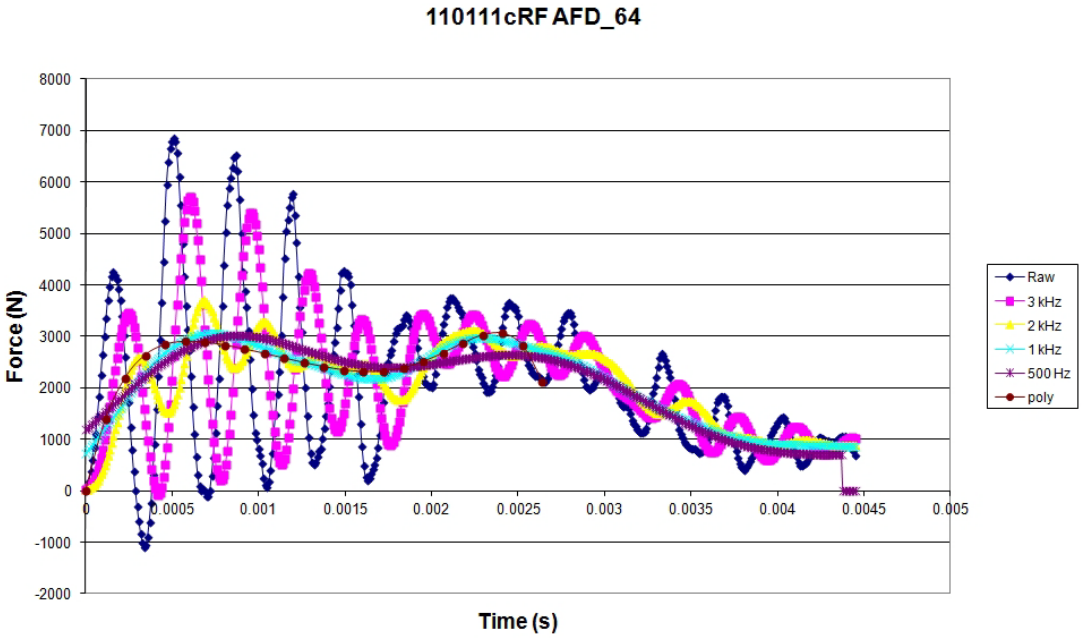
110111cRF AFD_64
Force (N)
Time (s)
Raw
3 kHz
2 kHz
1 kHz
500 Hz
poly

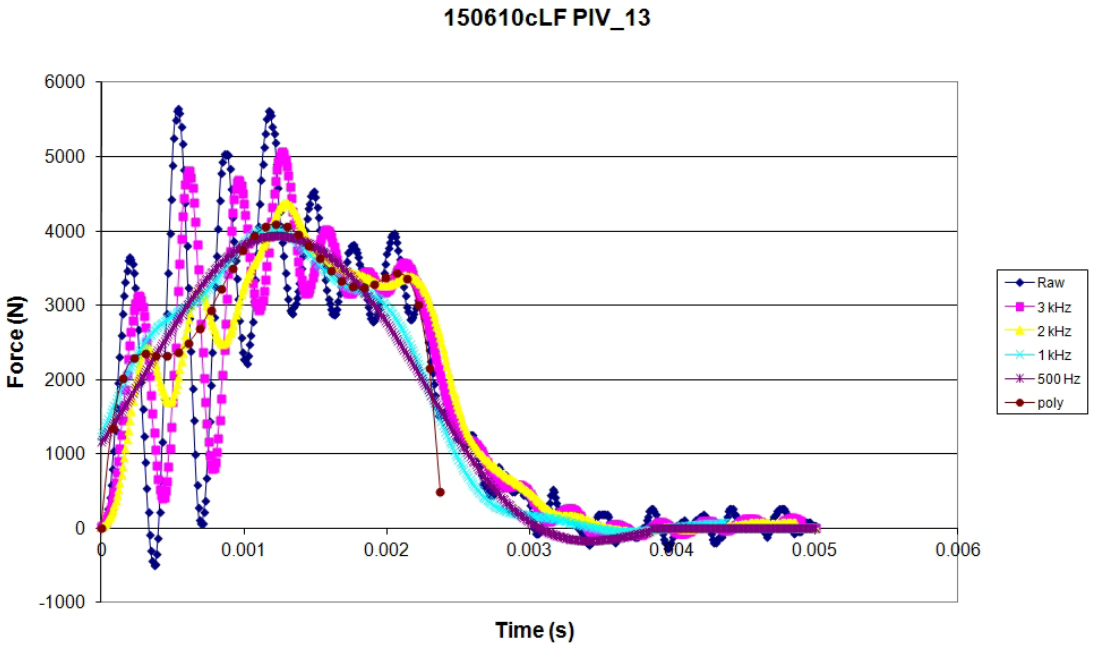
150610cLF PIV_13
Force (N)
Time (s)
Raw
3 kHz
2 kHz
1 kHz
500 Hz
poly

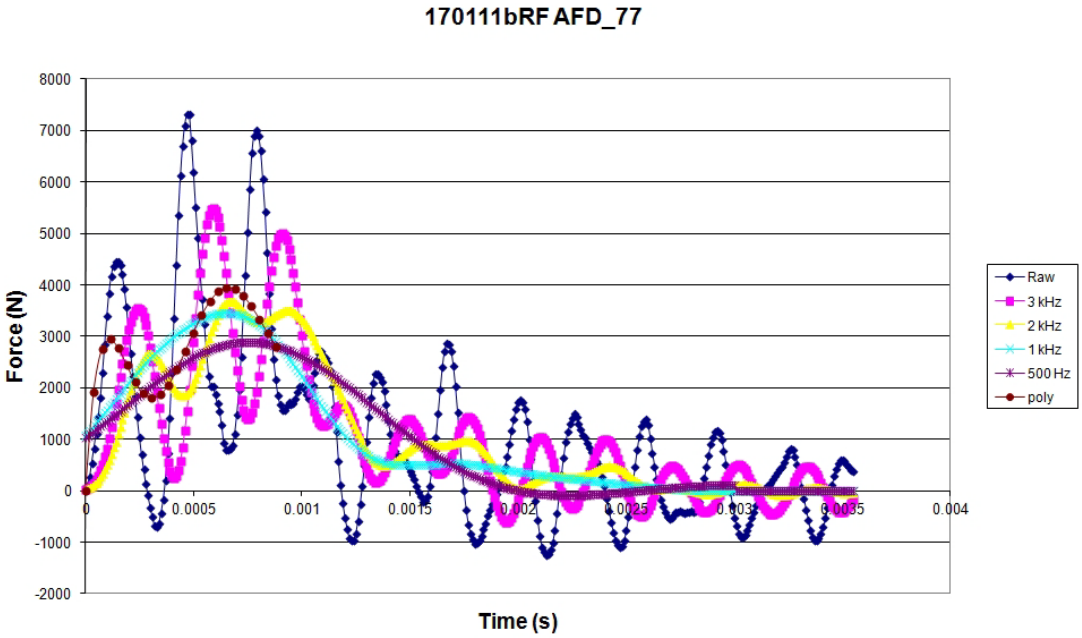
170111bRF AFD_77
Force (N)
Time (s)
Raw
3 kHz
2 kHz
1 kHz
500 Hz
poly

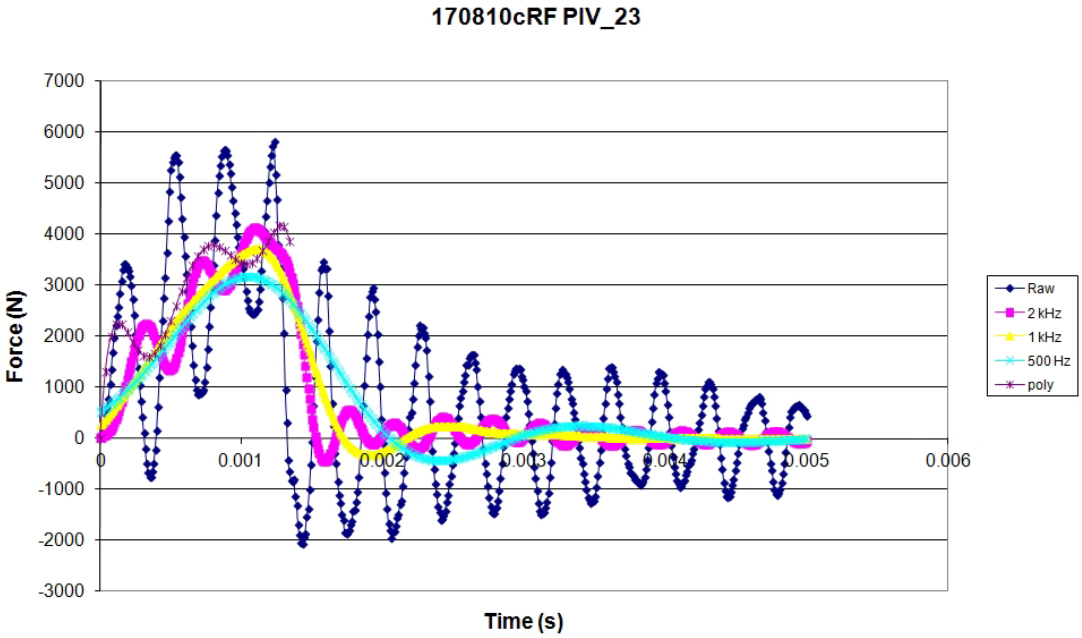
170810cRF PIV_23
Force (N)
Time (s)
Raw
2 kHz
1 kHz
500 Hz
poly

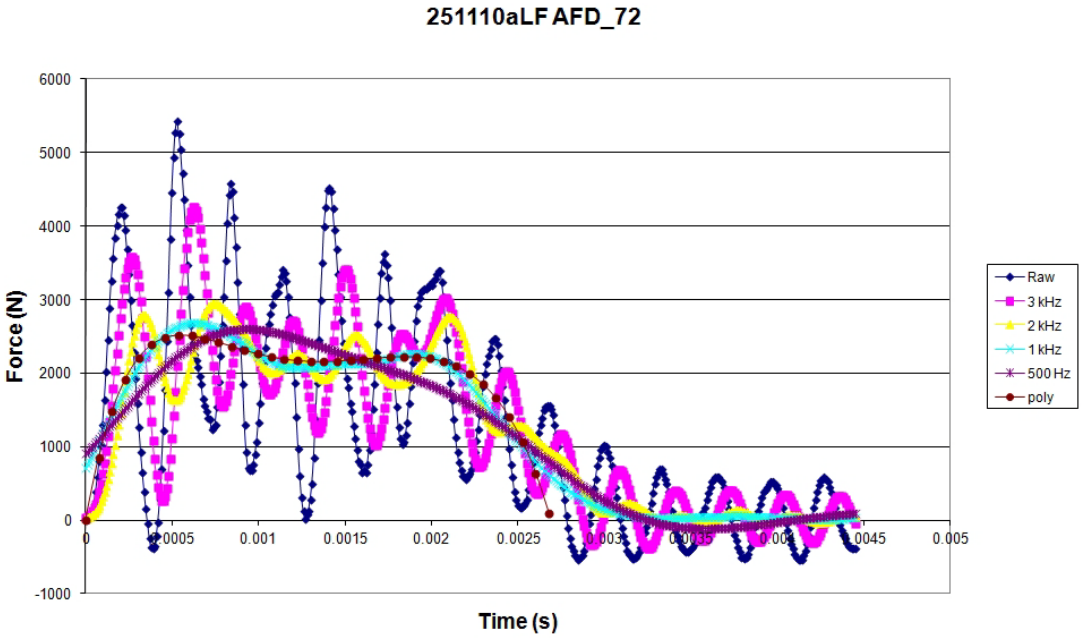
251110aLF AFD_72
Force (N)
Time (s)
Raw
3 kHz
2 kHz
1 kHz
500 Hz
poly

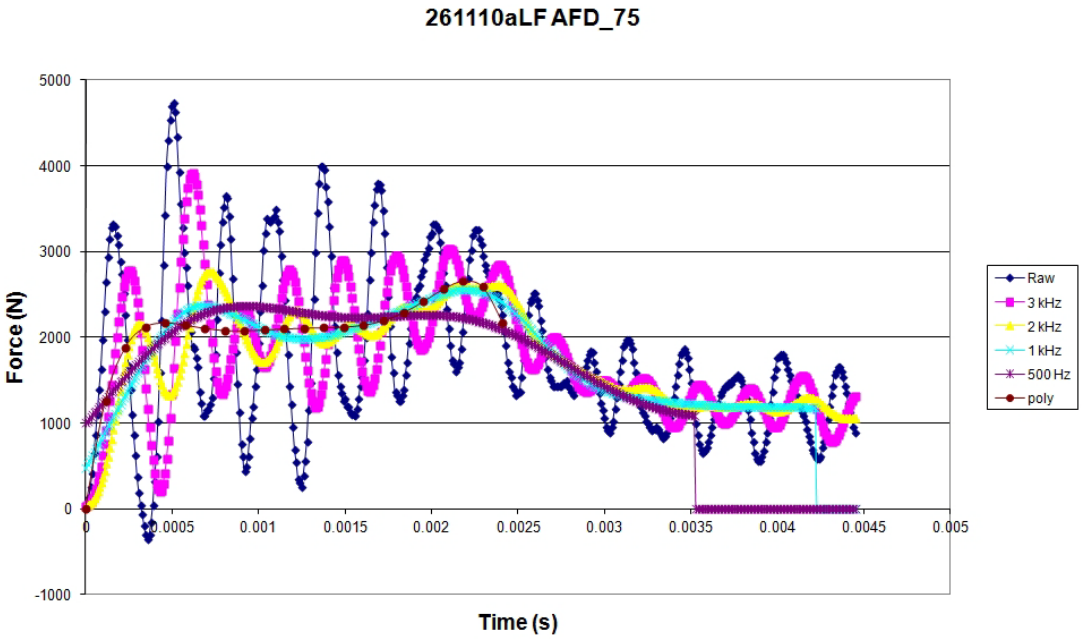
261110aLF AFD_75
Force (N)
Time (s)
Raw
3 kHz
2 kHz
1 kHz
500 Hz
poly

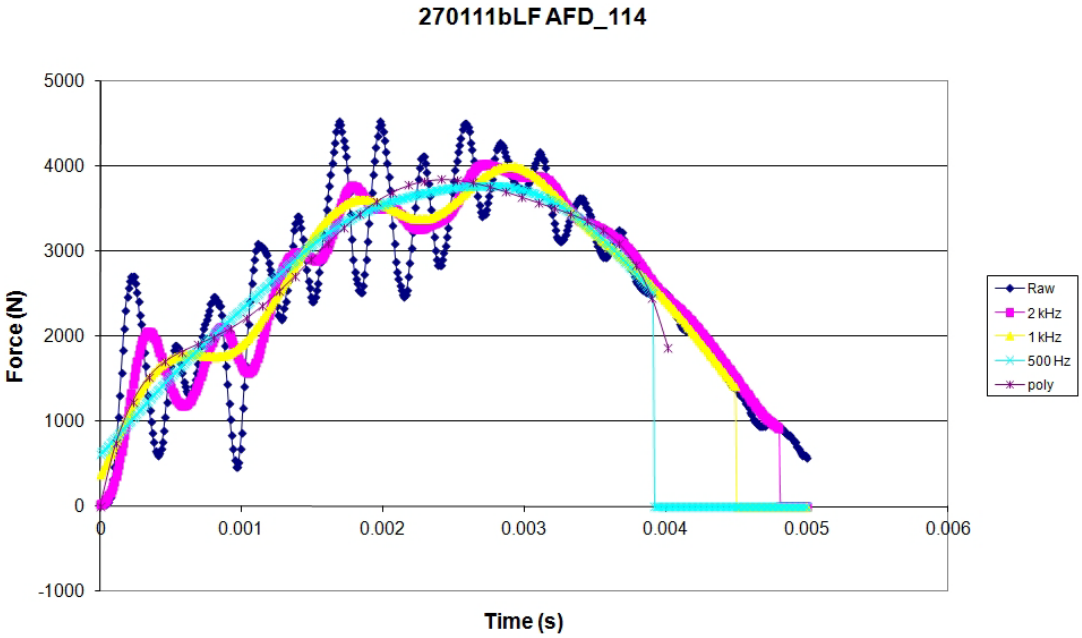
270111bLF AFD_114
Force (N)
Time (s)
Raw
2 kHz
1 kHz
500 Hz
poly

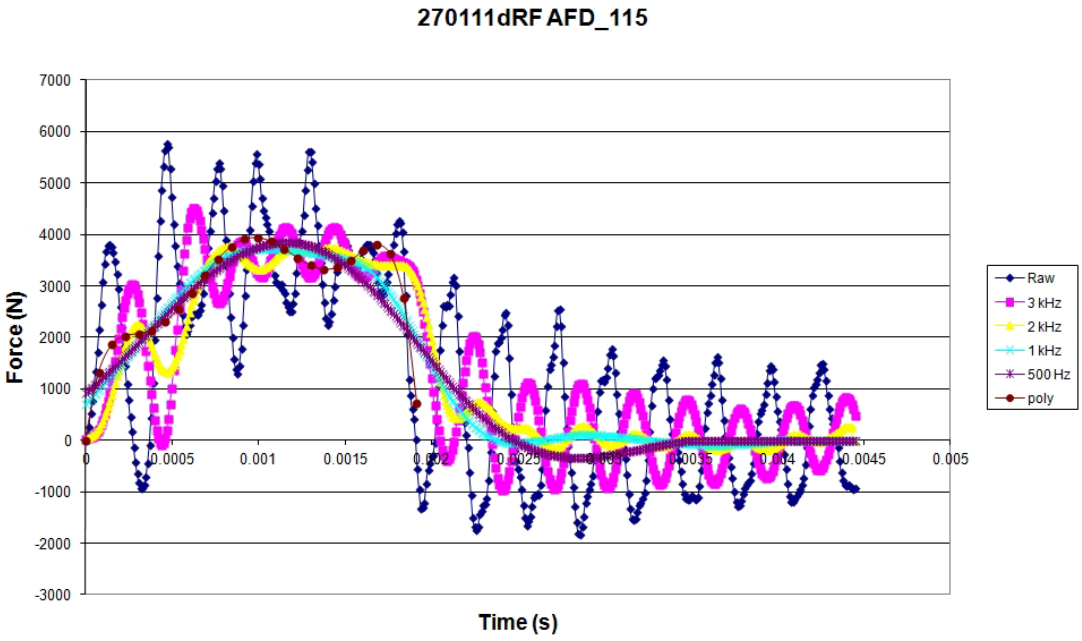
270111dRF AFD_115
Force (N)
Time (s)
Raw
3 kHz
2 kHz
1 kHz
500 Hz
poly

14.6 Appendix F: Radiographs

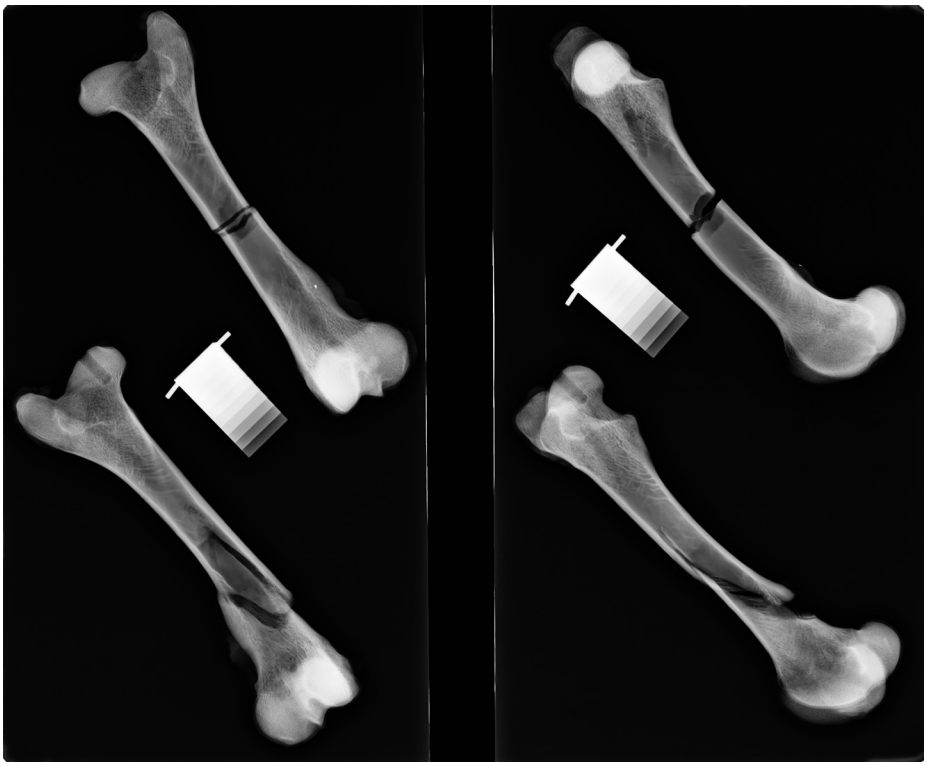

03aL+R

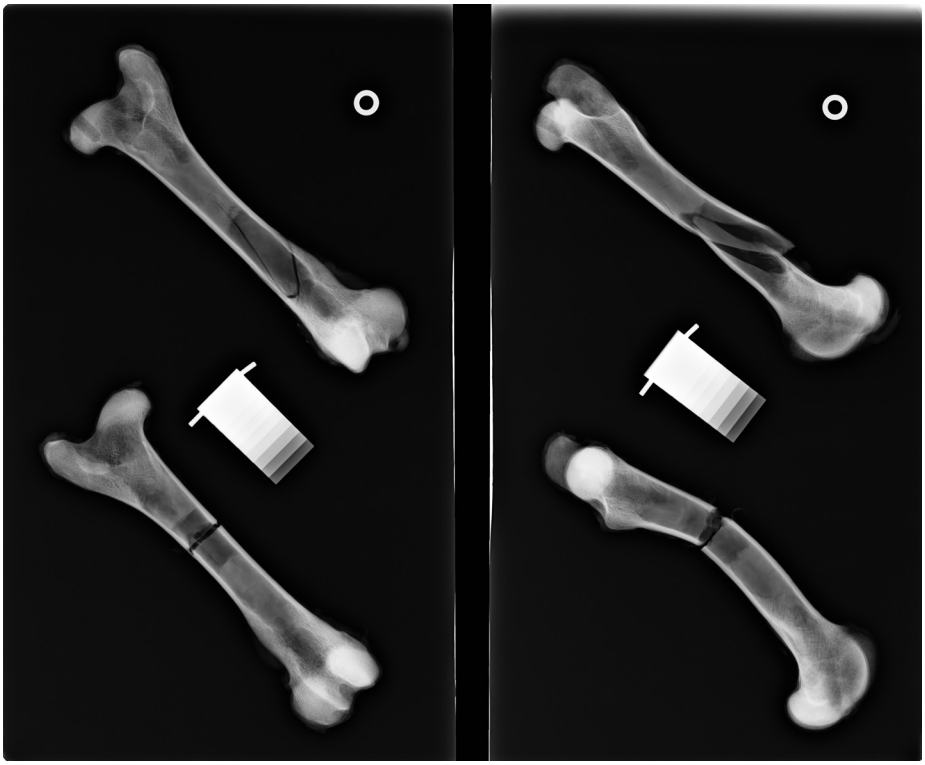

060111aL+R

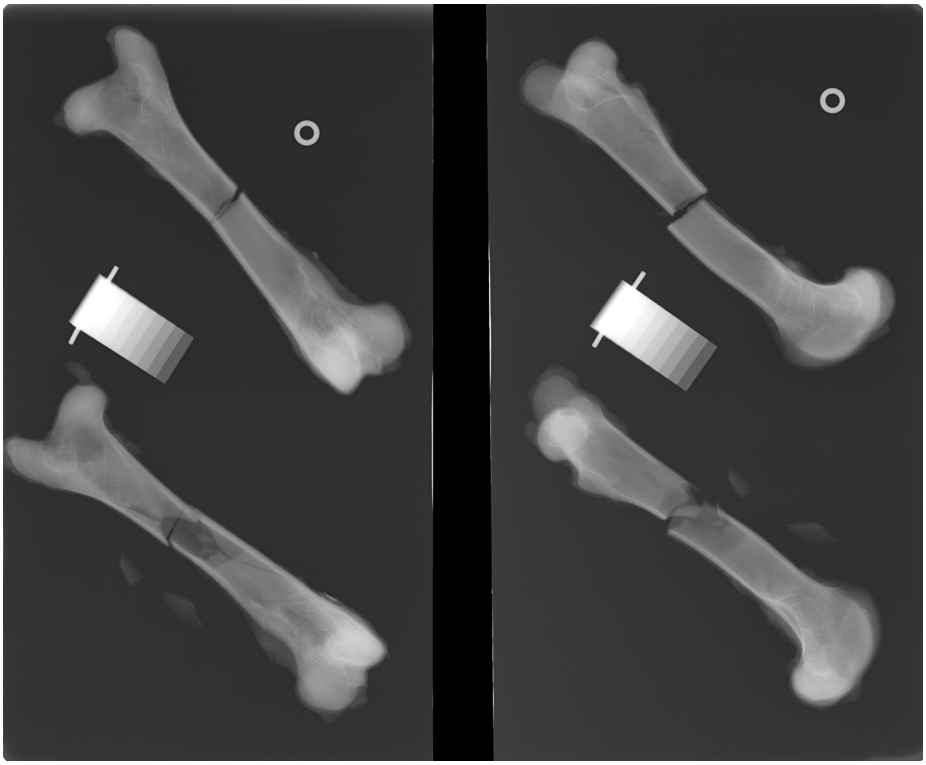

060111bL+R

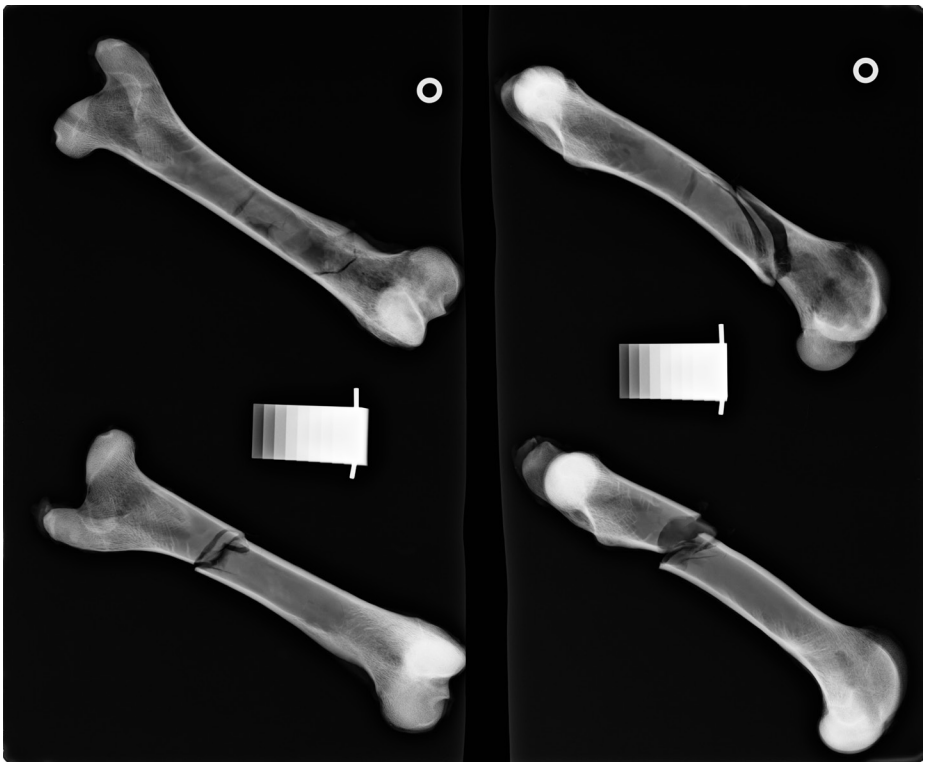

100111aL+R

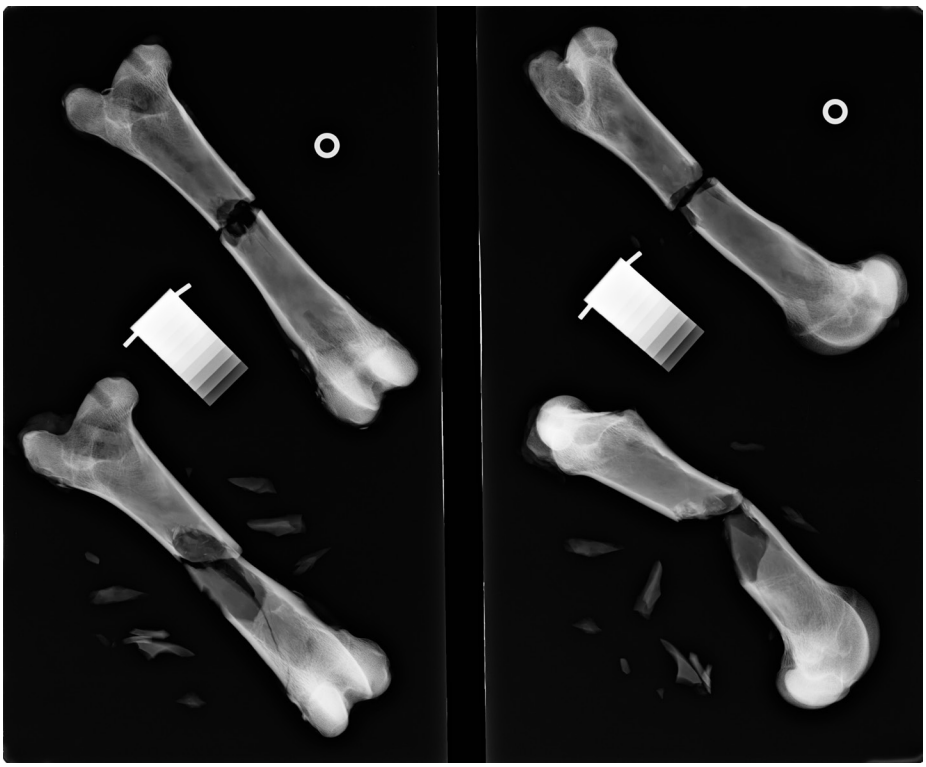

110111aL+R

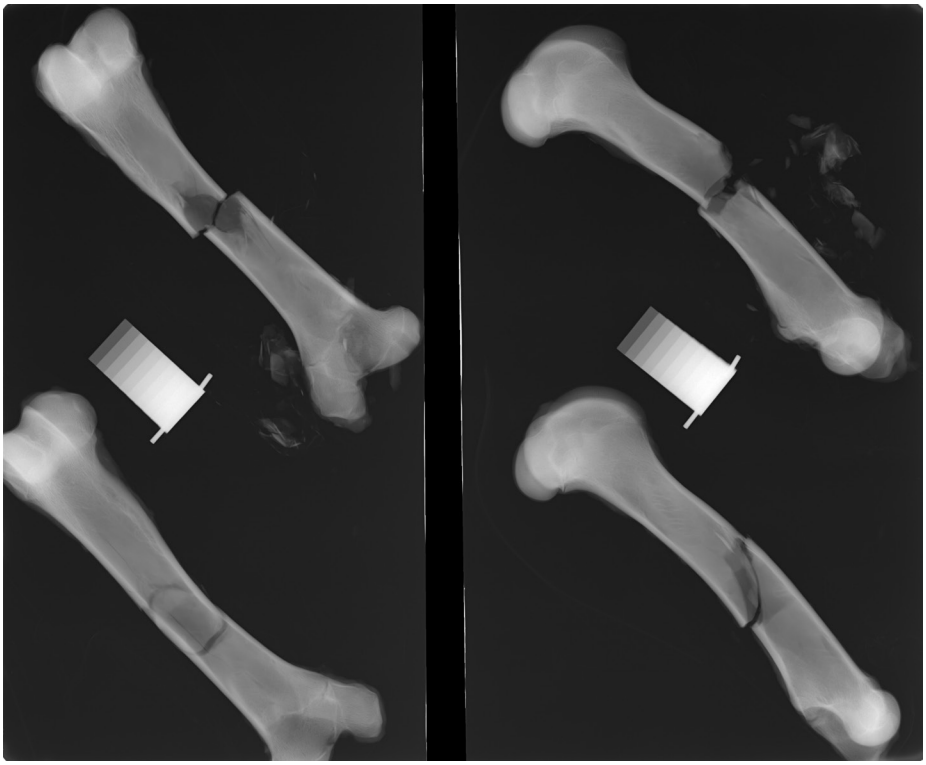

110111bL+R

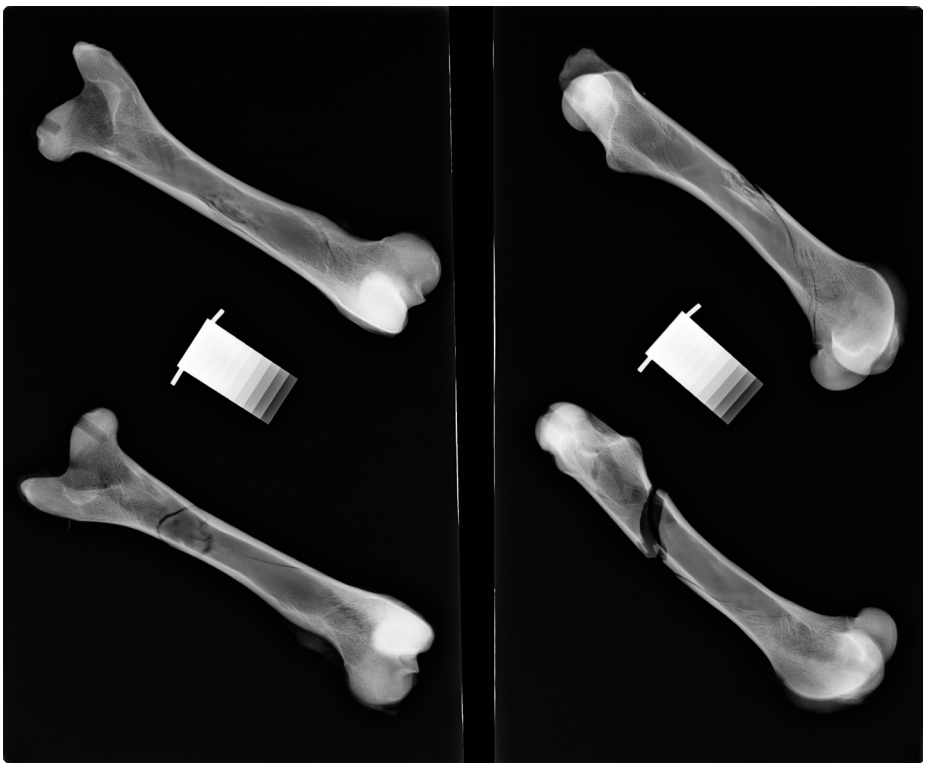

110111cL+R

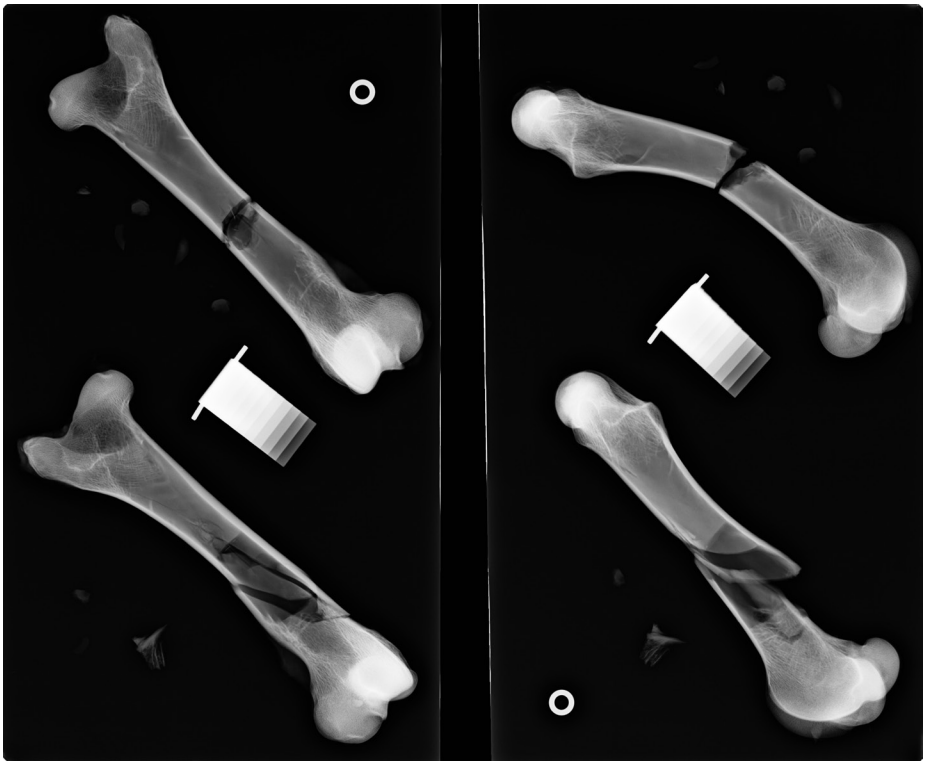

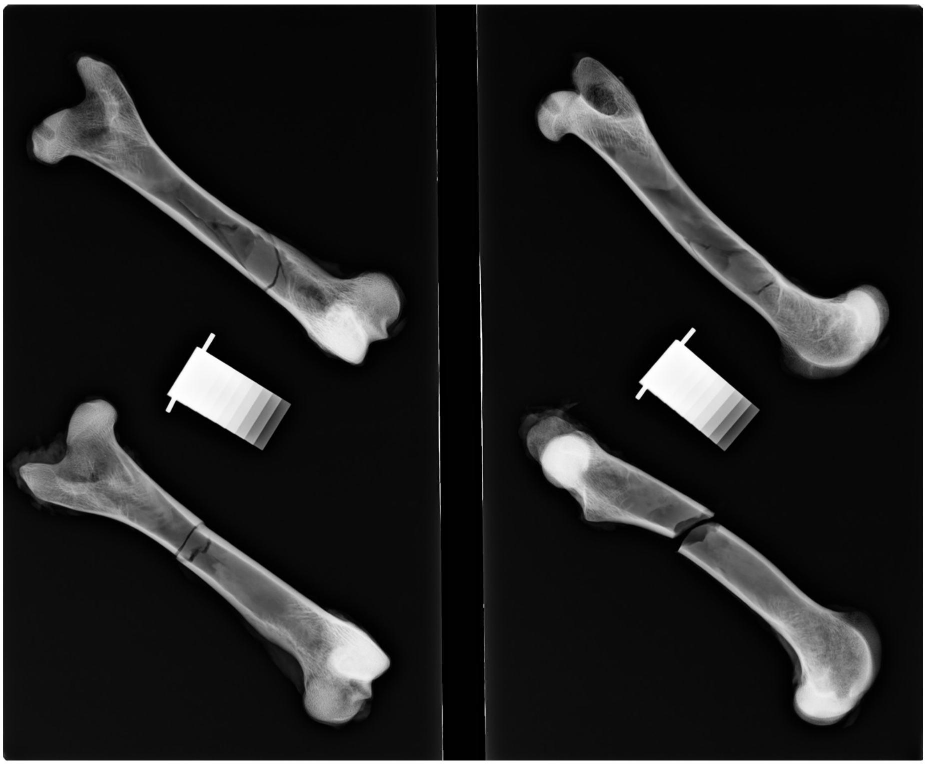

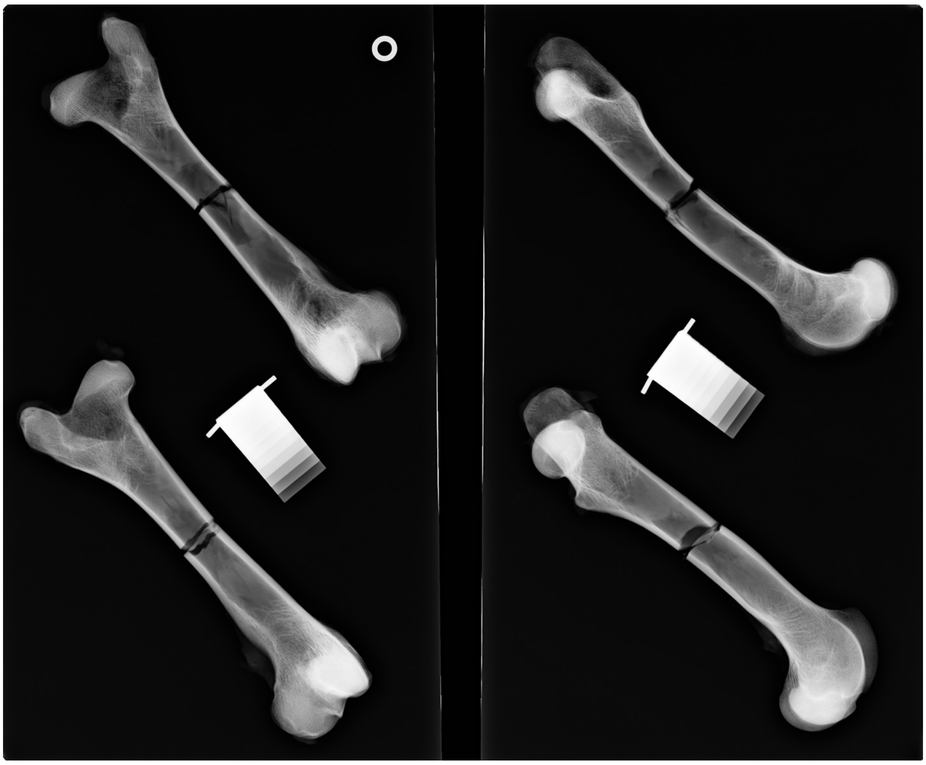

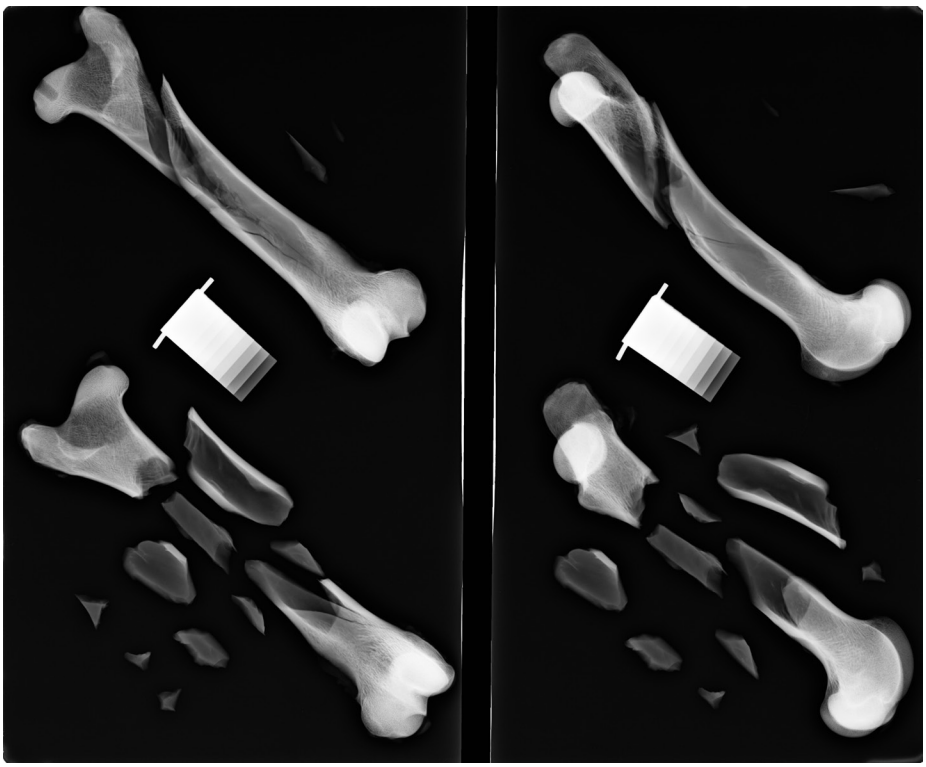

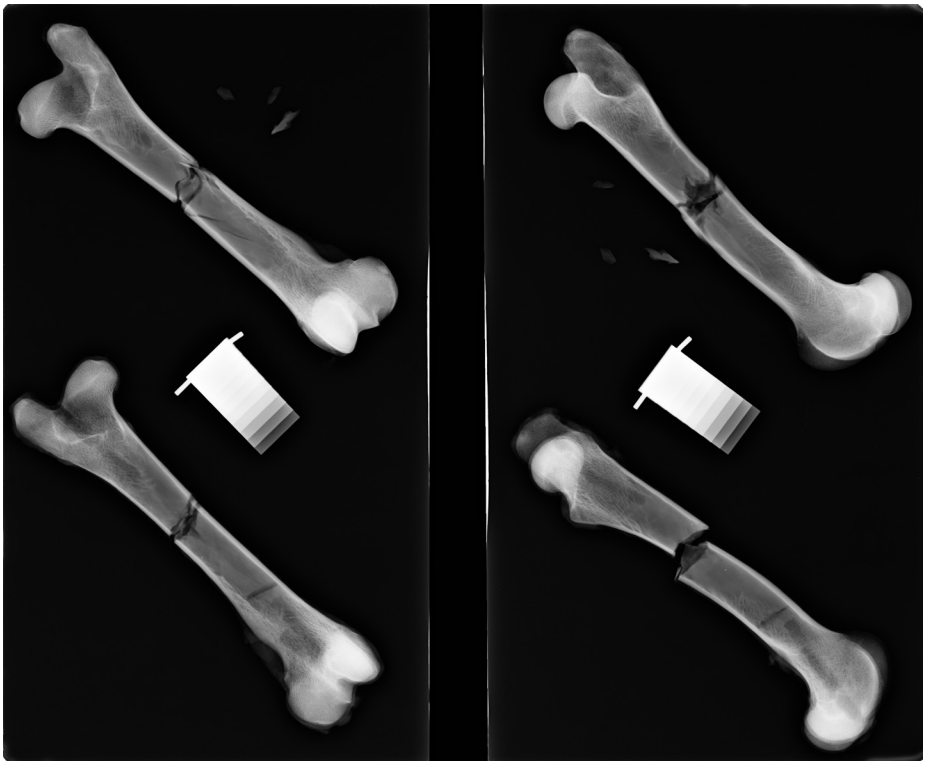

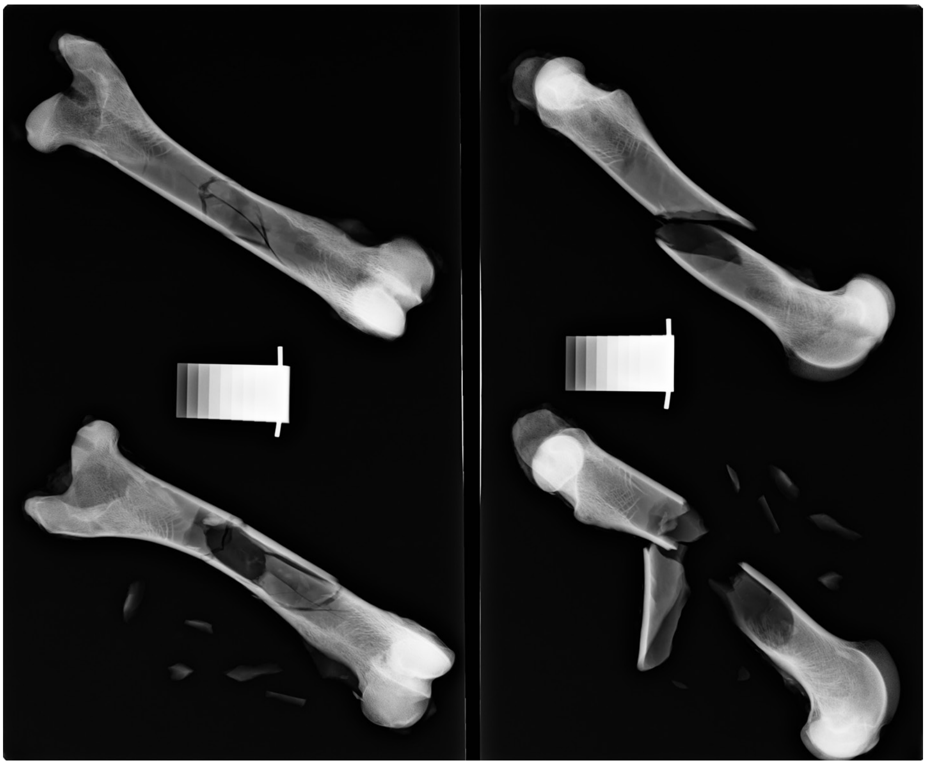

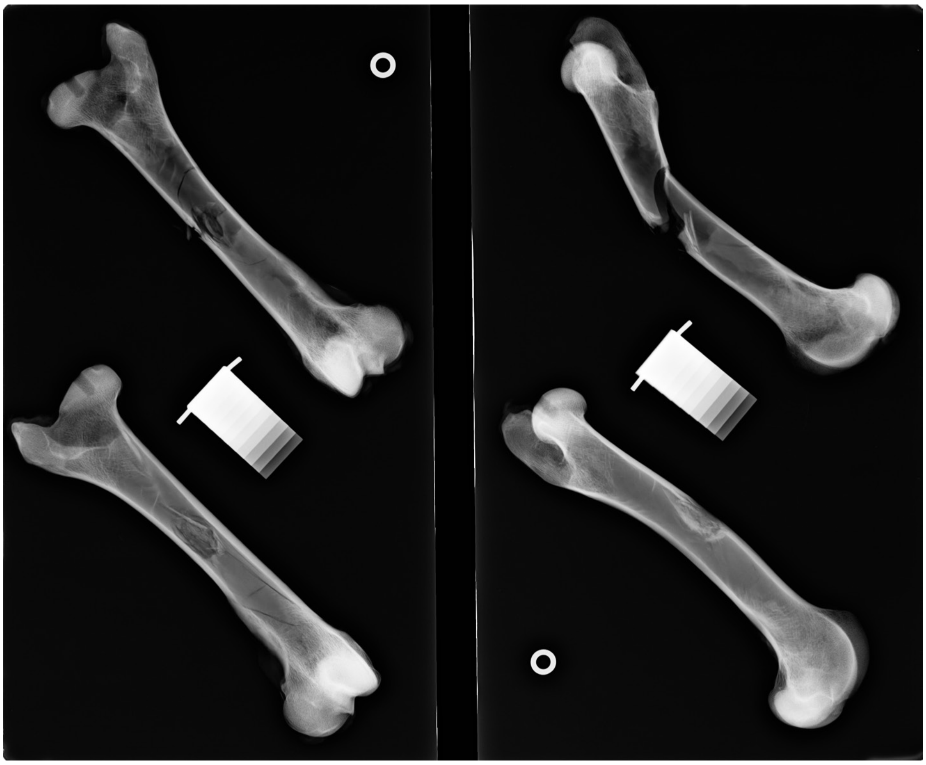

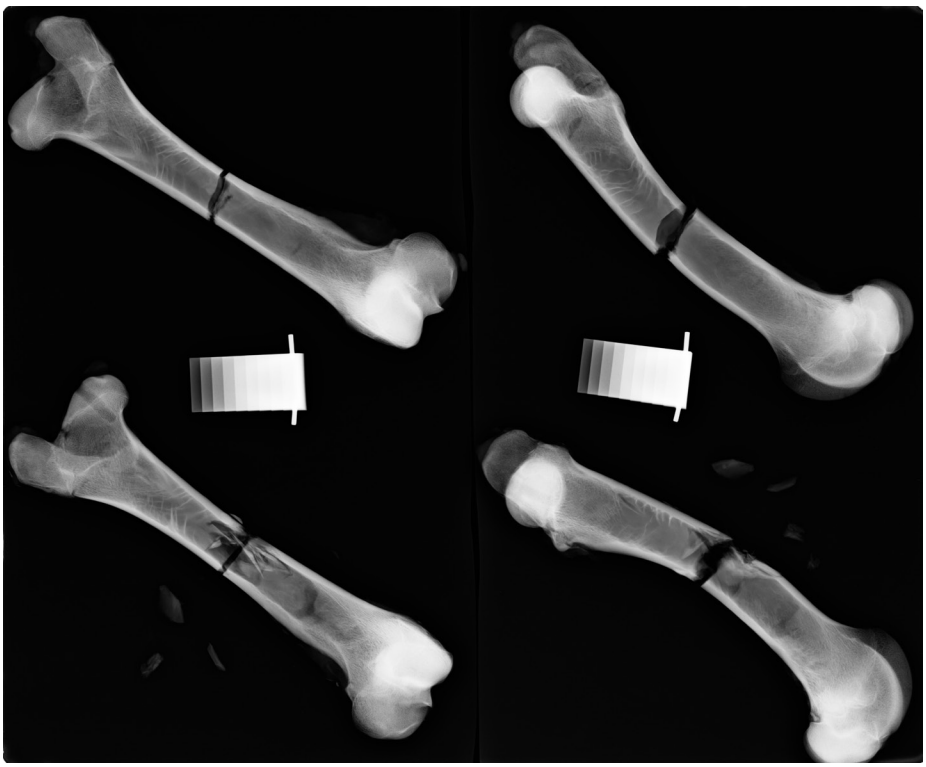

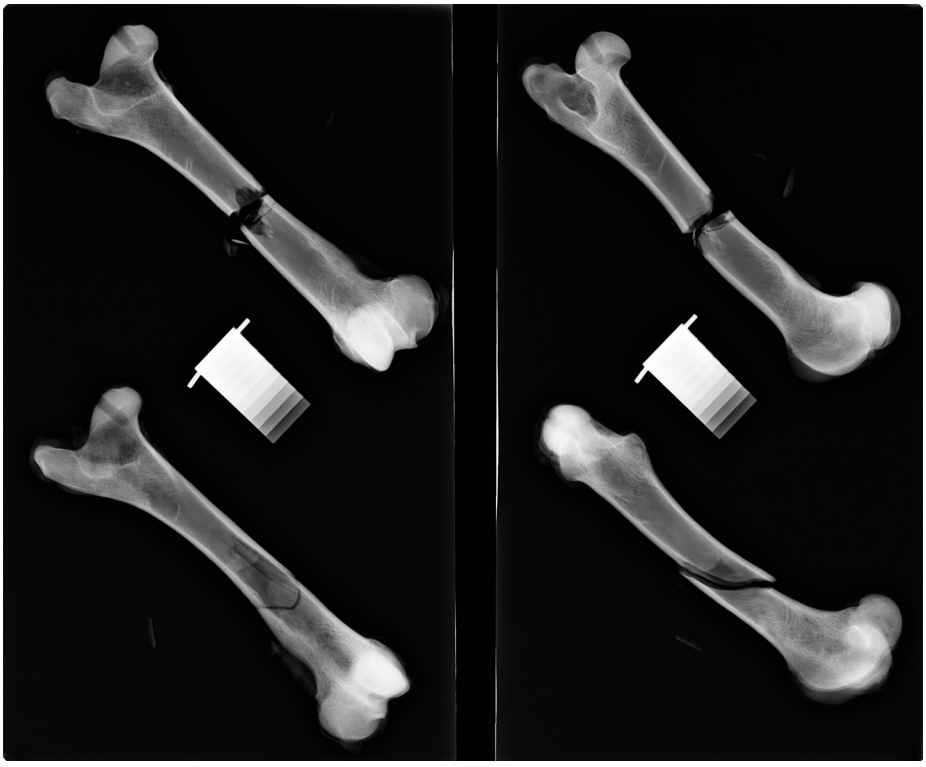

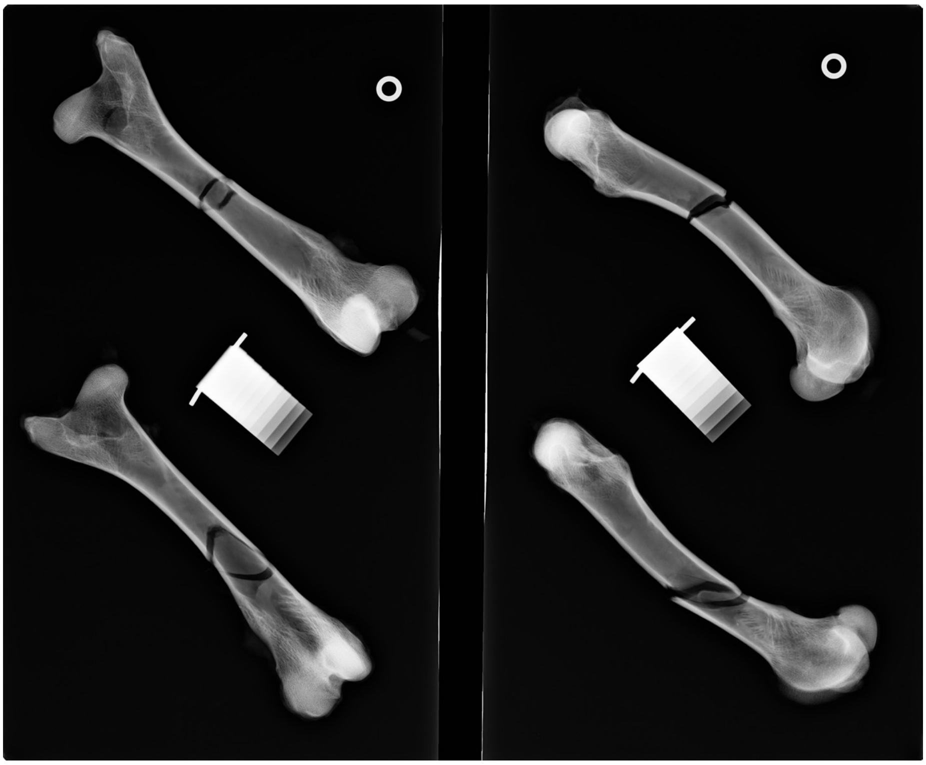

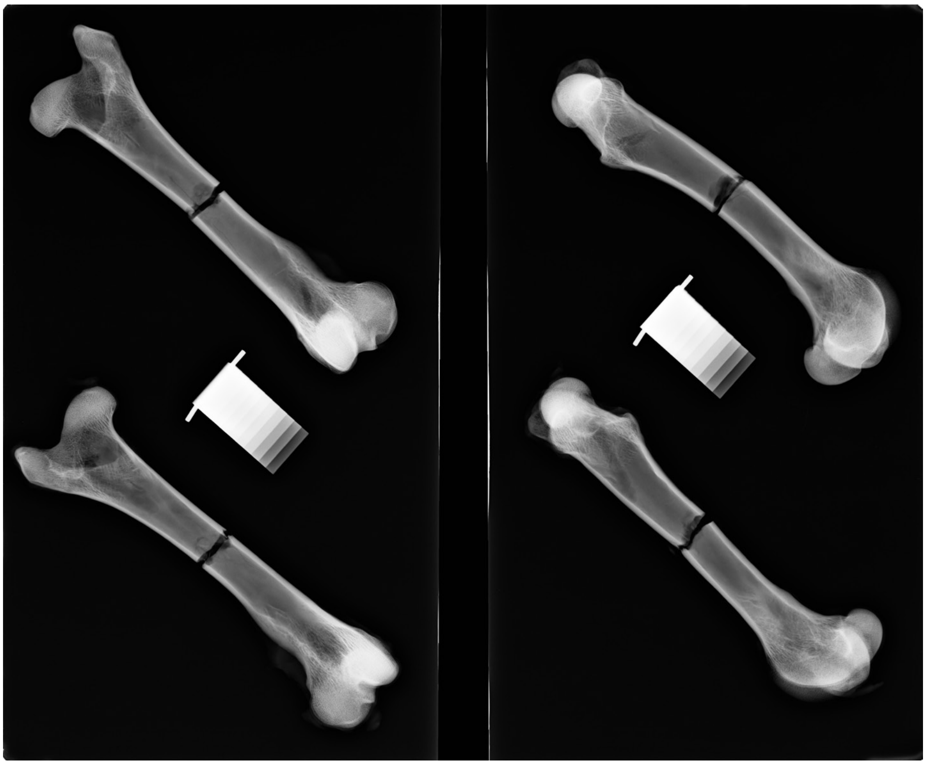

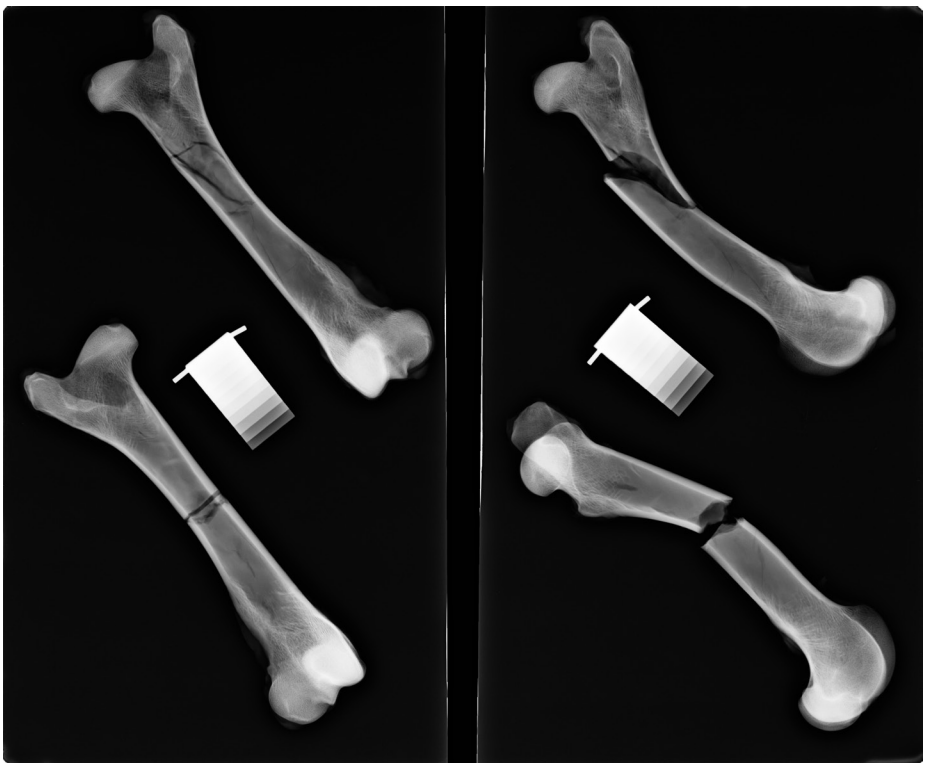

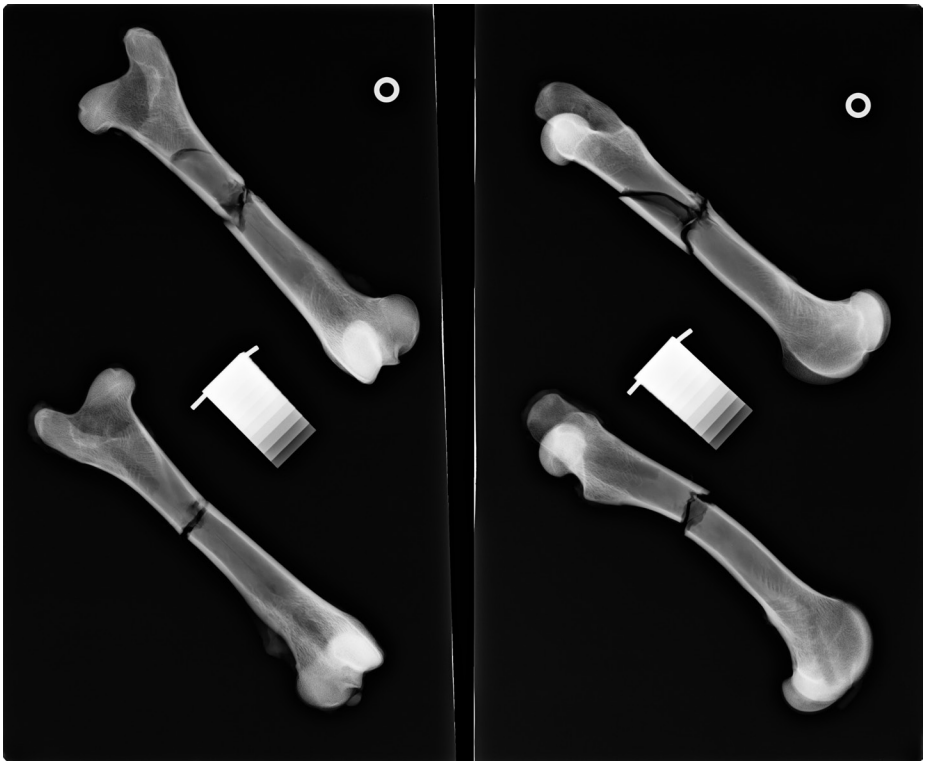

14.7 Appendix G: Stress strain graphs

14.7.1 Slow loaded, Normal Bone Quality

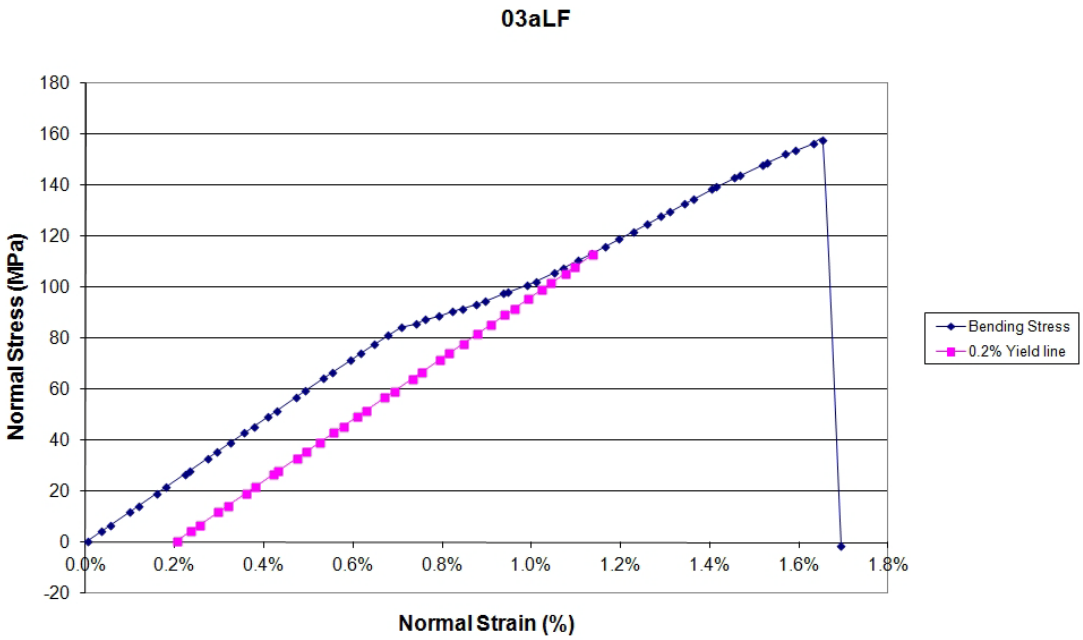

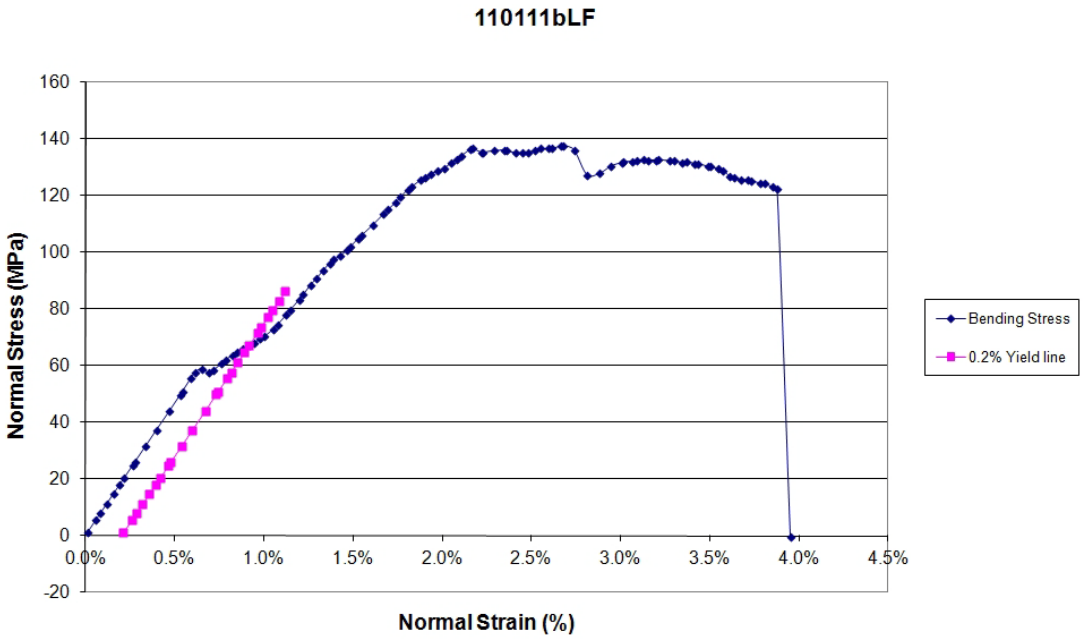

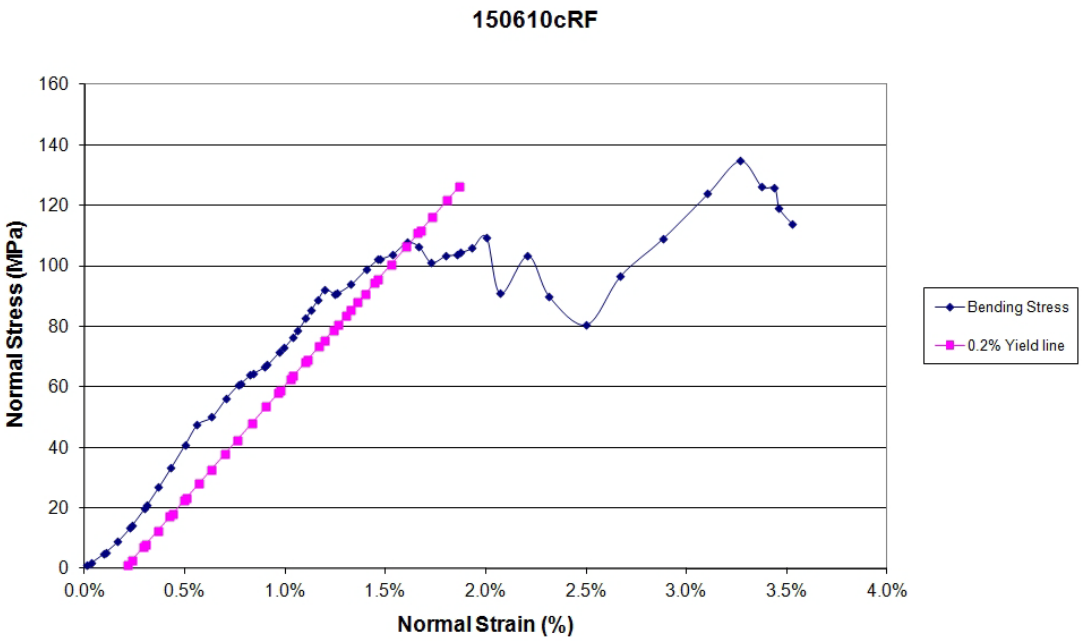
150610cRF
Normal Stress (MPa)
160
140
120
100
80
60
40
20
0
0.0%
0.5%
1.0%
1.5%
2.0%
2.5%
3.0%
3.5%
4.0%
Normal Strain (%)
Bending Stress
0.2% Yield line

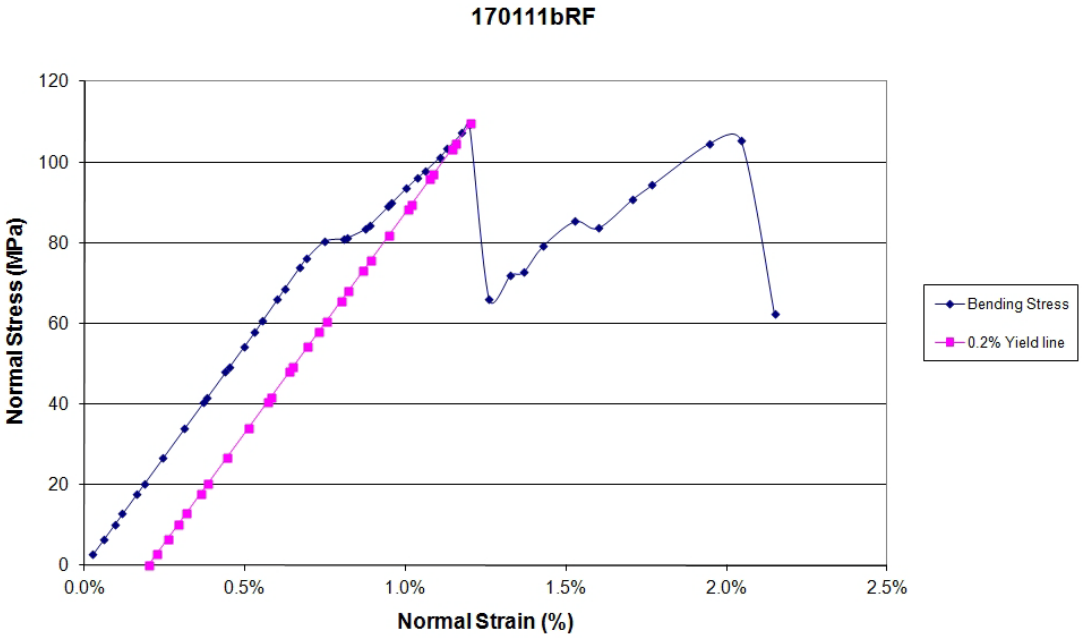
170111bRF
Normal Stress (MPa)
120
100
80
60
40
20
0
0.0%
0.5%
1.0%
1.5%
2.0%
2.5%
Normal Strain (%)
Bending Stress
0.2% Yield line

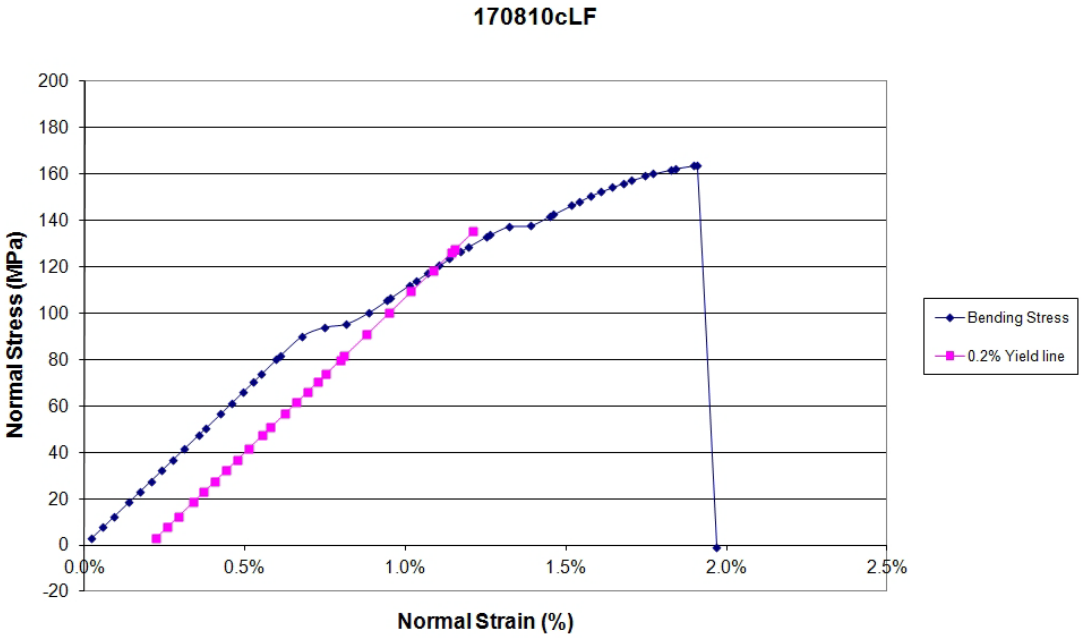
170810cLF
Normal Stress (MPa)
200
180
160
140
120
100
80
60
40
20
0
-20
0.0%
0.5%
1.0%
1.5%
2.0%
2.5%
Normal Strain (%)
Bending Stress
0.2% Yield line

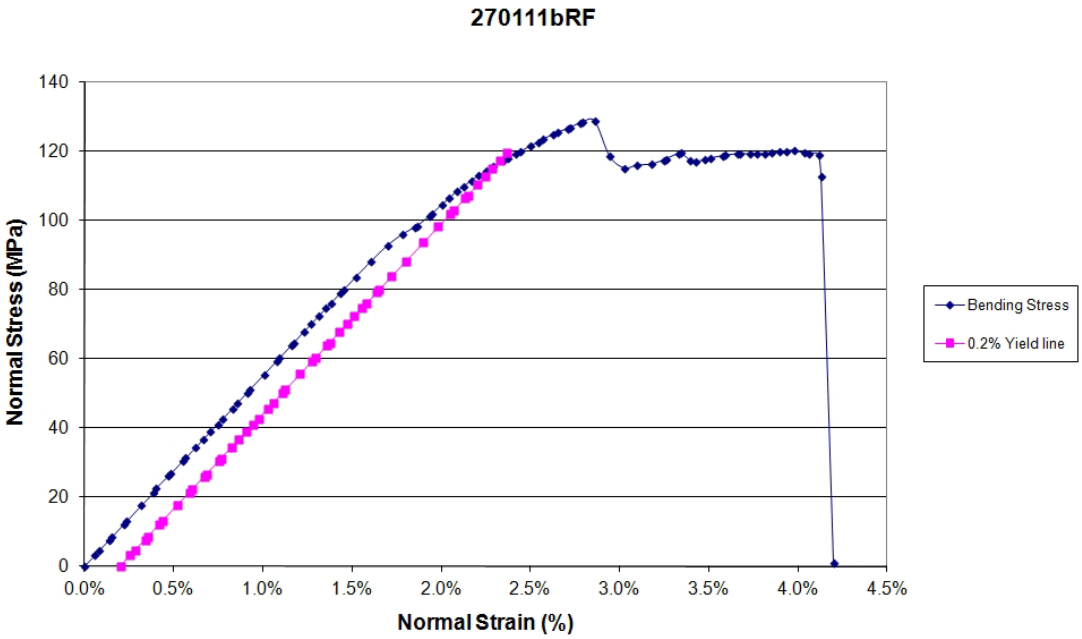
270111bRF
Normal Stress (MPa)
140
120
100
80
60
40
20
0
0.0%
0.5%
1.0%
1.5%
2.0%
2.5%
3.0%
3.5%
4.0%
4.5%
Normal Strain (%)
Bending Stress
0.2% Yield line

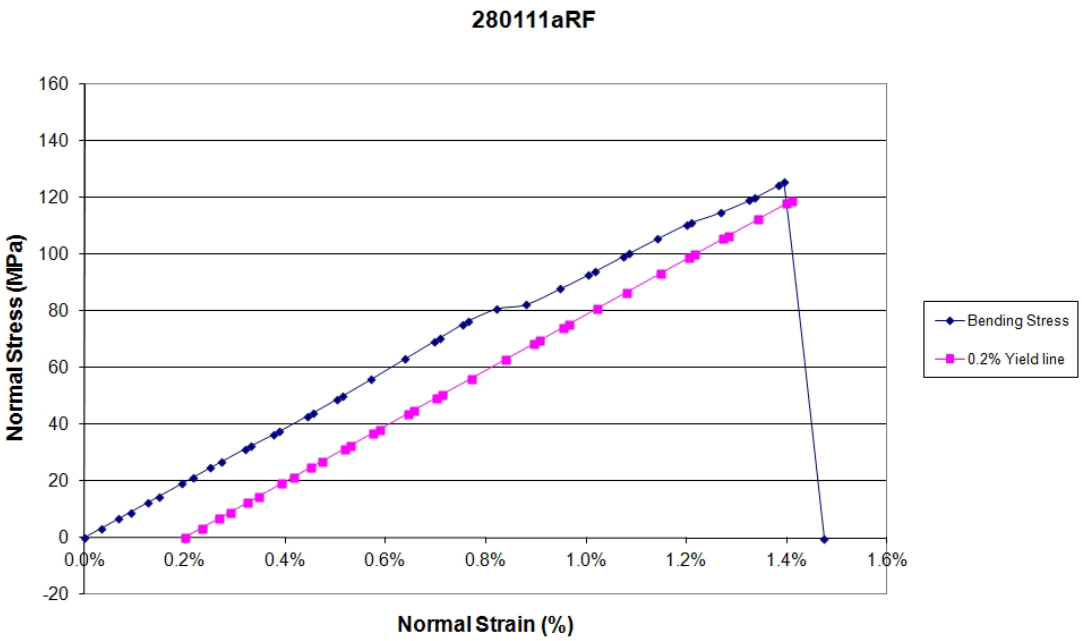
280111aRF
160
140
120
100
80
60
40
20
0
-20
0.0%
0.2%
0.4%
0.6%
0.8%
1.0%
1.2%
1.4%
1.6%
Normal Stress (MPa)
Normal Strain (%)
Bending Stress
0.2% Yield line

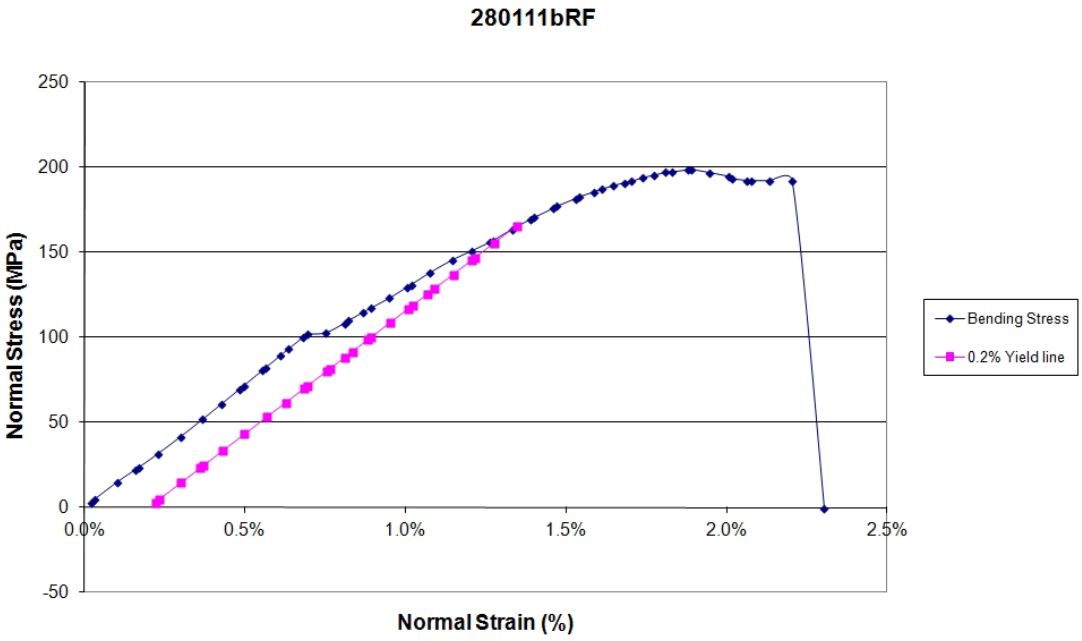
280111bRF
250
200
150
100
50
0
-50
0.0%
0.5%
1.0%
1.5%
2.0%
2.5%
Normal Stress (MPa)
Normal Strain (%)
Bending Stress
0.2% Yield line

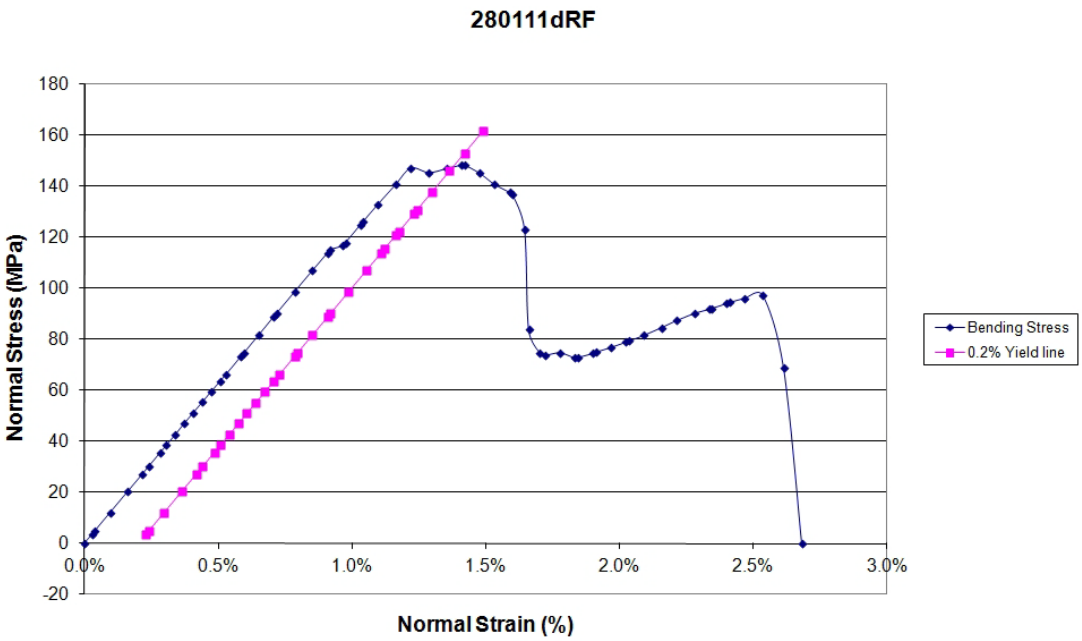
280111dRF
Normal Stress (MPa)
180
160
140
120
100
80
60
40
20
0
-20
0.0%
0.5%
1.0%
1.5%
2.0%
2.5%
3.0%
Normal Strain (%)
Bending Stress
0.2% Yield line

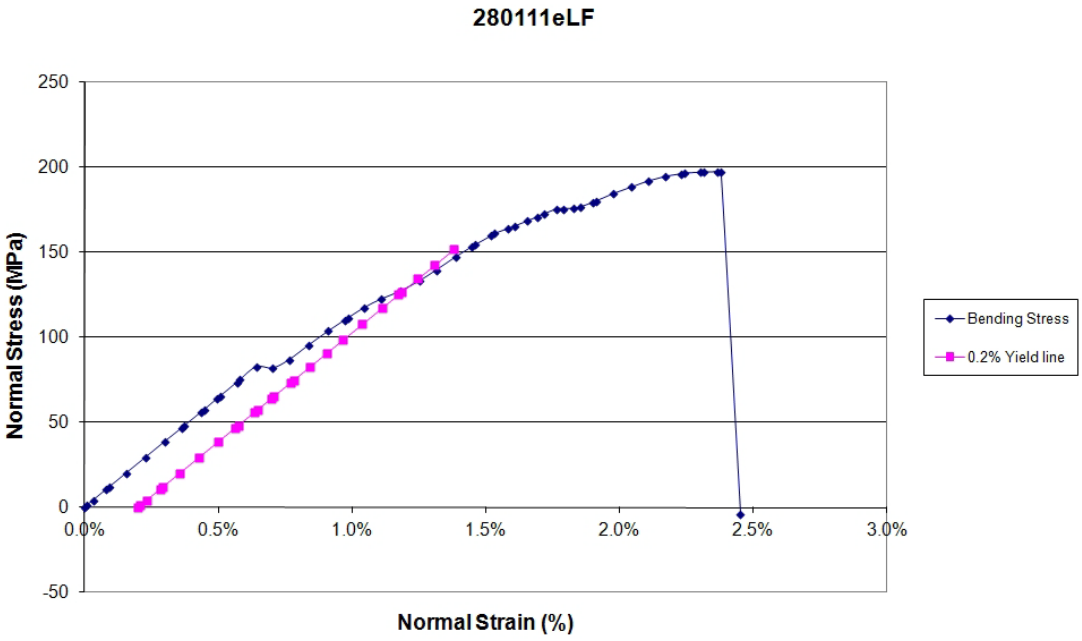
280111eLF
Normal Stress (MPa)
250
200
150
100
50
0
-50
0.0%
0.5%
1.0%
1.5%
2.0%
2.5%
3.0%
Normal Strain (%)
Bending Stress
0.2% Yield line

14.7.2 Slow Loading, Demineralised Bones

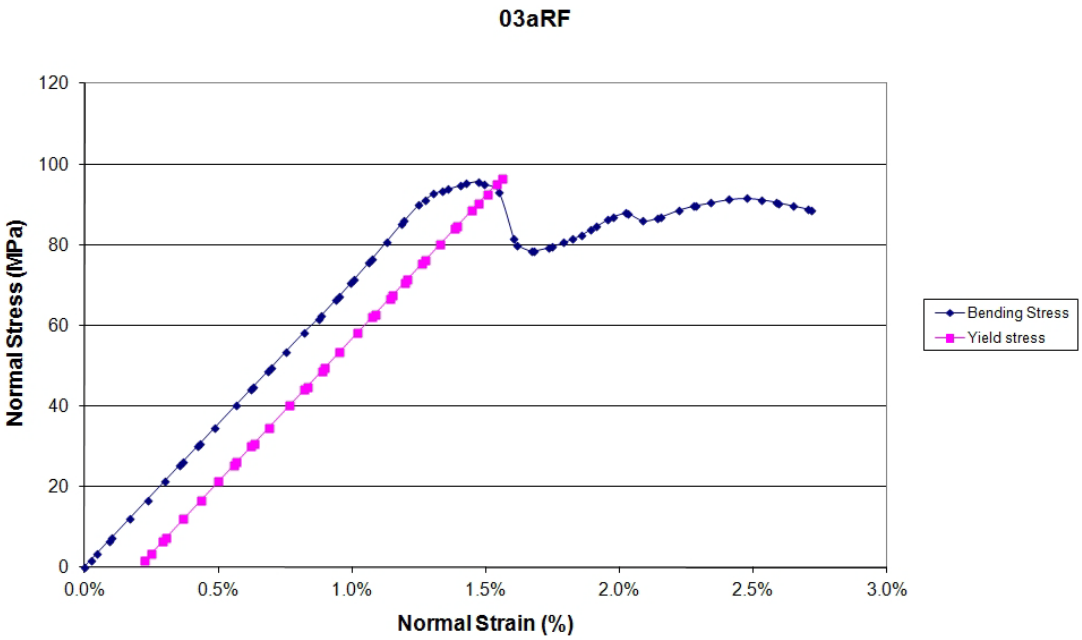

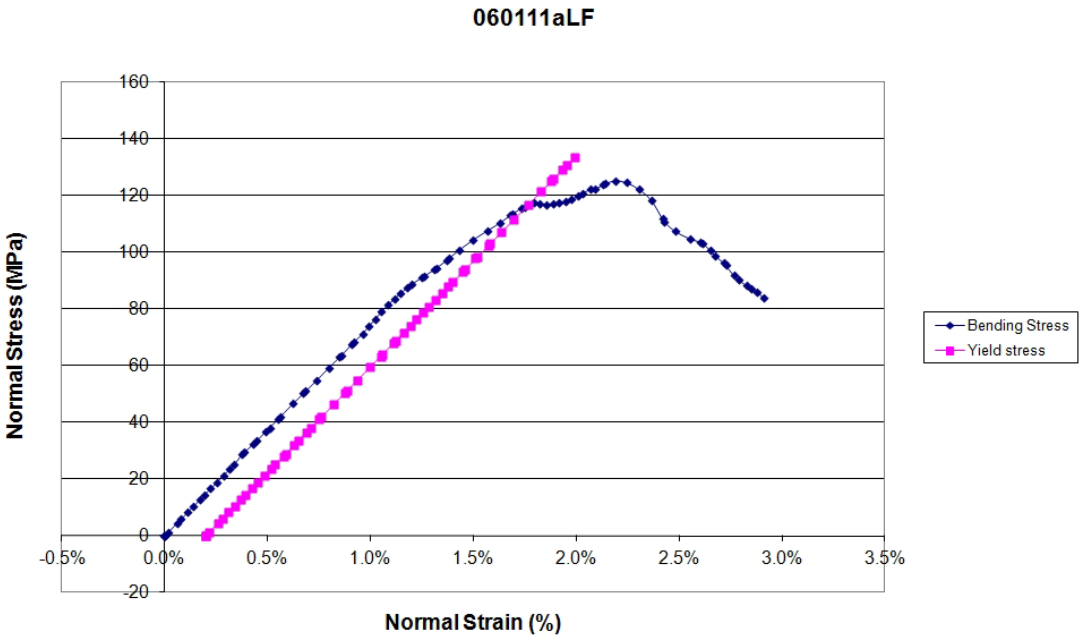

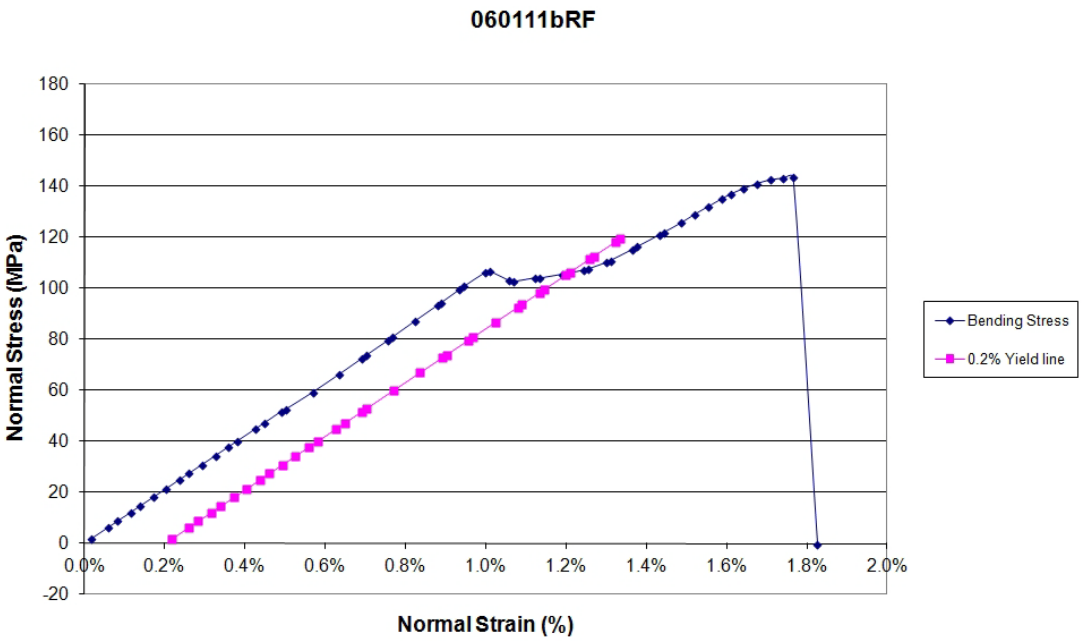
060111bRF
Normal Stress (MPa)
180
160
140
120
100
80
60
40
20
0
-20
0.0%
0.2%
0.4%
0.6%
0.8%
1.0%
1.2%
1.4%
1.6%
1.8%
2.0%
Normal Strain (%)
Bending Stress
0.2% Yield line

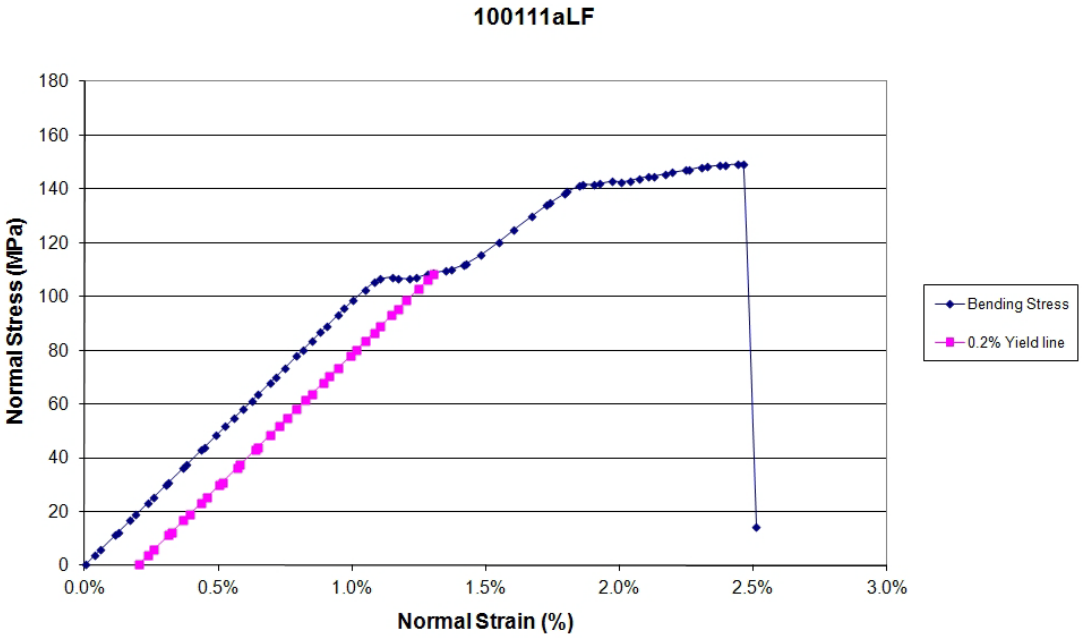
100111aLF
Normal Stress (MPa)
180
160
140
120
100
80
60
40
20
0
0.0%
0.5%
1.0%
1.5%
2.0%
2.5%
3.0%
Normal Strain (%)
Bending Stress
0.2% Yield line

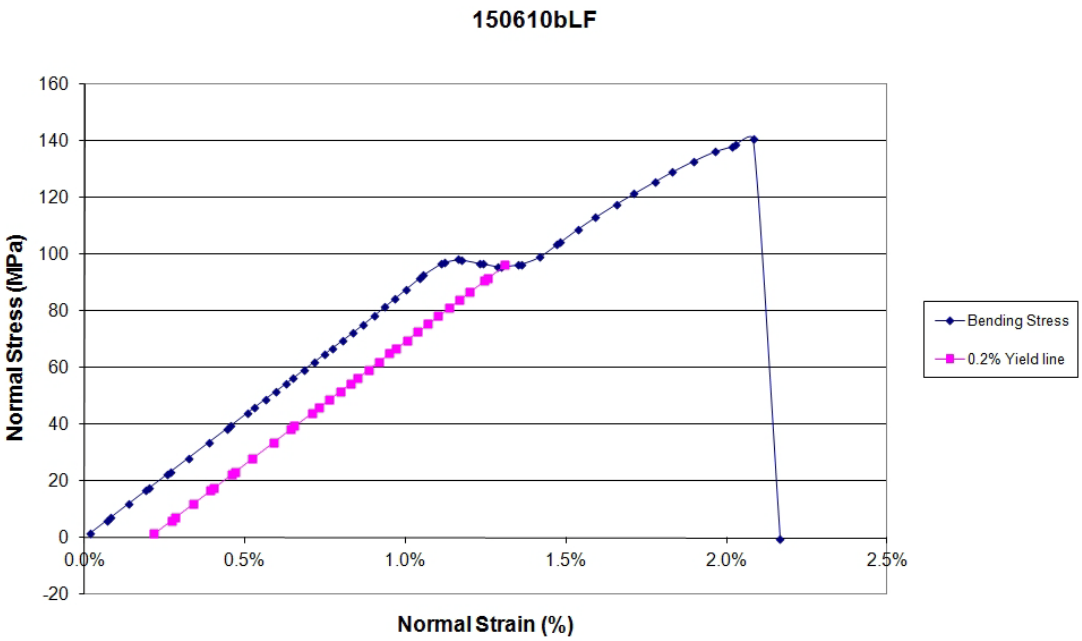
150610bLF
160
140
120
100
80
60
40
20
0
-20
0.0%
0.5%
1.0%
1.5%
2.0%
2.5%
Normal Stress (MPa)
Normal Strain (%)
Bending Stress
0.2% Yield line

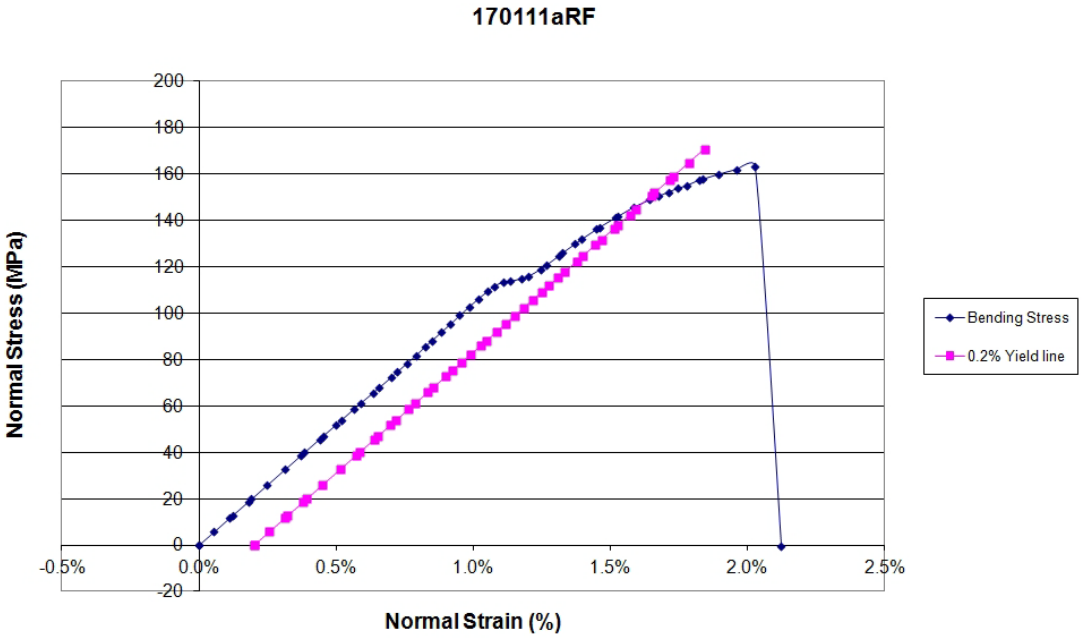
170111aRF
200
180
160
140
120
100
80
60
40
20
0
-20
-0.5%
0.0%
0.5%
1.0%
1.5%
2.0%
2.5%
Normal Stress (MPa)
Normal Strain (%)
Bending Stress
0.2% Yield line

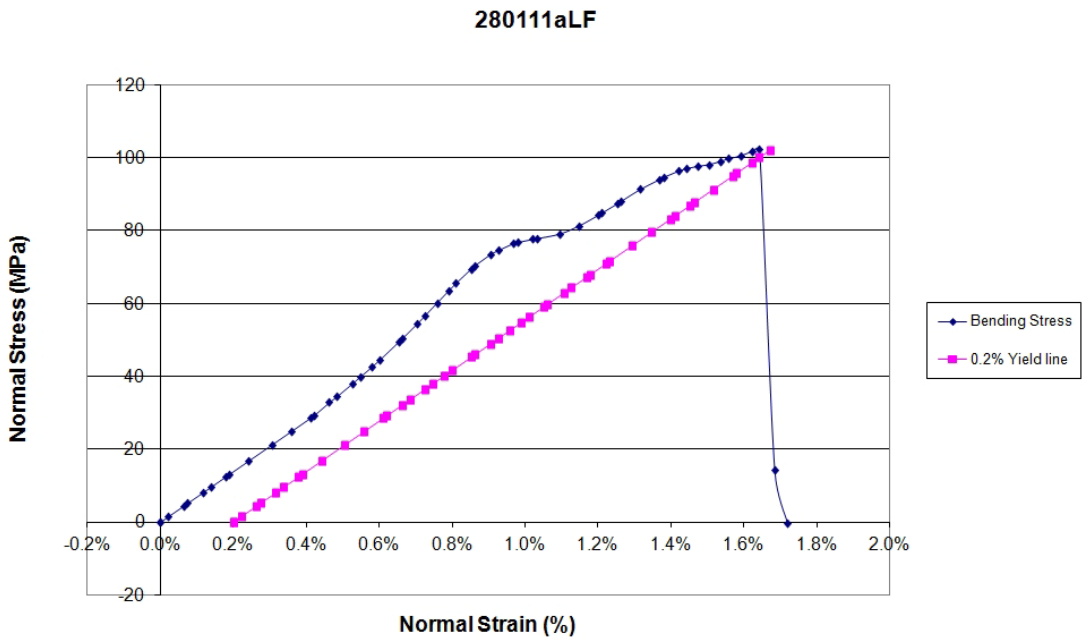
280111aLF
Normal Stress (MPa)
120
100
80
60
40
20
0
-20
-0.2%
0.0%
0.2%
0.4%
0.6%
0.8%
1.0%
1.2%
1.4%
1.6%
1.8%
2.0%
Normal Strain (%)
Bending Stress
0.2% Yield line

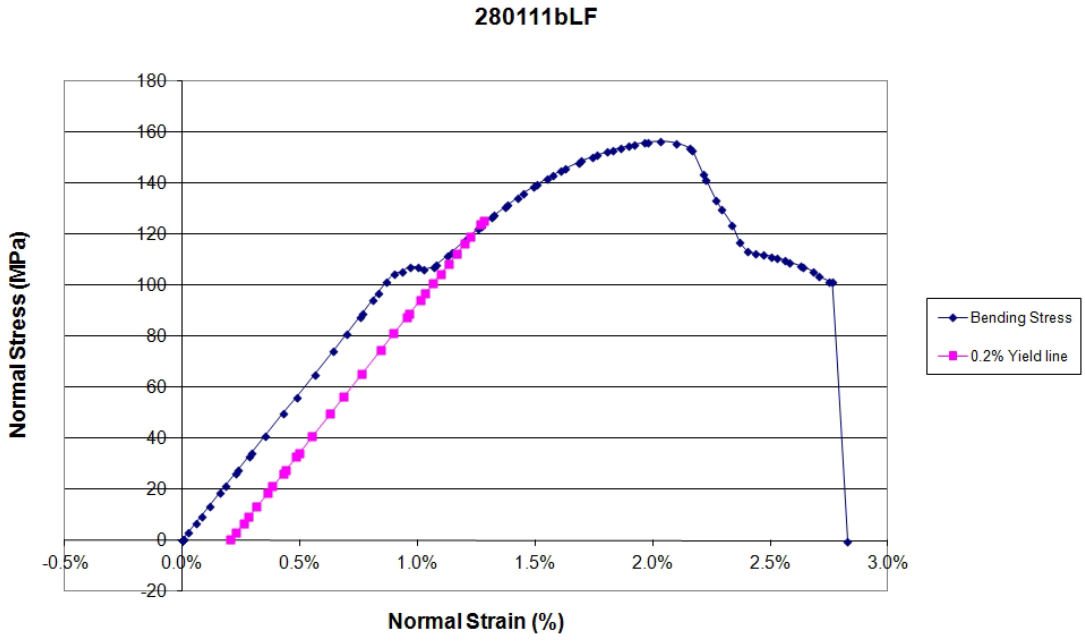
280111bLF
Normal Stress (MPa)
180
160
140
120
100
80
60
40
20
0
-20
-0.5%
0.0%
0.5%
1.0%
1.5%
2.0%
2.5%
3.0%
Normal Strain (%)
Bending Stress
0.2% Yield line

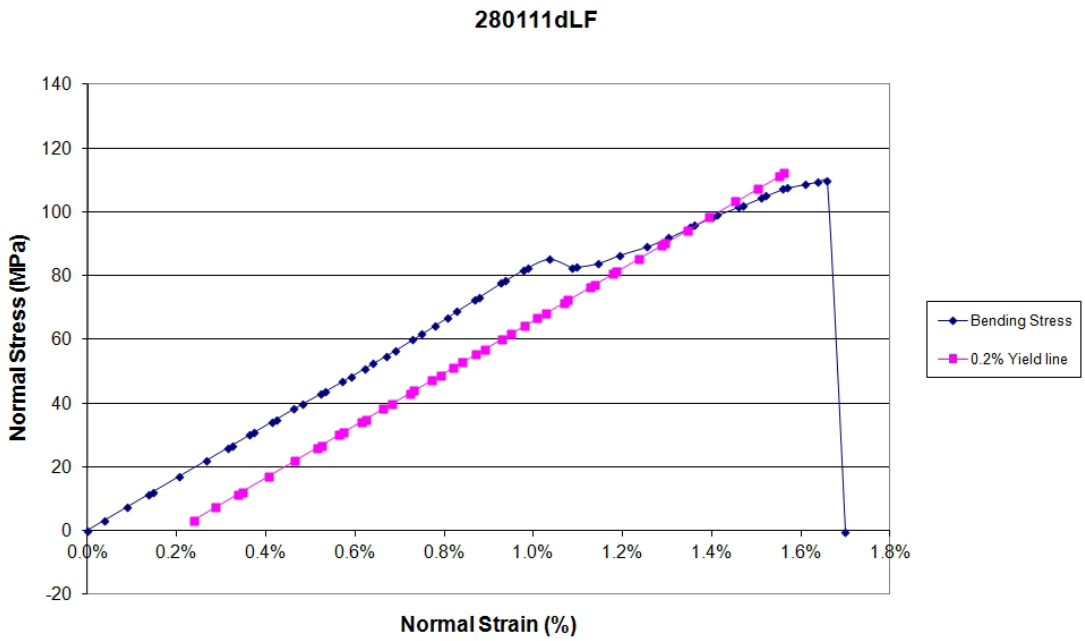
280111dLF
140
120
100
80
60
40
20
0
-20
0.0%
0.2%
0.4%
0.6%
0.8%
1.0%
1.2%
1.4%
1.6%
1.8%
Normal Stress (MPa)
Normal Strain (%)
Bending Stress
0.2% Yield line

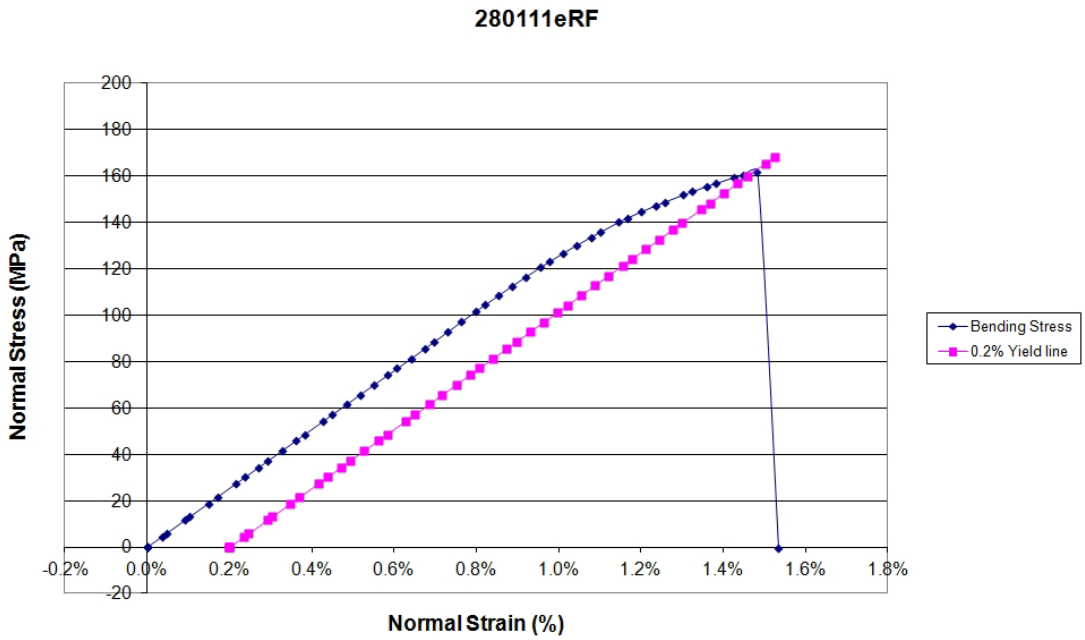
280111eRF
200
180
160
140
120
100
80
60
40
20
0
-20
-0.2%
0.0%
0.2%
0.4%
0.6%
0.8%
1.0%
1.2%
1.4%
1.6%
1.8%
Normal Stress (MPa)
Normal Strain (%)
Bending Stress
0.2% Yield line

14.7.3 Fast Loading, Normal Quality

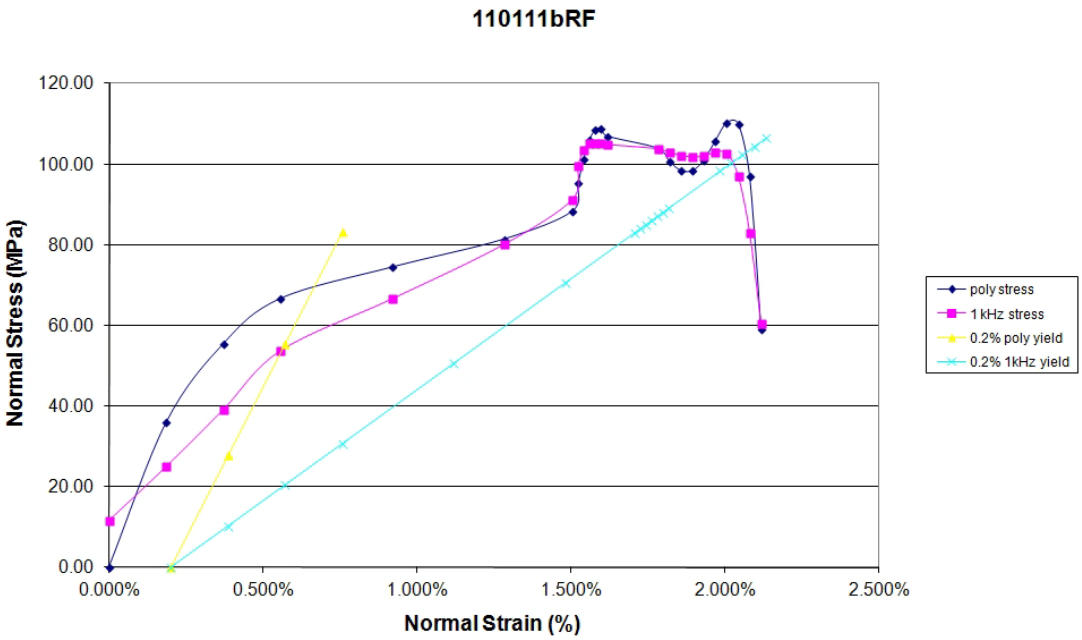

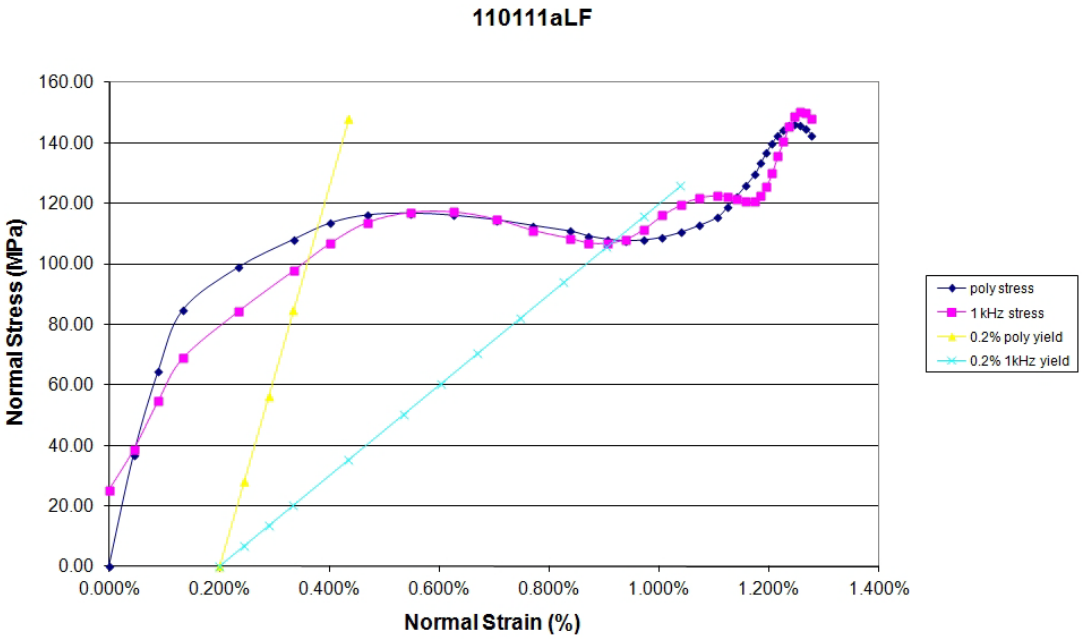

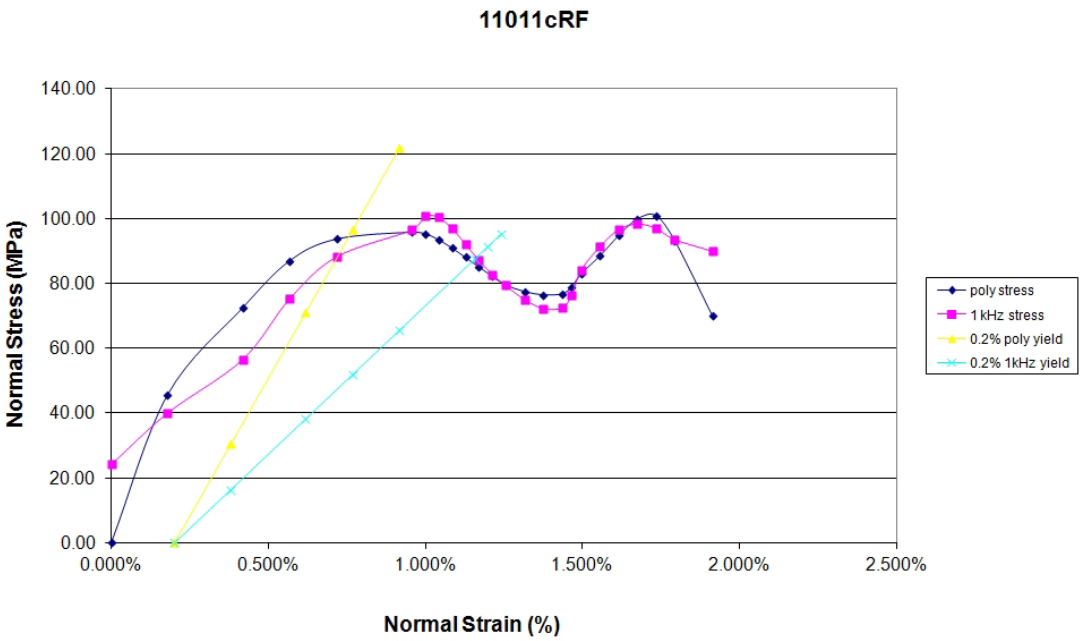
11011cRF
140.00
120.00
100.00
80.00
60.00
40.00
20.00
0.00
Normal Stress (MPa)
0.000%
0.500%
1.000%
1.500%
2.000%
2.500%
Normal Strain (%)
poly stress
1 kHz stress
0.2% poly yield
0.2% 1kHz yield

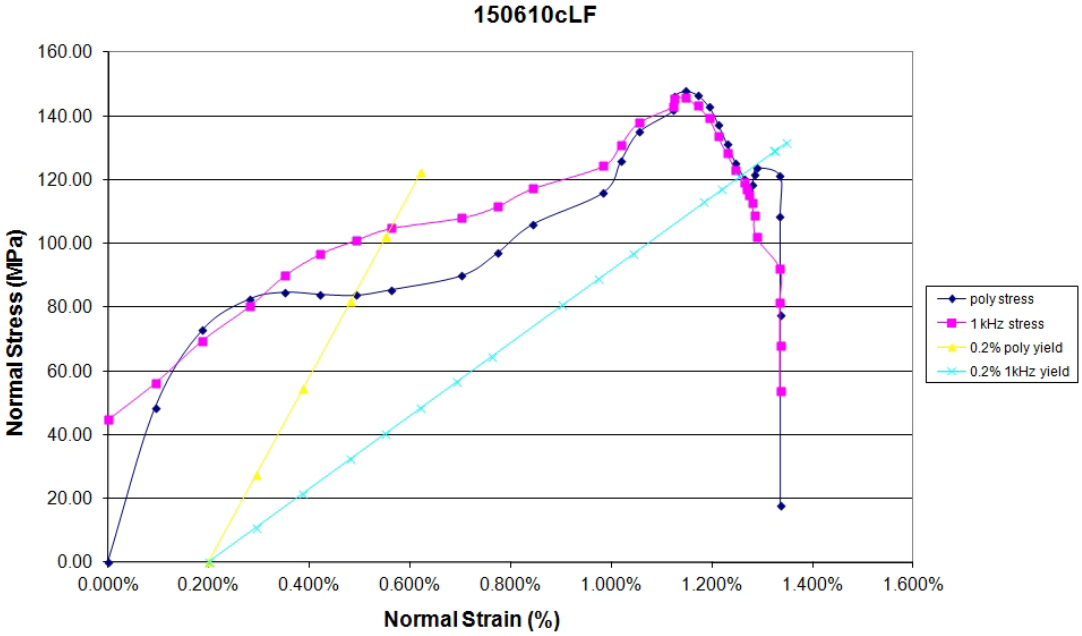
150610cLF
160.00
140.00
120.00
100.00
80.00
60.00
40.00
20.00
0.00
Normal Stress (MPa)
0.000%
0.200%
0.400%
0.600%
0.800%
1.000%
1.200%
1.400%
1.600%
Normal Strain (%)
poly stress
1 kHz stress
0.2% poly yield
0.2% 1kHz yield

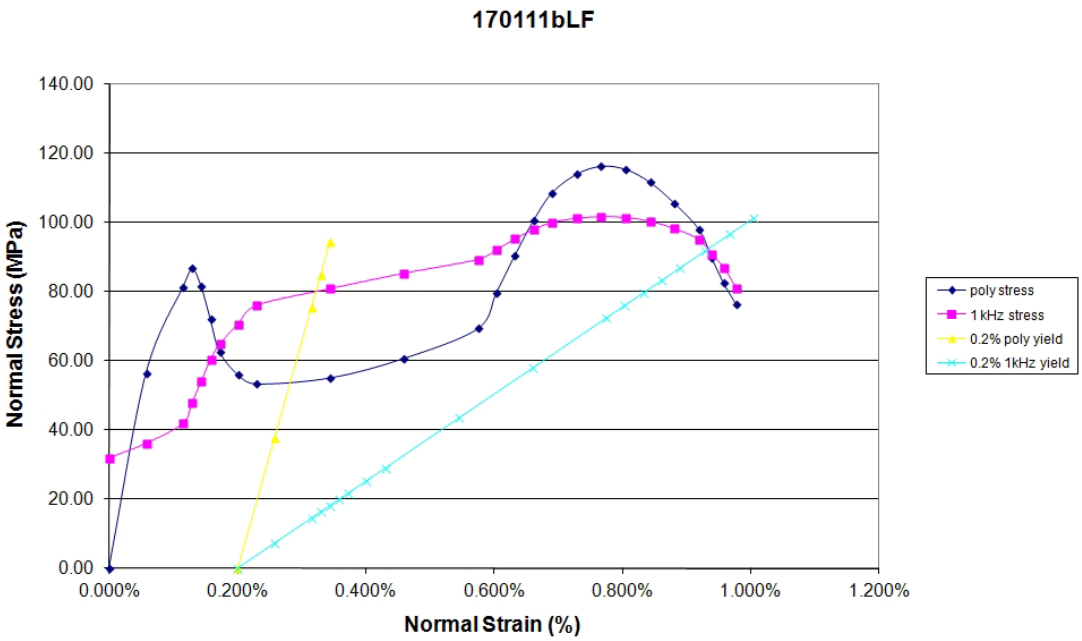
170111bLF
140.00
120.00
100.00
80.00
60.00
40.00
20.00
0.00
Normal Stress (MPa)
0.000%
0.200%
0.400%
0.600%
0.800%
1.000%
1.200%
Normal Strain (%)
poly stress
1 kHz stress
0.2% poly yield
0.2% 1kHz yield

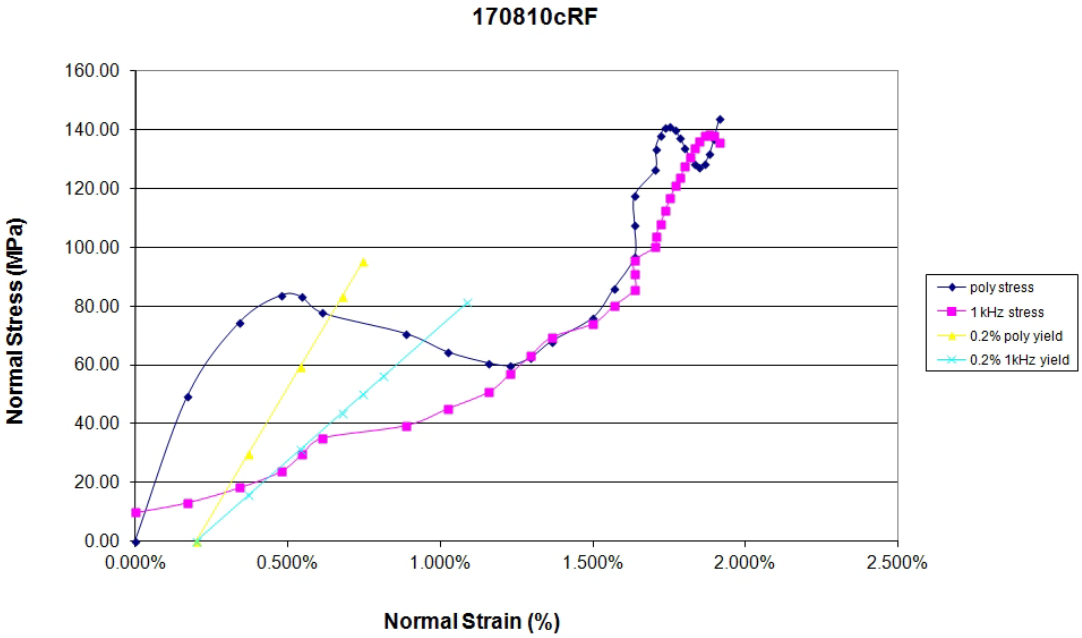
170810cRF
160.00
140.00
120.00
100.00
80.00
60.00
40.00
20.00
0.00
Normal Stress (MPa)
0.000%
0.500%
1.000%
1.500%
2.000%
2.500%
Normal Strain (%)
poly stress
1 kHz stress
0.2% poly yield
0.2% 1kHz yield

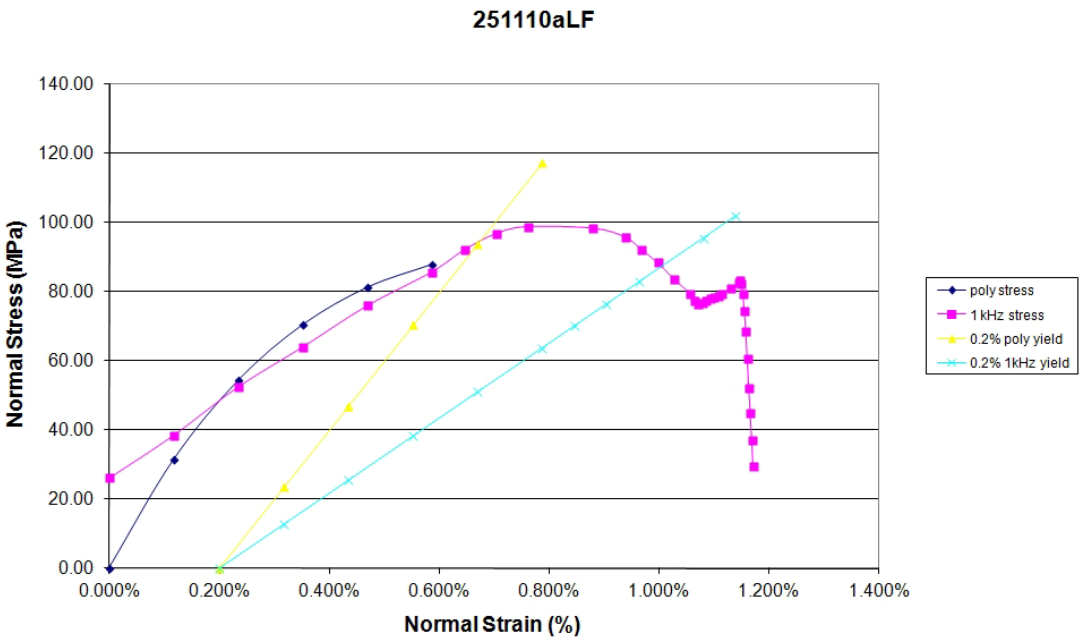
251110aLF
140.00
120.00
100.00
80.00
60.00
40.00
20.00
0.00
Normal Stress (MPa)
0.000%
0.200%
0.400%
0.600%
0.800%
1.000%
1.200%
1.400%
Normal Strain (%)
poly stress
1 kHz stress
0.2% poly yield
0.2% 1kHz yield

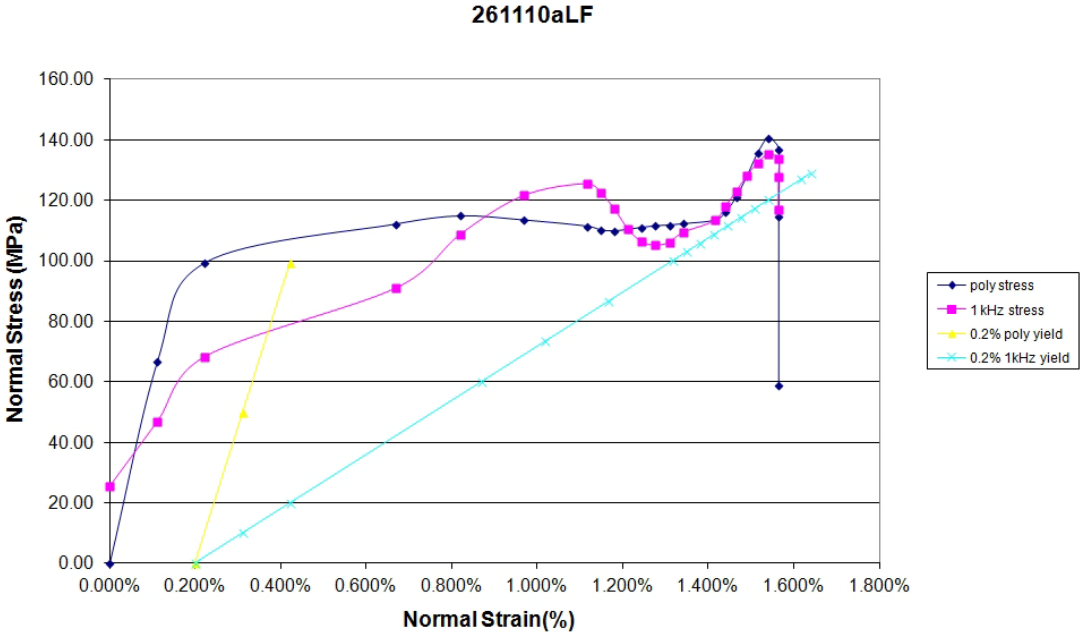
261110aLF
160.00
140.00
120.00
100.00
80.00
60.00
40.00
20.00
0.00
Normal Stress (MPa)
0.000%
0.200%
0.400%
0.600%
0.800%
1.000%
1.200%
1.400%
1.600%
1.800%
Normal Strain(%)
poly stress
1 kHz stress
0.2% poly yield
0.2% 1kHz yield

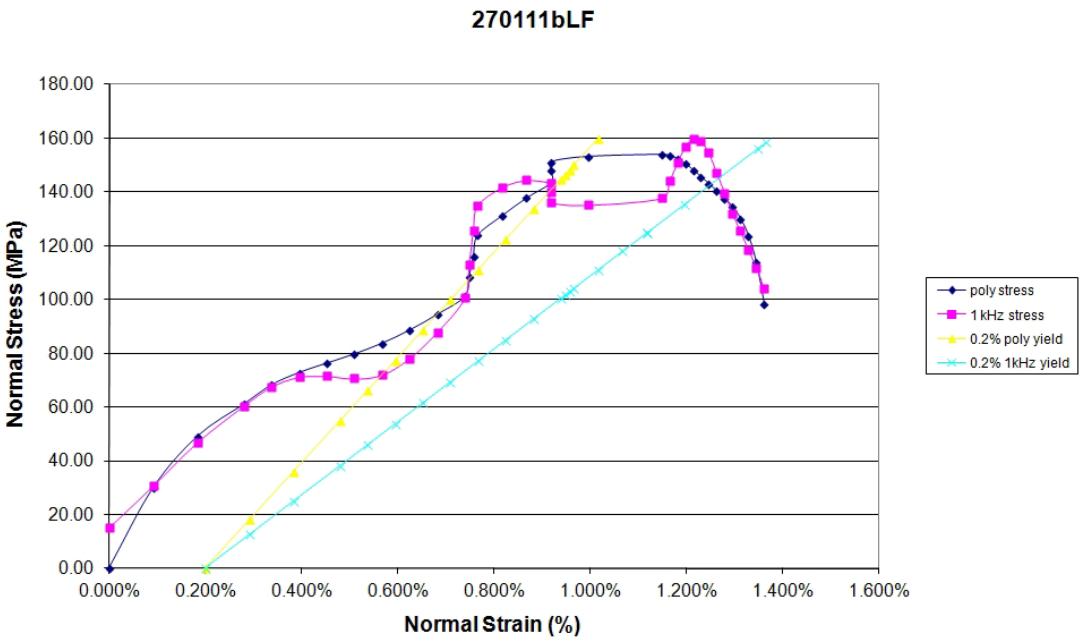
270111bLF
180.00
160.00
140.00
120.00
100.00
80.00
60.00
40.00
20.00
0.00
Normal Stress (MPa)
0.000%
0.200%
0.400%
0.600%
0.800%
1.000%
1.200%
1.400%
1.600%
Normal Strain (%)
poly stress
1 kHz stress
0.2% poly yield
0.2% 1kHz yield

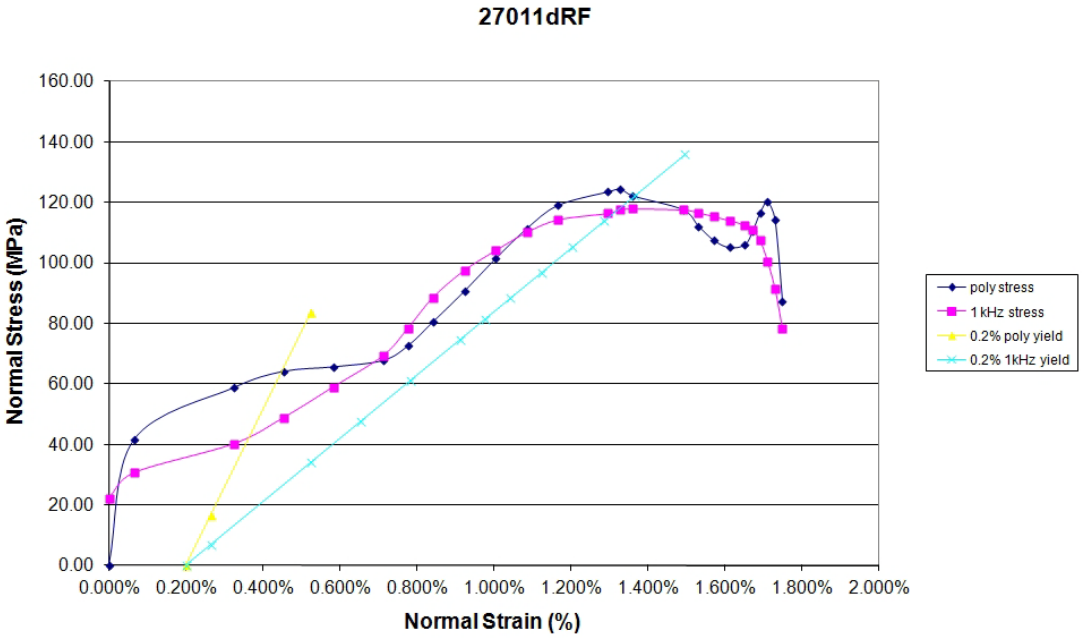
27011dRF
160.00
140.00
120.00
100.00
80.00
60.00
40.00
20.00
0.00
Normal Stress (MPa)
0.000%
0.200%
0.400%
0.600%
0.800%
1.000%
1.200%
1.400%
1.600%
1.800%
2.000%
Normal Strain (%)
poly stress
1 kHz stress
0.2% poly yield
0.2% 1kHz yield

14.7.4 Fast Loading Demineralised Bones

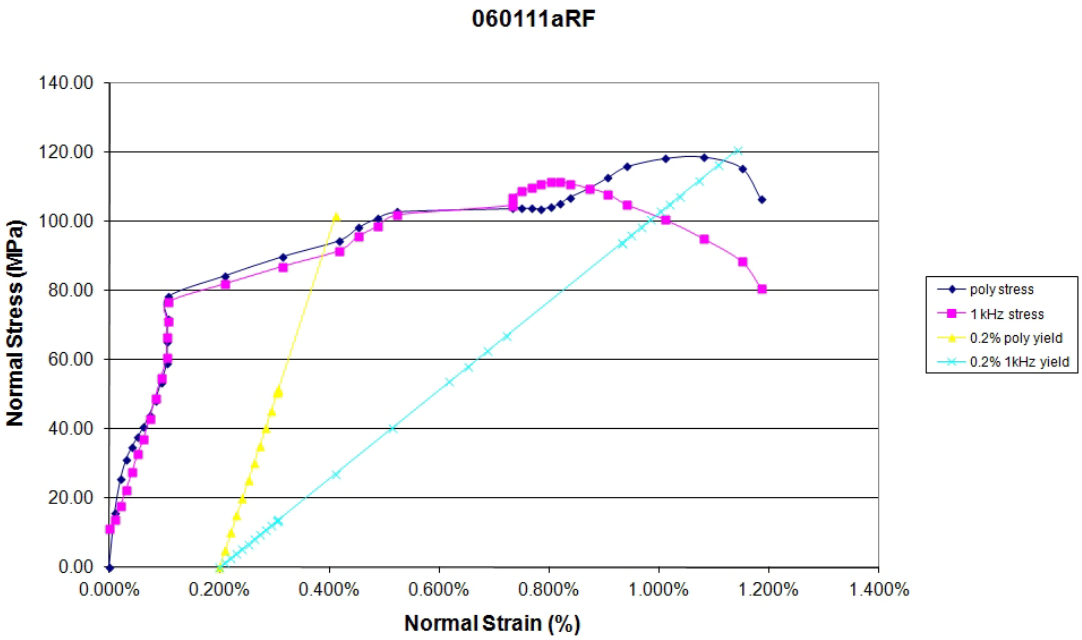

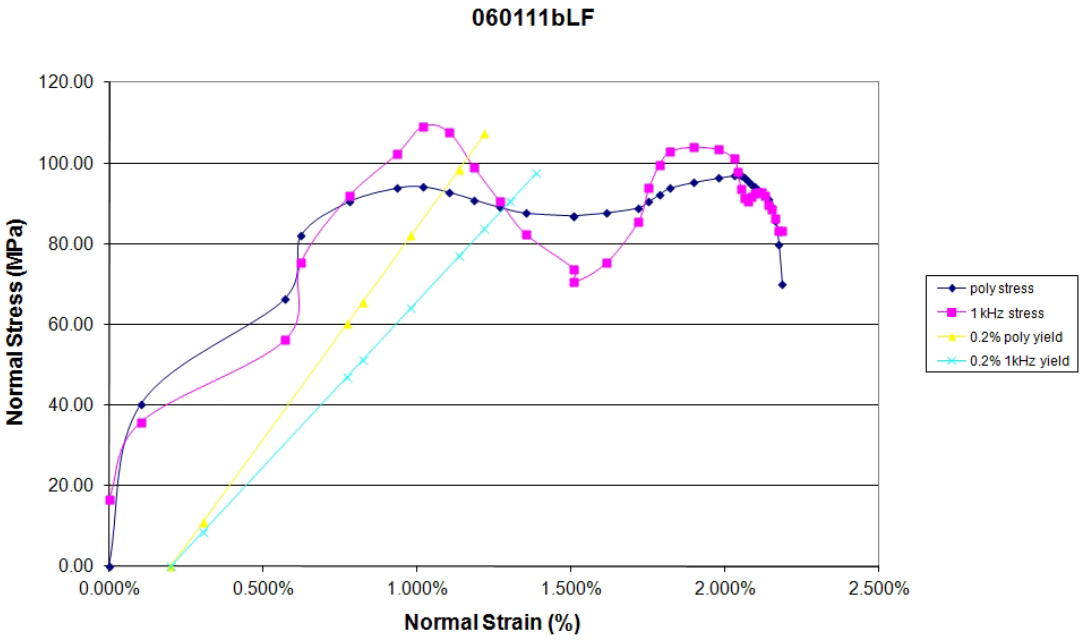

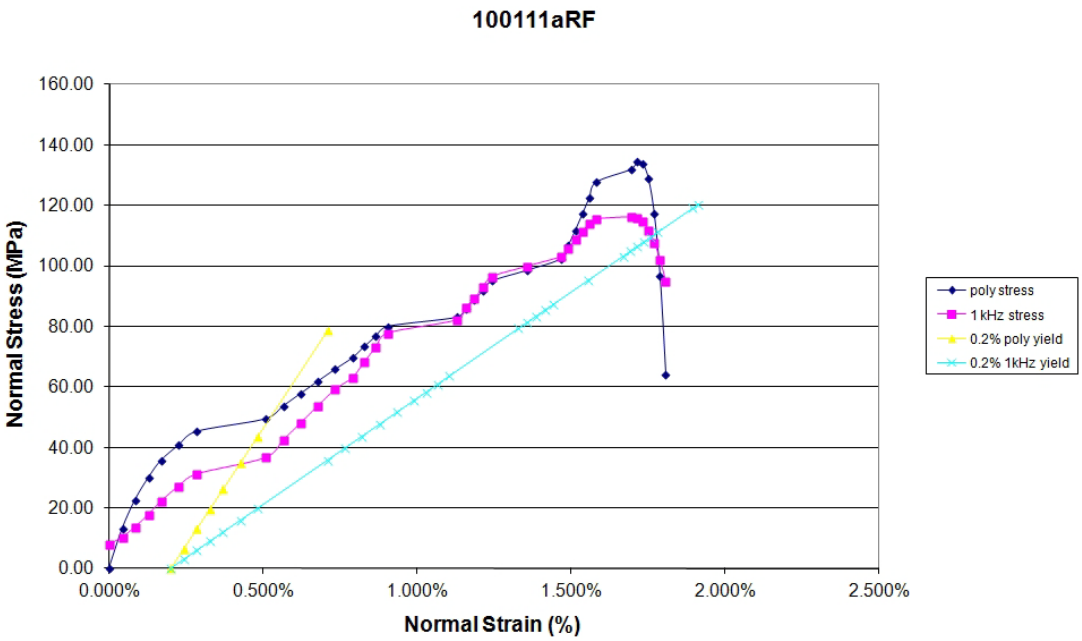
100111aRF
160.00
140.00
120.00
100.00
80.00
60.00
40.00
20.00
0.00
Normal Stress (MPa)
0.000%
0.500%
1.000%
1.500%
2.000%
2.500%
Normal Strain (%)
poly stress
1 kHz stress
0.2% poly yield
0.2% 1kHz yield

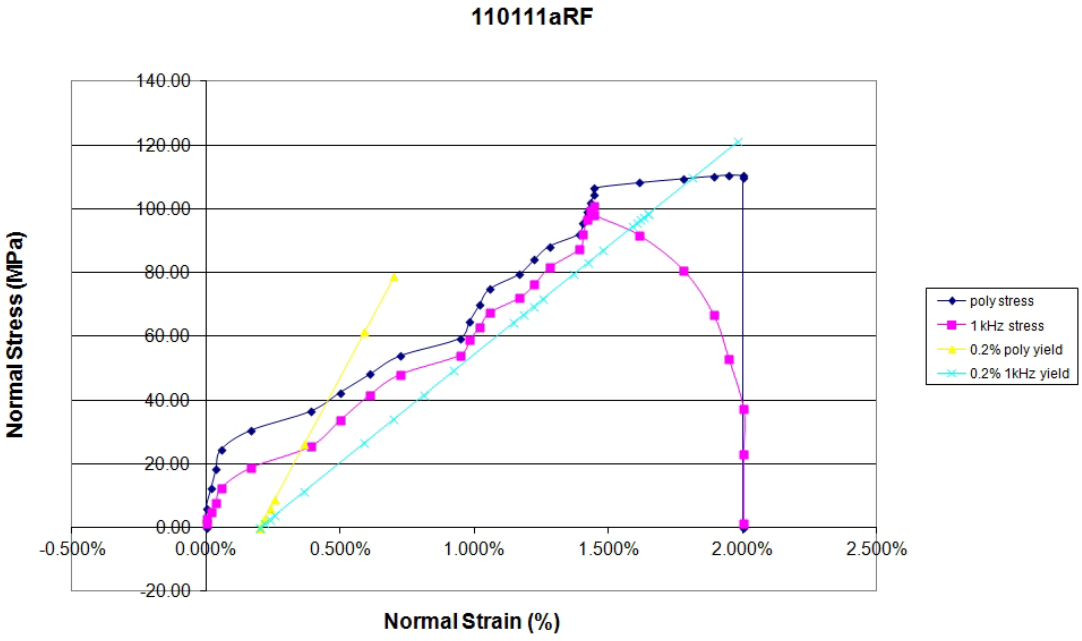
110111aRF
140.00
120.00
100.00
80.00
60.00
40.00
20.00
0.00
-20.00
Normal Stress (MPa)
-0.500%
0.000%
0.500%
1.000%
1.500%
2.000%
2.500%
Normal Strain (%)
poly stress
1 kHz stress
0.2% poly yield
0.2% 1kHz yield

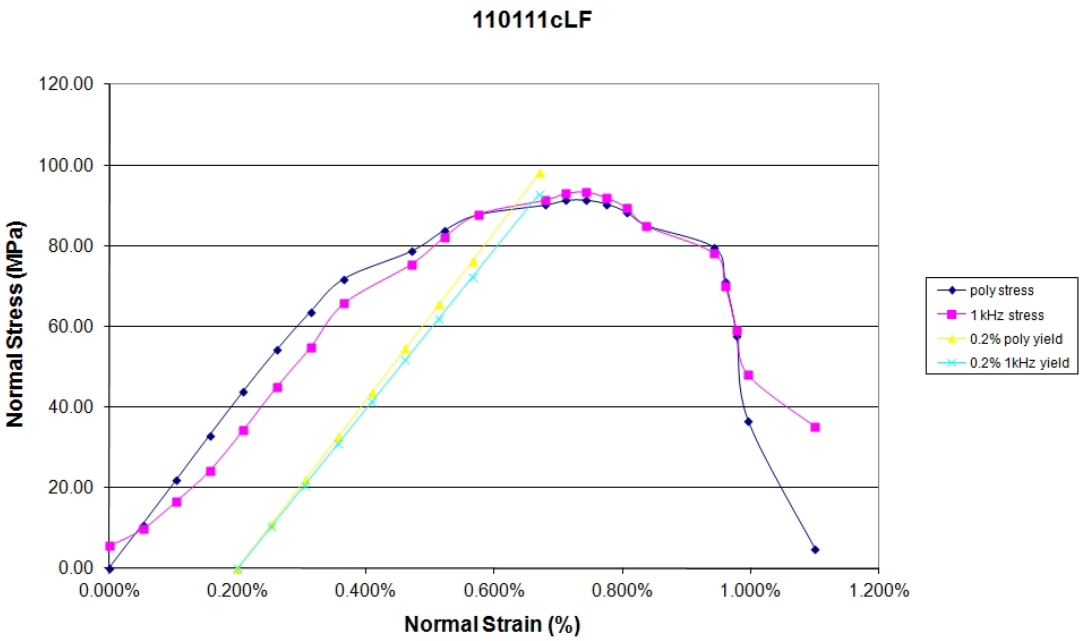
110111cLF
120.00
100.00
80.00
60.00
40.00
20.00
0.00
Normal Stress (MPa)
0.000%
0.200%
0.400%
0.600%
0.800%
1.000%
1.200%
Normal Strain (%)
poly stress
1 kHz stress
0.2% poly yield
0.2% 1kHz yield

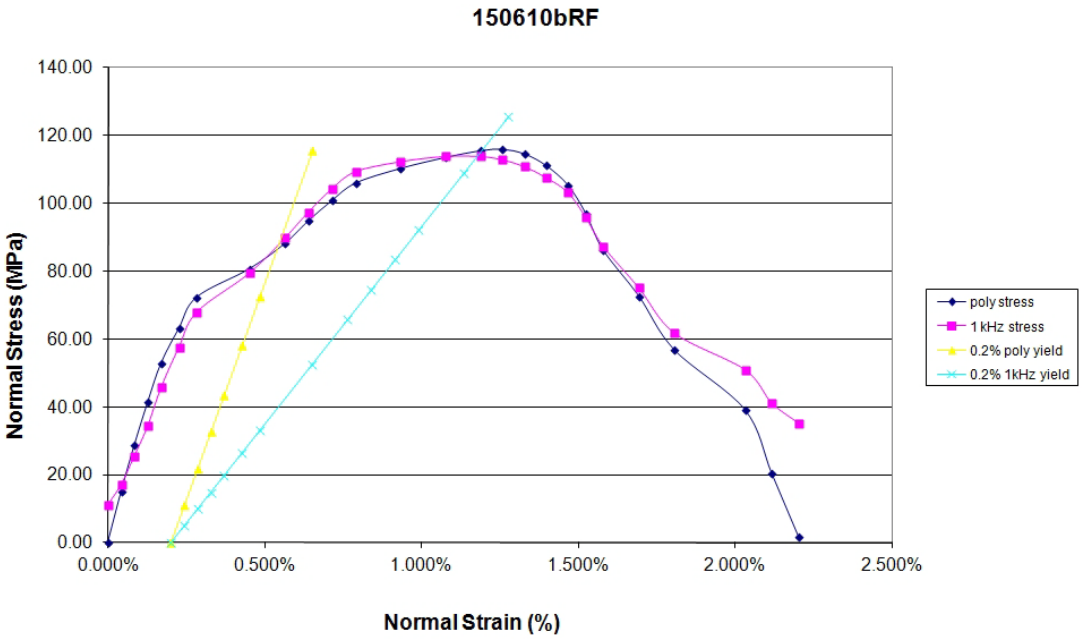
150610bRF
140.00
120.00
100.00
80.00
60.00
40.00
20.00
0.00
Normal Stress (MPa)
0.000%
0.500%
1.000%
1.500%
2.000%
2.500%
Normal Strain (%)
poly stress
1 kHz stress
0.2% poly yield
0.2% 1kHz yield

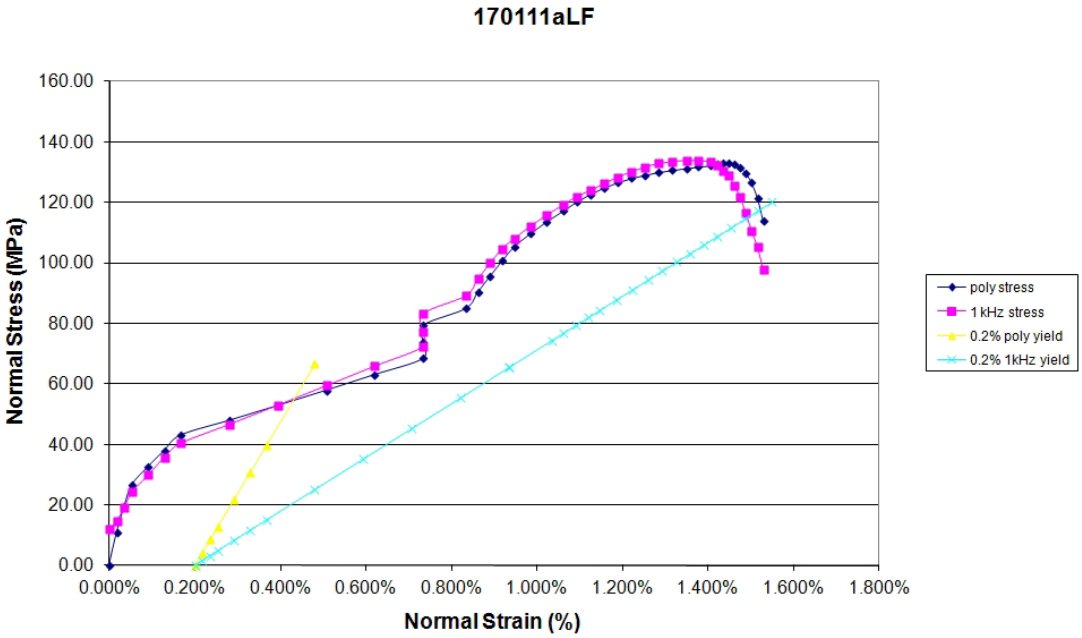
170111aLF
160.00
140.00
120.00
100.00
80.00
60.00
40.00
20.00
0.00
Normal Stress (MPa)
0.000%
0.200%
0.400%
0.600%
0.800%
1.000%
1.200%
1.400%
1.600%
1.800%
Normal Strain (%)
poly stress
1 kHz stress
0.2% poly yield
0.2% 1kHz yield

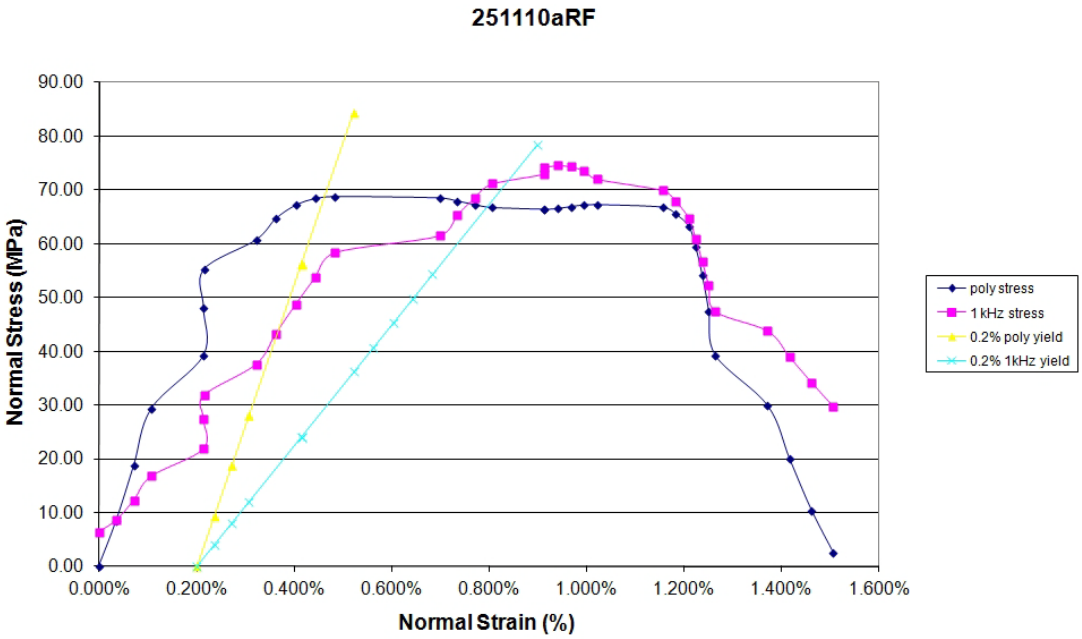
251110aRF
90.00
80.00
70.00
60.00
50.00
40.00
30.00
20.00
10.00
0.00
Normal Stress (MPa)
0.000%
0.200%
0.400%
0.600%
0.800%
1.000%
1.200%
1.400%
1.600%
Normal Strain (%)
poly stress
1 kHz stress
0.2% poly yield
0.2% 1kHz yield

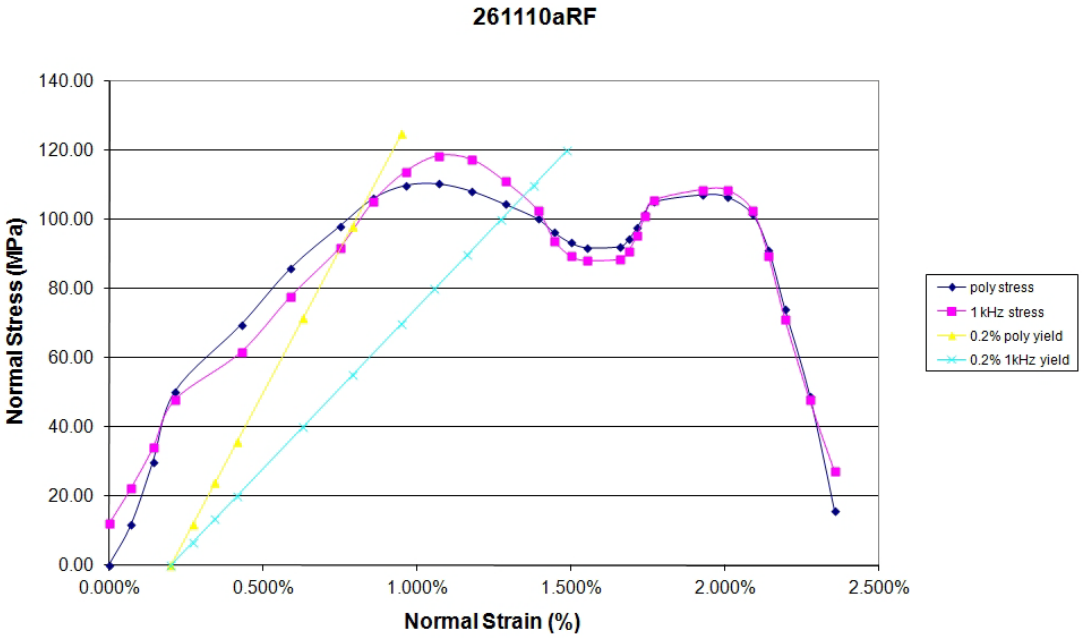
261110aRF
140.00
120.00
100.00
80.00
60.00
40.00
20.00
0.00
Normal Stress (MPa)
0.000%
0.500%
1.000%
1.500%
2.000%
2.500%
Normal Strain (%)
poly stress
1 kHz stress
0.2% poly yield
0.2% 1kHz yield

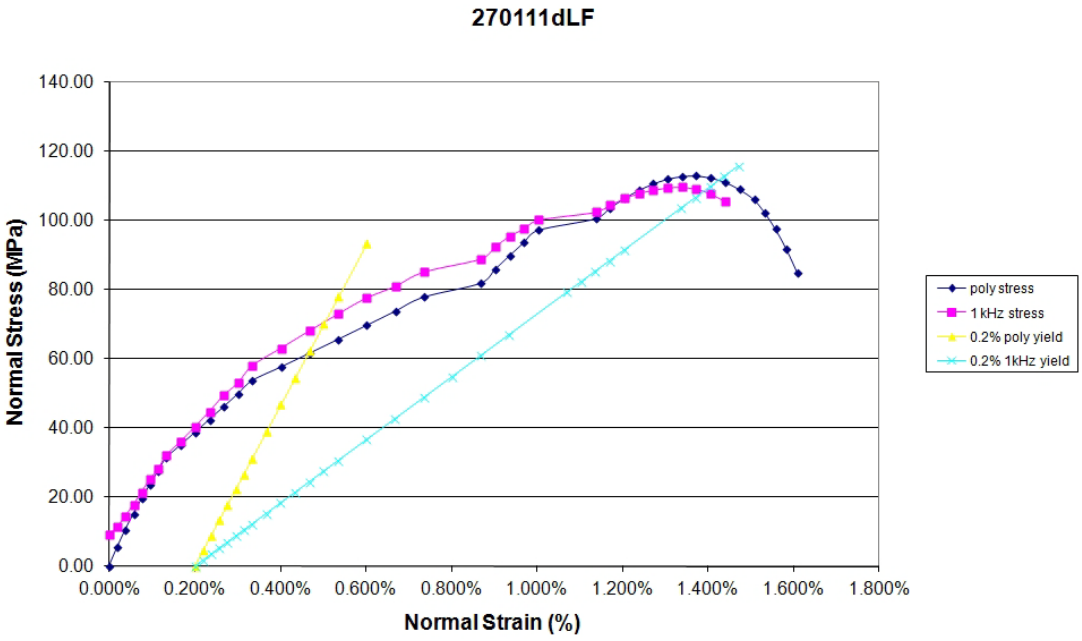
270111dLF
140.00
120.00
100.00
80.00
60.00
40.00
20.00
0.00
Normal Stress (MPa)
0.000%
0.200%
0.400%
0.600%
0.800%
1.000%
1.200%
1.400%
1.600%
1.800%
Normal Strain (%)
poly stress
1 kHz stress
0.2% poly yield
0.2% 1kHz yield

14.8 Appendix H: Interaction plots

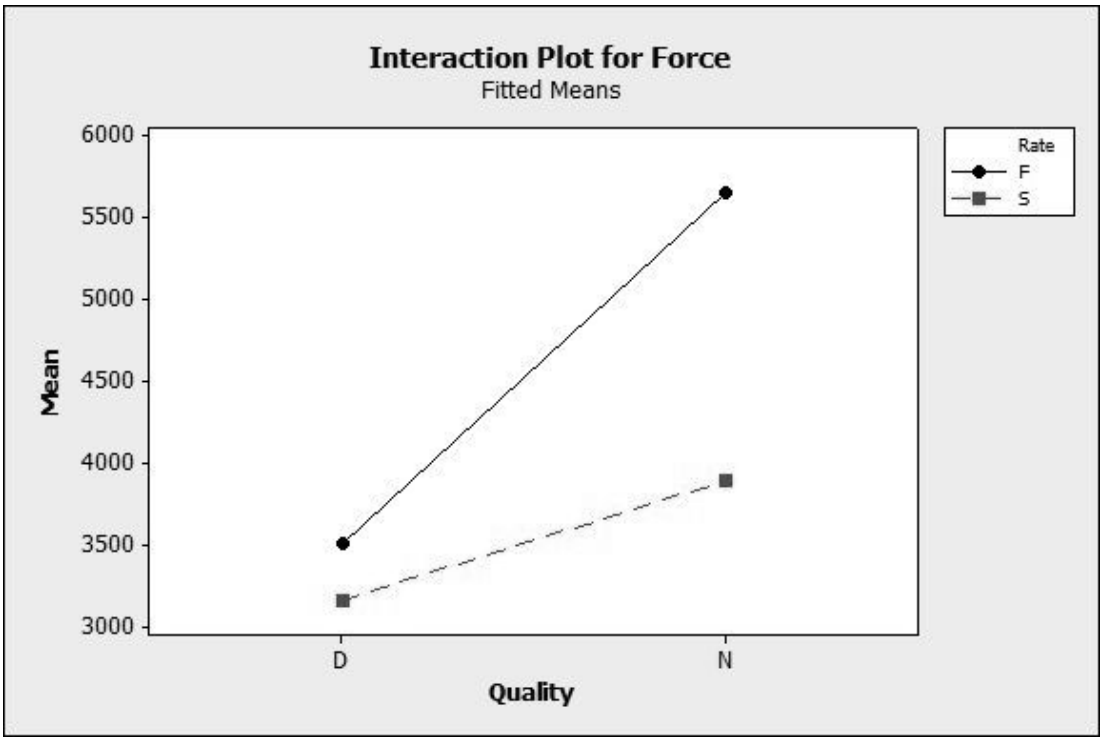

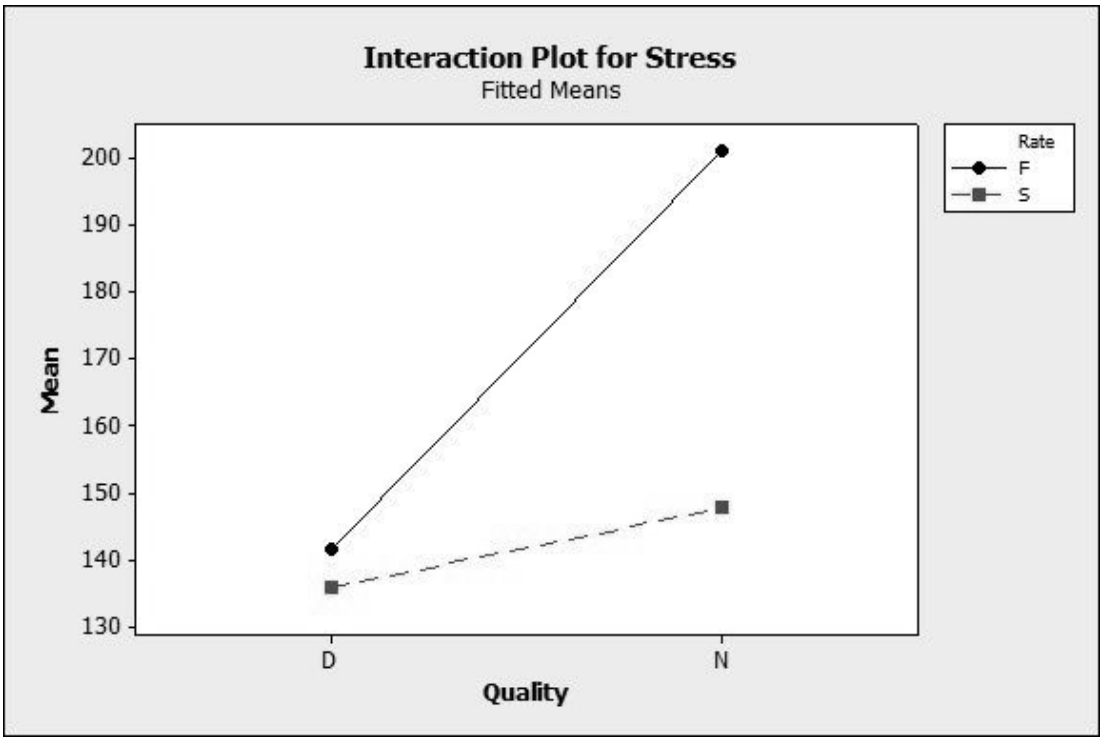

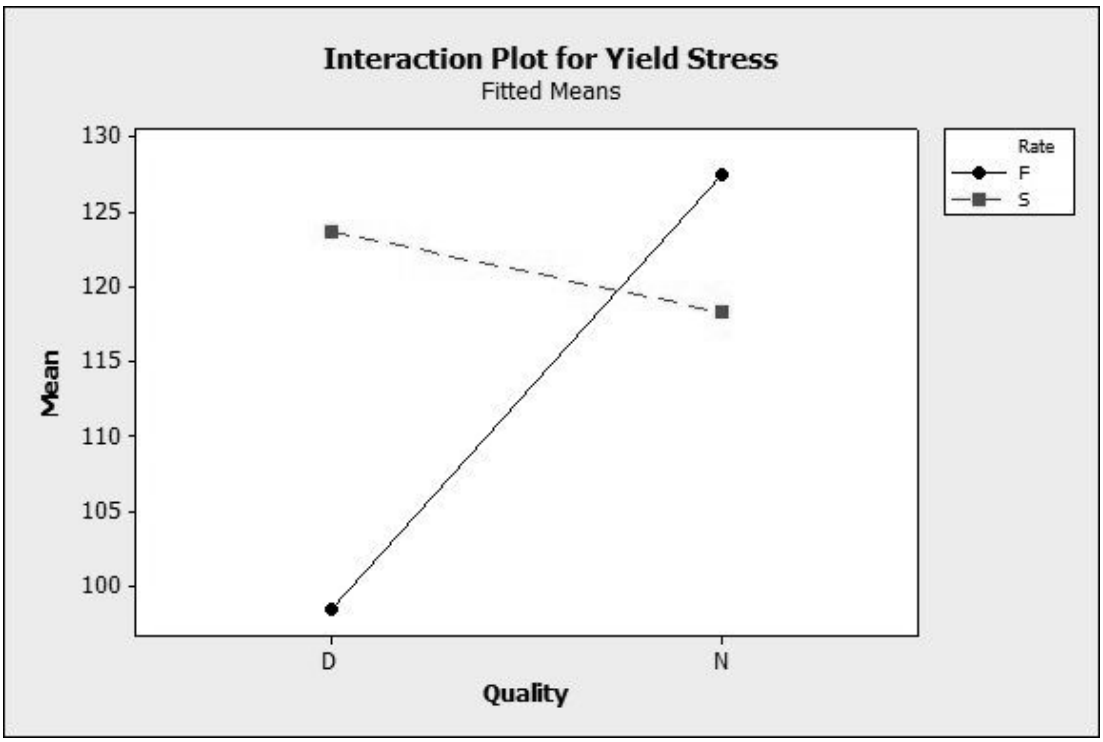
Interaction Plot for Yield Stress
Fitted Means
Mean
130
125
120
115
110
105
100
D
N
Quality
Rate
F
S

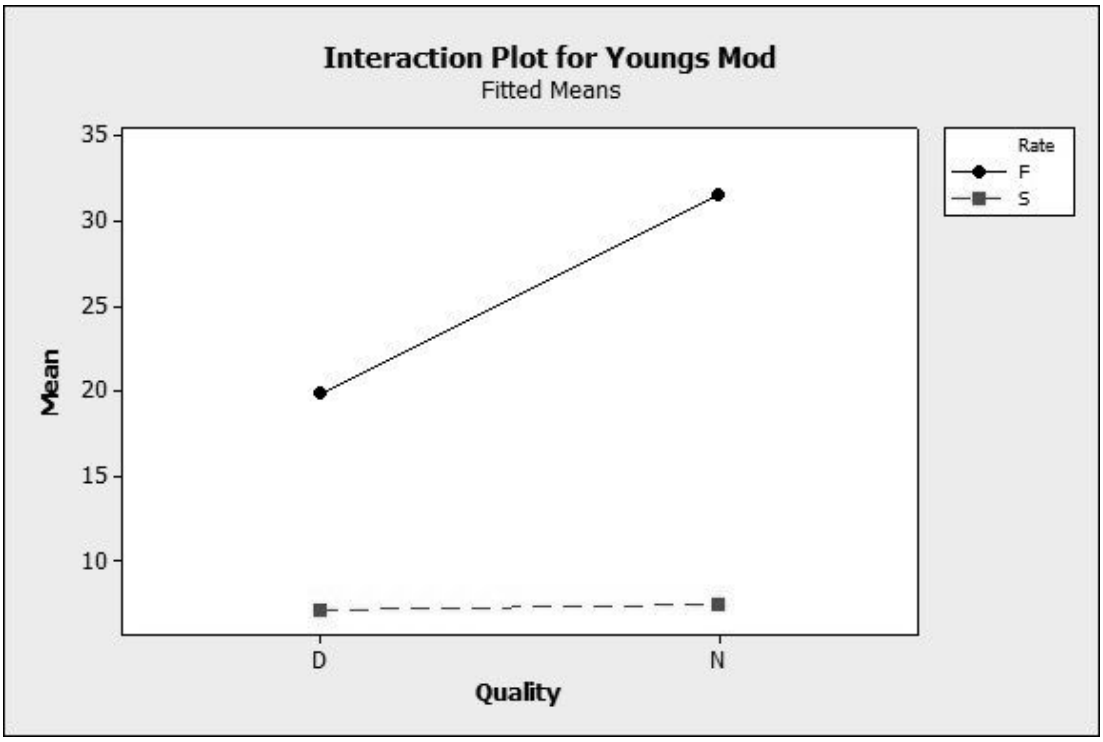
Interaction Plot for Youngs Mod
Fitted Means
Mean
35
30
25
20
15
10
D
N
Quality
Rate
F
S

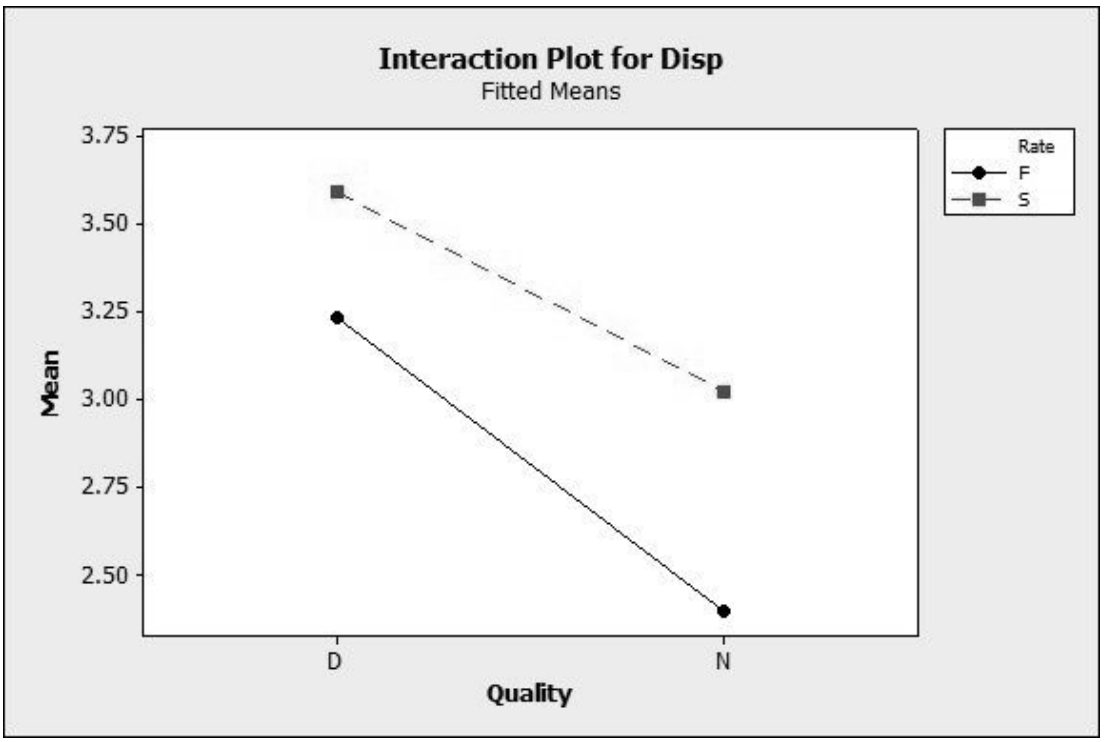
Interaction Plot for Disp
Fitted Means
Mean
3.75
3.50
3.25
3.00
2.75
2.50
D
N
Quality
Rate
F
S

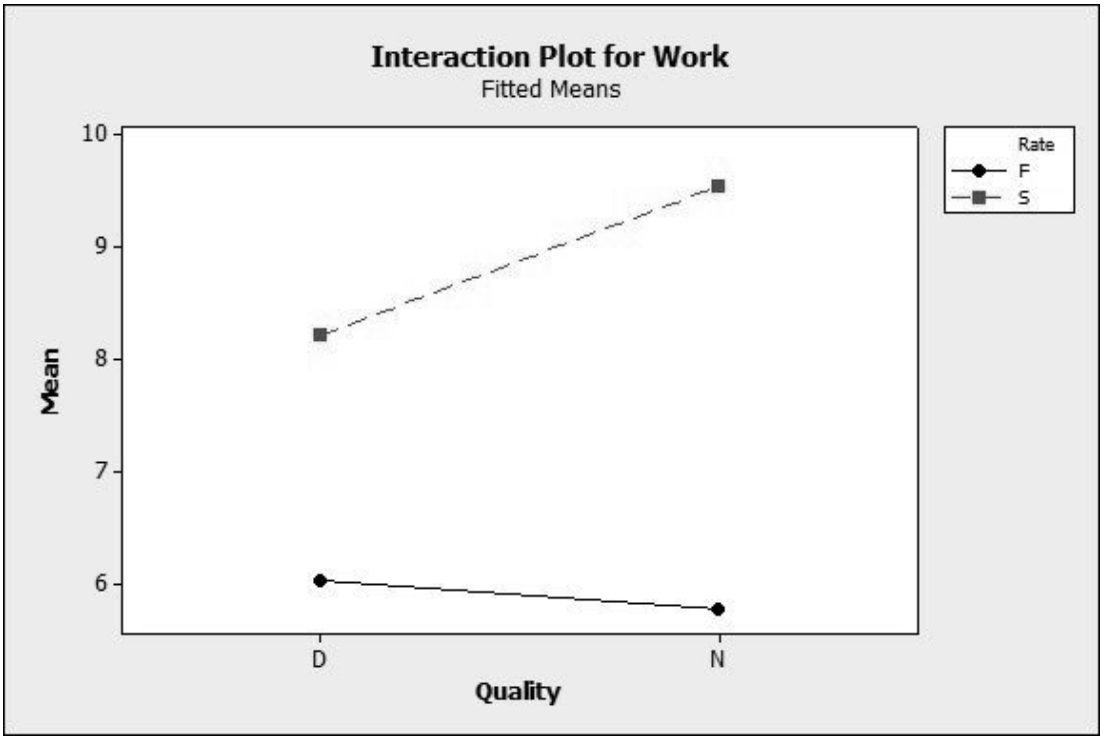
Interaction Plot for Work
Fitted Means
Mean
10
9
8
7
6
D
N
Quality
Rate
F
S

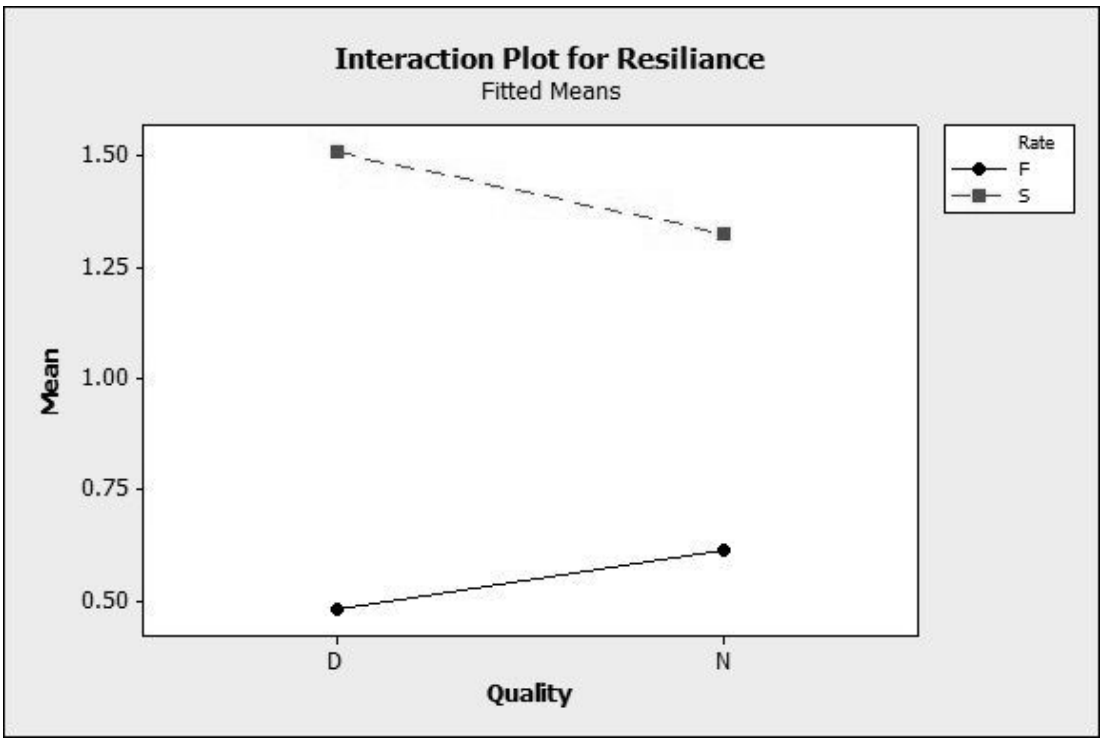
Interaction Plot for Resiliance
Fitted Means
Mean
1.50
1.25
1.00
0.75
0.50
D
N
Quality
Rate
F
S

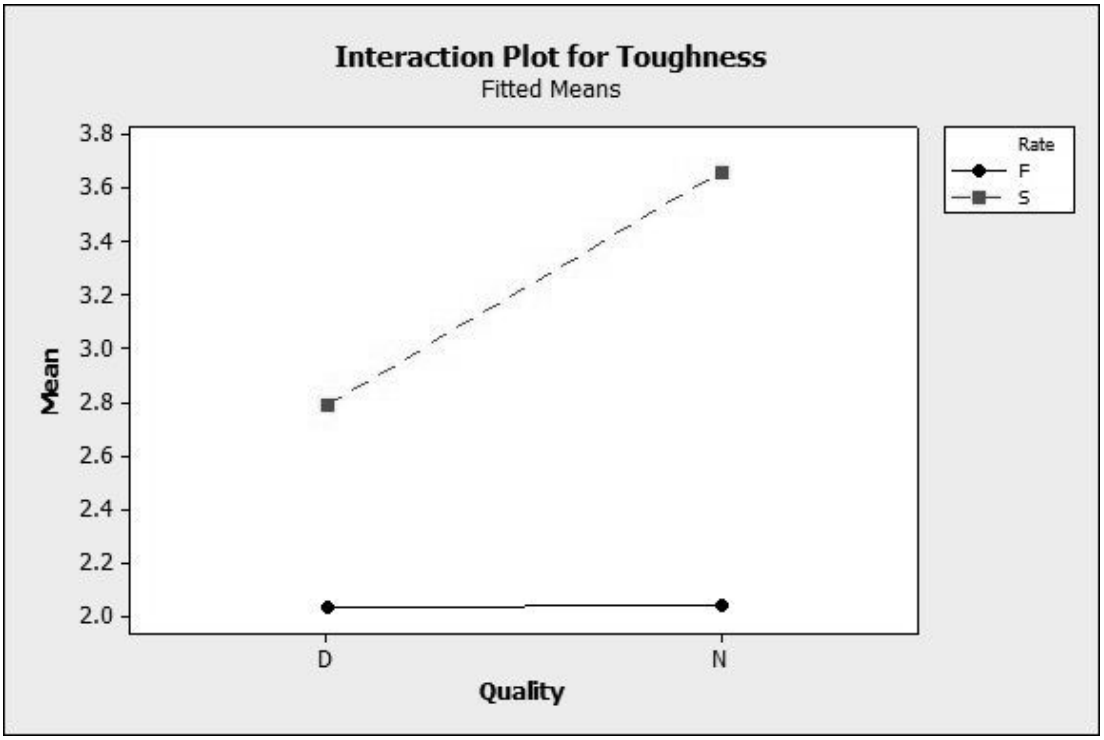
Interaction Plot for Toughness
Fitted Means
Mean
3.8
3.6
3.4
3.2
3.0
2.8
2.6
2.4
2.2
2.0
D
N
Quality
Rate
F
S

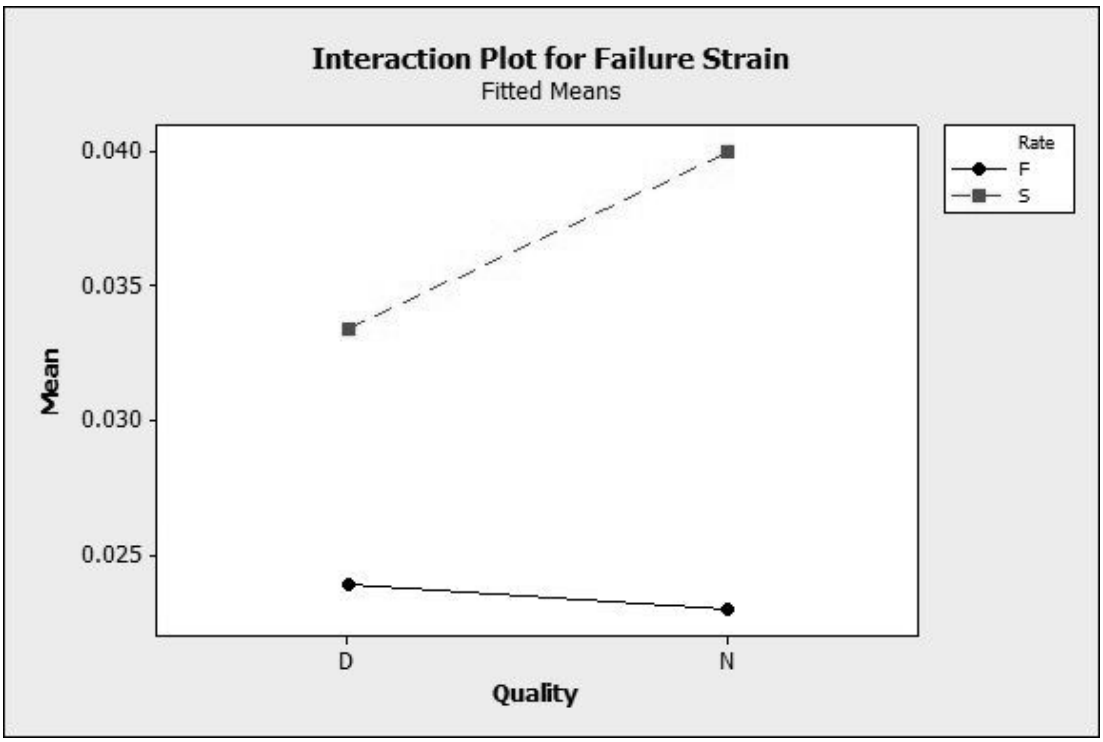
Interaction Plot for Failure Strain
Fitted Means
Mean
0.040
0.035
0.030
0.025
D
N
Quality
Rate
F
S

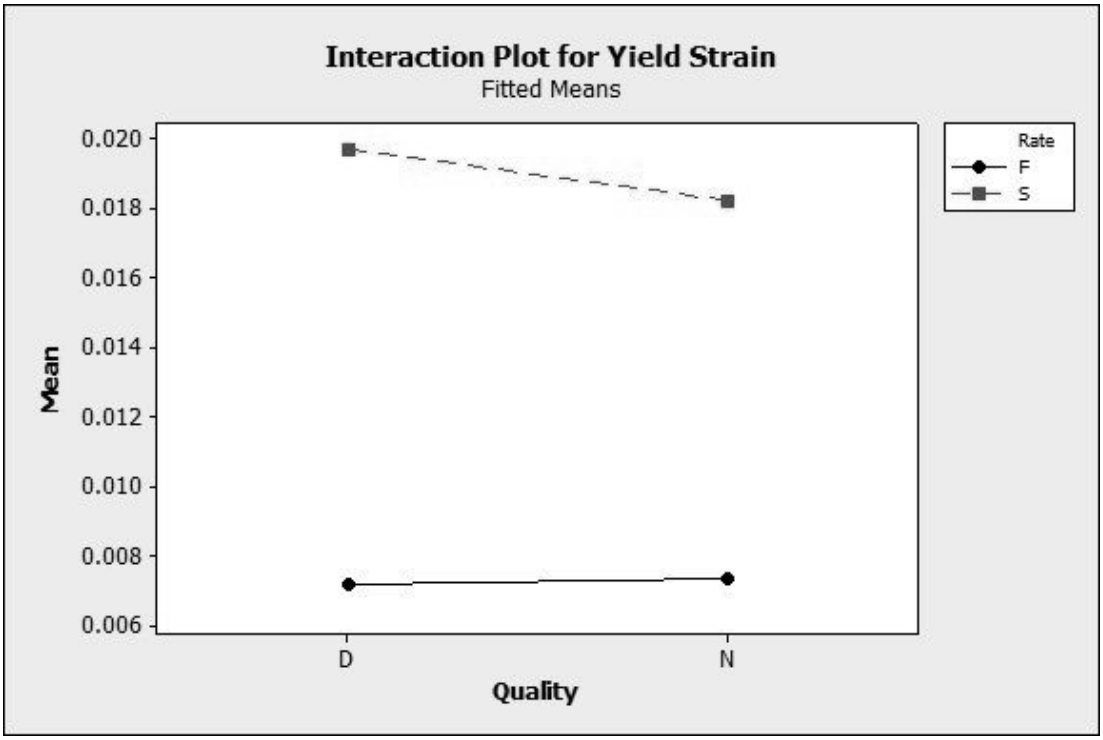
Interaction Plot for Yield Strain
Fitted Means
Mean
0.020
0.018
0.016
0.014
0.012
0.010
0.008
0.006
D
N
Quality
Rate
F
S

14.9 Appendix I: Conference papers

14.9.1 British Orthopaedic Research Society 2011

EFFECT OF BONE QUALITY ON STRAIN RATE AND FRACTURE RISK

*RJ Wallace, AHRW Simpson

Orthopaedic Engineering Collaboration, University of Edinburgh, UK

There is an established link between bone quality and fracture risk. It has been suggested that reduced bone quality will also reduce the toughening mechanisms displayed during loading at a high strain rate. We hypothesised that partially decalcified bone will not demonstrate an increase in force required to cause failure when comparing low and high strain rate loading.

Mechanical properties were defined by the maximum force at failure. Bone quality was defined by the mineral content. This was altered by subjecting the bones to ultrasonically assisted decalcification in 10M EDTA to achieve an average 18% mineral reduction (A 70 yr old woman has approx 18% of her peak bone mass). 20 pairs of sheep femurs were harvested and split into four equal groups: normal bone quality, fast strain rate (NF); normal bone quality, slow strain rate (NS); low bone quality, fast strain rate (LF) and low bone quality, slow strain rate (LS). All mechanical testing was carried out by means of 3-point bending. Load representing the slow strain rate was applied by a mechanical testing machine (Zwick) at a rate resulting in a deflection of 1mm/s. The dynamic loading was applied by a custom designed pneumatic ram at a mean rate of deflection between the specimens of 2983 mm/s (±SD 1155), this equates to strain rates experienced in a road traffic accident.

The following results for force at failure were found (mean ± SD). NF: Force 5503N (± 1012); NS: Force 3969N (± 572); LF: Force 3485N (± 772); LS: Force 3165N (± 605). Groups were compared using a Mann-Whitney U test. Significant results were found between the following groups: Normal bone quality, strain rate compared (NF-NS) $p<0.002$; Fast strain rate, bone quality compared (NF-LF) $p=0.008$; Slow strain rate, bone quality

compared (NS-LS) p=0.02. No statistical significance was found when comparing low bone quality, strain rate compared (LF-LS) p=0.47.

These results show that normal healthy bone has an ability to withstand higher strain rates which protects it against fracture. This ability to withstand high strain rates is lost in decalcified bone making it more susceptible to fracture. The results of this study indicate the importance of strain rate reduction as well as energy absorption in the design of hip protectors and in environmental modifications.

14.9.2 EFORT Madrid 2010

British Orthopaedic Research Society 2009

SICOT Pattaya 2010

DECALCIFICATION OF RAT TIBIA ON BENDING STRENGTH AND FAILURE MODE

RJ. Wallace [1], G. Hopper [2], AHRW Simpson [1]

[1] Edinburgh Orthopaedic Engineering Collaboration
University of Edinburgh
Chancellors Building
Edinburgh
[2] University of Glasgow Medical School

Decalcification of rat tibia on bending strength and failure mode

Aim

The aim of this study was to examine the relationship between amount of decalcification and bone strength and the different modes of failure that occur.

Method

40 rat tibias were harvested and split into 4 groups, each containing 10 tibias. Group A, the control group, underwent no decalcification. Group B, C and D underwent 7, 14 and 21 hours of sonification in 10% ethylenediaminetetraacetic acid (EDTA) respectively.

The tibias were loaded in four-point bending at a rate of 1N per-second till failure. After structural testing, the ash weight of half the tibias was calculated

Results

The following failure stresses and ash weights were found [mean ±SD]
Group A (control): Stress 243.5MPa ±59.70. Ash Weight 0.5154g ±0.0768
Group B (7 hours): Stress 55.48MPa ±22.56. Ash Weight 0.1902g ±0.0284
Group C (14 hours): Stress 39.13MPa ±21.18. Ash Weight 0.1536g ±0.0551
Group D (21 hours): Stress 12.15MPa ±12.79. Ash Weight 0.1140g ±0.0616

It was noted that different modes of failure occurred in the groups. Group A failed on the tension side resulting in a full thickness fracture. Group B failed on the tension side resulting in partial fracture. Group C failed on compression side with tearing on tension side. Group D suffered local buckling.

Conclusion

In addition to the well known relationship between bone strength and mineral content there is also a clearly observed relationship between mineral content and mode of failure: as bone quality reduces the mode of failure changes from the tension surface to the compression surface of the bone.

14.9.3 British Orthopaedic Research Society 2009

ULTRASONIC AGITATION CAN INREASE THE RATE OF DECALCIFICATION OF RAT BONE BY OVER 1000%

RJ. Wallace [1], SP Dawson [1], G. Hopper [2], AHRW Simpson [1]

[1] Edinburgh Orthopaedic Engineering Collaboration
University of Edinburgh
Chancellors Building
Edinburgh
[2] University of Glasgow Medical School

AIM

The aim of this study was to assess the increase in the rate of decalcification obtained by using ultrasound agitation in ethylene diamine tetra-acetic acid (EDTA) compared to EDTA exposure alone.

METHODS

The bones were split into 4 groups, each containing 10 rat tibias. Group A underwent no decalcification. Groups B, C and D underwent 7, 14 and 21 hours of sonification in 10% EDTA respectively. Additionally one bone was submerged in 10% EDTA without sonification to act as a control. This bone was decalcified for a total of 288 hours.

The bones subjected to ultrasonic agitation were x-rayed before and after decalcification. The percentage change of x-ray density was calculated for each bone. The control bone was x-rayed following the same protocol every 48 hours.

The ash weight of 20 of the tibias was determined to evaluate the amount of demineralisation that took place. Five bones were selected from each group at random.

RESULTS

The following percentage of x-ray density and ash weights were found [mean ± SD]

Group A (control): x-ray 100% ± 0. Ash Weight 0.5154g ± 0.0768
Group B (7 hours): x-ray 63% ± 9. Ash Weight 0.1902g ± 0.0284
Group C (14 hours): x-ray 51% ± 10. Ash Weight 0.1536g ± 0.0551
Group D (21 hours): x-ray 40% ± 14. Ash Weight 0.1140g ± 0.0616

The bone that was not subjected to sonification had the following percentage x-ray density; After 2 days 83%, 4 days 86%, 6 days 52%, 8 days 17%, 10 days 14%, 12 days 12 %

DISCUSSION

It can be seen that ultrasound increases the rate of decalcification. Similar levels of decalcification can be found from 14 hours sonification as can be achieved by 6 days of EDTA exposure alone. This is equivalent to a 1024% increase in rate of decalcification.

14.10 Appendix J: References

Adams, D. F. and J. L. Perry (1975). "Instrumented Charpy impact tests of several unidirectional composite materials." Fibre Science and Technology 8(4): 275-302.

Alers, J. C., P.-J. Krijtenburg, et al. (1999). "Effect of Bone Decalcification Procedures on DNA In Situ Hybridization and Comparative Genomic Hybridization: EDTA Is Highly Preferable to a Routinely Used Acid Decalcifier." Journal of Histochemistry & Cytochemistry 47(5): 703-709.

Ammann, P. and R. Rizzoli (2003). "Bone strength and its determinants." Osteoporosis International 14(0): 13-18.

Arakawa, K. and K. Takahashi (1991). "Relationships between fracture parameters and fracture surface roughness of brittle polymers." International Journal of Fracture 48(2): 103-114.

ASTM, 1985 "Standard test method for plane strain fracture toughness testing of metallic materials"ASTM Annual Book of Standards Section 2 (1985), pp. 898–933 Designation E 399-83

Barak, M. M., A. Sharir, et al. (2009). "Optical metrology methods for mechanical testing of whole bones." The Veterinary Journal 180(1): 7-14.

Bayraktar, H. H., E. F. Morgan, et al. (2004). "Comparison of the elastic and yield properties of human femoral trabecular and cortical bone tissue." Journal of Biomechanics 37(1): 27-35.

Beardsley, C. L., D. D. Anderson, et al. (2005). "Interfragmentary surface area as an index of comminution severity in cortical bone impact." Journal of Orthopaedic Research 23(3): 686-690.

Beardsley, C. L., C. R. Bertsch, et al. (2002). "Interfragmentary surface area as an index of comminution energy: proof of concept in a bone fracture surrogate." Journal of Biomechanics 35(3): 331-338.

Beck, T. J., C. B. Ruff, et al. (2000). "Stress fracture in military recruits: gender differences in muscle and bone susceptibility factors." Bone 27(3): 437-444.

Behiri, J. C. and W. Bonfield (1989). "Orientation dependence of the fracture mechanics of cortical bone." Journal of Biomechanics 22(8-9): 863-867.

Bergmann, G., G. Deuretzbacher, et al. (2001). "Hip contact forces and gait patterns from routine activities." Journal of Biomechanics 34(7): 859-871.

Boivin, G. and P. J. Meunier (2002). "The degree of mineralization of bone tissue measured by computerized quantitative contact microradiography." Calcified Tissue International 70(6): 503-511.

Boivin, G. and P. J. Meunier (2003). "The mineralization of bone tissue: a forgotten dimension in osteoporosis research." Osteoporosis International 14(0): 19-24.

Bonfield, W. and C. H. Li (1966). "Deformation and Fracture of Bone." Journal of Applied Physics **37**(2): 869-875.

Bonfield, W. and P. K. Datta (1976). "Fracture toughness of compact bone." Journal of Biomechanics **9**(3): 131-134.

Bonfield, W., M. D. Grynpas, et al. (1978). "Crack velocity and the fracture of bone." Journal of Biomechanics **11**(10–12): 473-479.

Boskey, A. L., T. M. Wright, et al. (1999). "Collagen and Bone Strength." Journal of Bone and Mineral Research 14(3): 330-335.

Bowman, S. M., J. Zeind, et al. (1996). "The tensile behavior of demineralized bovine cortical bone." Journal of Biomechanics 29(11): 1497-1501.

Bruce Martin, R. (2003). "Fatigue Damage, Remodeling, and the Minimization of Skeletal Weight." Journal of Theoretical Biology 220(2): 271-276.

Burr D.B, et al (1996) "In vivo measurement of human tibial strains during vigorous activity." Bone 18(5):405:410

Burr, D. B. (1997). "Muscle Strength, Bone Mass, and Age-Related Bone Loss." Journal of Bone and Mineral Research 12(10): 1547-1551.

Burr, D. B. (2002). "The contribution of the organic matrix to bone's material properties." Bone 31(1): 8-11.

Burr, D. B. (2002). "Targeted and nontargeted remodeling." Bone 30(1): 2-4.

Burr, D. B., M. R. Forwood, et al. (1997). "Bone Microdamage and Skeletal Fragility in Osteoporotic and Stress Fractures." Journal of Bone and Mineral Research 12(1): 6-15.

Burr, D. B., R. B. Martin, et al. (1985). "Bone remodeling in response to in vivo fatigue microdamage." Journal of Biomechanics 18(3): 189-200.

Burstein, A. H., J. D. Currey, et al. (1972). "The ultimate properties of bone tissue: The effects of yielding." Journal of Biomechanics 5(1): 35-42.

Burstein, A. H., J. M. Zika, et al. (1975). "Contribution of collagen and mineral to the elastic-plastic properties of bone." J Bone Joint Surg Am 57(7): 956-961.

Carter, D. R. and W. C. Hayes (1977). "Compact bone fatigue damage: a microscopic examination." Clin Orthop Relat Res(127): 265-74.

Carter, D. R. and W. C. Hayes (1977). "The compressive behavior of bone as a two-phase porous structure." J Bone Joint Surg Am 59(7): 954-62.

Catanese Iii, J., E. P. Iverson, et al. (1999). "Heterogeneity of the mechanical properties of demineralized bone." Journal of Biomechanics 32(12): 1365-1369.

Chavassieux, P., E. Seeman, et al. (2007). "Insights into Material and Structural Basis of Bone Fragility from Diseases Associated with Fractures: How Determinants of the

Biomechanical Properties of Bone Are Compromised by Disease." Endocr Rev 28(2): 151-164.

Choi, K. and S. A. Goldstein (1992). "A comparison of the fatigue behavior of human trabecular and cortical bone tissue." Journal of Biomechanics 25(12): 1371-1381.

Christina L. Beardsley, D. D. A. J. L. M. T. D. B. (2005). "Interfragmentary surface area as an index of comminution severity in cortical bone impact." Journal of Orthopaedic Research 23(3): 686-690.

Ciarelli, T. E., D. P. Fyhrie, et al. (2003). "Effects of vertebral bone fragility and bone formation rate on the mineralization levels of cancellous bone from white females." Bone 32(3): 311-315.

Compston, J. (2006). "Bone quality: what is it and how is it measured?" Arquivos Brasileiros de Endocrinologia & Metabologia 50: 579-585.

Courtney, A. C., W. C. Hayes, et al. (1996). "Age-related differences in post-yield damage in human cortical bone. Experiment and model." Journal of Biomechanics 29(11): 1463-1471.

Crowninshield, R. and M. Pope (1974). "The response of compact bone in tension at various strain rates." Annals of Biomedical Engineering 2(2): 217-225.

Currey, J. D. (1969). "The mechanical consequences of variation in the mineral content of bone." Journal of Biomechanics **2**(1): 1-11.

Currey, J. D. (1979). "Changes in the impact energy absorption of bone with age." Journal of Biomechanics 12(6): 459-465, 467-469.

Currey, J. D. (1988). "The effect of porosity and mineral content on the Young's modulus of elasticity of compact bone." Journal of Biomechanics 21(2): 131-139.

Currey, J. D. (1988). "Strain rate and mineral content in fracture models of bone." Journal of Orthopaedic Research 6(1): 32-38.

Currey, J. D. (1999). "What determines the bending strength of compact bone?" Journal of Experimental Biology 202(18): 2495-2503.

Curry, J. D. (2002) Bones : Structure and Mechanics, Princeton University Press

Currey, J. D. (2003). "How Well Are Bones Designed to Resist Fracture?" Journal of Bone and Mineral Research 18(4): 591-598.

Currey, J. D. (2004). "Incompatible mechanical properties in compact bone." Journal of Theoretical Biology 231(4): 569-580.

Currey, J. D., K. Brear, et al. (1996). "The effects of ageing and changes in mineral content in degrading the toughness of human femora." Journal of Biomechanics 29(2): 257-260.

Dawson, S, P., (2009), “Digital X-ray Analysis for Monitoring Fracture Healing” Thesis, (PhD). The University of Edinburgh.

Demade, A. I. H., M Goldthorpe, J Yates (2006). "Fracture Training Manual." Sheffield Fracture Mechanics.

Doube, M., M. M. Klosowski, et al. (2010). "BoneJ: Free and extensible bone image analysis in ImageJ." Bone 47(6): 1076-1079.

Einhorn, T. A. (1992). "Bone strength: The bottom line." Calcified Tissue International 51(5): 333-339.

Erdogan, F. (2000). "Fracture mechanics." International Journal of Solids and Structures 37(1-2): 171-183.

Felsenberg, D. and S. Boonen (2005). "The bone quality framework: Determinants of bone strength and their interrelationships, and implications for osteoporosis management." Clinical Therapeutics 27(1): 1-11.

Ferreira, F., M. A. Vaz, et al. (2006). "Mechanical properties of bovine cortical bone at high strain rate." Materials Characterization 57(2): 71-79.

Flügge, W. (1967). Viscoelasticity, Blaisdell Pub. Co.

Fratzl, P. (2008). "Bone fracture: When the cracks begin to show." Nat Mater 7(8): 610-612.

Fratzl, P. and R. Weinkamer (2007). "Nature's hierarchical materials." Progress in Materials Science 52(8): 1263-1334.

Frost, H. M. (1997). "On Our Age-Related Bone Loss: Insights from a New Paradigm." Journal of Bone and Mineral Research 12(10): 1539-1546.

Gallacher, S. and T. Dixon "Impact of Treatments for Postmenopausal Osteoporosis (Bisphosphonates, Parathyroid Hormone, Strontium Ranelate, and Denosumab) on Bone Quality: A Systematic Review." Calcified Tissue International 87(6): 469-484.

Gdoutos, E. E., D. D. Raftopoulos, et al. (1982). "A critical review of the biomechanical stress analysis of the human femur." Biomaterials 3(1): 2-8.

Gere J.M. (2006). Mechanics of Materials 6th Edition. Thompson Learning.

Griffith, A. A. (1921). "The Phenomena of Rupture and Flow in Solids." Philosophical Transactions of the Royal Society of London. Series A, Containing Papers of a Math. or Phys. Character (1896-1934) 221(-1): 163-198.

Gupta, H. S. and P. Zioupos (2008). "Fracture of bone tissue: The [`]hows' and the [`]whys'." Medical Engineering & Physics 30(10): 1209-1226.

Gurka R., L. A., Hefetz D., Rubinstein D. and Shavit U (1999). "Computation of Pressure Distribution Using PIV Velocity Data
" 3rd International Workshop on Particle Image Velocimetry.

Hansen, U., P. Zioupos, et al. (2008). "The Effect of Strain Rate on the Mechanical Properties of Human Cortical Bone." Journal of Biomechanical Engineering 130(1): 011011-8.

Hasegawa, K., C. Turner, et al. (1994). "Contribution of collagen and mineral to the elastic anisotropy of bone." Calcified Tissue International 55(5): 381-386.

Hasson, D. F. and R. W. Armstrong (1974). "A ductile-to-brittle transition in bone?" Journal of Materials Science 9(7): 1165-1170.

Hayes, W., E. Myers, et al. (1993). "Impact near the hip dominates fracture risk in elderly nursing home residents who fall." Calcified Tissue International 52(3): 192-198.

Hernandez, C. J. (2008). "How can bone turnover modify bone strength independent of bone mass?" Bone 42(6): 1014-1020.

Hernandez, C. J. and T. M. Keaveny (2006). "A biomechanical perspective on bone quality." Bone 39(6): 1173-1181.

Hertzberg, R. W. (1996). Deformation and fracture mechanics of engineering materials J. Wiley & Sons.

Hibbeler R.C. (1999). Structural Analysis 4th Edition. Prentice-Hall Inc.

Hight, T. K. and J. F. Brandeau (1983). "Mathematical modeling of the stress strain-strain rate behavior of bone using the Ramberg-Osgood equation." Journal of Biomechanics 16(6): 445-450.

ICB Dent, "Mechanical properties of bone". Available from http://www.feppd.org/ICB-Dent/campus/biomechanics_in_dentistry/ldv_data/mech/basic_bone.htm (accessed 2008)

Jarvinen, T. L. N., H. Sievanen, et al. (2005). "Revival of Bone Strength: The Bottom Line." Journal of Bone and Mineral Research 20(5): 717-720.

Jeffry, S. N., R. Anuradha, et al. (2007). "Age-related factors affecting the postyield energy dissipation of human cortical bone." Journal of Orthopaedic Research 25(5): 646-655.

Kanis, J. A., L. J. Melton, et al. (1994). "The diagnosis of osteoporosis." Journal of Bone and Mineral Research 9(8): 1137-1141.

Kanninen, M. F. (1985). Advanced fracture mechanics, Oxford University Press.

Katsamanis, F. and D. D. Raftopoulos (1990). "Determination of mechanical properties of human femoral cortical bone by the Hopkinson bar stress technique." Journal of Biomechanics 23(11): 1173-1184.

Katz. J. L., (1971). "Hard tissue as a composite material—I. Bounds on the elastic behavior." Journal of Biomechanics **4**(5): 455-473.

Keaveny, T. M., E. F. Wachtel, et al. (1994). "Differences between the tensile and compressive strengths of bovine tibial trabecular bone depend on modulus." Journal of Biomechanics 27(9): 1137-1146.

Keller, T. S., Z. Mao, et al. (1990). "Young's modulus, bending strength, and tissue physical properties of human compact bone." J Orthop Res 8(4): 592-603.

Kennedy, O. D., O. Brennan, et al. (2008). "The effects of increased intracortical remodeling on microcrack behaviour in compact bone." Bone 43(5): 889-893.

Kotha, S. P. and N. Guzelsu (2007). "Tensile behavior of cortical bone: Dependence of organic matrix material properties on bone mineral content." Journal of Biomechanics 40(1): 36-45.

Lakes, R. (1993). "Materials with structural hierarchy." Nature 361(6412): 511-515.

Leng, H., X. Dong, et al. (2008). "Aging effects on compressive energy dissipation of cortical bone." Bone 43(Supplement 1): S47-S47.

Leng, H., X. N. Dong, et al. (2009). "Progressive post-yield behavior of human cortical bone in compression for middle-aged and elderly groups." Journal of Biomechanics 42(4): 491-497.

Lotz, J. C., E. J. Cheal, et al. (1995). "Stress distributions within the proximal femur during gait and falls: Implications for osteoporotic fracture." Osteoporosis International 5(4): 252-261.

Madden, V. J. and M. M. Henson (1997). "Rapid decalcification of temporal bones with preservation of ultrastructure." Hearing Research 111(1-2): 76-84.

Makhutov, N. A. and Y. G. Matvienko (1993). "Griffith theory and development of fracture mechanics criteria." Materials Science 29(3): 316-319.

Malik, C. L., S. M. Stover, et al. (2003). "Equine cortical bone exhibits rising R-curve fracture mechanics." Journal of Biomechanics 36(2): 191-198.

Martin, R. B. and D. L. Boardman (1993). "The effects of collagen fiber orientation, porosity, density, and mineralization on bovine cortical bone bending properties." Journal of Biomechanics 26(9): 1047-1054.

Martin, R. B. and J. Ishida (1989). "The relative effects of collagen fiber orientation, porosity, density, and mineralization on bone strength." Journal of Biomechanics 22(5): 419-426.

McCalden R.W., et al (1993). “Age-related changes in the tensile properties of cortical bone. The relative importance of changes in porosity, mineralization, and microstructure.” Journal of Bone and Joint Surgery 75(8):1193-1205

McCreadie B.R., et al (2006) “Bone tissue compositional differences in women with and without osteoporotic fracture.” Bone 39(6):1190-1995

McElhaney, J. H. (1966). "Dynamic response of bone and muscle tissue." J Appl Physiol **21**(4): 1231-1236.

Meunier, P. J. and G. Boivin (1997). "Bone mineral density reflects bone mass but also the degree of mineralization of bone: Therapeutic implications." Bone 21(5): 373-377.

Milan, L. and M. C. Trachtenberg (1981). Ultrasonic decalcification of bone. [Article], American Journal of Surgical Pathology September 1981;5(6):573-580.

Miller, E., D. Delos, et al. (2007). "Abnormal Mineral-Matrix Interactions Are a Significant Contributor to Fragility in <i>oim/oim</i> Bone." Calcified Tissue International 81(3): 206-214.

MIL-HDBK-5H (1998). "Military Handbook - MIL-HDBK-5H: Metallic Materials and Elements for Aerospace Vehicle Structures", U.S. Department of Defense. Ch.3.

Morgan, E. F. and T. M. Keaveny (2001). "Dependence of yield strain of human trabecular bone on anatomic site." Journal of Biomechanics 34(5): 569-577.

Nalla, R. K., J. H. Kinney, et al. (2003). "Mechanistic fracture criteria for the failure of human cortical bone." Nat Mater 2(3): 164-168.

Nalla, R. K., J. J. Kruzic, et al. (2005). "Mechanistic aspects of fracture and R-curve behavior in human cortical bone." Biomaterials 26(2): 217-231.

Nalla, R. K., J. J. Kruzic, et al. (2004). "On the origin of the toughness of mineralized tissue: microcracking or crack bridging?" Bone 34(5): 790-798.

Nalla, R. K., J. S. Stölken, et al. (2005). "Fracture in human cortical bone: local fracture criteria and toughening mechanisms." Journal of Biomechanics 38(7): 1517-1525.

Norman, T. L., S. V. Nivargikar, et al. (1996). "Resistance to crack growth in human cortical bone is greater in shear than in tension." Journal of Biomechanics 29(8): 1023-1031.

O'Brien, F. J., D. Taylor, et al. (2003). "Microcrack accumulation at different intervals during fatigue testing of compact bone." Journal of Biomechanics 36(7): 973-980.

Olszta, M. J., X. Cheng, et al. (2007). "Bone structure and formation: A new perspective." Materials Science and Engineering: R: Reports 58(3-5): 77-116.

Panagiotopoulos, E., V. Kostopoulos, et al. (2005). "Impact energy absorption by specimens from the upper end of the human femur." Injury 36(5): 613-617.

Pérez-Heredia, M., C. M. Ferrer-Luque, et al. (2008). "Decalcifying effect of 15% EDTA, 15% citric acid, 5% phosphoric acid and 2.5% sodium hypochlorite on root canal dentine." International Endodontic Journal 41(5): 418-423.

Peterlik, H., P. Roschger, et al. (2006). "From brittle to ductile fracture of bone." Nat Mater 5(1): 52-55.

Pettifor, J. M. (2002). "Rickets." Calcified Tissue International 70(5): 398-399.

Piekarski, K. (1970). "Fracture of Bone." Journal of Applied Physics **41**(1): 215-223.

Pinilla, T., K. Boardman, et al. (1996). "Impact direction from a fall influences the failure load of the proximal femur as much as age-related bone loss." Calcified Tissue International 58(4): 231-235.

Pope, M. H. and J. O. Outwater (1972). "The fracture characteristics of bone substance." Journal of Biomechanics **5**(5): 457-465.

Raftopoulos, D., E. Katsamanis, et al. (1993). "An intermediate loading rate technique for the determination of mechanical properties of human femoral cortical bone." Journal of Biomedical Engineering 15(1): 60-66.

Rauch, F., C. Neu, et al. (2001). "The Development of Metaphyseal Cortex—Implications for Distal Radius Fractures During Growth." Journal of Bone and Mineral Research 16(8): 1547-1555.

Reilly, D. T. and A. H. Burstein (1975). "The elastic and ultimate properties of compact bone tissue." Journal of Biomechanics 8(6): 393-396.

Reilly, D. T., A. H. Burstein, et al. (1974). "The elastic modulus for bone." Journal of Biomechanics 7(3): 271-272.

Rho, J.-Y., L. Kuhn-Spearing, et al. (1998). "Mechanical properties and the hierarchical structure of bone." Medical Engineering & Physics 20(2): 92-102.

Rockville, M. (2004). Bone Health and Osteoporosis: A Report of the Surgeon General. O. o. t. S. General, U.S. Department of Health and Human Services.

Rogers, L. L. and D. D. Moyle (1988). "Effect of specimen size on work-of-fracture measurements." Journal of Biomechanics 21(11): 919-926.

Rubin, C. T. and L. E. Lanyon (1984). "Regulation of bone formation by applied dynamic loads." J Bone Joint Surg Am 66(3): 397-402.

Russell, W. C. (2003). "Rickets: An old form for a new century." Pediatrics International 45(5): 509-511.

Sasaki, N., T. Nozoe, et al. (2008). "Effect of mineral dissolution from bone specimens on the viscoelastic properties of cortical bone." Journal of Biomechanics 41(16): 3511-3514.

Seeman, E. (1997). "From Density to Structure: Growing Up and Growing Old on the Surfaces of Bone." Journal of Bone and Mineral Research 12(4): 509-521.

Seeman, E. (2008). "Bone quality: the material and structural basis of bone strength." Journal of Bone and Mineral Metabolism 26(1): 1-8.

Seeman, E. and P. D. Delmas (2006). "Bone Quality -- The Material and Structural Basis of Bone Strength and Fragility." N Engl J Med 354(21): 2250-2261.

Shah, K., J. Goh, et al. (1995). "Effect of decalcification on bone mineral content and bending strength of feline femur." Calcified Tissue International 56(1): 78-82.

Sharir, A., M. M. Barak, et al. (2008). "Whole bone mechanics and mechanical testing." The Veterinary Journal 177(1): 8-17.

Sievanen, H. (2008). "Impact of physical activity on the skeleton." 2nd Joint meeting of the BRS & BORS.

Simkin, A. and G. Robin (1973). "The mechanical testing of bone in bending." Journal of Biomechanics 6(1): 31-36, IN3, 37-39.

Sinclair, G. B. and A. E. Chambers (1987). "Strength size effects and fracture mechanics: What does the physical evidence say?" Engineering Fracture Mechanics 26(2): 279-310.

Spatz, H. Ch., O'Leary, E.J., Vincent, J. F. V. (1996). "Young's moduli and shear moduli in cortical bone" Proceedings: Biological Sciences 263: 287-294

Summitt, M. C. and K. D. Reisinger (2003). "Characterization of the mechanical properties of demineralized bone." Journal of Biomedical Materials Research Part A 67A(3): 742-750.

Taylor, D. (2003). "Fracture mechanics: How does bone break?" Nat Mater 2(3): 133-134.

Taylor, D., J. G. Hazenberg, et al. (2007). "Living with cracks: Damage and repair in human bone." Nat Mater 6(4): 263-268.

Timoshenko S.P.,(1925*)* Applied Elasticity*,* J. M. Lessells, D. Van Nostrand Company,

Thorpe, E. J., B. B. Bellomy, et al. (1963). "Ultrasonic Decalcification of Bone: AN EXPERIMENTAL AND CLINICAL STUDY." J Bone Joint Surg Am 45(6): 1257-1259.

Thurner, P. J., B. Erickson, et al. (2007). "High-speed photography of compressed human trabecular bone correlates whitening to microscopic damage." Engineering Fracture Mechanics 74(12): 1928-1941.

Turner, C. H. (1998). "Three rules for bone adaptation to mechanical stimuli." Bone 23(5): 399-407.

Turner, C. H. and D. B. Burr (1993). "Basic biomechanical measurements of bone: A tutorial." Bone 14(4): 595-608.

van der Meulen, M. C. H., K. J. Jepsen, et al. (2001). "Understanding bone strength: size isn't everything." Bone 29(2): 101-104.

Vashishth, D. (2004). "Rising crack-growth-resistance behaviour in cortical bone:: implications for toughness measurements." Journal of Biomechanics 37(6): 943-946.

Vashishth, D. (2007). "Hierarchy of bone microdamage at multiple length scales." International Journal of Fatigue 29(6): 1024-1033.

Vashishth, D., G. J. Gibson, et al. (2001). "Influence of nonenzymatic glycation on biomechanical properties of cortical bone." Bone 28(2): 195-201.

Vashishth, D., K. E. Tanner, et al. (2000). "Contribution, development and morphology of microcracking in cortical bone during crack propagation." Journal of Biomechanics 33(9): 1169-1174.

Vashishth, D., K. E. Tanner, et al. (2003). "Experimental validation of a microcracking-based toughening mechanism for cortical bone." Journal of Biomechanics 36(1): 121-124.

Verhulp, E., B. van Rietbergen, et al. (2008). "Load distribution in the healthy and osteoporotic human proximal femur during a fall to the side." Bone 42(1): 30-35.

Wang, X. and J. S. Nyman (2007). "A novel approach to assess post-yield energy dissipation of bone in tension." Journal of Biomechanics 40(3): 674-677.

Wang, X. and C. Qian (2006). "Prediction of microdamage formation using a mineral-collagen composite model of bone." Journal of Biomechanics 39(4): 595-602.

Wang, X., X. Shen, et al. (2002). "Age-related changes in the collagen network and toughness of bone." Bone 31(1): 1-7.

Washington University, Available from: http://courses.washington.edu/bonephys/opbmd.html (accessed 2009)

Weiner, S. and W. Traub (1992). "Bone structure: from angstroms to microns." FASEB J. 6(3): 879-885.

Weiner, S. and H. D. Wagner (1998). "THE MATERIAL BONE: Structure-Mechanical Function Relations." Annual Review of Materials Science 28(1): 271-298.

Wolff, J. (1892). "Das Gesetz der Transformation der Knochen."

Wright, T. and W. Hayes (1976a). "The fracture mechanics of fatigue crack propagation in compact bone." Journal of Biomedical Research 10:637-648

Wright, T. and W. Hayes (1976b). "Tensile testing of bone over a wide range of strain rates: effects of strain rate, microstructure and density." Medical and Biological Engineering and Computing 14(6): 671-680.

Wright, T. M. and W. C. Hayes (1977). "Fracture mechanics parameters for compact bone—Effects of density and specimen thickness." Journal of Biomechanics **10**(7): 419-430.

Yan, J., J. J. J. Mecholsky, et al. (2007). "How tough is bone? Application of elastic-plastic fracture mechanics to bone." Bone 40(2): 479-484.

Yang, Q. D., B. N. Cox, et al. (2006). "Fracture length scales in human cortical bone: The necessity of nonlinear fracture models." Biomaterials 27(9): 2095-2113.

Yeni, Y. N. and D. P. Fyhrie (2002). "Fatigue damage-fracture mechanics interaction in cortical bone." Bone 30(3): 509-514.

Yeni, Y. N. and D. P. Fyhrie (2003). "A rate-dependent microcrack-bridging model that can explain the strain rate dependency of cortical bone apparent yield strength." Journal of Biomechanics 36(9): 1343-1353.

Yerramshetty, J. S. and O. Akkus (2008). "The associations between mineral crystallinity and the mechanical properties of human cortical bone." Bone 42(3): 476-482.

Young W.C., (1989) Roark's Formulas for Stress and Strain 6th Edition McGraw-Hill

Zioupos, P. (1998). "Recent developments in the study of failure of solid biomaterials and bone: `fracture' and `pre-fracture' toughness." Materials Science and Engineering: C 6(1): 33-40.

Zioupos, P., R. B. Cook, et al. (2008). "Some basic relationships between density values in cancellous and cortical bone." Journal of Biomechanics 41(9): 1961-1968.

Zioupos, P. and J. D. Currey (1998). "Changes in the Stiffness, Strength, and Toughness of Human Cortical Bone With Age." Bone 22(1): 57-66.

Zioupos, P., U. Hansen, et al. (2006). "The development of microdamage as a function of strain rate in human cortical bone." Journal of Biomechanics 39(Supplement 1): S16-S17.

Zioupos, P., U. Hansen, et al. (2008). "Microcracking damage and the fracture process in relation to strain rate in human cortical bone tensile failure." Journal of Biomechanics 41(14): 2932-2939.